ANTIBODY-DRUG CONJUGATES IN CANCER

Cover art: Joost Bakker, SCICOMVISUALS, Amsterdam, The Netherlands
Production: Joost Bakker, SCICOMVISUALS, Amsterdam, The Netherlands
Design & Dtp: De vliegende kiep, Amsterdam, The Netherlands
Printed by: Ipskamp Printing, Amsterdam

ISBN/EAN: 978-94-028-0102-6

Proefschrift Universiteit Leiden, Faculteit Geneeskunde

Dit proefschrift werd mede mogelijk gemaakt met financiële steun van Genmab

Antibody-drug conjugates in cancer

PROEFSCHRIFT

Ter verkrijging van de graad
van doctor aan de Universiteit Leiden,
op gezag van Rector Magnificus
prof.mr. C.J.J.M. Stolker
volgens besluit van het College voor Promoties
te verdedigen op
woensdag 13 april 2016
klokke 15:00 uur

door

Bart Egbertus Cornelis Gijsbertus de Goeij

Geboren op 6 februari 1981,
te Utrecht

Promotor
Prof. dr. Paul W.H.I. Parren

Co-promotor
Dr. Esther C. Breij

Promotiecommissie
Prof. dr. C. van Kooten
Prof. dr. F.A. Ossendorp
Prof. dr. W. Jiskoot
Prof. dr. M. van Egmond, Vrije Universiteit medisch centrum, Amsterdam
Dr. P.H.C. van Berkel, ADC Therapeutics

Table of Contents

1 General outline and aim of the thesis

Antibodies (Abs) are part of the adaptive humoral immune response, which provides long-lasting protection against pathogens such as viruses and bacteria. During this immune response naïve B-cells recognize an antigen through their B-cell receptor. This results in clonal expansion of the B-cells and differentiation into plasma cells, which secrete large amounts of Abs. These Abs can bind to pathogens thereby flagging the opsonized pathogen for destruction. Abs of the IgG isotype contain two binding arms, each containing a Fab (fragment antigen binding) region through which they recognize their cognate antigen (**Figure 1**). The Abs selectivity for the antigen is determined by the complementary determining region (CDRs) located at the top of the Fab-region. The population of B-cells in the human body may be able to respond to as many as 1 x 10^{11} different antigens. This huge diversity is determined by the different gene segments encoding variable, joining and diversity regions that recombine randomly allowing for nearly 2.5 x 10^{6} combinations. Nucleotide insertions and hypermutations further diversify the CDRs.

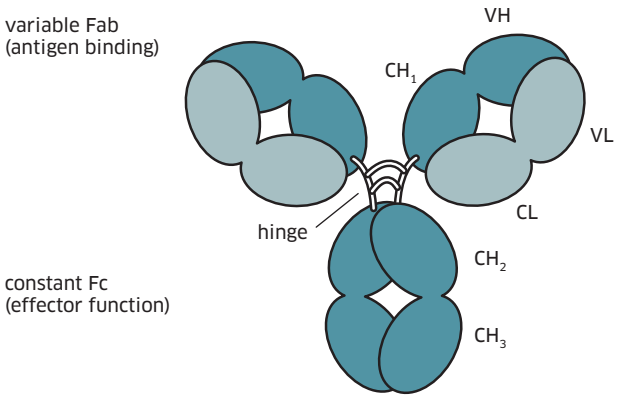

FIGURE 1 *Schematic representation of an IgG1 antibody structure.*

Abs are able to interact with the immune system through the constant Fc (fragment crystallizable) region. In humans, nine different antibody isotypes exist (IgA1 and 2, IgD, IgE, IgG1, 2, 3 and 4 and IgM), each having a unique Fc region. The most abundant class in circulation is IgG1 (~50%). This antibody class is able to eliminate pathogens through a number of Fc-mediated effector mechanisms. Each of these mechanisms requires that the pathogen is opsonized with antibodies resulting in a

high density of Fc regions on the pathogen surface. These Fc regions may interact to form a high-avidity binding scaffold for C1q, which initiates complement dependent cytotoxicity (CDC) [1]. Alternatively, the IgG Fc region can be recognized by Fcγ-receptors that are expressed on immune effector cells such as NK-cells, granulocytes and macrophages. Binding of Fcγ-receptors expressed on NK-cells and granulocytes triggers the release of cytotoxic granules that kill the pathogen through a mechanism called antibody-dependent cellular cytotoxicity (ADCC) [2]. Binding of Fcγ-receptors on macrophages leads to the engulfing of the opsonized pathogen, also known as antibody-dependent cellular phagocytosis (ADCP) [3].

The ability to engage the immune system to induce killing of opsonized cells via Fc-mediated mechanisms led to the notion that monoclonal Abs might have great potential for the treatment of cancer. Numerous monoclonal Abs for the treatment of cancer have been developed in the past two decades, some of which have revolutionized treatment of cancers such as non-Hodgkin lymphoma (Rituxan®) and breast cancer (Herceptin®). In addition to Fc-mediated effector functions, therapeutic antibodies can exert anti-tumor activity through a number of different mechanisms. For example, inhibition of growth factor receptor signaling and induction of receptor downmodulation (e.g. zalututumab). Furthermore, therapeutic antibodies may interact with the tumor microenvironment, for example by inhibiting regulatory interactions between tumor cells and the adaptive immune system (e.g. ipilumumab, PD-1, PD-L1). Although the generation of tumor-targeting antibodies has generally been very successful, only a limited number of antibodies have been clinically effective [4]. As of today, 17 monoclonal antibodies have been approved for the treatment of cancer by the Food and Drug Administration (FDA) and 15 by the European Medicines Agency (EMA) in addition to a comparable number of Abs for the treatment of inflammatory, cardiovascular, infectious and other diseases. The challenge in cancer treatment is that tumors often develop resistance to antibody therapy. Downstream signaling pathways can be mutated (KRAS/BRAF) which limits the antibody's capacity to inhibit growth factor receptor signaling [5]. Tumors can overexpress complement inhibitory receptors such as CD46, CD55 and CD59, thereby blocking CDC [6]. Overexpression of certain HLA molecules (i.e. HLA-E and -G) that inhibit NK-cell mediated ADCC has been described for various tumors [7,8] and the tumor microenvironment can be infiltrated by T-regulatory cells and myeloid-derived suppressor cells that serve to suppress the anti-tumor immune response [9].

One approach to overcome such limitations in efficacy is the conjugation of cytotoxic compounds to monoclonal antibodies. These antibody-drug conjugates (ADCs) combine the tumor specificity, pharmacokinetics and biodistribution properties of antibodies with the potent cell-killing activity of small molecules. This concept was already postulated in the early 20th century by Paul Ehrlich who reasoned that if a compound could be made that selectively targeted a disease-causing organism,

then a toxin for that organism could be delivered along with the agent of selectivity [10]. Hence, a "magic bullet" would be created that only killed the targeted organism. An antibody would be extremely suitable for this purpose as antibodies can selectively bind to tumor antigens while maintaining a long half-life in circulation (~21 days for IgG1). The first generation of ADCs were conjugated with clinically approved chemotherapeutic agents such as vinblastine, mitomycin, methotrexate and doxorubicin [11]. These ADCs showed limited clinical success which was mostly attributed to the low potency of the conjugated drug. The second generation of ADCs made use of more potent payloads, namely calicheamicin, auristatin and maytansin analogs. Besides, pharmacokinetics of the conjugation linker was optimized and fully human mAbs were used to solve immunogenicity problems observed with murine mAbs. In 2000 the first ADC, gemtuzumab ozogamicin (Mylotarg®), was clinically approved for use in refractory acute myeloid leukemia (AML) [12]. Here, a CD33 antibody was conjugated to calicheamicin, a drug that specifically binds to DNA and generates single and double strand DNA breaks. Gemtuzumab ozogamicin received accelerated approval for the treatment of patients with relapse AML. Unfortunately, ten years later, gemtuzumab ozogamicin was withdrawn from the US market due to lack of clinical benefit [13]. A confirmatory phase III trial showed no improvement in clinical benefit for patients who received standard chemotherapy plus gemtuzumab ozogamicin, but instead a greater number of deaths occurred in the group of patients who received gemtuzumab ozogamicin compared with those receiving chemotherapy alone [13]. Several factors have been identified that have limited the clinical efficacy of gemtuzumab ozogamicin, including poor stability of the acid-labile conjugation linker, heterogeneous drug loading (approximately 50% of the CD33 antibodies are unconjugated) and sensitivity to multidrug resistance pumps that are often overexpressed in AML.

More recently, two novel ADCs were approved by the FDA for the treatment of Hodgkin lymphoma and anaplastic large-cell lymphoma, brentuximab vedotin (Adcetris®) and HER2 positive breast cancer, trastuzumab emtansine (Kadcyla®) [14,15]. These ADCs showed improved liker stability and pharmacokinetics. Their clinical success has led to an impressive expansion of the clinical ADC pipeline (**Chapter 2, Table 1**). An overview of the recent developments in ADC based therapy is summarized in **Chapter 2**.

Although simple in concept, the success of a given ADC depends on careful selection of the tumor antigen, antibody, linker as well as the payload. The aim of this thesis was to better understand the antibody and antigen requirements that are essential for developing a therapeutically effective ADC. **Chapter 2** reviews the different cytotoxic compounds that are currently being used as payloads, and the type of tumor antigens that can be utilized for their intracellular delivery, as well as the interplay of ADCs with the immune system. In **Chapter 3** we explore tissue factor (TF) as a

novel target for an auristatin-based ADC. An effective ADC treatment requires that in circulation, the payload remains attached to the antibody. Following selective antigen binding, the ADC should be internalized and targeted to the lysosomes to be processed by lysosomal enzymes such as cathepsins. This leads to cleavage of the linker and/or degradation of the antibody moiety of the ADC, resulting in release of the payload. Once released, the payload can exert its cytotoxic effect through inhibition of microtubule formation (**Figure 2**).

To investigate the suitability of TF as a target for an ADC approach, we compared the distribution, internalization and lysosomal targeting of TF with that of the clinically validated ADC target HER2 as well as for EGFR, for which an ADC is currently in phase II clinical development. ADCs were generated by conjugating TF-, HER2- and EGFR- Abs with the microtubule inhibiting agent duostatin-3. These ADCs allowed us to compare efficacy of TF-, HER2- and EGFR-specific ADCs in different *in vitro* and *in vivo* tumor models. **Chapter 4** describes the selection of monoclonal antibody TF-011 as the optimal candidate for the development of a TF-specific ADC. A large panel of TF Abs was generated from which clone 011 was selected based on excellent target binding characteristics, rapid internalization and efficient lysososomal targeting and the capacity to inhibit TF-Factor VIIa (FVIIa)-dependent intracellular signaling, while having minimal impact on coagulation *in vitro*. The *in vivo* efficacy of the lead

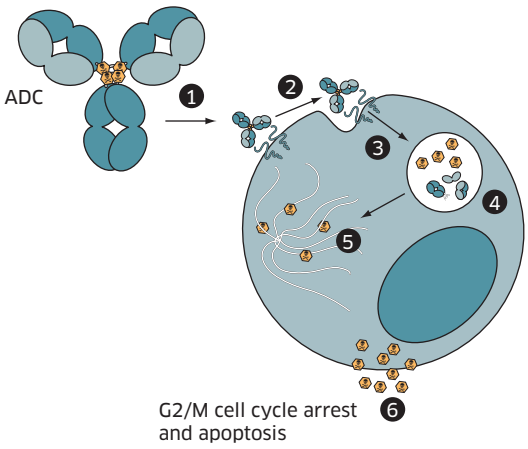

FIGURE 2 *Mechanism of action of auristatin-based ADCs.* The ADC should be stable in circulation (**1**) and bind (**2**) to its antigen when a tumor cell is encountered. The antigen/ADC complex has to be internalized and targeted to the lysosomes (**3**) where lysosomes enzymes can process the ADC and release the auristatin payload (**4**). The payload can then exert its cytotoxic effect by inhibition of tubulin formation (**5**), resulting in cell cycle arrest and apoptosis (**6**).

candidate HuMax-TF-ADC (TF-011-MMAE) is analyzed in detail. Different patient-derived xenograft (PDX) models with variable levels of TF expression were treated with TF-011-MMAE. In addition, tumor models that showed tumor recurrence after treatment with TF-011-MMAE and paclitaxel were retreated with TF-011-MMAE.

Chapter 5 describes the development of a high throughput assay that can be used to screen large antibody panels for their suitability to facilitate intracellular delivery of toxic payloads. A modified version of the Pseudomonas exotoxin-A was fused to a human kappa light chain binding antibody fragment. The resulting fusion protein (α-kappa-ETA') was tested for binding to Abs with a human kappa light chain and its ability to inhibit proliferation of EGFR expressing cells when non-covalently linked to an EGFR Ab. In **Chapter 6** we used the α-kappa-ETA' assay to screen a large and diverse panel of HER2 antibodies for their ability to deliver α-kappa-ETA' into tumor cells. **Chapter 7** describes the development of a Fab-arm that can be used to facilitate internalization and lysosomal delivery of poorly internalizing tumor antigens in a bispecific antibody approach. **Chapter 8** covers the general discussion of this thesis and addresses the key findings in comparison to the literature. General rules of thumb providing a road map for ADC development are presented and summarized.

To summarize, the clinical success of brentuximab vedotin and trastuzumab emtansine has led to an extensive expansion of the clinical ADC pipeline. Although the concept of an ADC seems simple, designing a successful ADC is complex and requires careful selection of the tumor antigen, antibody, linker and payload. In this thesis, different tumor antigens and targeting antibodies were compared for their capacity to deliver cytotoxic payloads to tumor cells, uncovering general mechanisms. In the course of this work, TF was identified as an excellent ADC target because of its rapid internalization and lysosomal targeting characteristics. Furthermore we have explored a novel Ab platform that improves the intracellular delivery of cytotoxic payloads. These findings provide a better insight in the Ab and antigen requirements needed for optimal payload delivery and support the development of novel and improved ADCs for the treatment of cancer.

REFERENCES

1 Diebolder CA, Beurskens FJ, de Jong RN, Koning RI, Strumane K, Lindorfer MA, Voorhorst M, Ugurlar D, Rosati S, Heck AJ *et al*: Complement is activated by IgG hexamers assembled at the cell surface. *Science* 2014, 343(6176):1260-1263.

2 Overdijk MB, Verploegen S, van den Brakel JH, Lammerts van Bueren JJ, Vink T, van de Winkel JG, Parren PW, Bleeker WK: Epidermal growth factor receptor (EGFR) antibody-induced antibody-dependent cellular cytotoxicity plays a prominent role in inhibiting tumorigenesis, even of tumor cells insensitive to EGFR signaling inhibition. *J Immunol* 2011, 187(6):3383-3390.

3 Overdijk MB, Verploegen S, Bogels M, van Egmond M, Lammerts van Bueren JJ, Mutis T, Groen RW, Breij E, Martens AC, Bleeker WK *et al*: Antibody-mediated phagocytosis contributes to the anti-tumor activity of the therapeutic antibody daratumumab in lymphoma and multiple myeloma. *MAbs* 2015, 7(2):311-321.

4 Nelson AL, Dhimolea E, Reichert JM: Development trends for human monoclonal antibody therapeutics. *Nat Rev Drug Discov* 2010, 9(10):767-774.

5 Van Cutsem E, Kohne CH, Lang I, Folprecht G, Nowacki MP, Cascinu S, Shchepotin I, Maurel J, Cunningham D, Tejpar S *et al*: Cetuximab plus irinotecan, fluorouracil, and leucovorin as first-line treatment for metastatic colorectal cancer: updated analysis of overall survival according to tumor KRAS and BRAF mutation status. *J Clin Oncol* 2011, 29(15):2011-2019.

6 Jurianz K, Maslak S, Garcia-Schuler H, Fishelson Z, Kirschfink M: Neutralization of complement regulatory proteins augments lysis of breast carcinoma cells targeted with rhumAb anti-HER2. *Immunopharmacology* 1999, 42(1-3):209-218.

7 Lin A, Yan WH, Xu HH, Gan MF, Cai JF, Zhu M, Zhou MY: HLA-G expression in human ovarian carcinoma counteracts NK cell function. *Ann Oncol* 2007, 18(11):1804-1809.

8 Levy EM, Bianchini M, Von Euw EM, Barrio MM, Bravo AI, Furman D, Domenichini E, Macagno C, Pinsky V, Zucchini C *et al*: Human leukocyte antigen-E protein is overexpressed in primary human colorectal cancer. *Int J Oncol* 2008, 32(3):633-641.

9 Greten TF, Manns MP, Korangy F: Myeloid derived suppressor cells in human diseases. *Int Immunopharmacol* 2011, 11(7):802-807.

10 Ehrlich P: Address in Pathology, ON CHEMIOTHERAPY: Delivered before the Seventeenth International Congress of Medicine. *Br Med J* 1913, 2(2746):353-359.

11 Perez HL, Cardarelli PM, Deshpande S, Gangwar S, Schroeder GM, Vite GD, Borzilleri RM: Antibody-drug conjugates: current status and future directions. *Drug Discov Today* 2014, 19(7):869-881.

12 Sievers EL, Larson RA, Stadtmauer EA, Estey E, Lowenberg B, Dombret H, Karanes C, Theobald M, Bennett JM, Sherman ML *et al*: Efficacy and safety of gemtuzumab ozogamicin in patients with CD33-positive acute myeloid leukemia in first relapse. *J Clin Oncol* 2001, 19(13):3244-3254.

13 Kopecky K, Stuart RK, Larson RA, Nevill TJ, Stenke L, Slovak ML, Tallman MS, Willman CL, Erba H, Appelbaum FR: Preliminary Results of Southwest Oncology Group Study S0106: An International Intergroup Phase 3 Randomized Trial Comparing the Addition of Gemtuzumab Ozogamicin to Standard Induction Therapy Versus Standard Induction Therapy Followed by a Second Randomization to Post-Consolidation Gemtuzumab Ozogamicin Versus No Additional Therapy for Previously Untreated Acute Myeloid Leukemia *Annual Meeting of the American Society of Hematology; New Orleans; 2009; abstract 790*.

14 Younes A, Bartlett NL, Leonard JP, Kennedy DA, Lynch CM, Sievers EL, Forero-Torres A: Brentuximab vedotin (SGN-35) for relapsed CD30-positive lymphomas. *N Engl J Med* 2010, 363(19):1812-1821.

15 Burris HA, Rugo HS, Vukelja SJ, Vogel CL, Borson RA, Limentani S, Tan-Chiu E, Krop IE, Michaelson RA, Girish S *et al*: Phase II study of the antibody drug conjugate trastuzumab-DM1 for the treatment of human epidermal growth factor receptor 2 (HER2)-positive breast cancer after prior HER2-directed therapy. *J Clin Oncol* 2011, 29(4):398-405.

2 New developments for antibody-drug conjugate-based therapeutic approaches

► Curr Opin Immunol. 2016 Mar 7;40:14-23.

► Bart ECG de Goeij[1] and John M. Lambert[2]

1 Genmab, Yalelaan 60, 3584 CM, Utrecht, The Netherlands

2 ImmunoGen, Inc., 830 Winter Street, Waltham, Massachusetts 02451, United States

Corresponding author: Bart E.C.G. de Goeij (b.degoeij@genmab.com)

Conflict of interest statement: John M. Lambert is an employee of ImmunoGen, Inc., the developer of the maytansinoid ADC platform utilized in ado-trastuzumab emtansine and in other ADCs in clinical development, and an ADC platform based on indolinobenzodiazepines. Bart E.C.G. de Goeij is an employee of Genmab, the developer of tisotumab vedotin.

ABSTRACT

The clinical success of Adcetris® (brentuximab vedotin) and Kadcyla® (ado-trastuzumab emtansine) has sparked clinical development of novel ADCs. These powerful anti-cancer agents are designed to allow specific targeting of highly potent cytotoxic agents to tumour cells while sparing healthy tissues. Despite the use of tumor-specific antibodies, the emerging clinical data with ADCs indicates that adverse effects frequently occur before ADCs have reached their optimal therapeutic dose, resulting in a relatively narrow therapeutic window. This review summarizes the therapeutic window of ADCs currently in clinical development, along with some strategies that may help to widen the window.

INTRODUCTION

The prospects for development of antibody-drug conjugates (ADCs) as effective, well-tolerated anti-cancer therapeutics have changed dramatically since the approval of Adcetris® (brentuximab vedotin) in 2011 and Kadcyla® (ado-trastuzumab emtansine) in 2013. Currently, over 50 different ADCs are in clinical development, the majority consisting of IgG1 antibodies conjugated with potent microtubule inhibitors, either derivatives of maytansine, or auristatins which are analogs of dolastatin 10 (Table 1). These compounds display cytotoxicity at ~1000-fold lower concentration than standard chemotherapeutic agents [1], which makes them too toxic for systemic treatment [2,3]. By conjugating these potent cytotoxins to tumor-specific antibodies, their cytotoxic effect can be concentrated at tumor cells. At the same time, the pharmacokinetic profile of the toxins will improve upon conjugation to antibodies, giving to the small molecular weight cytotoxin the long half-life of an immunoglobulin. Notwithstanding the clinical success of brentuximab vedotin and ado-trastuzumab emtansine, the development for therapeutic use of most ADCs is still hampered by a relatively narrow therapeutic window. Although tumor-specific antibodies allow enrichment of cytotoxic payloads in tumors, adverse effects frequently occur before ADCs have reached their optimal therapeutic dose, which may limit their clinical response. In this short review, we have summarized available data from clinical and preclinical studies to assess the therapeutic window of ADCs. In addition, this review will discuss three aspects of ADC design, that may be important factors in helping to increase the therapeutic window of ADCs (Figure 1): 1) the target selection requirements for ADC development; 2) the interaction of ADCs with the immune system; 3) the development of novel DNA damaging agents with low picomolar efficacy.

THERAPEUTIC WINDOW OF ADCS IN CLINICAL DEVELOPMENT

The majority of ADCs in clinical development make use of tubulin-targeting antimitotic agents. These agents (maytansinoids and auristatins [4]) bind to the vinca-binding domain of tubulin, thereby interfering with microtubule dynamics and causing cell cycle arrest in the G2/M phase [5]. Table 1 shows that antibodies coupled with the maytansinoids DM1 or DM4 typically reach a maximum tolerated dose (MTD) in humans in the range of 110-240 mg/m^2 (about 3–6.5 mg/kg) [6-8]. For antibodies conjugated with the dolastatin 10 analogs, monomethyl auristatin E or F (MMAE; MMAF), MTDs were established at doses around 80-110 mg/m^2 (about 2–3 mg/kg) [9-11]. It is not known what dose would be required to achieve optimal therapeutic efficacy in the clinic. However, some lessons may be drawn from preclinical studies in murine xenograft models. Given that both mice and humans have about 40–43 mL plasma per kg of body weight [12], and assuming that pharmacokinetic properties are approximately similar in mice and human, therapeutic activity should be observed at similar dose levels in mice and human. Thus, ADCs conjugated with maytansinoids or auristatins should show preclinical activity at doses at or below 3 – 6.5 mg/kg and 2–3 mg/kg, respectively. Preclinical studies in mice suggest that such doses levels are often suboptimal. For example, ado-trastuzumab emtansine has an MTD of 3.6 mg/kg in humans [6]. In preclinical models of breast cancer, ado-trastuzumab emtansine induced tumor regression at dose levels at or above 3 mg/kg, but more potent efficacy was observed at 15 mg/kg [13,14]. This suggests that at the clinically administered dose, ado-trastuzumab emtansine may not exert its maximal potential anti-tumor effect. Likewise, brentuximab vedotin has an MTD of 1.8 mg/ kg in humans [9], while in preclinical models of Hodgkin lymphoma, the lowest dose that induced partial tumor regression was generally about 1 mg/kg dose [15], suggesting that the therapeutic index of brentuximab vedotin is fairly narrow. Other examples can be drawn from compounds in development. For example, CR011-vcMMAE (glembatumumab vedotin), an ADC that targets GPNMB, showed modest clinical activity in humans at the MTD of 1.9 mg/kg [16]. In preclinical models of melanoma CR011-vcMMAE induced complete tumor regression upon treatment with 2.5 mg/kg ADC, but the 1.25 mg/kg dose showed only modest activity [17]. Another vcMMAE conjugated antibody, MLN0264 (indusatumab vedotin) that targets guanylyl cyclase C (GCC) positive tumors, has an MTD of 1.8 mg/kg in humans [10]. Yet it has been described to show significantly better inhibition of GCC-positive xenografts at a dose of 7.5 mg/ kg compared to 3.75 mg/kg dose [18].

In summary, these ADCs are highly active in preclinical tumor models but their therapeutic window in the clinic is narrow and dosing regimens seem hampered by dose-limiting toxicities that could not always be predicted based on data from preclinical models. This lack of predictability is especially illustrated by the fact that non-cleavable auristatin and maytansine conjugates are virtually devoid of toxicity

in preclinical models at doses equivalent to the MTD for cleavable auristatin and maytansine conjugates. Yet in the clinic they induce toxicity at doses that are the same or even lower as compared to their cleavable-linked counterparts [8,13,19]. In addition several other factors make it difficult to extrapolate preclinical data to the clinic, such as differences in proliferation rates, tumor burden, multidrug-resistance pumps and target-mediated clearance.

For most ADCs currently in clinical development, dose-limiting toxicities appear to be unrelated to the targeted antigen. For example, reversible ocular toxicity specific to the cornea has been reported as the dose-limiting toxicity (DLT) for disulfide-linked DM4-conjugated antibodies targeting antigens as diverse as CD19 [7], CanAg [20], folate receptor alpha [21] and mesothelin [22], none of which are thought to have significant expression in the eye. Similar toxicity has been reported for all ADCs conjugated with MMAF via an uncleavable linker [7,23]. In contrast, no ocular toxicity has been described for a MUC16 ADC conjugated with vcMMAE, despite the fact that MUC16 expression has been described in human ocular surface epithelia [24]. In fact, most, if not all, ADCs made with vcMMAE have a similar toxicity profile, with acute neutropenia and neuropathy (upon repeated dosing) being the dose-limiting adverse events, irrespective of the target antigen, CD30 [9], PSMA [25], gpNMB [16], NaPi2b [26], MUC16 [27], GCC [10], CD22 [28] and CD79b [29]. The fact that normal tissue expression often does not drive ADC toxicity is further illustrated by clinical experience with ado-trastuzumab emtansine. HER2 expression has been described in various healthy organs such as heart, skin and epithelial cells of the gastrointestinal tract [30]. Trastuzumab, the unconjugated antibody counterpart of ado-trastuzumab emtansine, has been reported to induce cardiotoxicity in combination with chemotherapy [31], which is thought to be related to HER2 expression in the heart. In contrast, the DLT of ado-trastuzumab emtansine is reversible thrombocytopenia, thought to be an off-target toxicity, with no clinically significant toxicity reported in heart, skin or epithelial tissue [6].

However, for some ADCs, certain toxicities observed in clinical trials appear to be on-target effects. For example, in the case of glembatumumab vedotin, development of skin rash was one of the observed dose-limiting toxicities [16], which is likely due to membrane expression of gpNMB in epithelial cells of the skin [32]. Previously, development of an ADC directed against CD44v6 (bivatuzumab mertansine) was discontinued due to severe skin toxicity [33], which was also linked to high CD44v6 expression in the skin.

In general, antigens that are internalized well, with low expression on normal tissue and high expression on tumors are preferred for an ADC approach. However, the results of clinical trials indicate that it may be difficult to predict the toxicity profile based on target expression in healthy tissue. Therefore selection of antigens that are

not particularly tumor specific, but highly overexpressed in tumors may, in certain circumstances, increase the efficacy of tubulin based ADCs without changing the MTD.

ADCS AND THE IMMUNE SYSTEM

The mechanism behind the off-target toxicity of ADCs is poorly understood. Neutropenia and thrombocytopenia could be explained by cytotoxicity of the free payload after processing of the linker-drug by the targeted cells or in the tumor microenvironment [34]. Alternatively, uptake and processing of ADCs by Fcγ-receptor bearing cells has been proposed as a potential mechanism of toxicity (Figure 2). For example, FcγRIIa binding has been proposed to be involved in the development of thrombocytopenia induced by ado-trastuzumab emtansine. Megakaryocytes showed uptake of trastuzumab and ado-trastuzumab emtansine which could be blocked with an FcγRIIa blocking antibody. The uptake of ado-trastuzumab emtansine as well as an isotype control ADC by megakaryocytes resulted in cytotoxicity, which was not observed with unconjugated trastuzumab [35]. However, these experiments were not done in the presence of non-immune human IgG at levels comparable to those found in human blood, so it is also possible that non-specific mechanisms such as pinocytosis may contribute to uptake of ADC by antigen-negative hematological cells *in vivo* at the relatively high initial concentrations of ADC in blood plasma after administration (~ 0.1 mg/mL).

Whereas, on the one hand interactions with Fcγ-receptors have been implicated in toxicity of ADCs, on the other hand at least one ADC with enhanced Fc-receptor binding has entered clinical development. J6M0-mcMMAF (GSK2857916), an ADC targeting the B-cell maturation antigen (BCMA) that is selectively expressed on multiple myeloma (MM) cells, was able to eliminate MM tumors in subcutaneous and disseminated MM models. The investigators used a defucosylated antibody with enhanced affinity for FcγRIIIa expressing immune cells. J6M0-mcMMAF induced antibody-dependent cell-mediated cytotoxicity (ADCC) and macrophage-mediated phagocytosis *in vitro* and enhanced macrophage infiltration in bone marrow tissues from SCID mice bearing MM1Sluc tumors [36].

Just as the role of IgG-FcγR interactions to toxicity is unknown, it is unclear to what extent FcγR-mediated effector functions contribute to the clinical efficacy of ADCs. Generally, antibody-mediated effector functions were similar between the naked antibody and the corresponding ADC. Considering the two approved ADCs, the capacity of trastuzumab to induce ADCC was not affected through conjugation with DM1 [37], while brentuximab has been described to induce antibody-dependent cellular phagocytosis *in vivo*, which is believed to contribute to the potent anti-tumor efficacy observed for brentuximab vedotin [38]. Although in the latter case, the naked anti-CD30

antibody had no clinical activity [39], it may be that Fc-receptor-mediated anti-tumor activity compliments payload delivery by the ADC, for increased clinical benefit.

More recently, ADCs based on auristatins have been suggested to stimulate a tumor-specific adaptive immune response [40]. Using fully immunocompetent mice with syngeneic RMAThy1.1 tumors, it was demonstrated that MMAE-coupled ADCs can induce dendritic cell (DC) homing to tumor draining lymph nodes. Analysis of PBMCs from Hodgkin lymphoma patients obtained before and after treatment with brentuximab vedotin showed activation of adaptive immunity as indicated by a significant decrease in the number of T-regulatory cells and increased activation of peripheral DCs and B-cells. These effects were not dependent on cytotoxicity towards the tumor cells, indicating a direct effect on DCs. Furthermore it was demonstrated that combined treatment of dolastatins with immune modulating antibodies targeting CTLA-4 and PD-1 resulted in slower outgrowth of MC38 tumors and altered ratio between regulatory and effector T-cells. These observations were also extended to maytansinoids and ado-trastuzumab emtansine [41]. The ability of chemotherapeutic agents to stimulate immunological cell death has been widely appreciated [42]. However, the potential clinical benefit of this effect may be limited during classical chemotherapy treatment regimens, that are associated with major immunosuppressive side effects [43]. The enhanced tumor-specificity of ADCs, however, may allow for reduced immunosuppressive side effects while increasing anti-tumor immunity.

TOWARDS MORE POTENT PAYLOADS

The clinical success of maytansinoid- and auristatin-based ADCs has sparked increased research into evaluation of even more potent cytotoxic compounds having different cell-killing mechanisms for utilization as ADC payloads. Most such research is with DNA-damaging agents such as pyrrolobenzodiazepine (PBD) dimers [44], calicheamicins, duocarmycins [45] and indolinobenzodiazepine dimers [46]. PBD dimers have shown promising cytotoxicity and displayed anti-tumor activity at ~10 fold lower concentration as compared to auristatins and maytansinoids. PBD dimers block cancer cell division by binding in the minor groove of DNA and crosslinking opposing strands of DNA without distorting the DNA helix, thus potentially avoiding DNA-repair mechanisms and emergent drug resistance [47]. Recently, several ADCs conjugated with PBD dimers have entered clinical development. SGN-CD33A, a humanized anti-CD33 antibody conjugated to a PBD dimer via a protease-cleavable valine-alanine dipeptide linker is being tested in acute myeloid leukemia [44]. SGN-CD33A showed impressive anti-tumor activity in xenograft models at doses as low as 0.1 mg/kg of ADC. This activity was dependent on the presence of cell surface antigen, although no correlation was observed between degree of efficacy and the levels of CD33 on the cell surface [44]. The same PBD-linker format was used to de-

velop a CD70 ADC (SGN-CD70A), for the treatment of patients with renal cell carcinoma (RCC) and non-Hodgkin lymphoma (NHL). Here too, the ADC showed impressive anti-tumor activity in preclinical models dosed at 0.1 and 0.3 mg/kg of ADC [48]. The potential of PBD dimers to target cell populations that are drug-resistant has been demonstrated with rovalpituzumab tesirine, an anti-DLL3 antibody conjugated to a PBD dimer. In patient-derived xenograft models of small cell lung cancer (SCLC) the ADC was able to eradicate DLL3-positive drug-resistant tumor-initiating cells [49]. Moreover, a phase I study in patients with relapsed and refractory SCLC demonstrated that at the MTD of 0.2 mg/kg, rovalpituzumab tesirine was able to induce partial responses in 7 out of 16 patients and stable disease in a further 8 patients [50].

Recently, SYD985, a HER2 ADC conjugated with the cleavable linker-duocarmycin analog, vc-*seco*-DUBA, entered clinical development. The ADC was able to inhibit growth of low HER2 expressing patient derived xenografts (PDX) at a single dose of 1 mg/kg [51]. This effect may even be underestimated because vc-*seco*-DUBA conjugated ADCs have poor PK properties in mouse plasma, due to presence of mouse-specific carboxylesterase (CES1c) which can release the payload from the ADC [51]. In human plasma, vc-*seco*-DUBA conjugated ADCs are quite stable. However, once released from the ADC, the active compound DUBA is rapidly degraded with a half-life of approximately 1 hour. Although this seems unfavorable from an efficacy point of view, the rapid degradation of DUBA may also translate to lower systemic toxicity and allow for higher dosing in clinical testing [45].

These exciting preclinical data and emerging clinical results with ADCs containing potent DNA-targeting payloads, both PBD dimers and duocarmycin based compounds, demonstrate that these ADCs are capable of inhibiting tumor growth at relatively low doses and require only modest expression of the targeted antigen. Studies addressing the safety and establishing the MTD will determine whether these extremely potent toxins can contribute to increasing the therapeutic index of ADCs towards such targets.

SUMMARY

The increased clinical experience with tubulin-based ADCs and emerging clinical data with ADCs containing DNA-targeting payloads, help us to better understand the target requirements needed for successful ADC design. The relative lack of immunosuppressive side effects of many ADCs, suggests that a potential component of the clinical benefit obtained with some ADCs may be the engagement of the immune system. There is still much to learn about the clinical application of ADC technologies, but the success of brentuximab vedotin and ado-trastuzumab emtansine have emboldened research into improved cancer treatments utilizing ADCs that has the prospect for improved outcomes for many cancer patients.

Drug Names	Sponsor	Phase	Indication	Target	Payload	Linker	Bystander	MTD mg/kg
Brentuximab Vedotin, Adcetris, SGN-35	Seattle Genetics, Inc.	approved	Hematological	CD30	MMAE	VC	Yes	1.8 [9] thrombocytopenia, neutropenia
Kadcyla, T-DM1, Trastuzumab Emtansine, PRO132365	Genentech, Inc.	approved	Solid	HER2	DM1	SMCC	No	3.6 [6] thrombocytopenia, neutropenia
Inotuzumab Ozogamicin, CMC-544	Pfizer	3	Hematological	CD22	Calicheamicin	Hydrazone Acetyl Butyrate	Yes	0.05 [52] thrombocytopenia, neutropenia
Gemtuzumab Ozogamicin	Pfizer	2	Hematological	CD33	Calicheamicin	Hydrazone Acetyl Butyrate	Yes	0.25 [53,54] no DLT*
ABT-414	Abbvie	2	Solid	EGFR	MMAF	MC	No	3.0 [55] ocular toxicity
Glembatumumab Vedotin, CDX-011, CR011-vcMMAE	Celldex therapeutics	2	Solid	gpNMB	MMAE	VC	Yes	1.9 [16] neutropenia, rash
IMMU-130, Labetuzumab Govitecan, Labetuzumab-SN-38, hMN14-SN38	Immunomedics, Inc.	2	Solid	CEACAM5	SN-38	CL2A	Yes	6-10 [56] neutropenia, typhlitis, nausea
IMMU-132, Sacituzumab Govitecan, hrS7-SN-38	Immunomedics, Inc.	2	Solid	TROP2, EGP1	SN-38	CL2A	Yes	8-10 [57] neutropenia
Lifastuzumab Vedotin, NaPi2b ADC, RG7599, DNIB0600A	Genentech, Inc.	2	Solid	NaPi2b	MMAE	VC	Yes	2.4 [26] dyspnea
Indusatumab Vedotin, MLN0264, 5F9-vcMMAE	Millennium Pharmaceuticals, Inc	2	Solid	GCC	MMAE	VC	Yes	1.8 [10] neutropenia
Polatuzumab Vedotin, RG7596, DCDS4501A	Genentech, Inc.	2	Hematological	CD79b	MMAE	VC	Yes	2.4 [29] neutropenia

Drug Names	Sponsor	Phase	Indication	Target	Payload	Linker	Bystander	MTD mg/kg
Pinatuzumab Vedotin, RG7593, DCDT2980S	Genentech, Inc.	2	Hematological	CD22	MMAE	VC	Yes	2.4 [28] neutropenia
PSMA ADC	Progenics Pharmaceuticals, Inc	2	Solid	PSMA	MMAE	VC	Yes	2.5 [25] neutropenia, liver toxicity
SAR3419, Coltuximab Ravtansine	ImmunoGen, Inc.	2	Hematological	CD19	DM4	SPDB	Yes	4.3 [7] ocular toxicity
BMS-986148	Bristol-Myers Squibb	1, 2	Solid	MSLN	unknown	unknown	unknown	
BT-062, Indatuximab Ravtansine	Biotest Pharmaceuticals Corporation	1, 2	Hematological	CD138, Syndecan1	DM4	SPDB	Yes	2.7 [58] mucositis, anemia
IMMU-110, Milatuzumab Doxorubicin, hLL1-DOX	Immunomedics, Inc.	1, 2	Hematological	CD74	Doxorubicin	Hydrazone	Yes	>16 [59] no DLT reported
MLN2704	Millennium Pharmaceuticals, Inc	1, 2	Solid	PSMA	DM1	SPP	Yes	No MTD reported neutropenia, neuropathy [60]
SAR408701	Sanofi	1, 2	Solid	CEACAM5	DM4	SPDB	Yes	
SC16LD6.5, Rovalpituzumab Tesirine	Stem CentRx, Inc.	1, 2	Solid	Delta-like protein 3 (DLL3)	D6.5 (PBD)	VA	Yes	0.2 [49,50] thrombocytopenia, capillary leak syndrome
ABBV-399	Abbvie	1	Solid	unknown	unknown	unknown	unknown	
AGS-16C3F	Astellas Pharma Inc.; Agensys, Inc.	1	Solid	ENPP3	MMAF	MC	No	1.8 [23] ocular toxicity, thrombocytopenia
ASG-22ME	Astellas Pharma Inc.; Agensys, Inc.	1	Solid	Nectin4	MMAE	VC	Yes	
AGS67E	Agensys, Inc.	1	Hematological	CD37	MMAE	VC	Yes	

Drug Names	Sponsor	Phase	Indication	Target	Payload	Linker	Bystander	MTD mg/kg
AMG 172	Amgen	1	Solid	CD27	DM1	Non-Cleavable	No	
AMG 595	Amgen	1	Solid	EGFRvIII	DM1	SMCC	No	
AGS-15E	Agensys, Inc.	1	Solid	SLTRK6	MMAE	VC	Yes	
BAY1129980	Bayer	1	Solid	C4.4a	unknown	unknown	unknown	
BAY1187982	Bayer	1	Solid	FGFR2	unknown	unknown	unknown	
BAY94-9343, Anetumab Ravtansine	Bayer	1	Solid	Mesothelin	DM4	SPDB	Yes	6.5 [22] ocular toxicity
GSK2857916	GlaxoSmithKline	1	Hematological	BCMA	MMAF	MC	No	
HuMax-TF-ADC, Tisotumab Vedotin	Genmab	1	Solid	TF	MMAE	VC	Yes	TBD [61]
IMGN289	ImmunoGen, Inc.	1	Solid	EGFR	DM1	SMCC	No	
IMGN529	ImmunoGen, Inc.	1	Hematological	CD37	DM1	SMCC	No	
IMGN853, Mirvetuximab Soravtansine	ImmunoGen, Inc.	1	Solid	FOLR1	DM4	Sulfo-SPDB	Yes	6.0 ocular toxicity [21]
LOP628	Novartis Pharmaceuticals	1	Solid	cKIT	Maytansine	Non-Cleavable	No	
PCA062	Novartis Pharmaceuticals	1	Solid	p-Cadherin	unknown	unknown	unknown	
MDX-1203, BMS936561	Bristol-Myers Squibb	1	Solid	CD70	Duocarmycin	VC	Yes	No MTD reported, neuropathy at 15 mg/kg [62]
MEDI-547, MI-CP177	Medimmune LLC	1	Solid	EphA2	MMAF	MC	No	
PF-06263507	Pfizer	1	Solid	5T4	MMAF	MC	No	
PF-06647020	Pfizer	1	Solid	unknown	unknown	unknown	unknown	
PF-06647263	Pfizer	1	Solid	EphrinA	Calicheamicin	Hydrazone Acetyl Butyrate	Yes	

Drug Names	Sponsor	Phase	Indication	Target	Payload	Linker	Bystander	MTD mg/kg
PF-06664178	Pfizer	1	Solid	Trop-2	microtubule inhibitor	unknown	unknown	
RG7450, DSTP3086S	Genentech, Inc.	1	Solid	STEAP1	MMAE	VC	Yes	2.4 [63] liver toxicity
RG7458, DMUC5754A	Genentech, Inc.	1	Solid	MUC16	MMAE	VC	Yes	2.4 [27] neutropenia
RG7598, DFRF4539A	Genentech, Inc.	1	Hematological	unknown	MMAE	unknown	unknown	
SAR566658	Sanofi	1	Solid	CA6	DM4	SPDB	Yes	6.5 [64] ocular toxicity, diarrhea
SGN-CD19A	Seattle Genetics, Inc.	1	Hematological	CD19	MMAF	MC	No	Not yet reached at 6 mg/kg
SGN-CD33A	Seattle Genetics, Inc.	1	Hematological	CD33	PBD	VA	Yes	neutropenia
SGN-CD70A	Seattle Genetics, Inc.	1	Solid	CD70	PBD	VA	Yes	
SGN-LIV1A	Seattle Genetics, Inc.	1	Solid	LIV1	MMAE	VC	Yes	
SYD985, Trastuzumab vc-seco DUBA	Synthon BV	1	Solid	HER2	Duocarmycin	VC	Yes	

TABLE 1 *Overview of ADCs in clinical development*. The last column shows the maximum tolerated dose in mg/kg, as well as the reported dose-limiting toxicities. *No severe dose-limiting toxicity found, but two of seven evaluable patients had prolonged drug-related neutropenia after 9 mg/m2 treatment MTD, maximum tolerated dose; DLT, dose-limiting toxicity; VC, valine-citrulline; VA, valine-alanine; MC, maleimidocaproyl linker; SMCC, N-succinimidyl 4-(N-maleimidomethyl) cyclohexane-1 carboxylate; SPDB, N-succinimidyl 4-(2-pyridyldithio)butyrate; SPP, N-succinimidyl 4-(2-pyridyldithio)pentanoate; sulfo-SPDB, N-succinimidyl 4-(2-pyridyldithio)-2-sulfobutanoate; CL2A, maleimido-[short PEG]-Lys-PABOCO-20-O.

REFERENCES

1 Chari RV, Martell BA, Gross JL, Cook SB, Shah SA, Blattler WA, McKenzie SJ, Goldmacher VS: **Immunoconjugates containing novel maytansinoids: promising anticancer drugs**. *Cancer Res* 1992, **52**(1):127-131.

2 Issell BF, Crooke ST: **Maytansine**. *Cancer Treat Rev* 1978, **5**(4):199-207.

3 Banerjee S, Wang Z, Mohammad M, Sarkar FH, Mohammad RM: **Efficacy of selected natural products as therapeutic agents against cancer**. *J Nat Prod* 2008, **71**(3):492-496.

4 Dumontet C, Jordan MA: **Microtubule-binding agents: a dynamic field of cancer therapeutics**. *Nat Rev Drug Discov* 2010, **9**(10):790-803.

5 Oroudjev E, Lopus M, Wilson L, Audette C, Provenzano C, Erickson H, Kovtun Y, Chari R, Jordan MA: **Maytansinoid-antibody conjugates induce mitotic arrest by suppressing microtubule dynamic instability**. *Mol Cancer Ther* 2010, **9**(10):2700-2713.

6 Krop IE, Beeram M, Modi S, Jones SF, Holden SN, Yu W, Girish S, Tibbitts J, Yi JH, Sliwkowski MX *et al*: **Phase I study of trastuzumab-DM1, an HER2 antibody-drug conjugate, given every 3 weeks to patients with HER2-positive metastatic breast cancer**. *J Clin Oncol* 2010, **28**(16):2698-2704.

7 Younes A, Kim S, Romaguera J, Copeland A, Farial Sde C, Kwak LW, Fayad L, Hagemeister F, Fanale M, Neelapu S *et al*: **Phase I multidose-escalation study of the anti-CD19 maytansinoid immunoconjugate SAR3419 administered by intravenous infusion every 3 weeks to patients with relapsed/refractory B-cell lymphoma**. *J Clin Oncol* 2012, **30**(22):2776-2782.

8 Rodon J, Garrison M, Hammond LA, de Bono J, Smith L, Forero L, Hao D, Takimoto C, Lambert JM, Pandite L *et al*: **Cantuzumab mertansine in a three-times a week schedule: a phase I and pharmacokinetic study**. *Cancer Chemother Pharmacol* 2008, **62**(5):911-919.

9 Younes A, Bartlett NL, Leonard JP, Kennedy DA, Lynch CM, Sievers EL, Forero-Torres A: **Brentuximab vedotin (SGN-35) for relapsed CD30-positive lymphomas**. *N Engl J Med* 2010, **363**(19):1812-1821.

10 Zambrano CC, Almhanna K, Messersmith WA, Ahnert JR, Ryan DP, Faris JE, Jung JA, Fasanmade A, Wyant T, Kalebic T: **MLN0264, an investigational antiguanylyl cyclase C (GCC) antibody-drug conjugate (ADC), in patients (pts) with advanced gastrointestinal (GI) malignancies: Phase I study**. *J Clin Oncol 32:5s, 2014 (suppl; abstr 3546)*.

11 Coveler AL, Von Hoff DD, Ko AH, Whiting NC, Zhao B, Wolpin BM: **A phase I study of ASG-5ME, a novel antibody-drug conjugate, in pancreatic ductal adenocarcinoma**. *J Clin Oncol 31, 2013 (suppl 4; abstr 176)*.

12 Davies B, Morris T: **Physiological parameters in laboratory animals and humans**. *Pharm Res* 1993, **10**(7):1093-1095.

13 Lewis Phillips GD, Li G, Dugger DL, Crocker LM, Parsons KL, Mai E, Blattler WA, Lambert JM, Chari RV, Lutz RJ *et al*: **Targeting HER2-positive breast cancer with trastuzumab-DM1, an antibody-cytotoxic drug conjugate**. *Cancer Res* 2008, **68**(22):9280-9290.

14 Jumbe NL, Xin Y, Leipold DD, Crocker L, Dugger D, Mai E, Sliwkowski MX, Fielder PJ, Tibbitts J: **Modeling the efficacy of trastuzumab-DM1, an antibody drug conjugate, in mice**. *J Pharmacokinet Pharmacodyn* 2010, **37**(3):221-242.

15 Francisco JA, Cerveny CG, Meyer DL, Mixan BJ, Klussman K, Chace DF, Rejniak SX, Gordon KA, DeBlanc R, Toki BE *et al*: **cAC10-vcMMAE, an anti-CD30-monomethyl auristatin E conjugate with potent and selective antitumor activity**. *Blood* 2003, **102**(4):1458-1465.

16 Yardley D, Melisko M, Forero A, Daniel B, Montero A, Guthrie T, Canfield V, Oakman C, Chew H, Ferrario C: **METRIC: A randomized international study of the antibody-drug conjugate glembatumumab vedotin (GV or CDX-011) in patients (pts) with metastatic gpNMB-overexpressing triple-negative breast cancer (TNBC).** *J Clin Oncol 33, 2015 (suppl; abstr TPS1110)*.

17 Pollack VA, Alvarez E, Tse KF, Torgov MY, Xie S, Shenoy SG, MacDougall JR, Arrol S, Zhong H, Gerwien RW *et al*: **Treatment parameters modulating regression of human melanoma xenografts by an antibody-drug conjugate (CR011-vcMMAE) targeting GPNMB**. *Cancer Chemother Pharmacol* 2007, **60**(3):423-435.

18 Zhang J, Gallery M, Wyant T, Stringer B, Manfredi M, Danaee H, Veiby P: **Abstract PR12: MLN0264, an investigational, first-in-class antibody-drug conjugate (ADC) targeting guanylyl cyclase C (GCC), demonstrates antitumor activity alone and in combination with gemcitabine in human pancreatic cancer xenograft models expressing GCC**. *Mol Cancer Ther 2013;12(11 Suppl):PR12*.

19 Doronina SO, Mendelsohn BA, Bovee TD, Cerveny CG, Alley SC, Meyer DL, Oflazoglu E, Toki BE, Sanderson RJ, Zabinski RF *et al*: **Enhanced activity of monomethylauristatin F through monoclonal antibody delivery: effects of linker technology on efficacy and toxicity**. *Bioconjug Chem* 2006, **17**(1):114-124.

20 Goff LW, Papadopoulos K, Posey JA, Phan AT, Patnaik T, Miller JG, Zildjian S, O'Leary JJ, Qin A, Tolcher A: **A phase II study of IMGN242 (huC242-DM4) in patients with CanAg-positive gastric or gastroesophageal (GE) junction cancer.** *J Clin Oncol 27, 2009 (suppl; abstr e15625)*.

21 Moore KN, Ponte J, LoRusso P, Birrer MJ, Bauer TM, Borghaei H, O'Malley DM, Ruiz-Soto R, Lutz R, Malik L: **Relationship of pharmacokinetics (PK), toxicity, and initial evidence of clinical activity with IMGN853, a folate receptor alpha (FRa) targeting antibody drug conjugate in patients (Pts) with epithelial ovarian cancer (EOC) and other FRa-positive solid tumors.** *J Clin Oncol 32:5s, 2014 (suppl; abstr 5571)*.

22 Bendell J, Blumenschein G, Zinner R, Hong D, Jones S, Infante J, Burris H, Rajagopalan P, Kornacker M, Henderson D *et al*: **First-in-human Phase I dose-escalation study of a novel anti-mesothelin antibody drug conjugate, BAY 94-9343, in patients with advanced solid tumors**. *AACR, April 6-10, 2013, Washington, DC*.

23 Thompson JA, Motzer R, Molina AM, Choueiri TK, Heath EI, Kollmannsberger CK, Redman BG, Sangha RS, Ernst DS, Pili R *et al*: **Phase I studies of anti-ENPP3 antibody drug conjugates (ADCs) in advanced refractory renal cell carcinomas (RRCC).** *Journal of Clinical Oncology, May 2015 vol 33 no 15_suppl 2503*

24 Argueso P, Spurr-Michaud S, Russo CL, Tisdale A, Gipson IK: **MUC16 mucin is expressed by the human ocular surface epithelia and carries the H185 carbohydrate epitope**. *Invest Ophthalmol Vis Sci* 2003, **44**(6):2487-2495.

25 Petrylak DP, Kantoff PW, Mega AE, Vogelzang NJ, Stephenson J, Fleming MT, Stambler N, Petrini M, Blattman S, Israel RJ: **Prostate-specific membrane antigen antibody drug conjugate (PSMA ADC): A phase I trial in metastatic castration-resistant prostate cancer (mCRPC) previously treated with a taxane.** *J Clin Oncol 31, 2013 (suppl; abstr 5018)*.

26 Burris HA, Gordon MS, Gerber DE, Spigel D, Mendelsohn DS, Schiller JH, Wang Y, Choi YJ, Kahn R, Wood K *et al*: **A phase I study of DNIB0600A, an antibody-drug conjugate (ADC) targeting NaPi2b, in patients (pts) with non-small cell lung cancer (NSCLC) or platinum-resistant ovarian cancer (OC).** *J Clin Oncol 32:5s, 2014 (suppl; abstr 2504)*.

27 Liu J, Moore K, Birrer M, Berlin S, Matulonis U, Infante JR, Xu J, Kahn R, Wang Y, Wood K *et al*: **Targeting MUC16 with the Antibody-Drug Conjugate DMUC5754A in Patients with Platinum-Resistant Ovarian Cancer: A Phase I Study of Safety and Pharmacokinetics**. *AACR Annual Meeting 2013, April 6-10 Washington DC*.

28 Advani R, Chen A, Lebovic D, Brunvand M, Goy A, Chang J, Hochberg E, Yalamanchili S, Kahn R, Lu D *et al*: **Final Results of a Phase I Study of the Anti-CD22 Antibody-Drug Conjugate Pinatuzumab Vedotin (DCDT2980S) with or without Rituximab in Patients with Relapsed or Refractory B-Cell Non-Hodgkin's Lymphoma**. *ASH Annual Meeting, December 7-10, 2013 # 4399*.

29 Palanca-Wessels MC, Czuczman M, Salles G, Assouline S, Sehn LH, Flinn I, Patel MR, Sangha R, Hagenbeek A, Advani R *et al*: **Safety and activity of the anti-CD79B antibody-drug conjugate polatuzumab vedotin in relapsed or refractory B-cell non-Hodgkin lymphoma and chronic lymphocytic leukaemia: a phase 1 study**. *Lancet Oncol* 2015.

30 Press MF, Cordon-Cardo C, Slamon DJ: **Expression of the HER-2/neu proto-oncogene in normal human adult and fetal tissues**. *Oncogene* 1990, **5**(7):953-962.

31 Ewer MS, Vooletich MT, Durand JB, Woods ML, Davis JR, Valero V, Lenihan DJ: **Reversibility of trastuzumab-related cardiotoxicity: new insights based on clinical course and response to medical treatment**. *J Clin Oncol* 2005, **23**(31):7820-7826.

32 Maric G, Rose AA, Annis MG, Siegel PM: **Glycoprotein non-metastatic b (GPNMB): A metastatic mediator and emerging therapeutic target in cancer**. *Onco Targets Ther* 2013, **6**:839-852.

33 Tijink BM, Buter J, de Bree R, Giaccone G, Lang MS, Staab A, Leemans CR, van Dongen GA: **A phase I dose escalation study with anti-CD44v6 bivatuzumab mertansine in patients with incurable squamous cell carcinoma of the head and neck or esophagus**. *Clin Cancer Res* 2006, **12**(20 Pt 1):6064-6072.

34 Mohamed MM, Sloane BF: **Cysteine cathepsins: multifunctional enzymes in cancer**. *Nat Rev Cancer* 2006, **6**(10):764-775.

35 Uppal H, Doudement E, Mahapatra K, Darbonne WC, Bumbaca D, Shen BQ, Du X, Saad O, Bowles K, Olsen S *et al*: **Potential mechanisms for thrombocytopenia development with trastuzumab emtansine (T-DM1)**. *Clin Cancer Res* 2015, **21**(1):123-133.

36 Tai YT, Mayes PA, Acharya C, Zhong MY, Cea M, Cagnetta A, Craigen J, Yates J, Gliddon L, Fieles W *et al*: **Novel anti-B-cell maturation antigen antibody-drug conjugate (GSK2857916) selectively induces killing of multiple myeloma**. *Blood* 2014, **123**(20):3128-3138.

37 Junttila TT, Li G, Parsons K, Phillips GL, Sliwkowski MX: **Trastuzumab-DM1 (T-DM1) retains all the mechanisms of action of trastuzumab and efficiently inhibits growth of lapatinib insensitive breast cancer**. *Breast Cancer Res Treat* 2011, **128**(2):347-356.

38 Oflazoglu E, Stone IJ, Gordon KA, Grewal IS, van Rooijen N, Law CL, Gerber HP: **Macrophages contribute to the antitumor activity of the anti-CD30 antibody SGN-30**. *Blood* 2007, **110**(13):4370-4372.

39 Foyil KV, Bartlett NL: **Anti-CD30 Antibodies for Hodgkin lymphoma**. *Curr Hematol Malig Rep* 2010, **5**(3):140-147.

40 Muller P, Martin K, Theurich S, Schreiner J, Savic S, Terszowski G, Lardinois D, Heinzelmann-Schwarz VA, Schlaak M, Kvasnicka HM *et al*: **Microtubule-depolymerizing agents used in antibody-drug conjugates induce antitumor immunity by stimulation of dendritic cells**. *Cancer Immunol Res* 2014, **2**(8):741-755.

41 Muller P, Kreuzaler M, Khan T, Thommen DS, Martin K, Glatz K, Savic S, Harbeck N, Nitz U, Gluz O *et al*: **Trastuzumab emtansine (T-DM1) renders HER2+ breast cancer highly susceptible to CTLA-4/PD-1 blockade**. *Sci Transl Med* 2015, **7**(315):315ra188.

42 Bracci L, Schiavoni G, Sistigu A, Belardelli F: **Immune-based mechanisms of cytotoxic chemotherapy: implications for the design of novel and rationale-based combined treatments against cancer**. *Cell Death Differ* 2014, **21**(1):15-25.

43 Zitvogel L, Galluzzi L, Smyth MJ, Kroemer G: **Mechanism of action of conventional and targeted anticancer therapies: reinstating immunosurveillance**. *Immunity* 2013, **39**(1):74-88.

44 Kung Sutherland MS, Walter RB, Jeffrey SC, Burke PJ, Yu C, Kostner H, Stone I, Ryan MC, Sussman D, Lyon RP *et al*: **SGN-CD33A: a novel CD33-targeting antibody-drug conjugate using a pyrrolobenzodiazepine dimer is active in models of drug-resistant AML**. *Blood* 2013, **122**(8):1455-1463.

45 Elgersma RC, Coumans RG, Huijbregts T, Menge WM, Joosten JA, Spijker HJ, de Groot FM, van der Lee MM, Ubink R, van den Dobbelsteen DJ *et al*: **Design, Synthesis, and Evaluation of Linker-Duocarmycin Payloads: Toward Selection of HER2-Targeting Antibody-Drug Conjugate SYD985**. *Mol Pharm* 2015, **12**(6):1813-1835.

46 Krystal W, Walker R, Fishkin N, Audette C, Kovtun Y, Romanelli A: **IMGN779, a CD33-Targeted Antibody-Drug Conjugate (ADC) with a Novel DNA-Alkylating Effector Molecule, Induces DNA Damage, Cell Cycle Arrest, and Apoptosis in AML Cells** *ASH annual meeting 2015, abstract number 1366 (poster)*.

47 Hartley JA: **The development of pyrrolobenzodiazepines as antitumour agents**. *Expert Opin Investig Drugs* 2011, **20**(6):733-744.

48 Jeffrey SC, Burke PJ, Lyon RP, Meyer DW, Sussman D, Anderson M, Hunter JH, Leiske CI, Miyamoto JB, Nicholas ND *et al*: **A potent anti-CD70 antibody-drug conjugate combining a dimeric pyrrolobenzodiazepine drug with site-specific conjugation technology**. *Bioconjug Chem* 2013, **24**(7):1256-1263.

49 Saunders LR, Bankovich AJ, Anderson WC, Aujay MA, Bheddah S, Black K, Desai R, Escarpe PA, Hampl J, Laysang A *et al*: **A DLL3-targeted antibody-drug conjugate eradicates high-grade pulmonary neuroendocrine tumor-initiating cells in vivo**. *Sci Transl Med* 2015, **7**(302):302ra136.

50 Rudin CM, Pietanza MC, Spigel DR, Bauer T, Glisson G, Robert F, Ready N, Morgensztern D, Kochendoerfer MD, Patel M *et al*: **A DLL3-Targeted ADC, Rovalpituzumab Tesirine, Demonstrates Substantial Activity in a Phase I Study in Relapsed and Refractory SCLC** *IASLC conference Abstract number 1598* 2015.

51 van der Lee MM, Groothuis PG, Ubink R, van der Vleuten MA, van Achterberg TA, Loosveld EM, Damming D, Jacobs DC, Rouwette M, Egging DF *et al*: **The Preclinical Profile of the Duocarmycin-Based HER2-Targeting ADC SYD985 Predicts for Clinical Benefit in Low HER2-Expressing Breast Cancers**. *Mol Cancer Ther* 2015, **14**(3):692-703.

52 Advani A, Coiffier B, Czuczman MS, Dreyling M, Foran J, Gine E, Gisselbrecht C, Ketterer N, Nasta S, Rohatiner A *et al*: **Safety, pharmacokinetics, and preliminary clinical activity of inotuzumab ozogamicin, a novel immunoconjugate for the treatment of B-cell non-Hodgkin's lymphoma: results of a phase I study**. *J Clin Oncol* 2010, **28**(12):2085-2093.

53 Stasi R: **Gemtuzumab ozogamicin: an anti-CD33 immunoconjugate for the treatment of acute myeloid leukaemia**. *Expert Opin Biol Ther* 2008, **8**(4):527-540.

54 Sievers EL, Appelbaum FR, Spielberger RT, Forman SJ, Flowers D, Smith FO, Shannon-Dorcy K, Berger MS, Bernstein ID: **Selective ablation of acute myeloid leukemia using antibody-targeted chemotherapy: a phase I study of an anti-CD33 calicheamicin immunoconjugate**. *Blood* 1999, **93**(11):3678-3684.

55 Gan HK, Papadopoulos KP, Fichtel L, Lassman AB, Merrell R, Van Den Bent MJ, Kumthekar P, Scott AM, Pedersen M, Gomez EJ *et al*: **Phase I study of ABT-414 mono- or combination therapy with temozolomide (TMZ) in recurrent glioblastoma (GBM).** *J Clin Oncol 33, 2015 (suppl; abstr 2016)*.

56 Dotan E, Starodub A, Berlin J, Lieu CH, Guarino MJ, Marshall J, Hecht JR, Cohen SJ, Messersmith WA, Maliakal PP *et al*: **A new anti-CEA-SN-38 antibody-drug conjugate (ADC), IMMU-130, is active in controlling metastatic colorectal cancer (mCRC) in patients (pts) refractory or relapsing after irinotecan-containing chemotherapies: Initial results of a phase I/II study.** *J Clin Oncol 33, 2015 (suppl; abstr 2505)*.

57 Starodub AN, Ocean A, Shah MA, Guarino MJ, Picozzi VJ, Jr., Vahdat LT, Thomas SS, Govindan SV, Maliakal PP, Wegener WA *et al*: **First-in-Human Trial of a Novel Anti-Trop-2 Antibody-SN-38 conjugate, Sacituzumab Govitecan, for the Treatment of Diverse Metastatic Solid Tumors**. *Clin Cancer Res* 2015.

58 Kelly KR, Chanan-Khan A, Somlo G, Heffner LT, Siegel DS, Zimmerman TM, Jagannath S, Munshi NC, Lonial S, Roy V *et al*: **Indatuximab Ravtansine (BT062) In Combination With Lenalidomide and Low-Dose Dexamethasone In Patients With Relapsed and/Or Refractory Multiple Myeloma: Clinical Activity In Len/Dex-Refractory Patients**. *Blood: 2013; 122 (21)*.

59 Kaufman JL, Niesvizky R, Stadtmauer EA, Chanan-Khan A, Siegel D, Horne H, Wegener WA, Goldenberg DM: **Phase I, multicentre, dose-escalation trial of monotherapy with milatuzumab (humanized anti-CD74 monoclonal antibody) in relapsed or refractory multiple myeloma**. *Br J Haematol* 2013, **163**(4):478-486.

60 Galsky MD, Eisenberger M, Moore-Cooper S, Kelly WK, Slovin SF, DeLaCruz A, Lee Y, Webb IJ, Scher HI: **Phase I trial of the prostate-specific membrane antigen-directed immunoconjugate MLN2704 in patients with progressive metastatic castration-resistant prostate cancer**. *J Clin Oncol* 2008, **26**(13):2147-2154.

61 Lassen U, Hong D, Diamantis N, Subbiah V, Kumar R, Sorensen M, Lisby S, Coleman R, De Bono J: **A phase I, first-in-human study to evaluate the tolerability, pharmacokinetics and preliminary efficacy of HuMax-tissue-factor-ADC (TF-ADC) in patients with solid tumors.** *J Clin Oncol 33, 2015 (suppl; abstr 2570)*.

62 Owonikoko TK, Hussain A, Stadler WM, Smith DS, Sznol M, Molina AM, Gulati P, Shah A, Ahlers CM, Cardarelli J *et al*: **A phase 1 multicenter open-label dose-escalation study of BMS-936561 (MDX-1203) in clear cell renal cell carcinoma (ccRCC) and B-cell non Hodgkin lymphoma (B-NHL)**. *J Clin Oncol 32:5s, 2014 (suppl; abstr 2558)*.

63 Danila DC, Szmulewitz RZ, David Baron A, Higano CS, Scher HI, Morris MJ, Gilbert H, Brunstein F, Lemahieu V, Kabbarah O *et al*: **A phase I study of DSTP3086S, an antibody-drug conjugate (ADC) targeting STEAP-1, in patients (pts) with metastatic castration-resistant prostate cancer (CRPC).** *J Clin Oncol 32:5s, 2014 (suppl; abstr 5024)*.

64 Boni B, Rixe O, Rasco D, Gomez-Roca C, Calvo E, Morris JC, Tolcher AW, Assadourian S, Guillemin H, JP. D: **A Phase I first-in-human (FIH) study of SAR566658, an anti CA6-antibody drug conjugate (ADC), in patients (Pts) with CA6-positive advanced solid tumors (STs)**. *Mol Cancer Ther 2013;12(11 Suppl):A73* 2013.

3 High turnover of Tissue Factor enables efficient intracellular delivery of antibody-drug conjugates

► Mol Cancer Ther. 2015 May;14(5):1130-40.

► Bart ECG de Goeij[1], David Satijn[1], Claudia M Freitag[1], Richard Wubbolts[2], Wim K Bleeker[1], Alisher Khasanov[3], Tong Zhu[3], Gary Chen[3], David Miao[3], Patrick HC van Berkel[1] and Paul WHI Parren[1,4,5]

1 Genmab, Yalelaan 60, 3584 CM, Utrecht, The Netherlands

2 Department of Biochemistry and Cell Biology, Faculty of Veterinary Medicine, Utrecht University, Yalelaan 2, 3584 CM, Utrecht, The Netherlands

3 Concortis Biosystems Corp., San Diego, 11760 Sorrento Valley, CA 92121, USA

4 Dept. of Cancer and Inflammation Research, Institute of Molecular Medicine, University of Southern Denmark, Odense, Denmark

5 Dept. of immunohematology and Blood Transfusion, Leiden University Medical Center, 2333 ZA Leiden, The Netherlands

ABSTRACT

Antibody drug conjugates (ADC) are emerging as powerful cancer treatments that combine antibody-mediated tumor targeting with the potent cytotoxic activity of toxins. We recently reported the development of a novel ADC that delivers the cytotoxic payload monomethyl auristatin E (MMAE) to tumor cells expressing tissue factor (TF). By carefully selecting a TF-specific antibody that interferes with TF:FVIIa-dependent intracellular signaling, but not with the pro-coagulant activity of TF, an ADC was developed (TF-011-MMAE/HuMax-TF-ADC) that efficiently kills tumor cells, with an acceptable toxicology profile.

To gain more insight in the efficacy of TF-directed ADC treatment we compared the internalization characteristics and intracellular routing of TF with the epidermal growth factor receptor (EGFR) and human epidermal growth factor receptor 2 (HER2). Both in absence and presence of antibody, TF demonstrated more efficient internalization, lysosomal targeting and degradation than EGFR and HER2. By conjugating TF, EGFR and HER2 specific antibodies with duostatin-3, a toxin that induces potent cytotoxicity upon antibody-mediated internalization but lacks the ability to induce bystander killing, we were able to compare cytotoxicity of ADCs with different tumor specificities. TF-ADC demonstrated effective killing against tumor cell lines with variable levels of target expression. In xenograft models, TF-ADC was relatively potent in reducing tumor growth compared to EGFR- and HER2- ADCs. We hypothesize that the constant turnover of TF on tumor cells, makes this protein especially suitable for an ADC approach.

INTRODUCTION

Therapeutic antibodies are currently used in the clinic to treat a variety of diseases, including cancer. The tumor-killing capacity of therapeutic antibodies can be greatly enhanced by conjugation with cytostatic toxins, this way combining antibody-mediated tumor targeting with the potent cytotoxic activity of toxins. This was also demonstrated through the FDA approval of brentuximab vedotin, a CD30 specific antibody coupled to the potent microtubule disrupting agent monomethyl auristatin E (MMAE), for the treatment of patients with Hodgkin's lymphoma or anaplastic T-cell lymphoma [1]. In addition, the approval of trastuzumab emtansine (T-DM1), an ADC composed of the HER2 antibody trastuzumab and the tubulin inhibitor maytansine (DM1), for the treatment of patients with HER2-positive breast cancer [2,3] emphasizes that the potential of ADCs is not limited to hematological malignanices. The number of ADCs in clinical development has markedly increased in the last couple of years. This includes the development of HuMax-TF-ADC (TF-011-MMAE), a novel

ADC designed to deliver the cytotoxic payload MMAE to tumor cells expressing tissue factor (TF) [4].

Tissue factor, also called thromboplastin, factor III or CD142, is aberrantly expressed in many types of cancers including NSCLC [5], colorectal cancer [6], genito-urethal [7,8] and gyneacological cancers [9-11], pancreatic cancer [12], head and neck cancer [13], glioma [14] and metastatic breast cancer [15]. Under physiological conditions, TF is expressed by fibroblasts, pericytes and smooth muscle cells in the sub-endothelial vessel wall. In these cells, the majority of TF is localized in intracellular pools and remains sequestered from circulating factor VII (FVII) until vascular integrity is disrupted or until TF expression is induced [16-18]. Upon vascular damage, TF binds activated FVII (FVIIa) and forms the proteolytically active TF:FVIIa complex that can initiate the coagulation pathway. The TF:FVIIa complex can also activate cells by cleavage of the G-protein coupled receptor protease-activated receptor 2 (PAR2) thereby inducing an intracellular signaling cascade that promotes proliferation, thrombosis and angiogenesis [19]. This makes TF an interesting yet challenging target for cancer immunotherapy.

TF-011-MMAE was designed to specifically target tumor cells that aberrantly express TF, without interfering with the role of TF in coagulation. TF-011-MMAE showed potent anti-tumor activity in xenograft models derived from a broad range of solid cancers, and an acceptable safety profile in non-clinical toxicology studies [4]. TF-011-MMAE and unconjugated TF-011 induced efficient antibody-dependent cell-mediated cytoxicity and inhibition of TF:FVIIa-dependent intracellular signaling, both of which may contribute to the anti-tumor activity of TF-011-MMAE. However, MMAE-mediated tumor cell killing was shown to be the dominant mechanism of action *in vivo*. This indicates that TF is a highly suitable target for the intracellular delivery of cytoxic agents through an ADC. To gain more insight in the target characteristics, particularly the internalization characteristics of TF and TF-specific antibodies, that contribute to the efficacy of TF-directed ADC treatment, we compared TF-specific ADCs with ADCs directed against HER2 and EGFR. HER2 is a well-known and clinically validated ADC target [3,20], and an EGFR antibody conjugated with DM1 through a non-cleavable linker system is currently being evaluated in a phase I clinical study. Antibodies targeting TF, HER2 and EGFR were conjugated with the cytotoxic compound duostatin-3, which blocks tubulin polymerization. This toxin lacks the ability to induce bystander killing and therefore only affects target-positive cells. Because tumor antigens are often heterogeneously expressed and therefore not always accessible to ADC treatment, an ADC capable of inducing bystander killing may be preferred from an efficacy point-of-view [4]. However, to study the target requirements needed for optimal intracellular delivery of cytotoxic agents, we selected a drug-linker combination that only affects antigen expressing cells.

By comparing *in vitro* and *in vivo* cytotoxicity of ADCs targeting TF, HER2 and EGFR we found that TF-ADC was more effective compared to ADCs targeting the EGF-receptor family. TF-ADC induced relatively potent tumor cell killing, even in cell lines where TF expression was lower than expression of HER2 or EGFR. Confocal microscopy analysis demonstrated faster and enhanced transport of TF-antibodies into lysosomes of tumor cells compared to EGFR and HER2 antibodies. Strikingly, also without antibody treatment, large quantities of TF were found to internalize and colocalize with markers of endosomes and lysosomes, indicating that TF was constitutively being replenished. Therefore, it seems that the high turnover of TF on tumor cells, inherent to its biological role, makes this protein specifically suitable for an ADC approach.

MATERIALS AND METHOD

Cell lines

Human SK-OV-3 (ovarian cancer), AU565 (breast adenocarcinoma) and HCC1954 (breast ductal carcinoma) cells were obtained from American Type Culture Collection (ATCC). Human A431 (epithelial squamous carcinoma) and Jurkat (T-cell leukemia) cells were obtained from the Deutsche Sammlung von Mikroorganismen und Zellkulturen (DSMZ). SK-OV-3 cells were cultured in Minimal Essential Medium Eagles (ATCC) containing 10% heat inactivated calf serum (Hyclone). HCC1954, A431 and Jurkat cells were cultured in RPMI 1640 (Lonza) containing 10% heat inactivated calf serum. AU565 cells were cultured in RPMI 1640 supplemented with 10% heat inactivated calf serum, 1% sodium bicarbonate (Lonza), 0.5% natrium pyruvate (Lonza) and 0.5% glucose (Sigma). To guarantee cell line authenticity, cell lines were aliquoted and banked, and cultures were grown and used for a limited number of passages before starting a new culture from stock. Cell lines were routinely tested for mycoplasma contamination. TF, HER2 and EGFR cell surface expression was quantified by QIFIKIT analysis (DAKO) according to the manufacturer's guidelines, using a mouse anti-human TF antibody (CLB), mouse anti-human HER2 antibody (R&D) and mouse anti-human EGFR antibody (BD) as described in supplementary method S1.

Antibody generation and conjugation

Human IgG1κ monoclonal antibodies were generated in human antibody transgenic mice; HuMAb® mice (Medarex), using hybridoma technolgy [21]. Tissue Factor antibodies were previously described [4]. In brief, TF-011 binds TF, interferes with FVIIa binding and inhibits ERK-phosphorylation. TF-111 binds TF and partially interferes with FVIIa binding and ERK-phosphorylation. The HER2 mAbs 153 and 005 were described by de Goeij et al. [22]. Both antibodies bound to epitopes distinct from those recognized by trastuzumab and pertuzumab. Upon binding to HER2, mAb 153 inhibits ligand-induced HER2 proliferation. mAb 005 has no effect on HER2 induced

proliferation. The EGFR mAbs zalutumumab and nimotuzumab (Biacon) both inhibit ligand binding and EGFR driven proliferation. Zalutumumab does so with high affinity [23], while nimotuzumab blocks EGF binding with low affinity [24].

Duostatin-3 conjugated antibodies were generated by covalent conjugation of valine-citrulline-duostatin-3 on antibody lysine groups as described in WO/2013/173391. The synthesis of duostatin-3 is also described in the supplementary method S2. Each resulting duostatin-3 conjugated ADC contained an average of 2 drug molecules per antibody, as determined by hydrophobic interaction chromatography (HIC). Duostatin-3 conjugated antibodies were referred to as TF-ADC, HER2-ADC and EGFR-ADC. TF-011 was also conjugated with maleimidocaproyl-valine-citrulline-*p*-aminobenzoyl-monomethyl auristatin E (vcMMAE, licensed from Seattle Genetics) on cysteine groups in the antibody hinge region, to generate TF-011-MMAE (HuMax-TF-ADC), as described [4]. This ADC was referred to as TF-011-MMAE throughout the manuscript. TF-011-MMAE contained an average of 4 drug molecules per antibody.

Confocal microscopy

Cells were grown on glass coverslips (Thermo Fisher Scientific) at 37°C for 16 hours. In case of antibody stimulation, cells were pre-incubated 1 hour with 50 µg/mL leupeptin (Sigma) to block lysosomal activity followed by 1 or 16 hours incubation with 1 µg/mL EGFR-, HER2- or TF-antibody. Cells were fixed, permeabilizedand incubated 45 min with mouse anti-human TF (CLB), HER2 (R&D) and EGFR (BD Pharmingen) antibodies, followed by goat anti-mouse IgG1-FITC (DAKO) to identify receptors, or goat anti-human IgG1-FITC (Jackson) to stain for human EGFR-, HER2- and TF- antibodies. Endosomes were stained with rabbit anti-human transferrin (Life Technology) and goat anti-rabbit IgG-Alexa-568 (Bio-connect), lysosomes were stained with mouse anti-human CD107a-APC (BD). Finally, coverslips were mounted (Calbiochem) on microscope slides and imaged with a Leica SPE-II confocal microscope (Leica Microsystems) equipped with LAS-AF software. 12-bit grayscale TIFF images were analyzed for colocalisation using MetaMorph® software (Molecular Devices). Colocalisation was calculated as the FITC pixel intensity overlapping with APC (lysosomes) or AlexaFluor568 (endosomes) and expressed as percentage of total FITC intensity.

Surface protein downmodulation assay

SK-OV-3 and A431 cells were seeded in 96-wells non-binding plates (Greiner), 100,000 cells/well, in serum-free culture medium, with or without 100 µM monensin (Dako) to block recycling of endosomes (30 minutes, 37°C) [25]. Next, human TF-, HER2- and EGFR- antibodies (10 µg/mL), EGF (Biosource, 50 ng/mL) or FVIIa (Novoseven, 100 ng/mL) were added for 3 hours (37°C). Remaining TF, HER2 or EGFR at the plasma membrane were stained with non-competing mouse TF (CLB), HER2 (R&D) and EGFR antibodies (BD) (30 min, 4°C), followed by incubation with goat anti-mouse IgG-FITC (Jackson, 30 min, 4°C). Mean Fluorescence Intensity (MFI) of

FITC was measured on a flow cytometer (BD). Quantification of cell surface proteins was done using QIFIKIT® (Dako) according to the manufacturer's instructions [26].

Total protein downmodulation assay

Cells were seeded (100,000 cells/well) in 96-wells culture plates (Greiner). After 4 hours cells were pre-incubated with 100 µM chloroquine (Sigma) or 100 µg/mL leupeptin (Sigma, 30 min, 37°C), followed by incubation with 10 µg/mL human TF, HER2 or EGFR antibodies. After 48 hours, cells were washed, lysed and total protein levels were quantified using bicinchoninic acid (BCA) protein assay reagent (Pierce), according to manufacturer's instruction. Next, ELISA plates (Greiner) were coated with 1 µg/mL mouse anti-human EGFR (Millipore), rabbit anti-human HER2 (Cell Signalling Technology) or mouse anti-human TF (CLB), blocked with 2% chicken serum (Hyclone) and incubated with 50 µL cell lysate. Subsequently, EGFR, HER2 and TF were detected with mouse anti-human EGFR-biotin (Leica Technologies, 0.5 µg/mL), goat anti-human HER2-biotin (R&D, 50 ng/mL) and goat anti-human TF-biotin (R&D, 0.5 µg/mL). The reaction was visualized as described [27].

Intracellular antibody accumulation

Cells were incubated with 5 µg/mL FITC-conjugated antibodies at either 4°C or 37°C. At the indicated time points, cells were transferred on ice to stop internalization and washed with ice-cold phosphate buffered saline (B.Braun Melsungen). 50 µL ice-cold acid wash buffer (0.2M glycine [Sigma], 4M urea [Sigma], pH2.0) was added for 5 minutes to remove extracellular bound antibodies and removed through centrifugation. Remaining FITC-fluorescence, originating from internalized FITC-conjugated antibodies, was measured using flow cytometry.

CypHer5E internalization assay

Cells were seeded in 96-well plates (Greiner, 20,000 cells/well) and cultured overnight at 37°C. Ice-cold culture medium with or without 100 µM chloroquine (Sigma) was added for 1 hour at 4°C, to trap internalized antibody in endosomal compartments. Next, 1 µg/mL HER2, EGFR or TF antibody, conjugated with CypHer5E according to manufacturer's instructions (GE Healthcare), was added. CypHer5E is a pH-sensitive dye which is non-fluorescent at basic pH (extracellular: culture medium) and fluorescent at acidic pH (intracellular: endosomes, lysosomes). After 30 minutes, the cells were washed and fresh culture medium (37°C) was added. The cells were incubated 24 hours at 37°C. At indicated time points MFI of internalized CypHer5E was measured per well using homogeneous Fluorometric Microvolume Assay Technology (FMAT, Applied Biosystems). As read out, fluorescence per cell was multiplied with the number of positive cells per well (counts x fluorescence).

Cytotoxicity assay

Mixed cell cultures were treated with ADC to simultaneously determine the amount of target cell kill and bystander kill. HER2, EGFR and TF expressing tumor cells were used as target cells and seeded (5,000 cells/well) in 96-well culture plates. Antigen negative Jurkat cells were used as bystander cells and added to the plate (20,000 cells/well). To discriminate between both cell populations, Jurkat cells were labelled with CellTraceTM carboxyfluorescein diacetate succinimidyl ester (CFSE) according to manufacturer's instructions (Invitrogen). Next, serially diluted ADCs (10-0.000001 µg/mL) were added and the cells were incubated 4 days at 37^{0}C. Cells were harvested and viability was assessed through live/dead staining on a flow cytometer. Target cell kill was plotted as the percentage of viable CFSE-negative cells. Bystander kill was plotted as the percentage of viable CFSE-positive cells.

Alternatively, 500,000 CFSE labeled cells were cultured in T25 flasks (Greiner) in presence of 2 µg/mL ADC. After 3 days the viable cells were harvested and analyzed for antigen expression using mouse TF (CLB), HER2 (R&D) and EGFR antibodies (BD) and goat anti-mouse IgG1-APC (Jackson). Each sample was spiked with 10,000 CFSE-negative Jurkat cells. During flow cytometry analysis, the CFSE-negative Jurkat cells were gated and 3,000 events were measured in this gate, while all events were stored and analyzed.

Tumor xenograft models

6-11 week old female SCID mice (C.B-17/IcrPrkdc-scid/CRL) were purchased from Charles River. Subcutaneous tumors were induced by inoculation of 5 x 10^{6} cells in the right flank of the mice. Tumor volumes were calculated from digital caliper measurements as 0.52 x length x width^{2} (mm^{3}). When tumors reached 200-400 mm^{3}, mice were grouped into groups of 7 mice with equal tumor size distribution and mAbs were injected intraperitoneally at indicated time points (1 or 4 mg/kg). During the study, blood samples were collected into heparin-containing tubes to confirm the presence of human IgG in plasma. IgG levels were quantified using a Nephelometer (Siemens Healthcare). Mice that did not show human IgG in plasma were excluded from the analysis. Some mice developing ulcerations not related to tumor size, were euthanized for ethical reasons before the end of the study, which is indicated by the censored data points.

Statistical analysis

Data analysis was done using GraphPad Prism 5 software. Group data were reported as mean ± SD. One-way ANOVA was applied for statistical analysis. Statistical analysis of xenograft studies was done with one-way ANOVA at the last day that all groups were complete. Mantel-Cox analysis of Kaplan-Meier curves was performed to analyze statistical differences in progression-free survival time.

RESULTS

Tissue Factor distribution in unstimulated tumor cells

In healthy tissue, TF is primarily expressed in intracellular pools and remains sequestered from circulating FVII [17,18,28]. To determine TF distribution in cancer cells we applied confocal microscopy. For this, we selected two cell lines based on aberrant expression of HER2 and TF (SK-OV-3, ovarian cancer) or EGFR and TF (A431, epithelial carcinoma), as depicted in Table 1. The cells were grown on glass coverslips, left unstimulated and stained for TF, EGFR and HER2. Markers of recycling endosomes (i.e. transferrin) and lysosomes (i.e. LAMP1) were included to determine compartmentalization of the different proteins. Figure 1A-C demonstrates that, in resting SK-OV-3 cells, TF is primarily localized intracellularly and partially colocalizes with the lysosomal marker LAMP1. EGFR and HER2 staining on the other hand was mainly localized to the plasma membrane.

Cell line	Origin	TF (molecules/cell)	EGFR (molecules/cell)	HER2 (molecules/cell)
HCC1954	Breast cancer	400,000	100,000	600,000
A431	Epithelial cancer	200,000	500,000	30,000
SK-OV-3	Ovarian cancer	100,000	50,000	200,000
AU565	Breast cancer	20,000	100,000	500,000

TABLE 1 *Number of molecules on plasma membrane*. Average number of EGFR, HER2 and TF molecules expressed on the cell surface, calculated with quantitative flow cytometry as described in supplementary method S1.

Also in A431 cells (Figure 1D) and HCC1954 cells (Supplementary Figure S1), TF was more abundantly present in lysosomes as compared to EGFR and HER2, suggesting that TF has a high turnover in these tumor cells. This was confirmed by ELISA where total protein levels of TF, EGFR and HER2 were measured in absence and presence of inhibitors of lysosomal degradation (Figure 1E). Total protein levels of EGFR and HER2 were unaffected by addition of chloroquine, an inhibitor of endosomal acidification [29] or leupeptin, an inhibitor of lysosomal proteases. However, TF protein levels were increased over 2-fold when lysosomal degradation was blocked with chloroquine, indicating that TF is continuously transported from endosomal to lysosomal compartments to undergo degradation.

The enhanced colocalisation of TF with transferrin (Figure 1D) suggests that at least a part of the intracellular TF pool originated from the plasma membrane [30]. Therefore we next investigated downmodulation of surface expressed receptors using quantitative flow cytometry. SK-OV-3 cells were incubated with the TF ligand FVIIa or the EGFR ligand EGF, after which residual receptor expression was quantified.

Monensin was added to block transport of intracellular receptors to the cell surface and thereby trap internalized proteins in the cell. Figure 1F shows that FVIIa alone had no effect on surface expression of TF, whereas monensin significantly reduced TF expression, indicating that TF is constitutively recruited from intracellular pools to the plasma membrane. Previous reports have described the internalization of TF in presence of FVIIa [16,31], our data demonstrate that TF is also internalized in absence of FVIIa. EGF on the other hand induced significant downmodulation of surface expressed EGFR which was in line with previous reports [32], while HER2 expression was unaffected by EGF and monensin.

In summary, unlike EGFR and HER2, TF was continuously internalized and degraded, even in resting tumor cells. This suggests that the efficacy of TF-specific ADCs may be at least partly related to the endogenous internalization characteristics of TF.

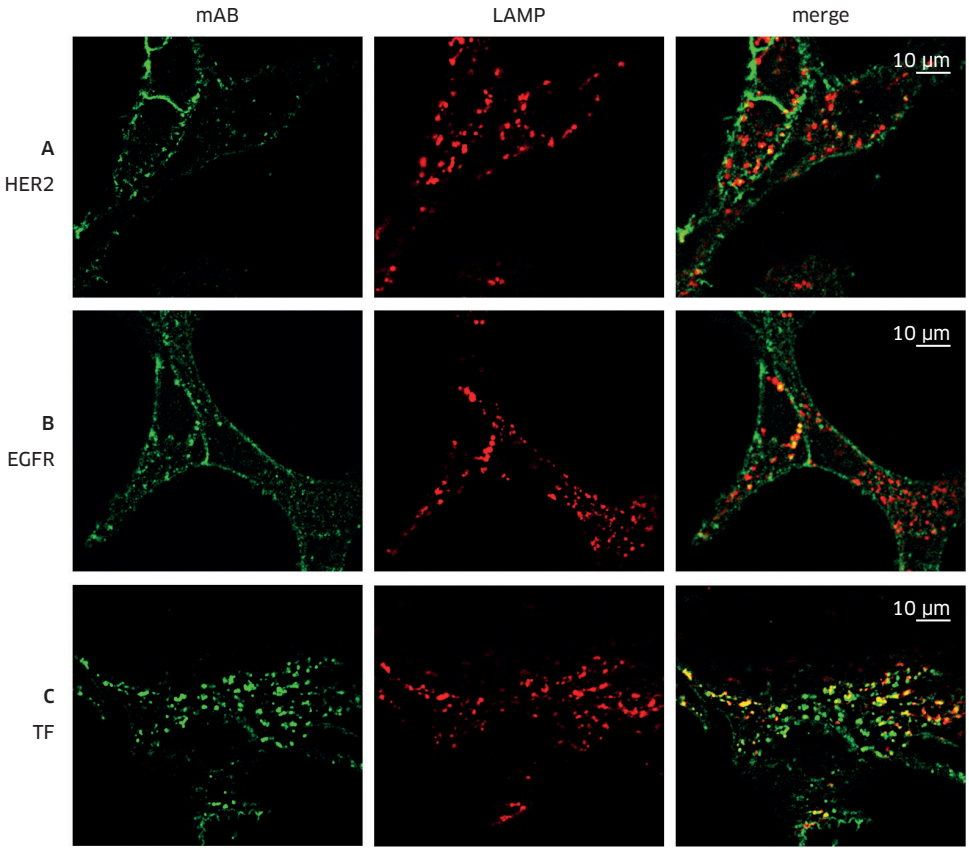

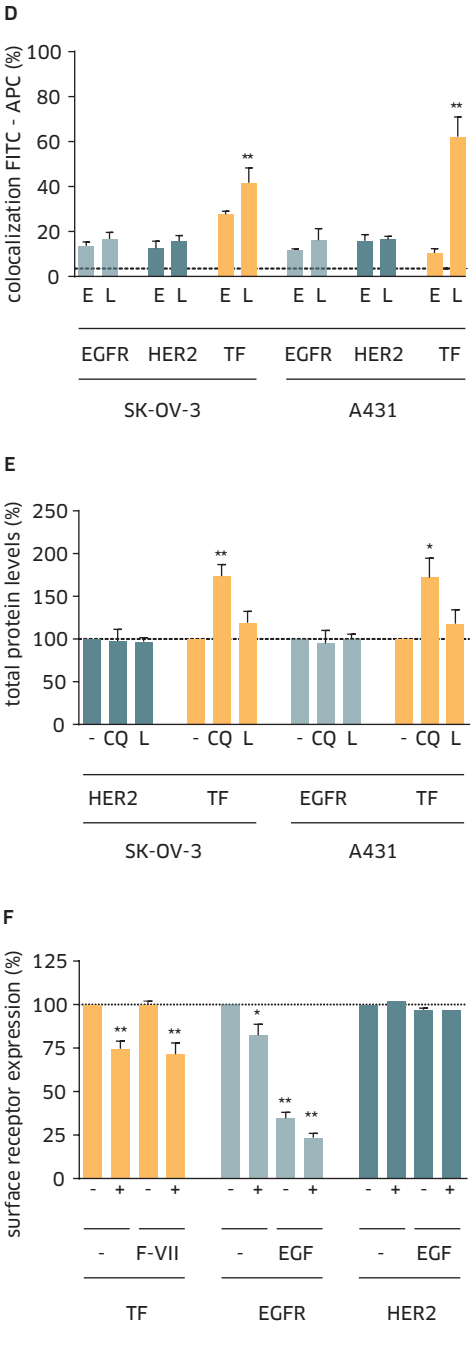

FIGURE 1 *Distribution of HER2, EGFR and TF in unstimulated tumor cells.* **(A-C, page 44)** Confocal microscopy images (8-bit) of unstimulated SK-OV-3 cells. The left panel shows staining of HER2 **(A)**, EGFR **(B)** and TF **(C)** with murine antibodies and goat anti-mouse IgG-FITC (green). In the middle panel lysosomes were stained with mouse anti-human LAMP1-APC (red). The right panel shows the overlay (yellow). **(D)** Quantification of endosomal and lysosomal receptor colocalisation. Each bar represents 4 different 12-bit images ± standard deviation. E=endosomes L=lysosomes. **(E)** Downmodulation of total protein expression. Cells were incubated for 2 days with 100 µM chloroquine or 100 µg/mL leupeptin, after which protein levels were measured with ELISA and expressed as percentage compared to untreated cells. Data shown are mean ± standard deviatin. **(F)** Surface protein downmodulation on SK-OV-3 cells measured with quantitative flow cytometry. Cells were preincubated 30 minutes with (+) or without (-) monensin and incubated an additional 3 hours with 50 ng/mL EGF or 100 ng/mL FVIIa. Surface expression of remaining TF, EGFR and HER2 was quantified and plotted as percentage relative to untreated cells. Data shown are mean ± standard deviation. *P<0.05, **P<0.001

Antibody binding to TF triggers internalization of mAb/TF-complexes

For certain receptors, antibody binding results in internalization of the Ab/receptor-complex [32]. To investigate whether Ab/TF-complexes were internalized, we incubated SK-OV-3 and A431 cells for three hours at 37°C with antibodies directed against TF, EGFR and HER2. The cells were cooled to 4°C and remaining extracellular proteins were quantified using non-competing murine TF, EGFR and HER2 antibodies. Figure 2A demonstrates that TF-011 and TF-111 induced significant downmodulation of extracellular TF, which was not observed with Fab fragments of mAb TF-011 or the TF physiological ligand FVIIa. The tested EGFR and HER2 antibodies had no effect on extracellular expression of EGFR and HER2 respectively. The experiment was also performed in presence of the recycling inhibitor monensin. For EGFR and TF, this further decreased extracellular expression (data not shown).

Next, it was investigated whether antibody-mediated downmodulation of total protein levels. SK-OV-3 and A431 cells were incubated for 2 days with EGFR, HER2 and TF antibodies, lysed and subjected to ELISA to measure the degree of protein. Figure 2B shows that TF-011 induced downmodulation of total TF protein in both cell lines. Also a slight reduction of EGFR protein levels was observed upon incubation with EGFR antibody zalutumumab, but no effect on HER2 protein levels was observed with any of the HER2 antibodies.

To exclude that the reduced protein levels depicted in Figure 2A result from antibody-induced shedding of TF, intracellular accumulation of FITC-conjugated antibodies was assessed to confirm that Ab/TF-complexes were indeed internalized. Cells were incubated with FITC-conjugated antibodies at 37°C for 0-9 hours. Prior to flow cytometry analysis, extracellular FITC-conjugated antibodies were removed through acid wash and residual FITC fluorescence, originating from internalized FITC-conjugated antibodies, was measured on a flow cytometer. As depicted in figure 2C and D, both TF antibodies showed accumulation of FITC fluorescence over time, demonstrating that these antibodies were efficiently internalized.

TF/TF-011 complexes are rapidly targeted to the lysosomes

For an ADC-approach, it is typically required that internalized antibodies traffic to lysosomes where cellular proteases can initiate drug release [33]. Using confocal microscopy, lysosomal transport of TF, EGFR and HER2 antibodies was analyzed. SK-OV-3 and A431 cells were incubated with the indicated antibodies, and after 1 or 16 hours cells were fixed, permeabilized and stained with FITC-conjugated goat-α-human IgG1. After one hour, TF-011 already demonstrated clear internalization and lysosomal colocalisation (Figure 3A). EGFR antibody zalutumumab was also internalized after one hour, but the internalized antibody had not yet reached the lysosomes (Figure 3C), while HER2 antibody 005 only stained at the plasma membrane (Figure 3E). After 16 hours, all antibodies demonstrated substantial internalization and ly-

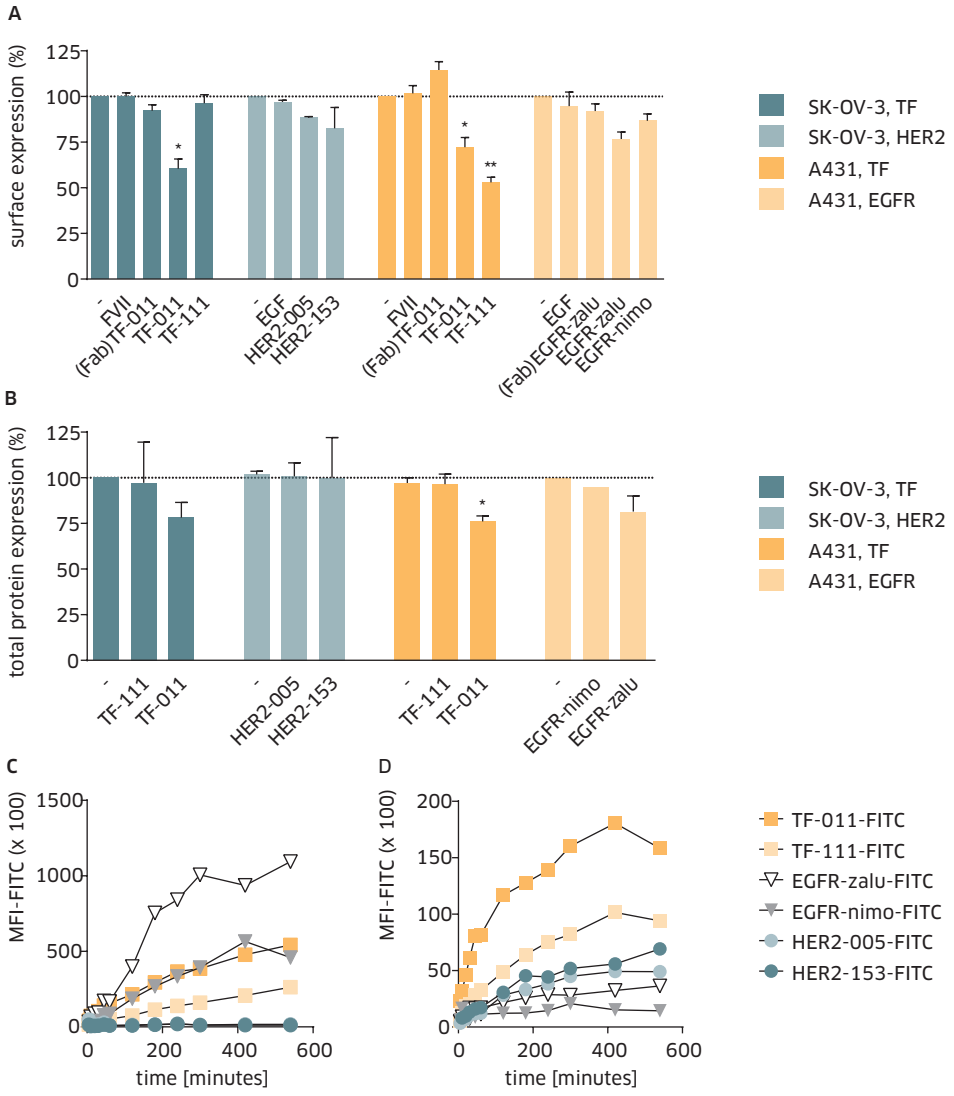

FIGURE 2 Antibody-mediated internalization and downmodulation of TF, EGFR and HER2. **(A)** Downmodulation of surface expressed proteins measured with flow cytometry. SK-OV-3 and A431 cells were incubated with 10 µg/mL antibody. After 3 hours, remaining surface expression of the different receptors was analyzed with quantitative flow cytometry and expressed as percentage relative to untreated cells. **(B)** Downmodulation of total protein levels. SK-OV-3 and A431 cells were incubated with 10 µg/mL antibody. After two days protein levels were measured with ELISA and expressed as percentage compared to untreated cells. Data shown are mean ± standard deviation. **(C-D)** Intracellular accumulation of FITC-conjugated antibodies measured with flow cytometry. **(C)** A431 and **(D)** SK-OV-3 cells were incubated with 10 µg/mL Ab-FITC at 4°C and 37°C. At the indicated timepoints, extracellular bound Ab-FITC was removed through acid wash and MFI of intracellular FITC was analyzed with flow cytometry. One representative experiment out of three is shown. *P<0.05, **P<0.001.

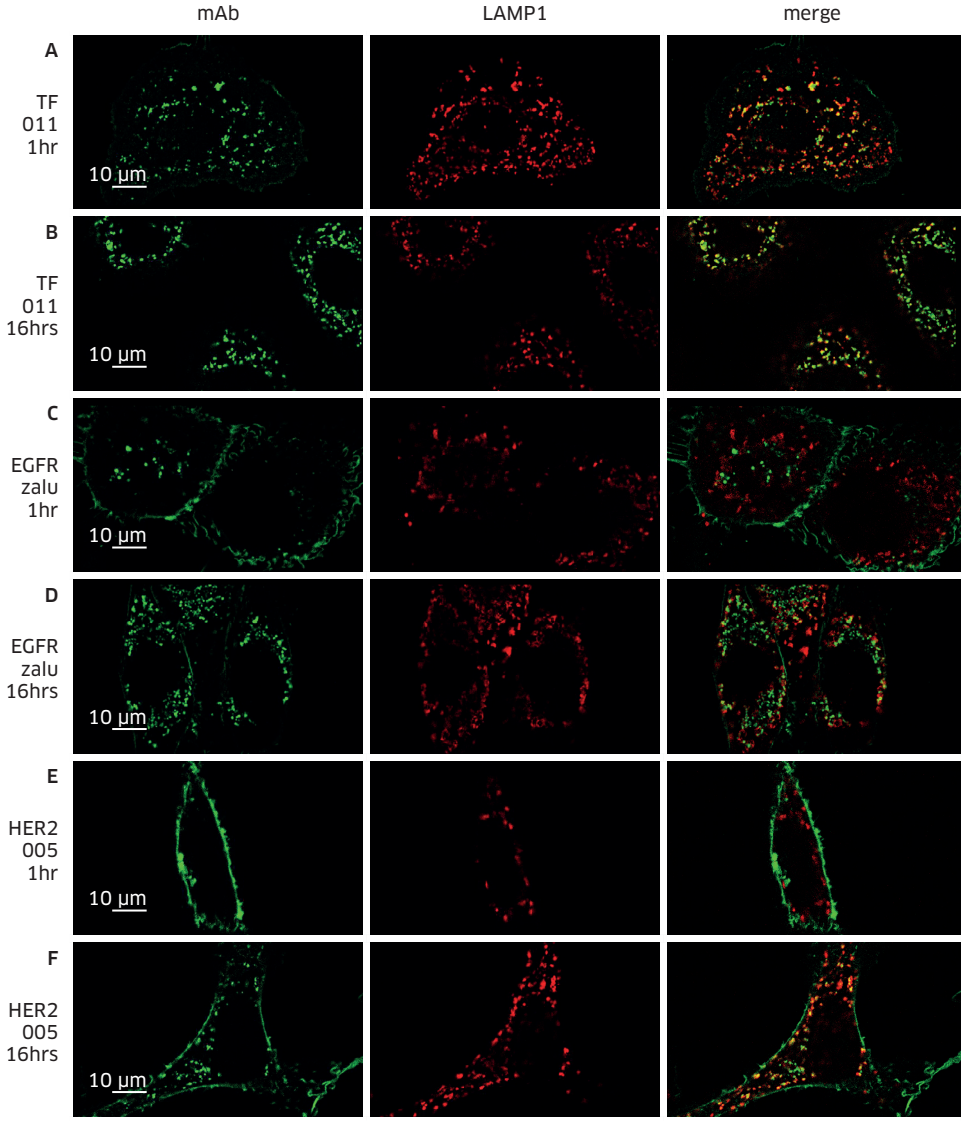

FIGURE 3 *Lysosomal colocalisation of TF, EGFR and HER2 antibodies*. **(A-F)** Confocal microscopy analysis of SK-OV-3 **(A-B, E-F)** and A431 **(C-D)** cells demonstrating fast and increased lysosomal transport of TF-011. Lysosomes were stained with mouse anti-human LAMP1-APC (red). Zalutumumab (anti-EGFR), 005 (anti-HER2) and TF-011 (anti-TF) were detected with goat anti-human IgG1-FITC (green). **(G)** Arbitrary units [AU] represent the total pixel intensity of antibody overlapping with the lysosomal marker LAMP1, divided by the total pixel intensity of LAMP1. Data shown are mean ± standard deviation of 4 images. **(H-K)** Lysosomal targeting of CypHer5E conjugated mAbs. SK-OV-3 cells, preincubated with or without 100 µM chloroquine, were incubated with CypHer5E-conjugated antibodies: TF-011 **(H)**, zalutumumab **(I)**, 005 **(J)** and 153 **(K)**. At the indicated time points, CypHer5E fluorescence was measured using homogeneous Fluorometric Microvolume Assay Technology. The grey area indicates antibody present in lysosomal compartments.

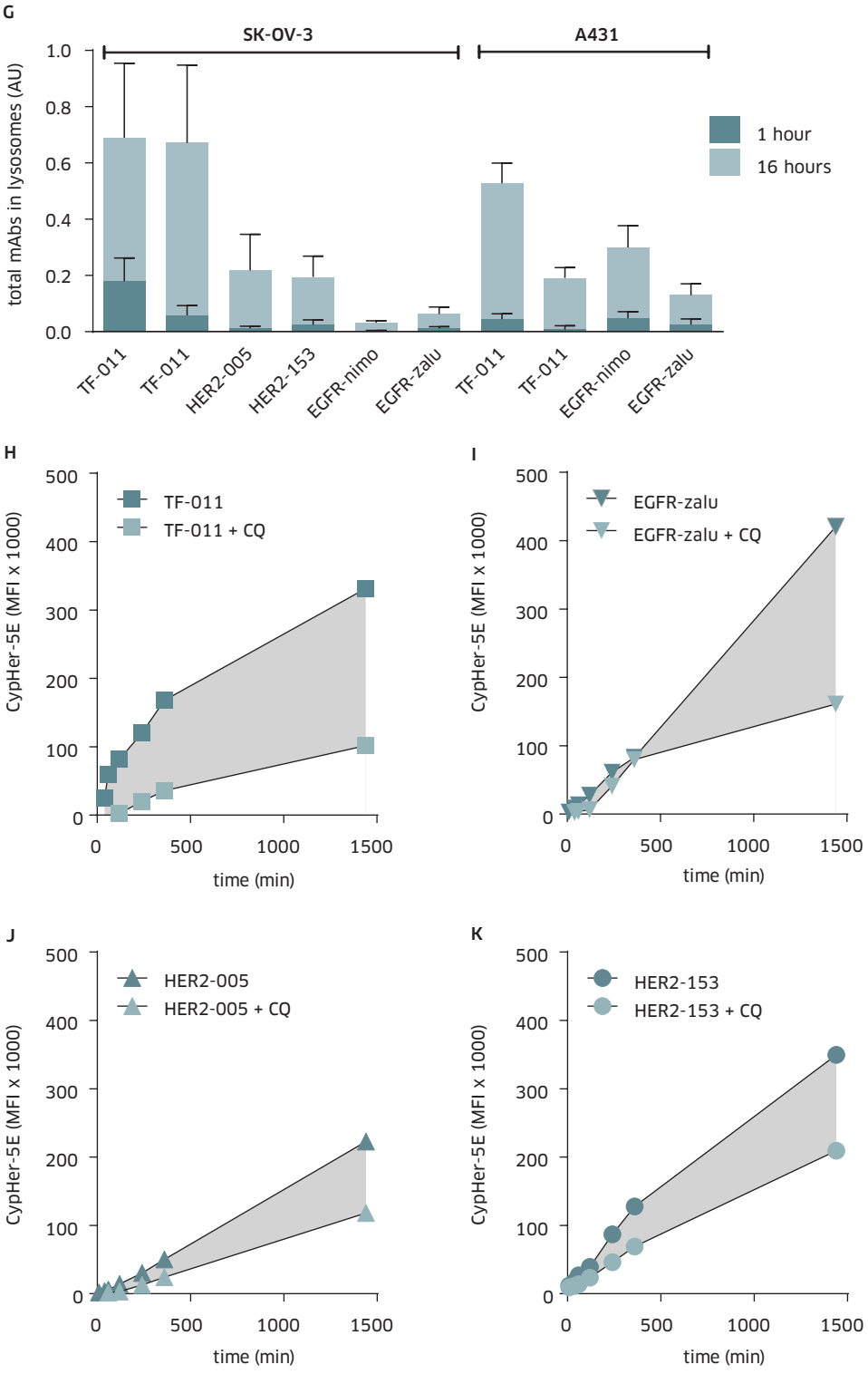
G
SK-OV-3
A431
total mAbs in lysosomes (AU)
1.0
0.8
0.6
0.4
0.2
0.0
1 hour
16 hours
TF-011
TF-011
HER2-005
HER2-153
EGFR-nimo
EGFR-zalu
TF-011
TF-011
EGFR-nimo
EGFR-zalu
H
CypHer-5E (MFI x 1000)
TF-011
TF-011 + CQ
time (min)
I
EGFR-zalu
EGFR-zalu + CQ
J
HER2-005
HER2-005 + CQ
K
HER2-153
HER2-153 + CQ

sosomal colocalisation, but TF mAbs were most abundantly present in lysosomes (Figure 3B, D, F and G). Additionally, receptor distribution was tested after antibody treatment (Supplementary Figure S2). Both TF-antibodies significantly increased the amount of TF in endosomes and lysosomes of SK-OV-3 and A431 cells. EGFR mAbs zalutumumab and nimotuzumab also enhanced endosomal and lysosomal colocalisation of EGFR in A431 cells. In contrast, cellular distribution of HER2 was hardly affected by HER2 antibodies 005 and 153.

The more rapid lysosomal colocalisation of TF-mAbs, led us to investigate TF mediated internalization and lysosomal targeting in more detail. By conjugating TF, HER2 and EGFR mAbs with CypHer5E, a dye that becomes fluorescent at acidic pH, we were able to follow internalization and lysosomal colocalisation over time. Both endosomes and lysosomes are acidic environments that induce fluorescence of CypHer5E. To distinguish between fluorescence resulting from endosomal and lysosomal transport, SK-OV-3 cells were preincubated with chloroquine, which inhibits the acidification and fusion of endosomes with lysosomes [34]. Thus, inhibition of CypHer5E fluorescence by chloroquinine is indicative of lysosomal transport. This was most evident for TF-011 (Figure 3H). Whereas fluorescence of CypHer5E conjugated mAbs 005, 153 and zalutumumab was only inhibited after 24 hours incubation (Figure 3I-K), fluorescence of TF-011-CypHer5E was already inhibited within one hour. This shows that TF bound antibodies were rapidly transported to lysosomes, while lysosomal transport of EGFR and HER2 mAbs was relatively slow.

In vitro cytotoxicity induced by duostatin-3-conjugated TF, EGFR and HER2 antibodies

To investigate whether the more rapid lysosomal targeting observed with TF mAbs, results in increased cytotoxicity of TF-directed ADCs, we conjugated antibodies TF-011, 005 and zalutumumab with duostatin-3 using a valine-citrulline linker that is cleaved by intracellular proteases such as cathepsin B. Duostatin-3 is an antimitotic agent that inhibits cell division by blocking of tubulin polymerization. Unlike vcMMAE, duostatin-3 can not kill neighbouring tumor cells when the drug is released from the antibody. This was also demonstrated in Figures 4B, D and F, where duostatin-3 conjugated antibodies did not induce bystander kill. Whereas TF-011-MMAE induced potent bystander kill which was in line with results published previously [4,33]. To study the target requirements needed for efficient intracellular drug delivery, a drug-linker that only affects antigen expressing cells was preferred. Figure 4A, C and E, show that duostatin-3 conjugated HER2 and EGFR antibodies only induced cytotoxicity when tumor cells highly overexpress their targets HER2 (AU565 and SK-OV-3) and EGFR (A431 and AU565) respectively. Viability of tumor cells that display moderate overexpression of HER2 (A431) or EGFR (SK-OV-3) was hardly affected. In contrast, TF-mAbs conjugated with duostatin-3 induced cytotoxicity in all tested cell lines, including cells that express less than 20,000 TF molecules/cell. Analysis of

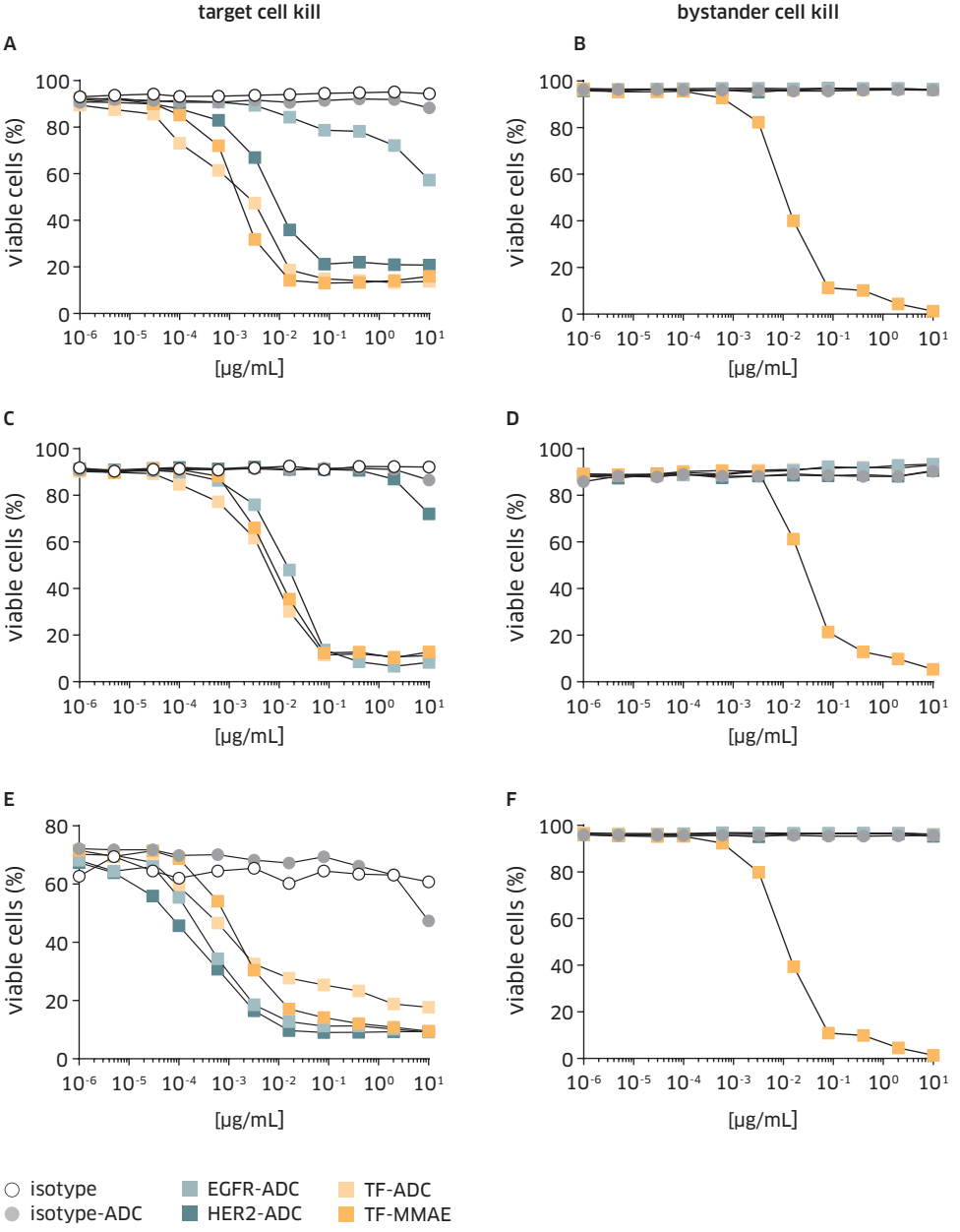

FIGURE 4 *Cytotoxicity of TF-ADC, EGFR-ADC, HER2-ADC and TF-011-MMAE in vitro.* SK-OV-3 **(A-B)**, A431 **(C-D)** and AU565 **(E-F)** cells were seeded in 96-wells tissue culture plates together with CFSE-labeled Jurkat cells. Serially diluted ADCs and isotype control antibody were added to the cells. After 4-days incubation at 37°C viability was assessed on a flow cytometer. Target cell kill was plotted as the percentage of viable CFSE- SK-OV-3, A431, and AU565 cells (left panel). Bystander kill was plotted as the percentage of viable CFSE+ cells (right panel).

TF-expression in SK-OV-3 cells that survived TF-ADC-treatment demonstrated that TF expression was similar before and after treatment (Table 2 and supplementary figure S3). However, the proliferation-rate of the surviving cells was reduced, as indicated by the high CFSE fluorescence of the surviving cells. This indicates that lack of efficacy against these cells was caused by their low proliferation-rate, rather than lack of target expression.

Anti-tumor activity of duostatin-3-conjugated TF, EGFR and HER2 antibodies *in vivo*

Finally, the effect of ADC treatment on tumor growth was assessed *in vivo*. The ADCs were compared in two different tumor xenograft models, starting with the breast cancer model HCC1954 (Figure 5A-B) which highly overexpressed HER2 and TF (Table 1). Figure 5B demonstrates that treatment with a single dose of 1 mg/kg TF-ADC resulted in significant inhibition of HCC1954 tumor growth as compared to animals treated with isotype control ADC. At the same dose, HER2-ADC had no effect on tumor growth. At 4 mg/kg, both ADCs induced tumor regression, which was sustained until at least 67 days post treatment.

Using the epidermal carcinoma model A431, ADCs targeting TF and EGFR were compared (Figure 5C-D). A single dose of 1 mg/kg TF-ADC induced significant inhibition of tumor growth, which was increased at 4 mg/kg. EGFR-ADC only reduced tumor growth at 4 mg/kg, a dose at which TF-ADC treatment was significantly more effective. Overall, TF-ADC treatment induced significant inhibition of tumor growth. Despite the reduced expression of TF as compared to HER2 and EGFR, TF-ADC outperformed HER2- and EGFR- ADCs. Hence these data demonstrate the potential of TF as tumor target for an ADC approach.

DISCUSSION

Antibodies conjugated with tubulin inhibitors have demonstrated impressive preclinical and clinical anti-tumor activity [1,20,35,36]. However, the optimal target characteristics for ADC development are not entirely clear. Most ADCs are dependent on internalization and lysosomal targeting to release their cytotoxic compound. Thus the internalization characteristics of a tumor target may greatly contribute to the efficacy of ADCs directed against that target. In addition, binding of antibodies or ADCs to specific tumor targets may change the internalization characteristics of the tumor target. In this study, the internalization characteristics of three different tumor targets, TF, EGFR and HER2, as well as antibodies and ADCs specific for those targets, were compared. Internalization, lysosomal sorting and intracellular degradation of the three proteins were analysed in absence and presence of monoclonal antibodies. The combination of TF and antibody TF-011 was the only combination demonstrating efficacy in all assays. TF demonstrated significant and constitutive

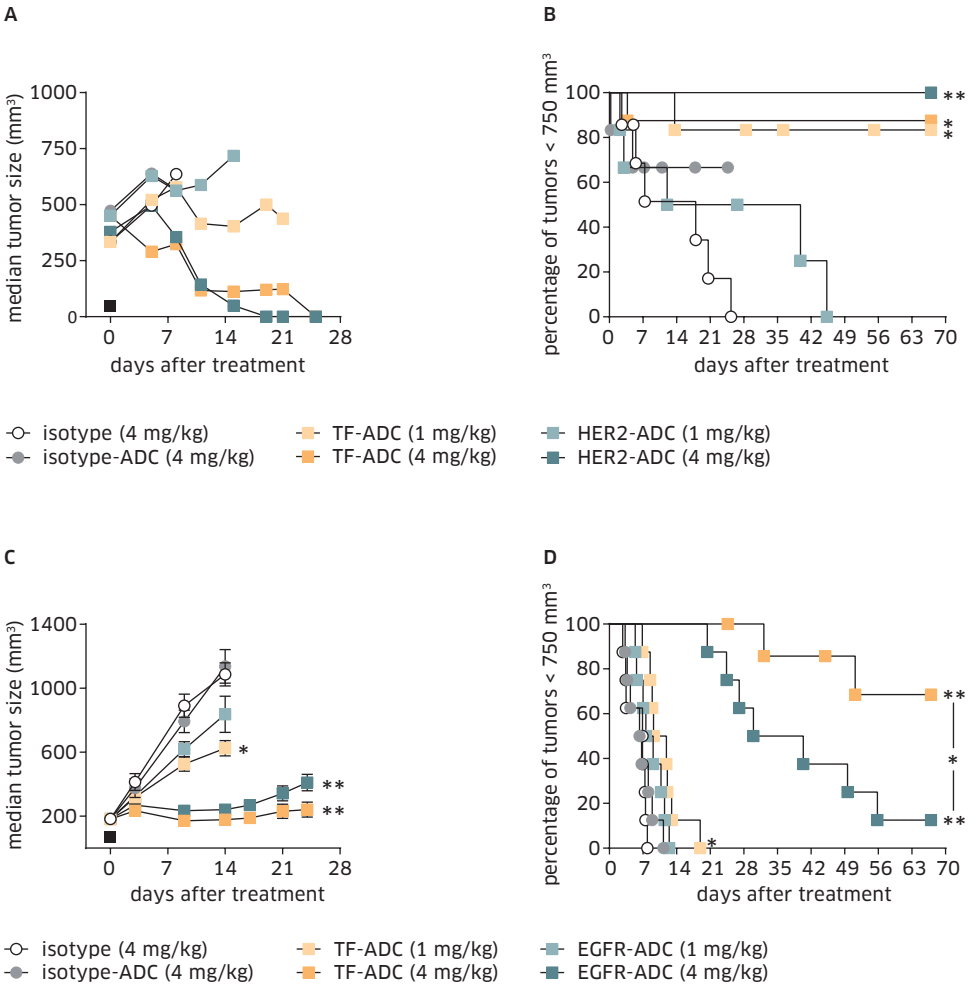

FIGURE 5 *Efficacy of TF-ADC, HER2-ADC and EGFR-ADC in tumor xenograft models.* Mice were inoculated subcutaneously with 5 x 10^6 HCC1954 **(A-B)** or A431 **(C-D)** cells. When average tumor volume reached >200 mm^3, mice were divided in groups of 7 mice with equal tumor size distribution and injected intraperitoneally at indicated time points with 4 mg/kg or 1 mg/kg mAb or ADC. Tumors were measured twice a week by using calipers, and the median **(A)** or mean ± SE **(C)** tumor volume (mm^3) was plotted against time, as well as time to progression indicated by the percentage of tumors <750mm^3 **(B)** or <500mm^3 **(D)**. In the HCC1954 model, some mice developed ulcerations unrelated to tumor size or Ab-treatment. These mice were withdrawn from the study as indicated by the censored data points **(B)**. Median tumor volumes were not calculated when more than 3 mice had been withdrawn **(A)**. *P<0.05, ** P<0.001

internalization, lysosomal colocalisation and degradation in tumor cells, all of which were increased upon incubation with TF-011. Given the potential of TF as target for an ADC approach, TF-, EGFR- and HER2- mAbs were conjugated with the cleavable linker-drug vcDuostatin-3, generating ADCs that provide specific tumor targeting with a payload only affecting proliferating cells. We found that TF-ADC outperformed HER2-ADC and EGFR-ADC in two different tumor xenograft models.

Quantitative flow cytometry analysis of tumor cell lines revealed that, like EGFR and HER2, TF can be aberrantly expressed on tumor cells. Compared with normal melanocytes, more than 1000-fold increased TF expression has been reported on metastatic human melanoma cells [37]. In the tumor models selected here, extracellular expression of TF was lower compared to EGFR and HER2. However, despite the lower antigen expression, the anti-tumor activity of TF-ADC was more potent compared to HER2- and EGFR- ADCs. This can be explained by the efficient transport of TF-011 from the plasma membrane into lysosomes of tumor cells as demonstrated with confocal microscopy. Previous publications also indicate that TF has a higher turnover rate compared to EGFR and HER2. Hamik et al. demonstrated that the half-life of TF on monocytes was 3.7 hours, which could be reduced to 1.3 hours when TF was bound by tissue factor protein inhibitor and FVII [38]. Unstimulated EGFR and HER2 on the other hand have a half-life of 6-24 hours depending on the cell line used [39]. Since TF is the main physiological initiator of the coagulation cascade, which represents a system that needs to be tightly regulated it makes sense that TF is more efficiently internalized and degraded compared to EGFR and HER2.

	Cytotoxicity (number of events)	Antigen expression (MFI APC)	Proliferation rate (MFI CFSE)
EGFR	40100	26613	65493
EGFR + EGFR-ADC	17858	21380	93951
HER2	39836	90735	65493
HER2 + HER2-ADC	7034	76490	122213
TF	42522	51237	65493
TF + TF-ADC	2403	45816	175662

TABLE 2 *Flow cytometry analysis of SK-OV-3 cells after ADC-treatment.* SK-OV-3 cells were labeled with CFSE, a dye that is stably fluorescent and that is transferred to daughter cells upon cell division with its fluorescence being halved. Thus reduced CFSE fluorescence indicates SK-OV-3 proliferation. CFSE labeled cells were treated 3 days with 2 µg/mL ADC after which cytotoxicity was analysed as well as expression of the antigen targeted by the respective ADC. Cytotoxicity was expressed as number of events measured on a flow cytometer. Antigen expression was detected with mouse anti-HER2, anti-EGFR and anti-TF antibodies in combination with APC-conjugated rabbit anti-mouse and depicted as MFI of APC.

Internalization of TF has been studied previously [16,40] and is believed to be an active process which can be enhanced through binding of FVIIa. We did not observe FVIIa mediated internalization of TF. Instead we found that TF was constitutively being turned over on tumor cells, a process which was not influenced by presence of FVIIa. Most studies focussing on internalization of TF:FVIIa complexes made use of radiolabelled FVIIa [16,31,41]. Our studies, using TF expression as read out, demonstrate that FVIIa most likely piggy-backs with internalizing TF. Various cancer cells including ovarian cancer cells have been reported to produce FVII themselves [42], however we did not detect FVII production in culture supernatant (data not shown).

Although the more rapid internalization and lysosomal targeting of TF seem fundamental for effective ADC treatment, the potent anti-tumor effect of TF-ADC can not be fully ascribed to the target characteristics of TF alone. Antibody selection plays an important role as well. This was illustrated by the increased internalization and lysosomal targeting observed with TF-011. While TF-011 is expected to crosslink extracellular TF, Fab-011 and FVII lack the ability to crosslink TF, indicating that mAb-induced crosslinking may be critical to increase downmodulation of extracellular TF. TF-111 on the other hand only seems to crosslink TF when highly overexpressed. Moreover differential antibody binding at low pH may influence intracellular trafficking of ADCs and consequently increase their lysosomal transport. Flow cytometry analysis of antibody binding at pH6 and pH7.4 revealed no differences in binding at reduced pH (Supplementary Table S1). Also no substantial differences were observed between apparent affinities of antibodies targeting TF, EGFR and HER2 (Supplementary Table S1). The low affinity EGFR mAb nimotuzumab was an exception to this and showed low apparent affinity binding to EGFR expressing cells (EC50 value 15.6 nM). Furthermore, inhibition of receptor signalling and engagement of immune effector cells may contribute to the anti-tumor activity of ADCs as well. However, treatment of established A431 xenografts with comparable dosing of unconjugated mAbs induced significantly less (EGFR-mAb [43]) or no (TF-mAbs [4]), inhibition of tumor growth. The unconjugated HER2 antibody 005 demonstrated modest inhibition of *in vivo* tumor growth, when tested at >10-fold higher dose in a high HER2 expressing tumor model (data not shown).

While EGFR and HER2 belong to a family of receptor tyrosine kinases, for which endocytic trafficking has been extensively investigated, TF is a member of the class II cytokine receptor superfamily. To date, little is known about intracellular trafficking of these proteins and their potential use in ADC based therapy. Our data indicate that such targets can be very attractive for an ADC-approach because of their rapid internalization, lysosomal targeting and degradation, which may be inherent to their physiological roles in regulating immune responses [44,45]. Taken together, these

data support the use of TF-ADC in cancer therapy and a clinical study is underway to assess the safety and efficacy of TF-011-MMAE, an auristatin-conjugate of antibody TF-011, for the treatment of patients with solid cancers.

Acknowledgements
We would like to thank Maarten Dokter, Hendrik ten Napel and Ester van 't Veld for technical support and Esther Breij for reviewing the manuscript.

REFERENCE LIST

1 Senter PD, Sievers EL: The discovery and development of brentuximab vedotin for use in relapsed Hodgkin lymphoma and systemic anaplastic large cell lymphoma. *Nat Biotechnol* 2012, 30(7):631-637.

2 LoRusso PM, Weiss D, Guardino E, Girish S, Sliwkowski MX: Trastuzumab emtansine: a unique antibody-drug conjugate in development for human epidermal growth factor receptor 2-positive cancer. *Clin Cancer Res* 2011, 17(20):6437-6447.

3 Burris HA: Trastuzumab emtansine: a novel antibody-drug conjugate for HER2-positive breast cancer. *Expert Opin Biol Ther* 2011, 11(6):807-819.

4 Breij EC, de Goeij BE, Verploegen S, Schuurhuis DH, Amirkhosravi A, Francis J, Miller VB, Houtkamp M, Bleeker WK, Satijn D *et al*: An antibody-drug conjugate that targets tissue factor exhibits potent therapeutic activity against a broad range of solid tumors. *Cancer Res* 2014, 74(4):1214-1226.

5 Goldin-Lang P, Tran QV, Fichtner I, Eisenreich A, Antoniak S, Schulze K, Coupland SE, Poller W, Schultheiss HP, Rauch U: Tissue factor expression pattern in human non-small cell lung cancer tissues indicate increased blood thrombogenicity and tumor metastasis. *Oncol Rep* 2008, 20(1):123-128.

6 Shigemori C, Wada H, Matsumoto K, Shiku H, Nakamura S, Suzuki H: Tissue factor expression and metastatic potential of colorectal cancer. *Thromb Haemost* 1998, 80(6):894-898.

7 Gonzalez-Gronow M, Gawdi G, Pizzo SV: Tissue factor is the receptor for plasminogen type 1 on 1-LN human prostate cancer cells. *Blood* 2002, 99(12):4562-4567.

8 Patry G, Hovington H, Larue H, Harel F, Fradet Y, Lacombe L: Tissue factor expression correlates with disease-specific survival in patients with node-negative muscle-invasive bladder cancer. *Int J Cancer* 2008, 122(7):1592-1597.

9 Uno K, Homma S, Satoh T, Nakanishi K, Abe D, Matsumoto K, Oki A, Tsunoda H, Yamaguchi I, Nagasawa T *et al*: Tissue factor expression as a possible determinant of thromboembolism in ovarian cancer. *Br J Cancer* 2007, 96(2):290-295.

10 Cocco E, Hu Z, Richter CE, Bellone S, Casagrande F, Bellone M, Todeschini P, Krikun G, Silasi DA, Azodi M *et al*: hI-con1, a factor VII-IgGFc chimeric protein targeting tissue factor for immunotherapy of uterine serous papillary carcinoma. *Br J Cancer* 2010, 103(6):812-819.

11 Cocco E, Varughese J, Buza N, Bellone S, Glasgow M, Bellone M, Todeschini P, Carrara L, Silasi DA, Azodi M *et al*: Expression of Tissue factor in Adenocarcinoma and Squamous Cell Carcinoma of the Uterine Cervix: Implications for immunotherapy with hI-con1, a factor VII-IgGFc chimeric protein targeting tissue factor. *BMC Cancer* 2011, 11(263).

12 Khorana AA, Ahrendt SA, Ryan CK, Francis CW, Hruban RH, Hu YC, Hostetter G, Harvey J, Taubman MB: Tissue factor expression, angiogenesis, and thrombosis in pancreatic cancer. *Clin Cancer Res* 2007, 13(10):2870-2875.

13 Wojtukiewicz MZ, Zacharski LR, Rucinska M, Zimnoch L, Jaromin J, Rozanska-Kudelska M, Kisiel W, Kudryk BJ: Expression of tissue factor and tissue factor pathway inhibitor in situ in laryngeal carcinoma. *Thromb Haemost* 1999, 82(6):1659-1662.

14 Hamada K, Kuratsu J, Saitoh Y, Takeshima H, Nishi T, Ushio Y: Expression of tissue factor in glioma. *Noshuyo Byori* 1996, 13(2):115-118.

15 Jiang X, Zhu S, Panetti TS, Bromberg ME: Formation of tissue factor-factor VIIa-factor Xa complex induces activation of the mTOR pathway which regulates migration of human breast cancer cells. *Thromb Haemost* 2008, 100(1):127-133.

16 Hansen CB, Pyke C, Petersen LC, Rao LV: Tissue factor-mediated endocytosis, recycling, and degradation of factor VIIa by a clathrin-independent mechanism not requiring the cytoplasmic domain of tissue factor. *Blood* 2001, 97(6):1712-1720.

17 Mandal SK, Pendurthi UR, Rao LV: Cellular localization and trafficking of tissue factor. *Blood* 2006, 107(12):4746-4753.

18 Schecter AD, Giesen PL, Taby O, Rosenfield CL, Rossikhina M, Fyfe BS, Kohtz DS, Fallon JT, Nemerson Y, Taubman MB: Tissue factor expression in human arterial smooth muscle cells. TF is present in three cellular pools after growth factor stimulation. *J Clin Invest* 1997, 100(9):2276-2285.

19 Kasthuri RS, Taubman MB, Mackman N: Role of tissue factor in cancer. *J Clin Oncol* 2009, 27(29):4834-4838.

20 Verma S, Miles D, Gianni L, Krop IE, Welslau M, Baselga J, Pegram M, Oh D-Y, Diéras V, Guardino E *et al*: Trastuzumab Emtansine for HER2-Positive Advanced Breast Cancer. *N Eng J Med* 2012, 367(19):1783-1791.

21 Fishwild DM, O'Donnell SL, Bengoechea T, Hudson DV, Harding F, Bernhard SL, Jones D, Kay RM, Higgins KM, Schramm SR *et al*: High-avidity human IgG kappa monoclonal antibodies from a novel strain of minilocus transgenic mice. *Nat Biotechnol* 1996, 14(7):845-851.

22 de Goeij BE, Peipp M, De Haij S, van den Brink EN, Kellner C, Riedl T, de Jong R, Vink T, Strumane K, Bleeker WK *et al*: HER2 monoclonal antibodies that do not interfere with receptor heterodimerization-mediated signaling induce effective internalization and represent valuable components for rational antibody-drug conjugate design. *MAbs in press [published online January 3, 2014; doi:104161/mabs27705]*.

23 Bleeker WK, Lammerts van Bueren JJ, van Ojik HH, Gerritsen AF, Pluyter M, Houtkamp M, Halk E, Goldstein J, Schuurman J, van Dijk MA *et al*: Dual mode of action of a human anti-epidermal growth factor receptor monoclonal antibody for cancer therapy. *J Immunol* 2004, 173(7):4699-4707.

24 Ramakrishnan MS, Eswaraiah A, Crombet T, Piedra P, Saurez G, Iyer H, Arvind AS: Nimotuzumab, a promising therapeutic monoclonal for treatment of tumors of epithelial origin. *MAbs* 2009, 1(1):41-48.

25 Levkowitz G, Waterman H, Zamir E, Kam Z, Oved S, Langdon WY, Beguinot L, Geiger B, Yarden Y: c-Cbl/Sli-1 regulates endocytic sorting and ubiquitination of the epidermal growth factor receptor. *Genes Dev* 1998, 12(23):3663-3674.

26 Poncelet P, Carayon P: Cytofluorometric quantification of cell-surface antigens by indirect immunofluorescence using monoclonal antibodies. *J Immunol Methods* 1985, 85(1):65-74.

27 Labrijn AF, Meesters JI, de Goeij BE, van den Bremer ET, Neijssen J, van Kampen MD, Strumane K, Verploegen S, Kundu A, Gramer MJ *et al*: Efficient generation of stable bispecific IgG1 by controlled Fab-arm exchange. *Proc Natl Acad Sci U S A* 2013, 110(13):5145-5150.

28 Mandal SK, Pendurthi UR, Rao LV: Tissue factor trafficking in fibroblasts: involvement of protease-activated receptor-mediated cell signaling. *Blood* 2007, 110(1):161-170.

29 Vincent MJ, Bergeron E, Benjannet S, Erickson BR, Rollin PE, Ksiazek TG, Seidah NG, Nichol ST: Chloroquine is a potent inhibitor of SARS coronavirus infection and spread. *Virol J* 2005, 2::69.

30 Mellman I: Endocytosis and molecular sorting. *Annu Rev Cell Dev Biol* 1996, 12:575-625.

31 Iakhiaev A, Pendurthi UR, Voigt J, Ezban M, Vijaya Mohan Rao L: Catabolism of factor VIIa bound to tissue factor in fibroblasts in the presence and absence of tissue factor pathway inhibitor. *J Biol Chem* 1999, 274(52):36995-37003.

32 Lammerts van Bueren JJ, Bleeker WK, Bogh HO, Houtkamp M, Schuurman J, van de Winkel JG, Parren PW: Effect of target dynamics on pharmacokinetics of a novel therapeutic antibody against the epidermal growth factor receptor: implications for the mechanisms of action. *Cancer Res* 2006, 66(15):7630-7638.

33 Smith LM, Nesterova A, Alley SC, Torgov MY, Carter PJ: Potent cytotoxicity of an auristatin-containing antibody-drug conjugate targeting melanoma cells expressing melanotransferrin/p97. *Mol Cancer Ther* 2006, 5(6):1474-1482.

34 Koh YH, von Arnim CA, Hyman BT, Tanzi RE, Tesco G: BACE is degraded via the lysosomal pathway. *J Biol Chem* 2005, 280(37):32499-32504.

35 Flygare JA, Pillow TH, Aristoff P: Antibody-drug conjugates for the treatment of cancer. *Chem Biol Drug Des* 2013, 81(1):113-121.

36 Alley SC, Okeley NM, Senter PD: Antibody-drug conjugates: targeted drug delivery for cancer. *Curr Opin Chem Biol* 2010, 14(4):529-537.

37 Mueller BM, Reisfeld RA, Edgington TS, Ruf W: Expression of tissue factor by melanoma cells promotes efficient hematogenous metastasis. *Proc Natl Acad Sci U S A* 1992, 89(24):11832-11836.

38 Hamik A, Setiadi H, Bu G, McEver RP, Morrissey JH: Down-regulation of monocyte tissue factor mediated by tissue factor pathway inhibitor and the low density lipoprotein receptor-related protein. *J Biol Chem* 1999, 274(8):4962-4969.

39 Sorkin A, Goh LK: Endocytosis and intracellular trafficking of ErbBs. *Exp Cell Res* 2008, 314(17):3093-3106.

40 Rao LVM, Pendurthi UR: Regulation of tissue factor-factor VIIa expression on cell surfaces: A role for tissue factor-factor VIIa endocytosis. *Mol Cell Biochem* 2003, 253(1-2):131-140.

41 Chang GT, Kisiel W: Internalization and degradation of recombinant human coagulation factor VIIa by the human hepatoma cell line HuH7. *Thromb Haemost* 1995, 73(2):231-238.

42 Yokota N, Koizume S, Miyagi E, Hirahara F, Nakamura Y, Kikuchi K, Ruf W, Sakuma Y, Tsuchiya E, Miyagi Y: Self-production of tissue factor-coagulation factor VII complex by ovarian cancer cells. *Br J Cancer* 2009, 101(12):2023-2029.

43 Overdijk MB, Verploegen S, van den Brakel JH, Lammerts van Bueren JJ, Vink T, van de Winkel JG, Parren PW, Bleeker WK: Epidermal growth factor receptor (EGFR) antibody-induced antibody-dependent cellular cytotoxicity plays a prominent role in inhibiting tumorigenesis, even of tumor cells insensitive to EGFR signaling inhibition. *J Immunol* 2011, 187(6):3383-3390.

44 Ragimbeau J, Dondi E, Alcover A, Eid P, Uze G, Pellegrini S: The tyrosine kinase Tyk2 controls IFNAR1 cell surface expression. *EMBO J* 2003, 22(3):537-547.

45 Wei SH, Ming-Lum A, Liu Y, Wallach D, Ong CJ, Chung SW, Moore KW, Mui AL: Proteasome-mediated proteolysis of the interleukin-10 receptor is important for signal downregulation. *J Interferon Cytokine Res* 2006, 26(5):281-290.

SUPPLEMENTARY METHODS

Quantitative determination of cell surface antigens.
Qifikit (DAKO) was used to detect and quantify cell surface expression of TF, HER2 and EGFR, according to manufacturer's protocol (1). In brief; cells were stained with 10 µg/mL mouse anti-human TF (CLB), mouse anti-human HER2 (R&D), mouse anti-human EGFR (BD), following incubation with polyclonal goat anti-mouse IgG FITC (DAKO). In parallel a series of bead populations, containing a well-defined number of antibody molecules per bead, was stained with the polyclonal goat anti-mouse IgG FITC antibody. Mean fluorescence intensities (MFI) were measured using flow cytometry, and a calibration curve with the MFI of the individual bead populations was plotted against the number of mAb molecules on the beads. This curve was used to interpolate the number of TF, HER2 and EGFR molecules per cell.

Duostatin-3 synthesis

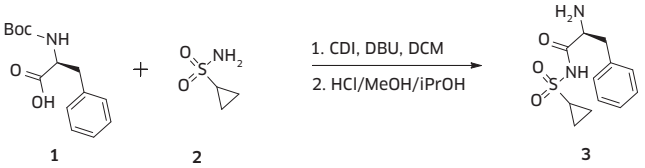

PREPARATION OF COMPOUND 3 To a solution of Boc-L-phenylalanine **1** (5.36 g, 20.2 mmol) in 30 mL of methylene chloride (DCM), carbonyldiimidazole (CDI, 4.26 g, 26.3 mmol) was added and stirred for 1 hour. Then added a solution of **2** (3.67 g, 30.3 mmol) and 2,4-diaminobutyric acid (DBU, 4.5 mL, 30 mmol) in 15 mL of DCM. The mixture was heated at 40°C for 16 hours. The mixture was diluted with 60 mL of DCM and 40 mL of water, then neutralized to pH 7 with conc. HCl. The DCM extract was collected, washed with 0.2M HCl (60 mL), then with brine (60 mL), dried over Na^2SO^4, and evaporated to give 7.47 g of Boc-protected sulfonamide. This material was suspended in 40 mL of methanol, then 200 mL of 6N HCl/isopropanol was added and the mixture was stirred for 2 hours. The solvent was evaporated under vacuum, 100 mL of ether was then added. The precipitate was collected by filtration and dried to give compound **3** as HCl salt (5.93 g, 96%); MS m/z 269.1 (M+H).

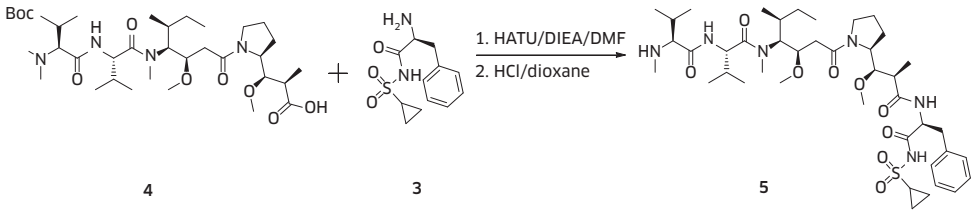

4 3 5

PREPARATION OF COMPOUND 5 To a solution of compound **4** (1.09 g, 1.6 mmol) in 10 mL of N,N-Dimethylformamide (DMF) was added 2-(lH-7-azabenzotriazol-l-yl)-l,l ,3,3-tetramethyl uranium hexafluorophosphate (HATU, 0.61 g, 1.6 mmol), diisopropylethylamine (DIEA, 0.56 mL), and compound **3** (0.49 g, 1.6 mmol) in that order. The mixture was stirred for 1 hour and diluted with 100 mL of water and 4 mL of acetic acid. The precipitate was collected by filtration, dried under vacuum and added to 10 mL of 4M HCl/dioxane. After 30 min, 200 mL of ether was added and insoluble precipitate was collected and purified by HPLC to give compound **5** as tetrahydrofuran salt (TFA, 1.3 g, 88%); MS m/z 835.5 (M+H). Compound **5** is referred to as duostatin-3 throughout the manuscript.

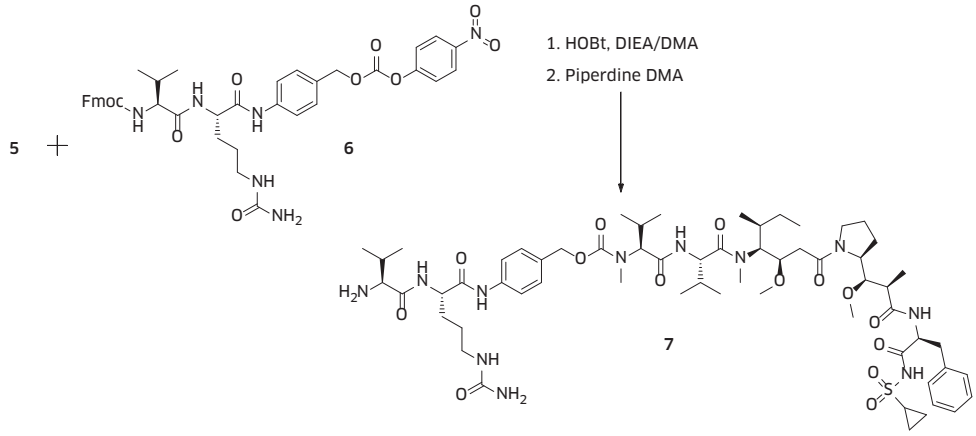

5 6 7

PREPARATION OF COMPOUND 7 To a solution of compound **5** (500 mg, 0.527 mmol) in 5 mL of DMF was added compound **6** (483 mg, 0.631 mmol), N-Hydroxybenzotriazole (HOBt, 40 mg, 0.296 mmol), and DIEA (0.27 mL). The mixture was stirred for 16 hours after which 0.4 mL of piperidine was added. After 1 hour, the mixture was diluted with 100 mL of ether and the precipitate was collected and dried to give compound **7** as HCl salt (640 mg, 95 %); MS m/z 1240.7 (M+H).

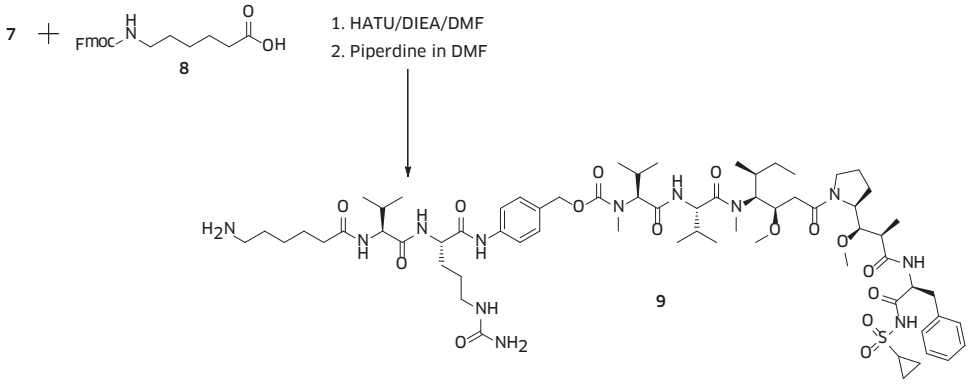

PREPARATION OF COMPOUND 9 To a solution of compound **8** (219 mg, 0.62 mmol) in 5 mL of DMF was added HATU (236 mg, 0.62 mmol), DIEA (0.15 mL), and compound **7** (316 mg, 1.6 mmol), respectively. After 1 hour, 0.2 mL of piperidine was added and the mixture was stirred for 30 min, then purified by HPLC to give compound **9** as TFA salt (235 mg, 64 %); MS m/z 1353.8 (M+H).

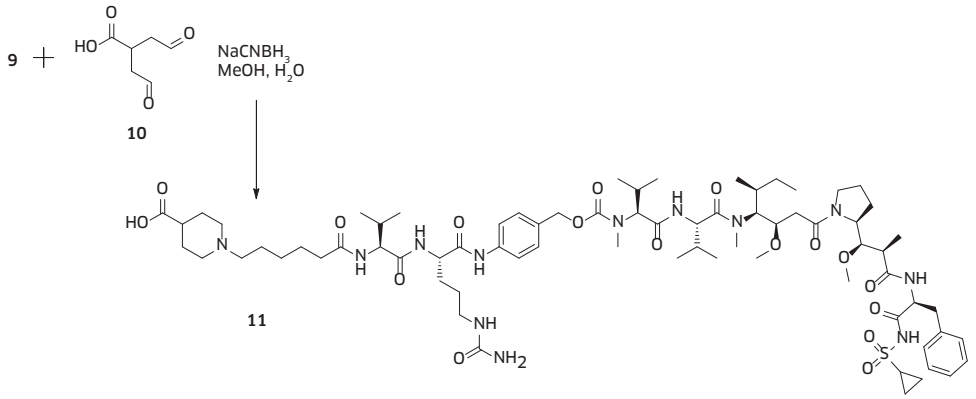

PREPARATION OF COMPOUND 11 To a solution of compound **9** (235 mg, 0.16 mmol) in 2 mL of methanol and 1 mL of water was added a solution of dialdehyde **10** (1.6 mL of 0.3M in iPrOH) and NaCNBH3 (180 mg, 2.85 mmol). The mixture was stirred for 2 hours at RT, and then purified by HPLC giving rise to compound **11** as TFA salt (126 mg, 50 %); MS m/z 1465.8 (M+H).

SUPPLEMENTARY TABLE

Antibody	Antigen	EC_{50} pH7.4 (nM)	EC_{50} pH6.0 (nM)
011	TF	0.69	0.61
111	TF	0.49	0.47
005	HER2	1.63	1.10
153	HER2	0.57	0.55
Zalutumumab	EGFR	0.93	1.45
Nimotuzumab	EGFR	15.6	13.8

SUPPLEMENTARY TABLE S1 *Apparent antibody affinities*. Apparent antibody affinities at pH7.4 and 6.0 measured using flow cytometry. SK-OV-3 cells, overexpressing TF, EGFR and HER2 were incubated with TF, EGFR and HER2 antibodies diluted in FACS-buffer at pH7.4 and FACS-buffer adjusted to pH6.0 with NaCl. Antibody binding was detected using a phycoerythrin (PE)-conjugated goat anti-human IgG antibody diluted in FACS-buffer at pH7.4. PE fluorescence was measured on a flow cytometer and EC_{50} values were calculated using GraphPad Prism 5 software.

SUPPLEMENTARY FIGURES

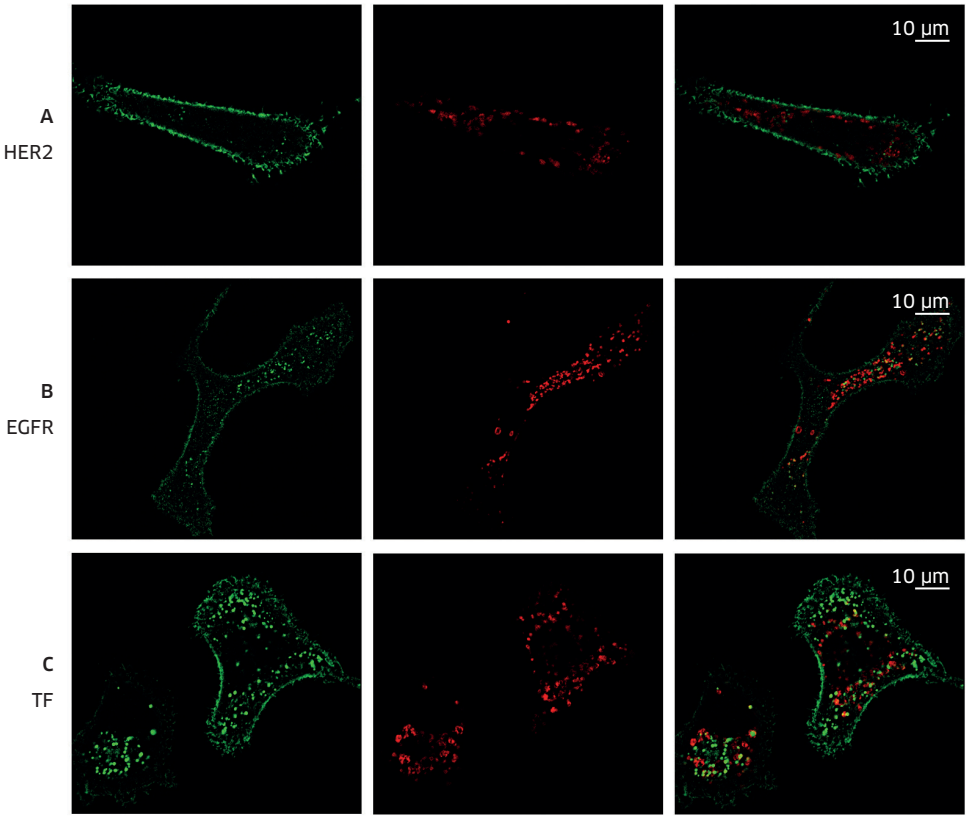

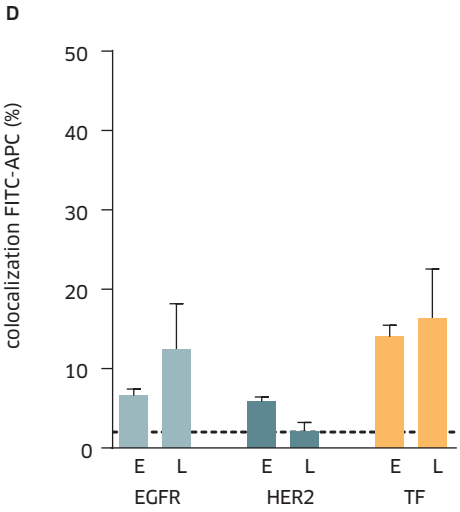

SUPPLEMENTARY FIGURE S1 *Distribution of HER2, EGFR and TF in unstimulated HCC1954 cells.* **(A-C, page 64)** Confocal microscopy images (12-bit) of unstimulated HCC1954 cells. The left panel shows staining of HER2 **(A)**, EGFR **(B)** and TF **(C)** with murine antibodies and goat anti-mouse IgG-FITC (green). In the middle panel lysosomes were stained with mouse anti-human LAMP1-APC (red). The right panel shows the overlay (yellow). **(D)** Quantification of endosomal and lysosomal receptor colocalisation. Each bar represents 4 different 12-bit images ± standard deviation. E=endosomes L=lysosomes.

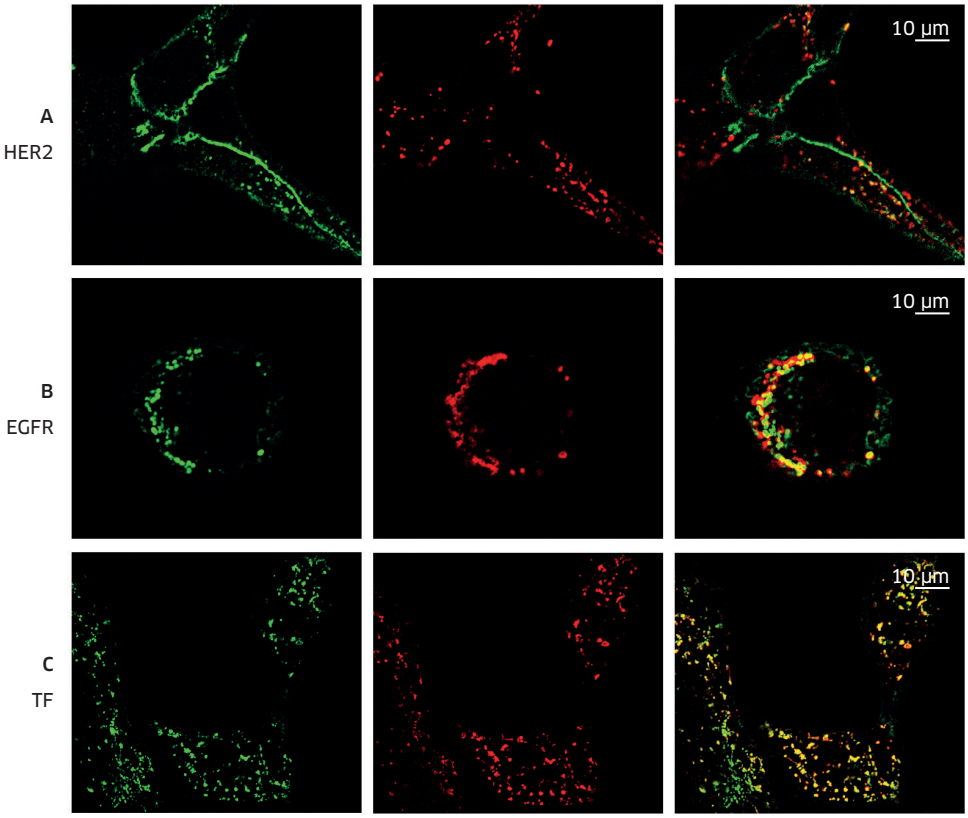
A
HER2
10 µm
B
EGFR
10 µm
C
TF
10 µm

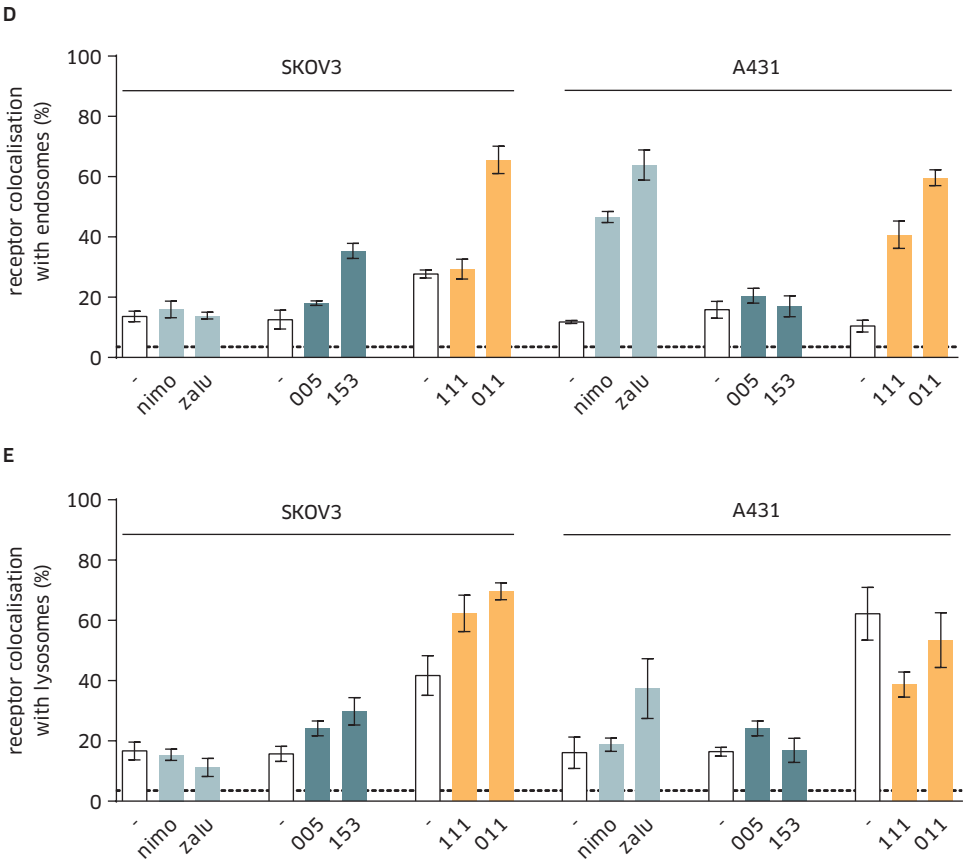

SUPPLEMENTARY FIGURE S2 *Endosomal and lysosomal colocalisation of TF, EGFR and HER2 in tumor cells after treatment with target-specific antibodies.* (**A-C, page 66)** Confocal analysis of SK-OV-3 cells demonstrating enhanced TF colocalisation with the lysosomal marker LAMP1 after incubation with TF-antibodies. Lysosomes were stained with mouse anti-human LAMP1-APC (red, middle panel). EGFR, HER2 and TF were stained with mouse monoclonal antibodies and visualized using goat anti-mouse IgG-FITC (green, left panel). Colocalisation of EGFR, HER2 and TF staining with the lysosomal marker LAMP1 is depicted in the overlay (yellow, right panel). (**D-E)** Pixel intensity of TF, HER2 and EGFR overlapping with **(D)** the endosomalmarker transferrin and **(E)** the lysosomal marker LAMP1, plotted as a percentage of total TF, HER2 and EGFR intensities. Data shown are mean ± standard deviation of 4 images. The dotted line indicates aspecific colocalisation.

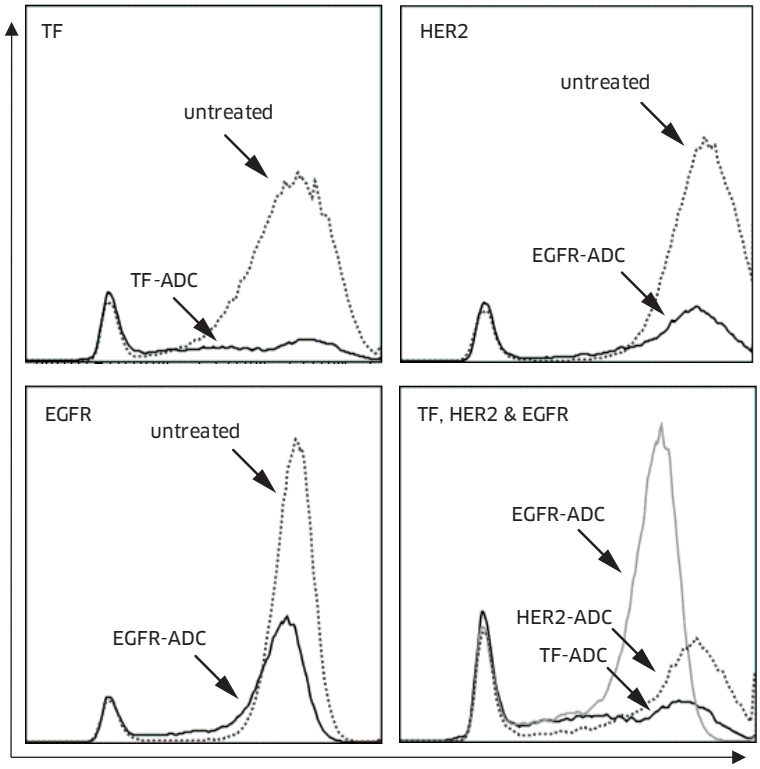

SUPPLEMENTARY FIGURE S3 *Flow cytometry analysis of SK-OV-3 cells after ADC-treatment.* Expression of TF, HER2 and EGFR on SK-OV-3 cells that survived ADC-treatment was analyzed using flow cytometry. Target expression was depicted on the X-axis as fluorescence intensity of APC. The number of surviving cells was depicted on the Y-axis as counts. The APC negative counts represent Jurkat cells that were spiked into each sample. Jurkat cells did not express EGFR, HER2 or TF and were used for quantification purposes.

4 An antibody-drug conjugate that targets tissue factor exhibits potent therapeutic activity against a broad range of solid tumors

► Cancer Res. 2014 Feb 15;74(4):1214-26.

► Esther C.W. Breij[1], Bart E.C.G. de Goeij[1], Sandra Verploegen[1], Danita H. Schuurhuis[1], Ali Amirkhosravi[3], John Francis[3], Vibeke Breinholt Miller[2], Mischa Houtkamp[1], Wim K. Bleeker[1], David Satijn[1] & Paul W.H.I. Parren[1]

1 Genmab, Utrecht, The Netherlands

2 Genmab, Copenhagen, Denmark

3 Center for Thrombosis Research, Florida Hospital, Orlando FL, United States

ABSTRACT

Tissue factor (TF) is aberrantly expressed in solid cancers and is thought to contribute to disease progression through its pro-coagulant activity and its capacity to induce intracellular signaling in complex with factor VIIa (FVIIa). To explore the possibility of using TF as target for an antibody-drug conjugate (ADC), a panel of human TF-specific antibodies (TF HuMab) was generated. Three TF HuMab, that induced efficient inhibition of TF:FVIIa-dependent intracellular signaling, antibody-dependent cell-mediated cytotoxicity and rapid target internalization, but had minimal impact on TF pro-coagulant activity *in vitro*, were conjugated with the cytotoxic agents monomethyl auristatin E (MMAE) or monomethyl auristatin F (MMAF). TF-specific ADCs showed potent cytotoxicity *in vitro* and *in vivo*, which was dependent on TF expression. TF-011-MMAE (HuMax-TF-ADC) was the most potent ADC and the dominant mechanism of action *in vivo* was auristatin-mediated tumor cell killing. Importantly, TF-011-MMAE showed excellent anti-tumor activity in patient-derived xenograft (PDX) models with variable levels of target TF expression, derived from seven different solid cancers. Complete tumor regression was observed in all PDX models, including models that showed TF expression in only 25-50% of the tumor cells. In conclusion, TF-011-MMAE is a promising novel anti-tumor agent with potent activity in xenograft models that represent the heterogeneity of human tumors, including heterogeneous target expression.

INTRODUCTION

Antibody-drug conjugates (ADCs), which combine the tumor-targeting capacity of monoclonal antibodies with the anti-tumor activity of cytotoxic agents, received renewed attention in recent years. Trastuzumab emtansine (T-DM1), an ADC composed of the HER2-specific antibody trastuzumab and the cytotoxic agent DM1, increased progression-free survival in patients that had received prior treatment with unconjugated trastuzumab [1], demonstrating the added value of toxin conjugation to a monoclonal antibody. In addition, brentuximab vedotin, a CD30-specific antibody coupled to the microtubule disrupting agent monomethyl auristatin E (MMAE), was approved for the treatment of relapsed Hodgkin's lymphoma and relapsed systemic anaplastic large cell lymphoma [2]. With at least thirty products in clinical development, ADCs represent an exciting new class of anti-cancer drugs.

Tissue factor (TF), also called thromboplastin, factor III or CD142, is aberrantly expressed in many solid cancers including pancreatic, lung, cervical, prostate, bladder, ovarian, breast and colon cancer. Expression has been described on tumor cells and the tumor vasculature, and has been associated with poor disease prognosis and increased metastatic properties (reviewed in [3]). This, in combination with the known

internalizing capacity of TF [4], led us to explore the possibility of using TF as a novel target for an ADC.

TF is the main physiological initiator of the extrinsic coagulation pathway. Proteolytic cleavage of factor VII (FVII), the physiological ligand of TF, generates activated FVII (FVIIa), which associates with TF to form the TF:FVIIa complex. This complex proteolytically activates coagulation factor X (FX) to generate FXa, eventually leading to thrombin generation and clot formation [5]. TF is expressed in a wide range of organs, including brain, heart, intestine, kidney, lung, placenta, uterus and testes [6]. Under physiological conditions, TF expression is mostly restricted to the cells of the sub-endothelial vessel wall, such as smooth muscle cells, pericytes and fibroblasts, that are not in direct contact with the blood [6]. In healthy individuals, blood leukocytes do not express TF on the cell surface, although TF expression has been described on 1-2% of monocytes [7,8]. Activation of the coagulation cascade occurs when membrane-bound TF is exposed to circulating FVII(a), for example after disruption of the vessel wall by injury or after up-regulation of TF on monocytes under inflammatory conditions [9].

In addition to initiation of coagulation, formation of the TF:FVIIa complex on the cell membrane induces an intracellular signaling cascade by activation of protease-activated receptor 2 (PAR-2), resulting in the production of pro-angiogenic factors, cytokines and adhesion molecules [10]. This signaling cascade is further amplified by coagulation factors generated downstream of the TF:FVIIa complex, such as FXa and thrombin, all of which recognize one or more receptors of the PAR family [10].

TF-expressing tumor cells are thought to exploit both TF pro-coagulant activity and TF:FVIIa-mediated intracellular signaling. Experimental tumor models showed that interference with TF using siRNA or monoclonal antibodies reduced tumor outgrowth, tumor-associated angiogenesis and metastatic potential *in vivo* [11-13]. Previous studies demonstrated that it is possible to generate TF-specific antibodies that have minimal impact on TF pro-coagulant capacity [13,14], potentially allowing specific targeting of TF-positive tumors without a major impact on hemostasis.

Here, we report the development of TF-011-MMAE, an ADC composed of a human TF-specific monoclonal antibody, a protease-cleavable linker and the potent cytotoxic agent MMAE. By carefully selecting TF-specific antibodies that interfere with TF:FVIIa-dependent intracellular signaling, but not with TF pro-coagulant activity, and that show efficient internalization and lysosomal targeting, we developed an ADC that efficiently kills tumor cells *in vivo* with only minimal effect on parameters of coagulation. TF-011-MMAE was extensively tested in pre-clinical efficacy studies, including studies in patient-derived xenograft (PDX) models that showed heterogeneous target expression.

MATERIALS AND METHOD

Cells

Human tumor cell lines AsPC-1 (pancreas adenocarcinoma; 100,000-300,000 TF molecules/cell), BxPC-3 (pancreas adenocarcinoma; >350,000 TF molecules/cell), HCT-116 (colorectal carcinoma; <15,000 TF molecules/cell), HPAF-II (pancreas adenocarcinoma; >350,000 TF molecules/cell), MDA-MB-231 (breast adenocarcinoma; >350,000 TF molecules/cell), SK-OV-3 (ovarian adenocarcinoma; 50,000-175,000 TF molecules/cell) and TOV-21G (ovarian adenocarcinoma; <7,000 TF molecules/cell) were obtained from the American Type Culture Collection. The epidermoid adenocarcinoma cell line A431 (>300,000 TF molecules/cell) was obtained from the Deutsche Sammlung von Mikroorganismen und Zellkulturen GmbH, and HaCaT human keratinocytes (150,000-200,000 TF molecules/cell) were a kind gift from Dr. Wiiger (Biotechnology Center of Oslo, Norway). To guarantee cell line authenticity, cell lines were aliquoted and banked, and cultures were grown and used for a limited number of passages before starting a new culture from stock. Cell lines were routinely tested for mycoplasma contamination. TF cell surface expression was quantified by QIFIKIT analysis (DAKO) according to the manufacturer's guidelines, using a mouse anti-human TF antibody (R&D systems).

Recombinant expression of full-length TF or the TF extracellular domain

A codon-optimized construct was generated for the expression of full-length TF (Genbank accession NP001984), cloned into the mammalian expression vector pEE13.4 (Lonza Biologics) and transfected into Freestyle™ 293-F cells (HEK-293F, Invitrogen) or NSO cells as described [15]. To generate recombinant His-tagged soluble TF, PCR was used to amplify the part encoding the extracellular domain (aa 1-251) of TF from the construct, adding a C-terminal His tag containing 6 His residues (TF-ECDHis). The construct was cloned in pEE13.4 and expressed in HEK-293F cells. TF-ECDHis was purified from cell supernatant using immobilized metal affinity chromatography.

Generation of human TF-specific antibodies and ADCs

Human IgG1κ TF-specific antibodies (TF HuMab) were generated by immunization of HuMAb mice (Medarex) [16] with TF-ECDHis and/or TFexpressing NSO cells. Hybridomas were generated from mice that showed TF-specific antibodies in serum, as assessed by binding to TF-transfected HEK293F or A431 cells, or to bead-coupled TF-ECDHis using Fluorimetric Microvolume Assay Technology (Applied Biosystems). TF-specific hybridomas were identified by screening supernatants for TF-specific antibodies as described above. To determine the antibody variable region sequences of TF-specific hybridomas, mRNA was extracted and the immunoglobulin variable heavy and light chain regions were amplified, cloned and sequenced. Recombinant antibodies were generated as described [17], and the recombinant IgG1κ was used for further characterization of the TF HuMab. Fab fragments were generated as de-

scribed [17]. The IgG1κ antibodies IgG1-b12 [18] and HuMab-KLH [19] were included as isotype control antibodies.

Antibodies TF-011, -098 and -111, as well as IgG1-b12, were conjugated with MMAE through a protease-cleavable valine-citrulline (vc) dipeptide and a maleimido-caproyl-containing (mc) linker, or with monomethyl auristatin F (MMAF) through an mc linker as described [20,21]. The average drug-antibody ratio was 4:1.

Flow cytometry

Binding of TF HuMab and TF-ADCs to membrane-bound TF was analyzed by flow cytometry as described [22], using phycoerythrin (PE)-conjugated goat anti-human IgG (Jackson ImmunoResearch Laboratories) to detect binding of TF HuMab or ADCs.

Biacore analysis

The affinity of TF HuMab for TF was measured by surface plasmon resonance in a Biacore 3000 (GE Healthcare). TF HuMab were immobilized on a CM-5 sensor chip (GE Healthcare), according to the manufacturer's guidelines, and a concentration series of TF-ECDHis was injected over the HuMab (30 µL/min; 180 seconds). The HuMab surface was regenerated using 10 mM glycine-HCl pH 2.0. Kinetic analysis was performed using double reference subtraction and model 1:1 (langmuir) binding analysis.

FVIIa ELISA

TF-ECDHis (0.5 µg/mL) was immobilized and incubated with recombinant FVIIa (100 nM, Novo Nordisk) in the presence of TF HuMab (1 hour (h), room temperature (RT)). Plates were washed and incubated with rabbit-anti-FVIIa (2.5 µg/mL; Abcam), followed by incubation with swine-anti-rabbit IgG-HRP (1:2,500; DAKO). Binding was visualized as described [17].

Phosphorylation inhibition assay – Western Blot

BxPC-3 or HaCaT cells were cultured in serum-free medium for 1.5 h, prior to pre-incubation with TF HuMab (30 min, 37°C). Next, cells were stimulated with 10 nM FVIIa (10 min, 37°C) and lysed. Phosphorylated ERK1/2 (p-ERK1/2) and total ERK1/2 were detected in cell lysates by Western Blot using standard procedures, using rabbit anti-p-ERK1/2 and rabbit-anti-ERK1/2 (Cell Signaling technology) as primary antibodies, and donkey-anti-rabbit-IgG-HRP (Jackson Immunoresearch) as detection antibody.

IL-8 release assay

MDA-MB-231 cells were cultured in serum-free medium for 105 min, prior to incubation with TF HuMab (15 min). FVIIa (10 nM) was added and after 5 h (37°C), IL-8 production was measured in culture supernatant by ELISA (Sanquin), according to the manufacturer's protocol.

FXa generation assay

Recombinant lipidated full-length TF (Innovin; Dade Behring) was incubated with TF HuMab in HEPES buffer containing 3 mM $CaCl^2$ (30 min, RT). FXa generation was initiated by adding 1 nM recombinant FVIIa and 200 nM FX (Enzyme Research Laboratories). After 30 min (37˚C), the reaction was stopped by adding 5 mM EDTA in HEPES buffer, and FXa was detected by measuring conversion of the FXa substrate Chromogenix-2765 (Instrumation Laboratory Company) according to the manufacturer's guidelines.

Thromboelastography

Citrated human whole blood was obtained from healthy volunteers with the donor's consent and approval from the Ethical committee of the Florida Hospital Center. Whole blood was incubated with 10 µg/mL lipopolysaccharide (LPS) or PBS without Ca^{2+} and Mg^{2+} (4 h, 37ºC), followed by incubation with TF HuMab (10 min, RT). Thromboelastography was performed as described [23]. In this system, the LPS-induced decrease in clotting lag time (R) represents a measure for TF activity. Antibody-mediated inhibition of TF activity was calculated as follows: % inhibition of TF activity = $100 - ([R_{No\text{-}LPS} - R_{test\ item+LPS}] / [R_{No\text{-}LPS} - R_{isotype\text{-}mAb+LPS}] \times 100)$.

Immunofluorescent confocal microscopy

SK-OV-3 and A431 cells were grown on glass coverslips (Thermo Fisher Scientific) at 37˚C for 16 h. Cells were incubated with 50 µg/mL leupeptin (Sigma) for 1 h to block lysosomal activity, followed by incubation with 1 µg/mL TF HuMab (1, 3 or 24 h, 37˚C). Cells were fixed with 4% formaldehyde (30 min, RT) and stained with fluorescein isothiocyanate (FITC)-labeled goat anti-human IgG (Jackson Immunoresearch) to identify TF HuMab, and mouse anti-human CD107a (LAMP-1)-allophycocyanin (APC) (BD Pharmingen) to identify lysosomes. Staining was analyzed with a Leica SPE-II confocal microscope and LAS-AF software.

Fab-TAMRA/QSY7 internalization and degradation assay

Goat-anti-human IgG Fab-fragments (Jackson Immunoresearch) were conjugated with the fluorophore and quencher pair TAMRA/QSY7 (Fab-TAMRA/QSY7) as described [24]. TF HuMab (1 µg/mL) were pre-incubated with Fab-TAMRA/QSY7 (2 µg/mL; 30 min, 4ºC) and the complex was added to SK-OV-3 or A431 cells while shaking (200 rpm, 37ºC). After 24 h, TAMRA-fluorescence was measured on a FACS Canto-II (BD Biosciences).

Cytotoxicity assay *in vitro*

Cells were seeded in 96-well plates (2,500-5,000 cells/well) and incubated for 6 h (37ºC), before adding ADCs. After 3-5 days (37ºC), the viability of the culture was assessed using Alamar Blue (Biosource International), according to the manufacturer's guidelines. Staurosporine (Sigma, 10 µg/mL) was used a positive control (100%

cell death) and untreated cells were used as a negative control. The percentage of viable cells was calculated as follows: % viable cells = [(fluorescence test sample – fluorescence staurosporine)/(fluorescence untreated cells-fluorescence staurosporine)]*100.

Antibody-dependent cell-mediated cytotoxicity (ADCC) assay

Lysis of tumor cells by ADCC was measured in a ^{51}Cr release assay as described [25], using A431, BxPC-3 and MDA-MB-231 cells as target cells and human peripheral blood mononuclear cells (PBMC), isolated from healthy donors (Sanquin), as effector cells.

Immunohistochemical analysis of TF expression in PDX models

A tissue microarray (TMA) containing formalin-fixed, paraffin-embedded (FFPE) PDX tissue (Oncotest GmbH) was incubated with FITC-labeled TF-011 or mouse anti-human cytokeratin antibody (Cell Marque) (1 h, RT), after antigen retrieval (citrate/EDTA buffer, pH8, in a pressure cooker for 5 min for TF-011-FITC and citrate buffer, pH6, for mouse anti-cytokeratin). Endogenous peroxidase (PO) activity was exhausted by incubation with H_2O_2 and non-specific antibody binding was blocked using chicken serum or normal human serum. Binding of TF-011-FITC was detected using rabbit anti-FITC (Zymed) and Powervision (anti-rabbit IgG1)-PO (Leica Biosystems). Mouse-anti-cytokeratin binding was detected using Ultravision-PO (Thermo Scientific). PO was visualized with amino-ethyl-carbazole, resulting in a red color. Nuclei were visualized using hematoxylin. Immunostaining was scored manually, by estimating the TF-positive tumor area in relation to the total tumor area as identified by human cytokeratin staining. The TF-positive tumor area was scored according to the following intervals: 0 (no TF-positive cells), 0-25%, 25-50%, 50-75% or >75% TF-positive cells.

Xenograft models

Cell line-derived xenograft models were established in female SCID mice by subcutaneous (s.c.) injection of $2\text{-}10*10^6$ (HPAF-II), $5*10^6$ (A431, AsPC-1 and BxPC-3) or $0.5*10^6$ (HCT-116) tumor cells as described [22]. TF HuMab were injected intraperitoneally 1 h after tumor injection (prophylactic treatment) or when tumors had reached a size of 100-400 mm^3 (therapeutic treatment, starting between day 8-13). All experiments were approved by the Utrecht University Animal Ethics Committee. PDX models were initiated by s.c. implantation of human tumor fragments in the flanks of NMRI nu/nu mice at Oncotest GmbH (Freiburg, Germany). When tumors had reached a size of 80-200 mm^3, mice were treated intravenously with 4 mg/kg ADC or 20 mg/kg paclitaxel (Teva-Gry Pharma). Tumor volume was determined as described above. All experiments were conducted according to the guidelines of the German Animal Welfare Act (Tierschutzgesetz).

Statistical analyses

Data were analyzed using GraphPad Prism 5 software. For mouse xenograft studies, differences in tumor size between treatment groups were analyzed by one-way ANOVA, using mean tumor sizes from the last day that all groups were complete (i.e. before mice in isotype control groups had to be sacrificed due to large tumor burden).

RESULTS

Target binding characteristics of TF HuMab

From a large panel of human TF-specific IgG1κ antibodies (TF HuMab), eight clones were selected for extensive functional characterization *in vitro* and *in vivo*. All TF HuMab showed dose-dependent binding to TF-positive MDA-MB-231 breast cancer cells (Figure 1A). EC_{50} values ranged from 0.07 µg/mL for TF-011 to 0.49 µg/mL for TF-109 (sub-nanomolar to nanomolar range) (Supplementary Table S1). Similar results were obtained using BxPC-3 pancreas adenocarcinoma and A431 epidermoid carcinoma cells (data not shown). Biacore analysis demonstrated that TF HuMab bound TF with affinities ranging from 1.8 nM for TF-025 to 307 nM for TF-098 (Supplementary Table S1).

TF-specific antibodies interfere with TF:FVIIa-mediated intracellular signaling

TFspecific antibodies may interfere with the interaction between TF and FVIIa, possibly resulting in inhibition of TF:FVIIa-dependent intracellular signaling. To measure competition between TF HuMab and FVIIa for TF binding, FVIIa was incubated with TF-ECDHis in the presence of TF HuMab and binding of FVIIa was detected by ELISA. Except for TF-044 and TF-013, TF HuMab efficiently inhibited binding of FVIIa to TF, with only 9-21% of FVIIa binding remaining at the highest antibody concentration tested (30 µg/mL) (Figure 1B, Table 1).

Next, the capacity of TF HuMab to interfere with TF:FVIIadependent PAR-2 signaling was assessed by measuring antibody-mediated inhibition of ERK1/2 phosphorylation and IL-8 production, both of which have been implicated in tumor cell proliferation, migration and metastatic potential [26,27]. When pre-incubated with BxPC-3 or HaCaT cells, all TF HuMab, except TF-013, inhibited TF:FVIIa-induced ERK phosphorylation, as shown by Western Blot analysis (Figure 1C and data not shown). Inhibition of TF:FVIIa-induced ERK phosphorylation was confirmed in A431 cells using Alphascreen, which allowed more quantitative detection of p-ERK1/2 (Table 1, Supplementary Figure S1). The TF HuMab that showed efficient inhibition of ERK1/2 phosphorylation, also inhibited TF:FVIIa-dependent production of IL-8 by MDA-MB-231 cells when antibodies were allowed to bind the cells before stimulation with FVIIa (Figure 1D). In the reverse experiment, where the tumor cells were incubated with FVIIa prior to adding TF HuMab, inhibition of TF:FVIIa-induced IL-8

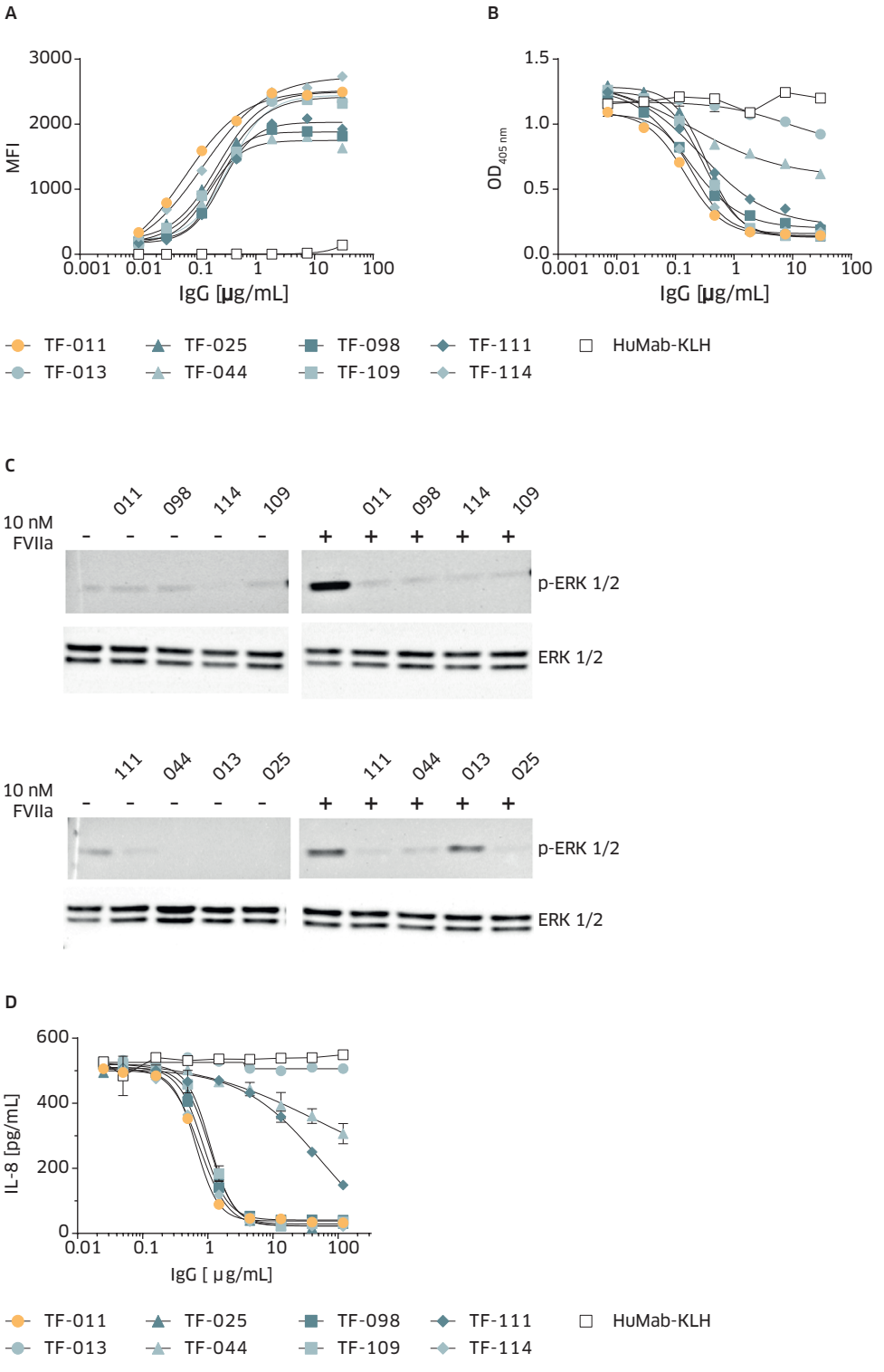
A
B
MFI
IgG [µg/mL]
OD405 nm
TF-011
TF-013
TF-025
TF-044
TF-098
TF-109
TF-111
TF-114
HuMab-KLH
C
10 nM FVIIa
011
098
114
109
p-ERK 1/2
ERK 1/2
111
044
013
025
D
IL-8 [pg/mL]
IgG [µg/mL]

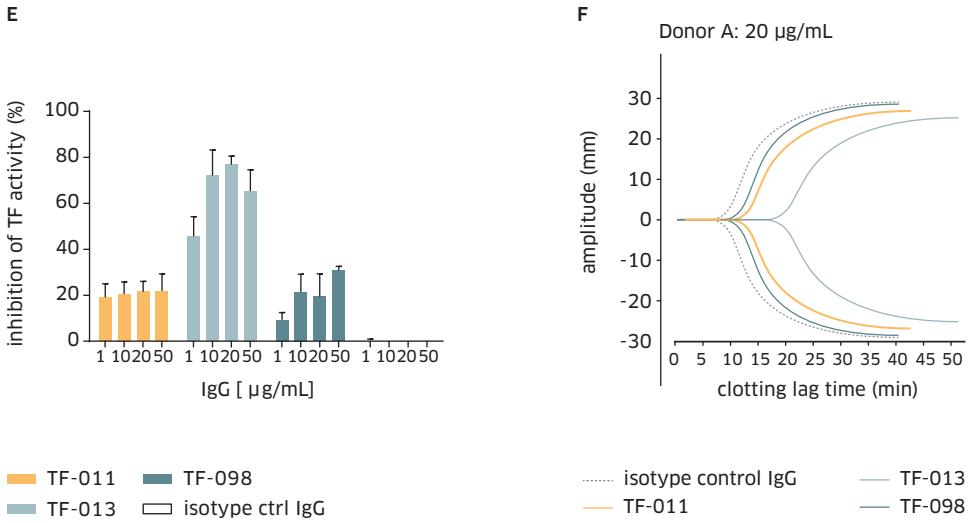

FIGURE 1 Functional characteristics of TF HuMab *in vitro*. **(A)** Binding of TF HuMab to MDA-MB-231 cells as assessed by flow cytometry. Results from a representative experiment are shown (n=3). **(B)** Competition between TF HuMab and FVIIa for TF binding. FVIIa was incubated with TF-ECDHis in the presence of TF HuMab, and binding of FVIIa was measured by ELISA. Results from a representative experiment are shown (n=3), error bars indicate SEM. **(C)** TF:FVIIa-induced ERK phosphorylation in the presence of TF HuMab. BxPC-3 cells were incubated with FVIIa after pre-incubation with TF HuMab, and p-ERK1/2 and total ERK1/2 were detected in cell lysates by Western Blot. Full-length blots are presented in Supplementary Figure S7. **(D)** TF:FVIIa-induced IL-8 production in MDA-MB-231 cells in the presence of TF HuMab. Cells were incubated with TF HuMab prior to stimulation with FVIIa. IL-8 production was measured in cell culture supernatants using ELISA. Results from a representative experiment are shown (n=3), error bars indicate SEM. **(E, F)** Effect of TF HuMab on whole blood coagulation as assessed by thromboelastography. Citrated whole blood was incubated with LPS to induce TF expression, followed by incubation with TF HuMab. Coagulation was initiated by re-calcification. **(E)** Inhibition of TF activity in the presence of TF HuMab. TF activity was defined as the difference in clotting lag time **(R)** between unstimulated and LPS-stimulated whole blood. TF HuMab-mediated inhibition of TF activity was expressed the percentage change in TF activity. Data represent the average of 3 donors, error bars represent SEM. **(F)** TEG trace overlays of coagulation in the presence of 20 µg/mL TF-011, TF-013, TF-098 or an isotype control IgG. Results from a representative donor are shown (n=3).

production was clearly less efficient, confirming competition between FVIIa and TF HuMab for TF binding (Supplementary Figure S2). In agreement with poor inhibition of FVIIa binding, TF-044 only moderately inhibited TF:FVIIa-dependent intracellular signaling, whereas TF-013 showed almost no inhibition.

These results suggest that TF HuMab recognize distinct functional epitopes in the TF extracellular domain. This was confirmed in a cross-competition study, which indicated that TF-011, -025, -098, -111, -109 and -114 bind different, but overlapping,

epitopes, whereas TF-013 and TF-044 recognize a non-overlapping epitope (Supplementary Table S2).

TF HuMab show minor interference with FXa generation and coagulation *in vitro*

Proteolytic activation of FX by the TF:FVIIa complex, generating FXa, is an important step in the extrinsic coagulation pathway. Depending on the binding domain, TF-specific antibodies may interfere with binding of FX to the catalytic domain of TF:FVIIa, thereby impairing FXa generation and coagulation [14]. None of the TF HuMab in our panel substantially inhibited FXa generation as shown in a chromogenic FXa generation assay (Table 1). TF-013 induced the highest inhibition of FXa generation, but even for this antibody, the reduction in FXa activity was maximally 22%.

The impact of TF HuMab (TF-011, TF-013 and TF-098) on whole blood coagulation was assessed by thromboelastography (TEG). Citrated whole blood, obtained from healthy donors, was incubated with LPS to activity (66%). Results obtained at 10, 20 and 50 µg/mL TF HuMab were comparable (Figure 1E). TF HuMab did not have impact on other parameters of clot formation such as the clot kinetics (K-value and α angle) or clot strength (maximal amplitude), as shown by the similar shape of the TEG trace in the presence or absence of TF HuMab (Figure 1F, Supplementary Table S3). This was as expected, as TF is thought to be important for the initiation but not the amplification or propagation of coagulation [9].

	FVIIa binding[a]		ERK phosphorylation[b]		IL-8 release[c]		
HuMab	**IC_{50} (SD) µg/mL**	**Maximal inhibition[d] (SD) %**	**IC_{50} (SD) µg/mL**	**Maximal inhibition[e] (SD) %**	**IC_{50} (SD) µg/mL**	**Maximal inhibition[f] (SD) %**	**FXa generation Maximal inhibition[g] (SD) %**
TF-011	0.19 (0.07)	91 (3)	0.12 (0.03)	69 (4)	1.4 (0.4)	62 (6)	19 (9)
TF-013	2.9 (4.2)	27 (10)	1.37 (0.31)	26 (6)	NA	0 (14)	22 (8)
TF-025	0.33 (0.01)	90 (2)	0.33 (0.06)	66 (0)	3.5 (2.7)	76 (5)	9 (2)
TF-044	0.21 (0.04)	54 (10)	60 (NA)	45 (5)	11.2 (4.8)	17 (19)	0 (3)
TF-098	0.16 (0.04)	85 (4)	0.28 (0.06)	64 (5)	1.4 (0.4)	59 (20)	14 (1)
TF-109	0.23 (0.10)	90 (2)	0.36 (0.08)	72 (4)	2.0 (0.8)	70 (14)	4 (1)
TF-111	0.33 (0.14)	79 (7)	>10,000	52 (1)	>10,000	40 (39)	0 (5)
TF-114	0.20 (0.05)	90 (4)	0.16 (0.05)	68 (0)	1.4 (0.7)	72 (6)	10 (4)

TABLE 1 *Tissue factor HuMab: functional characteristics in vitro.* [a]FVIIa ELISA, average of three experiments. [b]Alphascreen Surefire ERK assay, A431 cells, average of two experiments. [c]MDA-MB-231 cells, average of three experiments. [d-f]Inhibition measured at plateau of dose-response curve, at 30 µg/mL ([d]), 10 µg/mL ([e]) or 120 µg/mL ([f]). [g]Inhibition (percentage) measured at plateau of dose-response curve (at 0.9 µg/mL IgG); average of two experiments.

TF HuMab are rapidly internalized after target binding

Since ADCs generally rely on internalization for release of the payload, we characterized the internalization characteristics of TF HuMab in the TAMRA/QSY7 assay. This assay uses a fluorophore (TAMRA) and quencher (QSY7) pair. In close proximity, e.g. upon conjugation to the same protein, TAMRA fluorescence is quenched by QSY7. TF HuMab were complexed with TAMRA/QSY7-conjugated anti-human IgG Fab fragments (Fab-TAMRA/QSY7), and the complex was incubated with A431 or SK-OV-3 cells. After 6 h, TAMRA fluorescence was detected in cells that had been incubated with TF-011, TF-098 or TF-111 (Figure 2A-B), indicating internalization of the HuMab-Fab-TAMRA/QSY7 complex and degradation in the reducing environment of the endosomes and lysosomes. Internalization was most efficient for TF-011 and TF-098. Interestingly, internalization of TF-011 was reduced when Fab fragments were used instead of the intact antibody (Figure 2B), suggesting that internalization of TF-011 is stimulated by bivalent target binding. Efficient internalization of TF-011 was confirmed by confocal microscopy. 1 h after incubation with SK-OV-3 cells, TF-011 was already detectable in intracellular vesicles, some of which co-localized with the lysosomal marker LAMP-1, indicating internalization and lysosomal targeting. Co-localization of TF-011 and LAMP-1 was enhanced after 3 h, and after 24 h, most TF-011 co-localized with LAMP-1, indicating efficient accumulation in the lysosomal compartment (Figure 2C). Similar results were obtained with A431 cells (data not shown).

Our results demonstrate that TF HuMab are rapidly internalized and degraded upon target binding, indicating that TF may be a very suitable ADC target.

Generation of TF-specific ADCs and cytotoxicity *in vitro*

TF-specific ADCs were generated by conjugation of TF-011, -098 and -111 with the dolastatin analogs MMAE or MMAF. Auristatins are potent cytotoxic agents that induce cell death by disrupting microtubules [20,21]. MMAE was conjugated through the protease-cleavable vc linker, and can therefore be released from the antibody by lysosomal proteases, such as cathepsin B [21]. MMAF was conjugated through a non-cleavable linker, and relies on intracellular degradation of the ADC for release [20]. TF HuMab were conjugated with an average of four auristatins per antibody, a ratio that was shown to provide the optimal therapeutic index for brentuximab vedotin [29]. Direct comparison of TF HuMab and TF-specific ADCs (TF-ADCs) *in vitro*, confirmed that target binding and internalization characteristics were preserved in the ADCs (Figure 2A, Supplementary Figure S3).

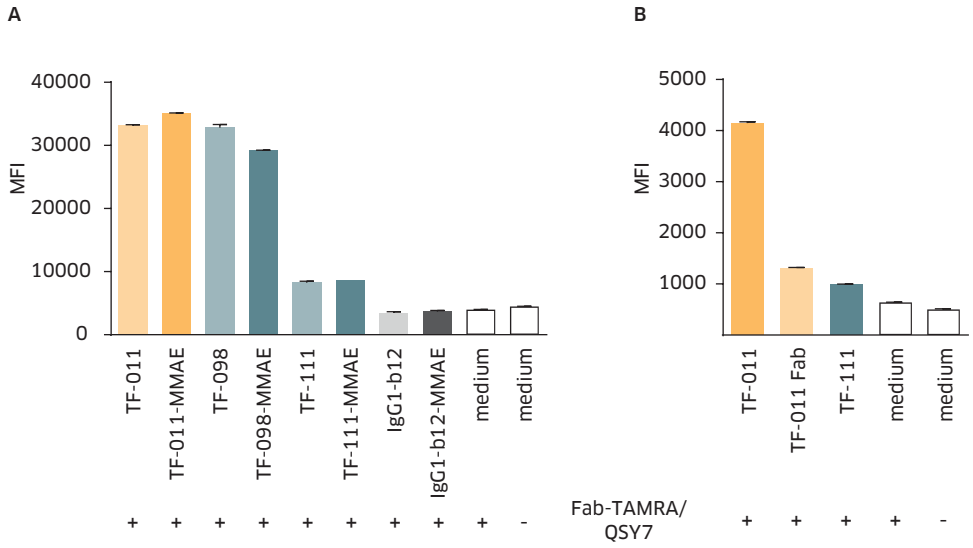
A
40000
30000
20000
10000
0
MFI
TF-011
TF-011-MMAE
TF-098
TF-098-MMAE
TF-111
TF-111-MMAE
IgG1-b12
IgG1-b12-MMAE
medium
medium
+ + + + + + + + + -
B
5000
4000
3000
2000
1000
MFI
TF-011
TF-011 Fab
TF-111
medium
medium
Fab-TAMRA/ QSY7
+ + + + -

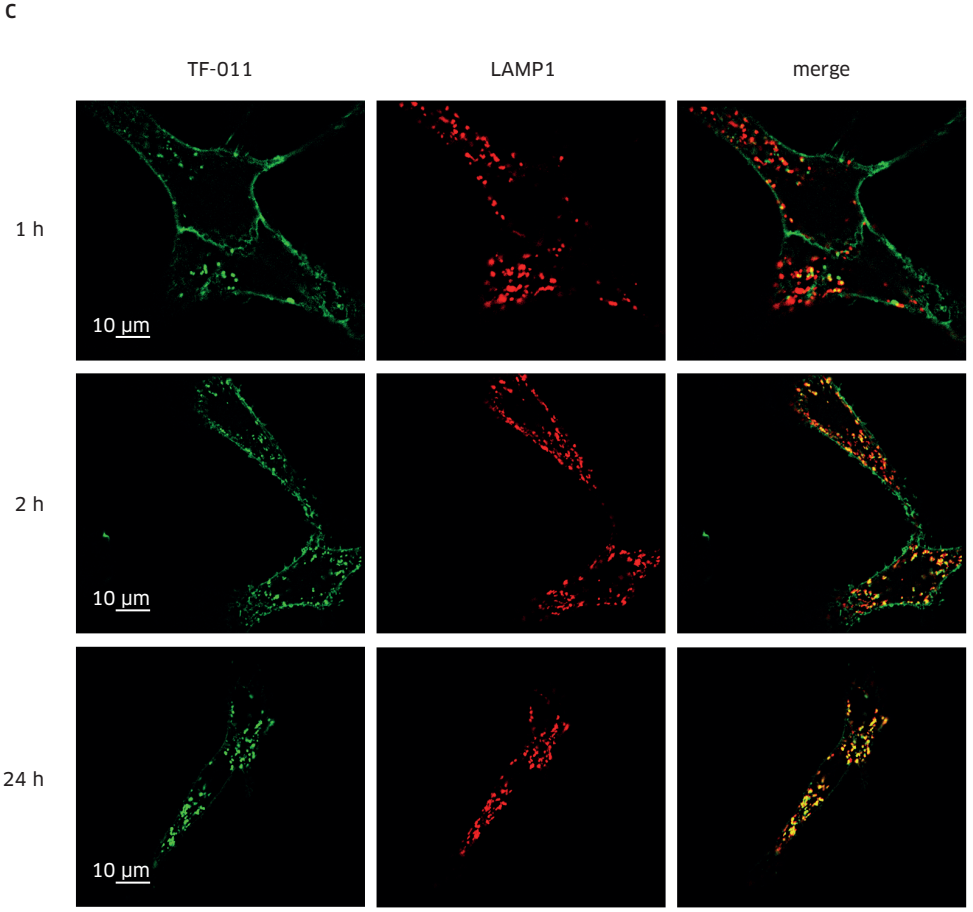
C
TF-011
LAMP1
merge
1 h
2 h
24 h
10 µm
10 µm
10 µm

FIGURE 2 *TF HuMab are rapidly internalized and trafficked to the lysosomes.* **(A, B)** TF HuMab or TF-ADCs were complexed with anti-human Fab-fragments that had been conjugated with the fluorophore and quencher pair TAMRA/QSY7 (Fab-TAMRA/QSY7), and the complex was added to A431 **(A)** or SK-OV-3 **(B)** cells. Upon internalization and degradation of the complex, dissociation of TAMRA and QSY results in de-quenching of TAMRA. The resulting fluorescent signal was measured by flow cytometry. Error bars indicate SEM of duplicates. **(C)** SK-OV-3 cells were incubated with TF-011 in the presence of an inhibitor of lysosomal degradation. After 1, 3 or 24 h, cells were fixed and TF-011 and the lysosomal protein LAMP-1 were detected using confocal microscopy. Left panel = TF-011 (green), middle panel = LAMP-1 (red), right panel = merge (yellow).

TF-ADCs showed excellent cytotoxicity *in vitro*. TF-ADCs efficiently and dose-dependently killed A431 and HPAF-II cells (Figure 3A,B), which express high levels of TF on the plasma membrane (>300,000 molecules per cell). The EC_{50} for TF-ADC-mediated tumor cell killing in A431 and HPAF-II cells ranged from 4-10 ng/mL, for TF-011-MMAE and TF-098-MMAE, to 5-80 ng/mL, for TF-111-MMAF. In cell lines that showed low (HCT-116; <15,000 molecules per cell) or very low (TOV-21G; <7,000 molecules per cell) TF expression, TF-ADCs showed very limited or no cytotoxic activity (Figure 3C,D). Similarly, TF-ADCs did not show cytotoxic activity in TF-negative tumor cells (data not shown). This, in addition to the lack of cytotoxic activity of the non-binding control ADCs IgG1-b12-MMAE and IgG1-b12-MMAF, indicates that the efficacy of TF-ADCs is dependent on target expression.

Unconjugated TF HuMab did not induce direct cytotoxicity *in vitro* (data not shown), indicating that the cytotoxicity of TF-ADCs was auristatin-dependent.

TF HuMab and TF-ADCs efficiently induce ADCC *in vitro*

Monoclonal antibodies of the IgG1 isotype may exert cytotoxicity through Fc-mediated effector functions such as ADCC, and these effector mechanisms may be preserved upon conjugation with cytotoxic agents [30]. Unconjugated TF-011, TF-098 and TF-111 potently induced killing of A431 cells by ADCC (Figure 3E), with median EC_{50} values of 15 ng/mL (range 0.5-19 ng/mL), 18 ng/mL (range 5.0-57 ng/mL) and 76 ng/mL (range 15-102 ng/mL), respectively. Similar results were observed with BxPC-3 and MDA-MB-231 cells (data not shown). Importantly, the capacity to induce ADCC was preserved after conjugation with MMAE (Figure 3E).

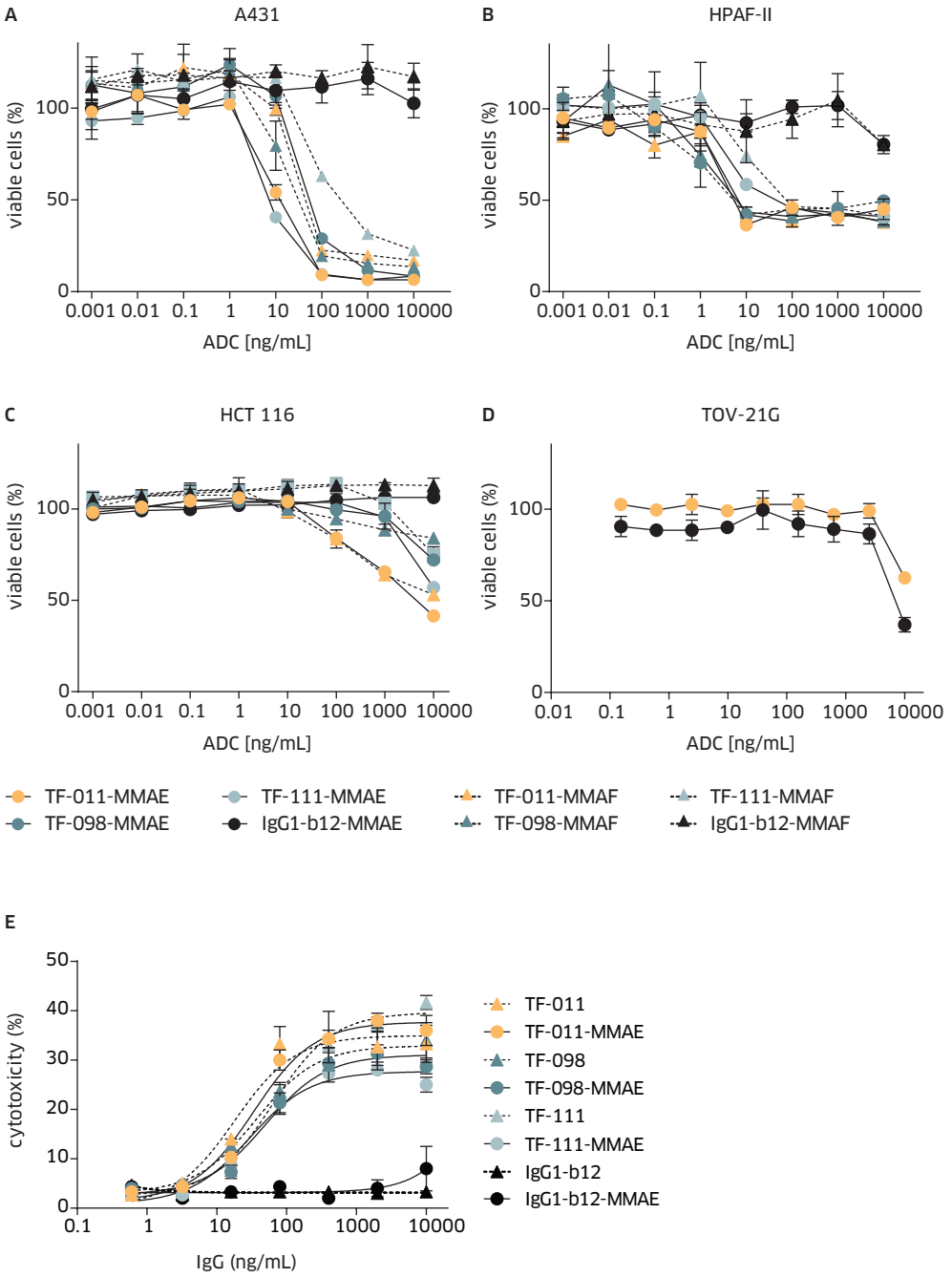
A
A431
B
HPAF-II
C
HCT 116
D
TOV-21G
viable cells (%)
ADC [ng/mL]
0.001 0.01 0.1 1 10 100 1000 10000
0.01 0.1 1 10 100 1000 10000
0 50 100
TF-011-MMAE
TF-098-MMAE
TF-111-MMAE
IgG1-b12-MMAE
TF-011-MMAF
TF-098-MMAF
TF-111-MMAF
IgG1-b12-MMAF
E
cytotoxicity (%)
IgG (ng/mL)
0.1 1 10 100 1000 10000
0 10 20 30 40 50
TF-011
TF-011-MMAE
TF-098
TF-098-MMAE
TF-111
TF-111-MMAE
IgG1-b12
IgG1-b12-MMAE

FIGURE 3 *Cytotoxicity of TF-specific ADCs in vitro.* **(A-D)** Cells were incubated in the presence of TF-ADCs and the viability of the cultures was assessed after 3-5 days using the Alamar Blue assay. IgG1-b12-MMAE and IgG1-b12-MMAF were included as isotype control ADCs. Curves represent dose-dependent cytotoxicity of TF-ADCs in the different cell lines. Results are representative of at least two experiments, error bars represent SEM. The inserts show TF expression in the different cell lines as assessed by flow cytometry, using 1 µg/mL mouse-anti-TF antibody (black lines) or an isotype control IgG (filled grey histograms). **(A-B)** Cytotoxicity of TF-ADCs in **(A)** A431 and **(B)** HPAF-II cells, which show high TF expression on the cell surface (>300,000 TF molecules/cell). **(C-D)** Cytotoxicity of TF-ADCs in cell lines with low (C; HCT-116, <15,000 molecules/cell) or very low (D; TOV-21G, <7,000 molecules/cell) TF expression. **(E)** TF HuMab and TF-ADCs induce ADCC. 51_{cr}-labeled A431 cells were incubated with TF HuMab or TF-ADCs in the presence of freshly isolated PBMC, as a source of effector cells. 51_{cr} release was measured to assess cytotoxicity, and the percentage kill was calculated. Results are representative of experiments performed with PBMC from six (TF HuMab) or two (TF-ADC) different donors. Error bars indicate SEM.

Anti-tumor activity of TF-specific ADCs in cell line-derived xenograft models

All TF-ADCs potently inhibited tumor growth in established xenografts derived from HPAF-II and A431 cells, at a dose of 3 mg/kg (four injections in two weeks; Figure 4A and Supplementary Figure S4A). MMAE-conjugates showed significantly better efficacy than their MMAF-conjugated counterparts (Figure 4B, Supplementary Figure S4B). Complete tumor regression, i.e. no measurable tumor remaining at 20-30 days after the last treatment, was observed for most mice in the TF-098-MMAE and TF-111-MMAE treatment groups, and for all mice in the TF-011-MMAE group. Strikingly, 3 out of 7 mice that had been treated with TF-011-MMAE, remained tumor-free until the end of the study (139 days after discontinuation of treatment). In mice that did show tumor recurrence after treatment with TF-011-MMAE (4 out of 7 mice in the HPAF-II model), measurable tumors were not detected until 56-70 days after discontinuation of treatment. Recurring tumors could successfully be re-treated with TF-011-MMAE, TF-098-MMAE or TF-111-MMAE (Figure 4C; Supplementary Figure S4C), indicating that TF expression was maintained in tumor cells that showed outgrowth after completion of the first treatment cycle.

The isotype control ADCs IgG1-b12-MMAE and IgG1-b12-MMAF did not inhibit tumor growth, indicating that the efficacy of TF-ADCs was dependent on target binding. This was supported by the lack of activity of TF-ADCs in the low TF expressing HCT-116 xenograft model (Supplementary Figure S4D).

To study the potential contribution of ADCC and inhibition of TF:FVIIa-dependent intracellular signaling to the anti-tumor activity of TF-ADCs *in vivo*, xenograft studies were performed using unconjugated TF-011, TF-098 or TF-111. Prophylactic treatment with TF-011, TF-098 or TF-111 significantly reduced outgrowth of BxPC-3, HPAF-II, AsPC-1 and A431 xenografts (Supplementary Figure S5A-D and data not shown). When treatment was initiated after the tumors had established (therapeutic

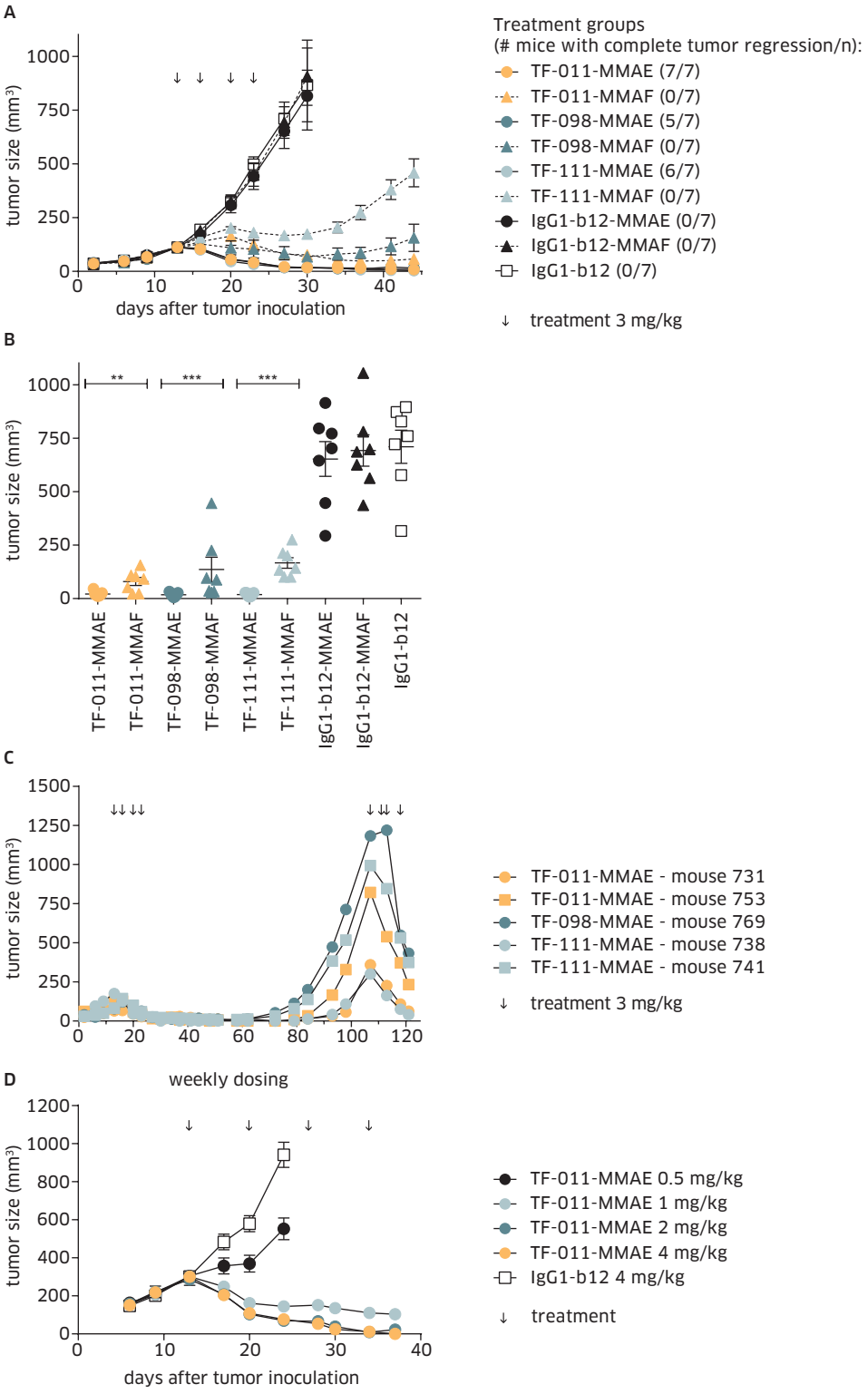
A
tumor size (mm³)
days after tumor inoculation
Treatment groups
(# mice with complete tumor regression/n):
TF-011-MMAE (7/7)
TF-011-MMAF (0/7)
TF-098-MMAE (5/7)
TF-098-MMAF (0/7)
TF-111-MMAE (6/7)
TF-111-MMAF (0/7)
IgG1-b12-MMAE (0/7)
IgG1-b12-MMAF (0/7)
IgG1-b12 (0/7)
treatment 3 mg/kg
B
tumor size (mm³)
**
***
***
TF-011-MMAE
TF-011-MMAF
TF-098-MMAE
TF-098-MMAF
TF-111-MMAE
TF-111-MMAF
IgG1-b12-MMAE
IgG1-b12-MMAF
IgG1-b12
C
tumor size (mm³)
weekly dosing
TF-011-MMAE - mouse 731
TF-011-MMAE - mouse 753
TF-098-MMAE - mouse 769
TF-111-MMAE - mouse 738
TF-111-MMAE - mouse 741
treatment 3 mg/kg
D
tumor size (mm³)
days after tumor inoculation
TF-011-MMAE 0.5 mg/kg
TF-011-MMAE 1 mg/kg
TF-011-MMAE 2 mg/kg
TF-011-MMAE 4 mg/kg
IgG1-b12 4 mg/kg
treatment

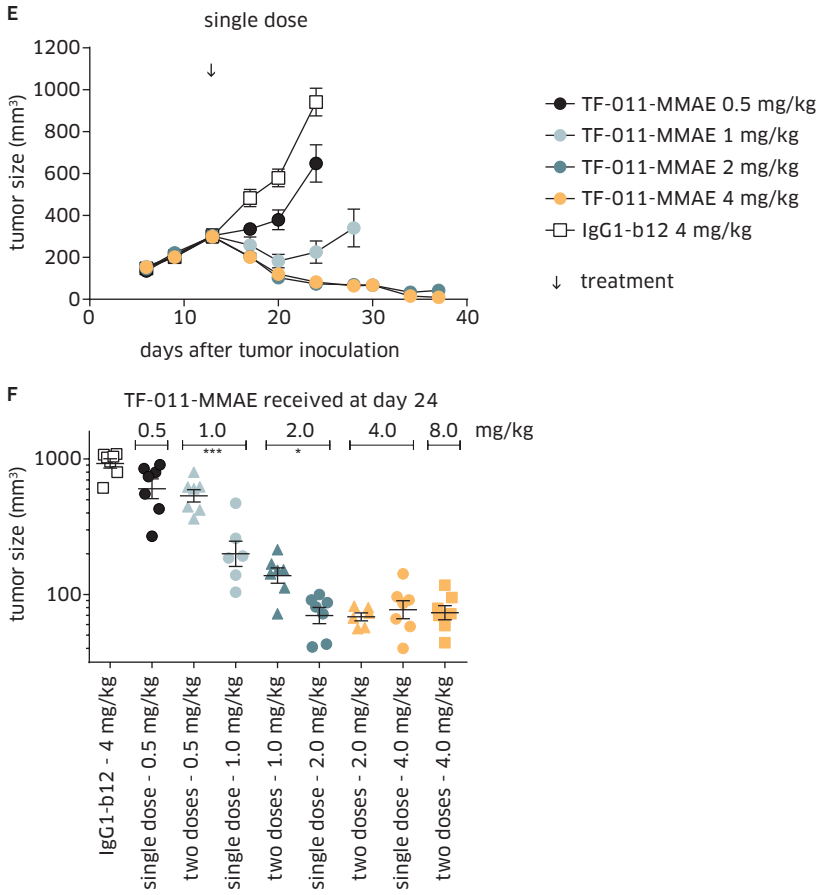

FIGURE 4 *TF-ADCs show potent anti-tumor activity in vivo.* HPAF-II xenografts were established by s.c. injection in SCID mice, and treatment with TF-ADCs was initiated at day 13 after tumor inoculation. **(A-C)** Treatment with 3 mg/kg TF-ADCs. **(A)** Tumor growth in the different treatment groups. IgG1-b12-MMAE and IgG1-b12-MMAF were included as isotype control ADCs, IgG1-b12 was included as isotype control IgG. Curves represent average tumor size per treatment group (7 mice per group), error bars indicate SEM. The number of mice that showed complete tumor regression (i.e. no measurable tumor remaining) in each of the treatment groups is indicated between brackets. **(B)** Tumor volumes in the different treatment groups at day 27 after tumor inoculation. Differences in average tumor size between treatment groups were analyzed by one-way ANOVA, ** P<0.01, *** P<0.001. **(C)** HPAF-II xenografts that showed outgrowth after completion of the first treatment cycle were re-treated with 3 mg/kg TF-ADC (four doses, at the indicated time points). Mice were re-treated with the same TF-ADC as they had received in the first treatment cycle. Curves represent individual mice. **(D-F)** Anti-tumor activity of TF-011-MMAE in the HPAF-II xenograft model at different dose levels and dosing frequencies. **(D-E)** Average tumor size after treatment with 0.5, 1, 2 or 4 mg/kg TF-011-MMAE (7 mice per group), at weekly dosing **(D)** or as a single dose **(E)**. IgG1-b12 was included as an isotype control antibody. Error bars indicate SEM. **(F)** Tumor volume per treatment group at day 24, when mice had received either one or two doses of TF-011-MMAE. Differences in average tumor size between groups that had received the same cumulative dose of TF-011-MMAE were compared by one-way ANOVA (* P<0.05, *** P<0.001).

treatment), TF-098 and TF-111 induced a small, albeit significant, reduction of tumor growth in the BxPC-3 model (Supplementary Figure S5E,F). However, therapeutic treatment with unconjugated TF HuMab was unable to inhibit tumor growth in the A431, AsPC-1 and HPAF-II xenograft models (Supplementary Figure S5G,H and data not shown). This suggests that the anti-tumor activity of TF-ADCs in the established xenografts tested here is to a large extent mediated by the cytotoxic activity of MMAE or MMAF.

The anti-tumor efficacy of the most potent ADC, TF-011-MMAE, was assessed at different dose levels and dosing schedules. At weekly dosing (four doses), treatment with 1 mg/kg TF-011-MMAE was sufficient to induce tumor regression (Figure 4D). When administered as a single dose, 2 and 4 mg/kg TF-011-MMAE induced tumor regression, whereas inhibition of tumor growth was observed after treatment with 0.5 or 1 mg/kg (Figure 4E). Interestingly, comparison of tumor volumes on day 24, when mice had received either one or two doses of TF-011-MMAE, demonstrated that a single dose of 1 mg/kg TF-011-MMAE was more effective than two doses of 0.5 mg/kg, although the cumulative dose was the same in both treatment groups. Similarly, treatment with a single dose of 2 mg/kg was more effective than two doses of 1 mg/kg (Figure 4F). This suggests that, at the same cumulative dose (exposure), dosing schedules giving a higher peak plasma level (C_{max}) are more effective. For treatment with a cumulative dose of 4 mg/kg, no difference in efficacy was observed between a single dose of 4 mg/kg and two doses of 2 mg/kg, because tumor regression was complete in both groups.

In summary, TF-ADCs showed potent anti-tumor activity *in vivo*, which was dependent on both TF targeting and conjugation with auristatins. TF-011-MMAE was selected for further preclinical studies and clinical development (designated as HuMax-TF-ADC).

TF-011-MMAE induces efficient tumor cell killing in PDX models with heterogeneous TF expression

Like most solid tumor targets, expression of TF in cancer is heterogeneous between patients, within patients and even within tumors [3]. We addressed the capacity of TF-011-MMAE to inhibit the growth of tumors with heterogeneous target expression using PDX models, which are thought to represent the heterogeneity that exists between human tumors [31-33]. Immunohistochemical (IHC) analysis of xenografted primary human tumor biopsies confirmed heterogeneity of TF expression, and seven PDX models were selected based on variable levels of TF expression. TF expression was observed in >75% of tumor cells in the PDX models for lung and pancreas adenocarcinoma (Figure 5A,B), and in 50-75% of tumor cells in the models for bladder carcinoma, prostate carcinoma and lung squamous cell carcinoma (Figure 5C-E). In PDX models for cervix squamous cell carcinoma and ovarian adenocarcinoma, only 25-50% of tumor cells were TF-positive (Figure 5F,G).

PDX tumors were implanted s.c. in nude mice, and when tumors had established, mice were treated with TF-011-MMAE (4 mg/kg, two doses). In models where the sensitivity to microtubule-targeting agents was not known, a paclitaxel treatment group (20 mg/kg, 3-4 doses) was included.

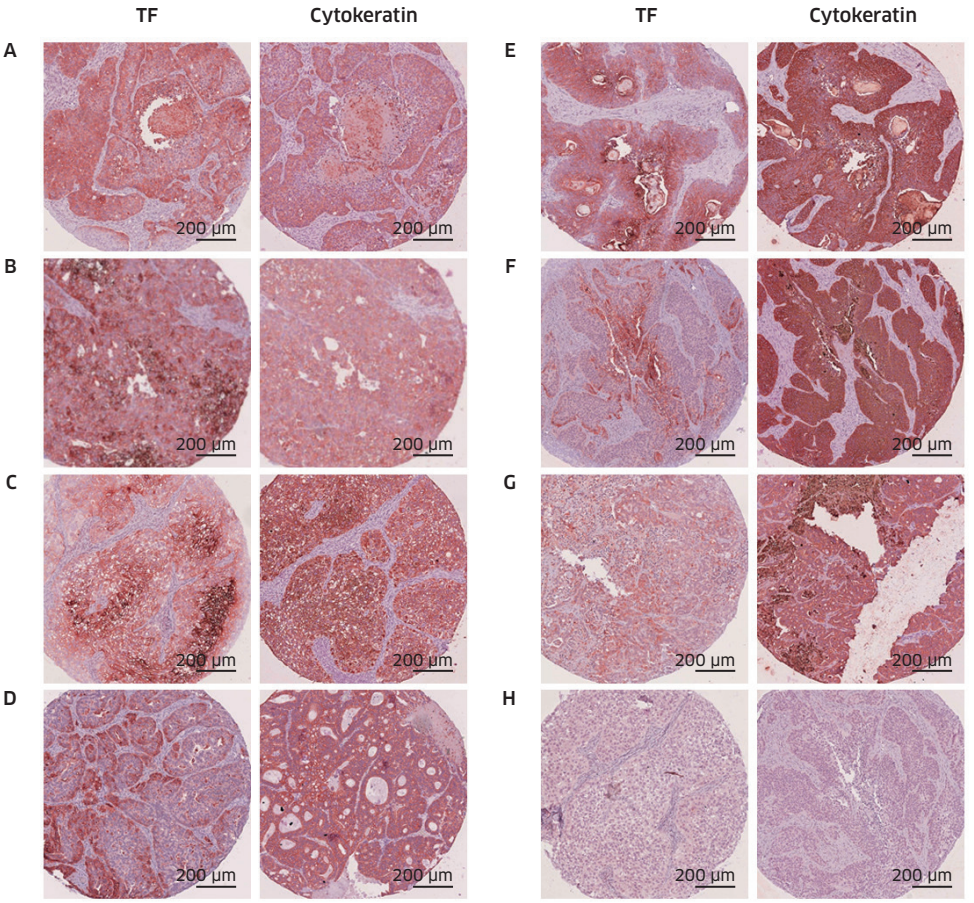

FIGURE 5 *Heterogeneous expression of TF in PDX models.* IHC analysis was performed to assess TF expression in PDX models. The percentage of TF-positive tumor cells was estimated by comparing human cytokeratin staining (which identifies human tumor cells) with TF staining (indicating TF-positive tumor cells). In PDX models for **(A)** lung adenocarcinoma and **(B)** pancreatic adenocarcinoma, >75% of the tumor cells showed TF expression. In PDX models for **(C)** bladder (urothelial) adenocarcinoma, **(D)** prostate adenocarcinoma and **(E)** lung squamous cell carcinoma, TF expression was observed in 50-75% of the tumor cells. In PDX models for **(F)** squamous cell carcinoma of the cervix and **(G)** ovarian adenocarcinoma, 25-50% of the tumor cells showed TF expression. **(H)** Representative pictures showing immunostaining with the isotype control antibody IgG1-b12.

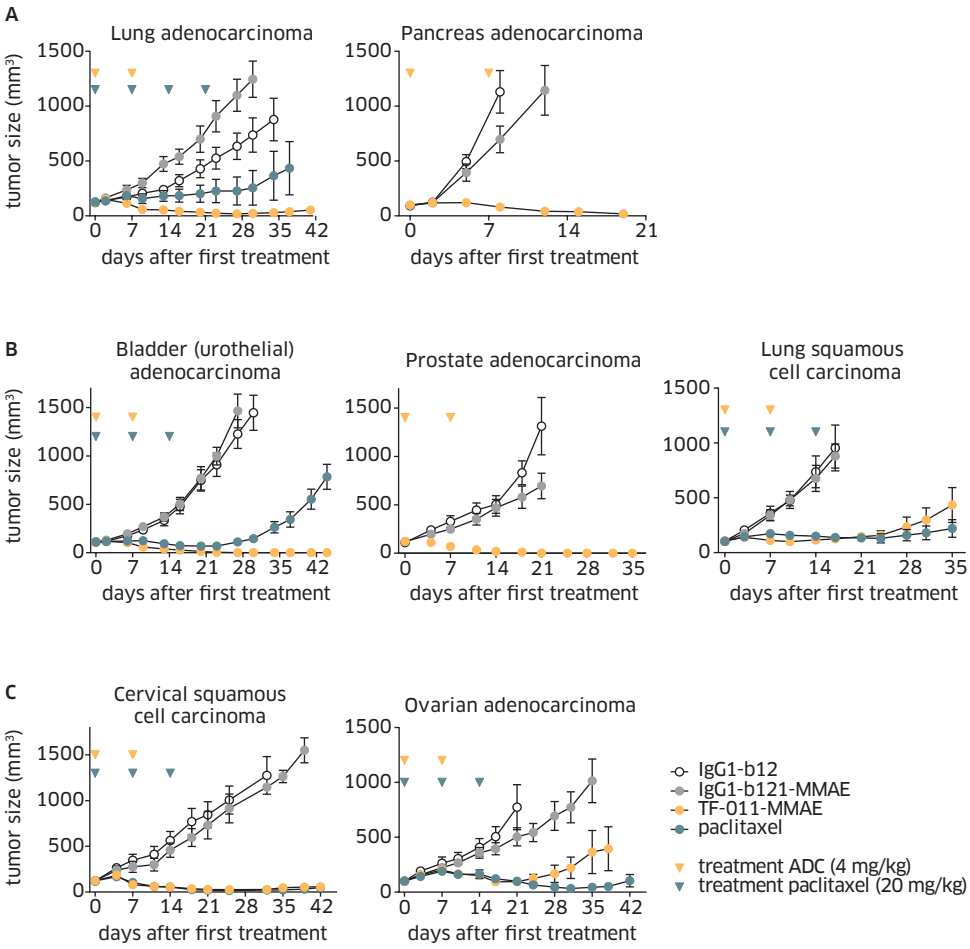

FIGURE 6 *Anti-tumor activity of TF-011-MMAE in PDX models with heterogeneous target expression.* PDX models were established by s.c. implantation of tumor fragments in mice. When tumors had reached a size of 80-200 mm³, mice were randomized and treatment was initiated. Mice were treated with TF-011-MMAE or paclitaxel at the indicated doses and time points. IgG1-b12-MMAE was included as an isotype control ADC, IgG1-b12 was included as an isotype control IgG. **(A)** Tumor growth in PDX models showing >75% TF-positive tumor cells (lung adenocarcinoma and pancreatic adenocarcinoma), **(B)** Tumor growth in PDX models showing 50-75% TF-positive tumor cells (bladder adenocarcinoma, prostate adenocarcinoma and lung squamous cell carcinoma) and **(C)** Tumor growth in PDX tumors with 25-50% TF-positive cells (cervical squamous cell carcinoma and ovarian adenocarcinoma). Data points represent average tumor size per group (8 mice per group). Error bars represent SEM.

In the models for pancreas and lung adenocarcinoma, that showed >75% TF-positive tumor cells, TF-011-MMAE induced complete tumor regression in all mice (Figure 6A). Similarly, TF-011-MMAE induced efficient tumor regression in PDX models that expressed TF in 50-75% of tumor cells (bladder cancer, prostate cancer and lung squamous cell carcinoma; Figure 6B). Importantly, tumor regression was also observed in models that showed TF expression in only 25-50% of the tumor cells (ovarian and cervical cancer; Figure 6C).

Treatment with two doses of HuMax-TF-ADC was at least as efficient as treatment with three or four doses of paclitaxel (Figure 6). Moreover, TF-011-MMAE induced tumor regression in mice that showed tumor recurrence after paclitaxel treatment, even in mice with relatively large tumors (Supplementary Figure S6). This demonstrates that prior treatment with paclitaxel did not affect the sensitivity of the tumors to treatment with TF-011-MMAE, indicating that TF expression and sensitivity to MMAE-mediated tumor cell killing was retained in tumors that showed outgrowth after paclitaxel treatment.

DISCUSSION

TF-011-MMAE was selected from a panel of six TF-specific ADCs, consisting of three different TF HuMab conjugated with vcMMAE or mcMMAF. TF-011-MMAE showed excellent anti-tumor activity *in vivo*, with auristatin-mediated tumor cell killing as the dominant mechanism of action. Furthermore, TF-011-MMAE and unconjugated TF-011 induced inhibition of TF:FVIIa-mediated intracellular signaling and ADCC *in vitro*, although it is unclear to what extent these mechanisms may contribute to the inhibition of tumor growth in cancer patients. To our knowledge, TF-011-MMAE is the first ADC that uses a TF-specific antibody to deliver a cytotoxic agent to tumor cells.

Importantly, TF-011-MMAE induced complete tumor regression in PDX models, even if only a sub-population of the tumor cells expressed TF. PDX models are thought to represent the genetic and histological heterogeneity in human tumors, and efficacy of treatment in such models was shown to have predictive value for the clinic [31-33]. The high potency of TF-011-MMAE in tumors with non-homogeneous target expression, may be related to the capacity of MMAE to cause a bystander effect by diffusion across cell membranes after intracellular release [34]. Especially in solid tumors, where antibody penetration may be limited [35,36], this may be a major advantage. As opposed to uncharged MMAE, the negative charge of MMAF is thought to prevent diffusion across membranes [20]. This difference in membrane permeability probably underlies the difference in efficacy observed between MMAE- and MMAF-conjugates.

Although TF plays a crucial role in coagulation and hemostasis, TF-011 showed minimal impact on coagulation *in vitro*. Previous studies suggested that TF-specific antibodies can roughly be divided into two categories: those that inhibit FVIIa binding and/or TF:FVIIa-induced intracellular signaling with minor impact on TF pro-coagulant activity, and those that interfere with FXa activation and coagulation without impacting on TF:FVIIa-induced intracellular signaling [14,37]. Our *in vitro* studies suggest that TF-011 belongs to the first category. This notion is supported by non-clinical toxicology studies in cynomolgus monkeys. TF-011 and TF-011-MMAE, which show comparable binding to cynomolgus monkey and human TF, did not significantly impact on functional bleeding time or systemic parameters of coagulation in cynomolgus monkeys at doses up to 100 mg/kg or 5-6 mg/kg, respectively (Genmab, data on file). It may seem counterintuitive that TF:FVIIa binding, the first step in the coagulation cascade, can be inhibited without impacting on hemostasis or clotting. This apparent paradox is most likely explained by the many amplification steps in the coagulation cascade downstream of TF:FVIIa [38]. As a result, only little TF:FVIIa binding is required to maintain hemostasis. The work of Parry and colleagues, who demonstrated that transgenic mice expressing only 1% of normal TF activity were viable and had relatively normal hemostasis [39], supports this.

In summary, TF-011-MMAE is a promising new ADC that is being developed for the treatment of solid tumors. TF is thought to be an excellent ADC target, due to its broad expression profile across solid cancer types and rapid internalization and degradation after antibody binding. TF-011-MMAE induced complete tumor regression in PDX models derived from a broad range of solid tumors, demonstrating the high potency of TF-011-MMAE for treatment of cancer.

Acknowledgements

We thank Elke Gresnigt-van den Heuvel, Imke Lodewijks, Gemma Rigter, Agnes de Goffau, Marije Overdijk, Patrick Engelberts and Antonio Ortiz-Buijsse for technical support, Dr. Tom Vink for help with the manuscript, Dr. Joost Bakker for help with the graphics and Dr. Wiiger for providing HaCaT cells.

REFERENCE LIST

1 Verma S, Miles D, Gianni L, Krop IE, Welslau M, Baselga J, et al. Trastuzumab Emtansine for HER2-Positive Advanced Breast Cancer. N Eng J Med 2012;367(19):1783-1791.

2 Senter PD, Sievers EL. The discovery and development of brentuximab vedotin for use in relapsed Hodgkin lymphoma and systemic anaplastic large cell lymphoma. Nat Biotech 2012;30(7):631-637.

3 Förster Y, Meye A, Albrecht S, Schwenzer B. Tissue factor and tumor: Clinical and laboratory aspects. Clinica Chimica Acta 2006;364(1-2):12-21.

4 Mandal SK, Pendurthi UR, Rao LV. Cellular localization and trafficking of tissue factor. Blood 2006;107(12):4746-4753.

5 Mackman N, Tilley RE, Key NS. Role of the extrinsic pathway of blood coagulation in hemostasis and thrombosis. Arterioscler Thromb Vasc Biol 2007;27(8):1687-1693.

6 Drake TA, Morrissey JH, Edgington TS. Selective cellular expression of tissue factor in human tissues. Implications for disorders of hemostasis and thrombosis. Am J Pathol 1989;134(5):1087-1097.

7 Egorina EM, Sovershaev MA, Bjorkoy G, Gruber FX, Olsen JO, Parhami-Seren B, et al. Intracellular and surface distribution of monocyte tissue factor: application to intersubject variability. Arterioscler Thromb Vasc Biol 2005;25(7):1493-1498.

8 Amirkhosravi A, Alexander M, May K, Francis DA, Warnes G, Biggerstaff J, et al. The importance of platelets in the expression of monocyte tissue factor antigen measured by a new whole blood flow cytometric assay. Thromb Haemost 1996;75(1):87-95.

9 Vine AK. Recent advances in haemostasis and thrombosis. Retina 2009;29(1):1-7.

10 Chu AJ. Tissue factor, blood coagulation, and beyond: an overview [published online September 24, 2011]. *Int J Inflam*. doi:10.4061/2011/367284.

11 Yu JL, May L, Lhotak V, Shahrzad S, Shirasawa S, Weitz JI, et al. Oncogenic events regulate tissue factor expression in colorectal cancer cells: implications for tumor progression and angiogenesis. Blood 2005;105(4):1734-1741.

12 Ngo CV, Picha K, McCabe F, Millar H, Tawadros R, Tam SH, et al. CNTO 859, a humanized anti-tissue factor monoclonal antibody, is a potent inhibitor of breast cancer metastasis and tumor growth in xenograft models. Int J Cancer 2007;120(6):1261-1267.

13 Versteeg HH, Schaffner F, Kerver M, Petersen HH, Ahamed J, Felding-Habermann B, et al. Inhibition of tissue factor signaling suppresses tumor growth. Blood 2008;111(1):190-199.

14 Kirchhofer D, Moran P, Chiang N, Kim J, Riederer MA, Eigenbrot C, et al. Epitope location on tissue factor determines the anticoagulant potency of monoclonal anti-tissue factor antibodies. Thromb Haemost 2000;84(6):1072-1081.

15 Vink T, Oudshoorn-Dickmann M, Roza M, Reitsma J-J, de Jong RN. A simple, robust and highly efficient transient expression system for producing antibodies [published online July 16, 2013]. *Methods*. doi:10.1016/j.ymeth.2013.07.018.

16 Fishwild DM, O'Donnell SL, Bengoechea T, Hudson DV, Harding F, Bernhard SL, et al. High-avidity human IgG kappa monoclonal antibodies from a novel strain of minilocus transgenic mice. Nat Biotechnol 1996;14(7):845-851.

17 Labrijn AF, Meesters JI, de Goeij BECG, van den Bremer ETJ, Neijssen J, van Kampen MD, et al. Efficient generation of stable bispecific IgG1 by controlled Fab-arm exchange. Proceedings of the National Academy of Sciences 2013;110(13):5145-5150.

18 Parren PW, Ditzel HJ, Gulizia RJ, Binley JM, Barbas CF, 3rd, Burton DR, et al. Protection against HIV-1 infection in hu-PBL-SCID mice by passive immunization with a neutralizing human monoclonal antibody against the gp120 CD4-binding site. AIDS 1995;9(6):F1-6.

19 Lammerts van Bueren JJ, Bleeker WK, Bogh HO, Houtkamp M, Schuurman J, van de Winkel JG, et al. Effect of target dynamics on pharmacokinetics of a novel therapeutic antibody against the epidermal growth factor receptor: implications for the mechanisms of action. Cancer Res 2006;66(15):7630-7638.

20 Doronina SO, Mendelsohn BA, Bovee TD, Cerveny CG, Alley SC, Meyer DL, et al. Enhanced activity of monomethylauristatin F through monoclonal antibody delivery: effects of linker technology on efficacy and toxicity. Bioconjug Chem 2006;17(1):114-124.

21 Doronina SO, Toki BE, Torgov MY, Mendelsohn BA, Cerveny CG, Chace DF, et al. Development of potent monoclonal antibody auristatin conjugates for cancer therapy. Nat Biotechnol 2003;21(7):778-784.

22 Overdijk MB, Verploegen S, van den Brakel JH, Lammerts van Bueren JJ, Vink T, van de Winkel JG, et al. Epidermal growth factor receptor (EGFR) antibody-induced antibody-dependent cellular cytotoxicity plays a prominent role in inhibiting tumorigenesis, even of tumor cells insensitive to EGFR signaling inhibition. J Immunol 2011;187(6):3383-3390.

23 Amirkhosravi A, Bigsby G, Desai H, Rivera-Amaya M, Coll E, Robles-Carrillo L, et al. Blood clotting activation analysis for preoperative differentiation of benign versus malignant ovarian masses. Blood Coagulation & Fibrinolysis 2013;24(5):510-517.

24 Ogawa M, Kosaka N, Longmire MR, Urano Y, Choyke PL, Kobayashi H. Fluorophore-quencher based activatable targeted optical probes for detecting *in vivo* cancer metastases. Mol Pharm 2009;6(2):386-395.

25 Bleeker WK, Lammerts van Bueren JJ, van Ojik HH, Gerritsen AF, Pluyter M, Houtkamp M, et al. Dual Mode of Action of a Human Anti-Epidermal Growth Factor Receptor Monoclonal Antibody for Cancer Therapy. The Journal of Immunology 2004;173(7):4699-4707.

26 Hjortoe GM, Petersen LC, Albrektsen T, Sorensen BB, Norby PL, Mandal SK, et al. Tissue factor-factor VIIa–specific up-regulation of IL-8 expression in MDA-MB-231 cells is mediated by PAR-2 and results in increased cell migration. Blood 2004;103(8):3029-3037.

27 Gessler F, Voss V, Dützmann S, Seifert V, Gerlach R, Kögel D. Inhibition of tissue factor/protease-activated receptor-2 signaling limits proliferation, migration and invasion of malignant glioma cells. Neuroscience 2010;165(4):1312-1322.

28 Aras O. Induction of microparticle- and cell-associated intravascular tissue factor in human endotoxemia. Blood 2004;103(12):4545-4553.

29 Hamblett KJ, Senter PD, Chace DF, Sun MM, Lenox J, Cerveny CG, et al. Effects of drug loading on the antitumor activity of a monoclonal antibody drug conjugate. Clin Cancer Res 2004;10(20):7063-7070.

30 Junttila TT, Li G, Parsons K, Phillips GL, Sliwkowski MX. Trastuzumab-DM1 (T-DM1) retains all the mechanisms of action of trastuzumab and efficiently inhibits growth of lapatinib insensitive breast cancer. Breast Cancer Res Treat 2011;128(2):347-356.

31 Moro M, Bertolini G, Tortoreto M, Pastorino U, Sozzi G, Roz L. Patient-derived xenografts of non small cell lung cancer: resurgence of an old model for investigation of modern concepts of tailored therapy and cancer stem cells [published online May 2, 2012]. *J Biomed Biotechnol*. doi:10.1155/2012/568567.

32 Tentler JJ, Tan AC, Weekes CD, Jimeno A, Leong S, Pitts TM, et al. Patient-derived tumour xenografts as models for oncology drug development. Nat Rev Clin Oncol 2012;9(6):338-350.

33 Hidalgo M, Bruckheimer E, Rajeshkumar NV, Garrido-Laguna I, De Oliveira E, Rubio-Viqueira B, et al. A pilot clinical study of treatment guided by personalized tumorgrafts in patients with advanced cancer. Mol Cancer Ther 2011;10(8):1311-1316.

34 Okeley NM, Miyamoto JB, Zhang X, Sanderson RJ, Benjamin DR, Sievers EL, et al. Intracellular activation of SGN-35, a potent anti-CD30 antibody-drug conjugate. Clin Cancer Res 2010;16(3):888-897.

35 Jain RK. Physiological Barriers to Delivery of Monoclonal Antibodies and Other Macromolecules in Tumors. Cancer Research 1990;50(3 Supplement):814s-819s.

36 Rudnick SI, Lou J, Shaller CC, Tang Y, Klein-Szanto AJP, Weiner LM, et al. Influence of Affinity and Antigen Internalization on the Uptake and Penetration of Anti-HER2 Antibodies in Solid Tumors. Cancer Research 2011;71(6):2250-2259.

37 Ahamed J, Belting M, Ruf W. Regulation of tissue factor–induced signaling by endogenous and recombinant tissue factor pathway inhibitor 1. Blood 2005;105(6):2384-2391.

38 Jesty J, Beltrami E. Positive Feedbacks of Coagulation: Their Role in Threshold Regulation. Arteriosclerosis, Thrombosis, and Vascular Biology 2005;25(12):2463-2469.

39 Parry GC, Erlich JH, Carmeliet P, Luther T, Mackman N. Low levels of tissue factor are compatible with development and hemostasis in mice. J Clin Invest 1998;101(3):560-569.

SUPPLEMENTARY METHODS

Antibody cross-competition studies.
ELISA plates were coated with each of the TF HuMab (0.5 or 2 µg/mL in PBS) at 4°C, overnight. Plates were washed with PBS, blocked with 2% (v/v) chicken serum in PBS (1 h, RT) and washed again with PBS. Subsequently, 50 µL anti-TF HuMab (10 µg/mL) was added, followed by 50 µL TF-ECDHis (0.5 or 1 µg/mL), and the mixture was incubated at RT (1 h) while shaking. Plates were washed three times with PBS+0.05% Tween-20, and incubated with a biotinylated polyclonal anti-His antibody (1:2,000 dilution; R&D Systems, Abingdon, UK) at RT while shaking, for 1 h. Plates were washed and incubated with Streptavidin-poly-HRP (Sanquin, Amsterdam, The Netherlands) at RT for 20 min, and washed again. The reaction was further developed with ABTS (Roche Diagnostics) at RT in the dark, stopped after 15 min by adding 2% (w/v) oxalic acid and absorbance at 405 nm was measured.

AlphaScreen assay to detect ERK phosphorylation.
A431 cells (30,000 cells/well) were seeded in 96-well tissue culture plates and cultured in serum-free medium (RPMI containing 20% HSA and penicillin/streptomycin), overnight. Medium was then replaced by DMEM without additives and cells were incubated for 1.5 h (37°C). Serial dilutions of TF HuMab or HuMab-KLH were added and cells were incubated for another 30 min (37°C). Cells were then stimulated with recombinant FVIIa at EC_{80} concentration (50 nM; 10 min). Cells were washed once with PBS, and lysed using 25 µL lysis buffer (Alphascreen® Surefire p-ERK1/2 assay kit, Perkin Elmer). Cell lysates were transferred to 384-well Proxiplates (Perkin Elmer), and levels of p-ERK1/2 were detected using the Alphascreen Surefire p-ERK1/2 assay kit (Perkin Elmer), according to the manufacturer's guidelines.

SUPPLEMENTARY TABLES

HuMab	Cell surface binding[a], EC_{50} (SD), µg/mL	Affinity (nM)[b]
TF-011	0.07 (0.02)	3.2
TF-013	0.25 (0.11)	2.8
TF-025	0.10 (0.10)	1.8
TF-044	0.14 (0.06)	9.7
TF-098	0.16 (0.10)	307
TF-109	0.49 (0.34)	4.8
TF-111	0.16 (0.11)	259
TF-114	0.11 (0.02)	11

SUPPLEMENTARY TABLE S1 *TF HuMab: target binding characteristics and inhibition of FXa generation.* [a]flow cytometry, MDA-MB-231 cells; average of 3 experiments. [b]Affinity for TF-ECDHis, measured by Biacore analysis.

	Immobilized antibody							
	0.5 µg coat	2 µg coat	0.5 µg coat	0.5 µg coat	2 µg coat	0.5 µg coat	0.5 µg coat	2 µg coat
Competing antibody (10 µg/mL)	**TF-013**	**TF-044**	**TF-011**	**TF-114**	**TF-098**	**TF-025**	**TF-109**	**TF-111**
TF-013	19	5	101	105	320	89	110	175
TF-044	93	40	109	105	330	108	94	175
TF-011	96	143	20	19	9	104	109	175
TF-114	101	143	21	13	9	47	26	5
TF-098	95	143	90	94	24	94	86	35
TF-025	102	143	117	28	10	34	11	6
TF-109	96	143	101	44	9	51	17	6
TF-111	89	143	110	99	37	104	93	43

SUPPLEMENTARY TABLE S2 *Cross-competition between TF HuMab.* Numbers indicate the binding of TF-ECDHis to immobilized TF HuMab in the presence of competing TF HuMab, expressed as a percentage of the binding in the absence of competing antibody. Green boxes indicate competition between TF HuMab (<40% residual binding of TF-ECDHis), grey boxes indicate partial competition (40-80% binding of TF-ECDHis) and light boxes indicate absence of competition (>80% binding of TF-ECDHis).

	R (min)[a] (SD)			K value (min)[b] (SD)			α angle (º)c (SD)			MA (mm)[d] (SD)		
Donor	**A[f,g]**	**B**	**C**	**A**	**B**	**C**	**A**	**B**	**C**	**A**	**B**	**C**
Isotype ctrl[e]	6.7 (0.1)[f]	4.8 (0.0)	6.3 (0.1)	3.0 (0.1)	2.5 (0.1)	4.4 (2.1)	52 (2)	58 (0)	39 (12)	60 (1)	63 (1)	59 (1)
TF-011	9.5[f]	6.8	16.1	3.1	2.6	3.3	50	56	49	56	60	58
TF-013	17.7[f]	16.2	29.2	3.6	2.9	6.8	43	47	31	51	56	60
TF-098	6.6[g]	8.8	16.0	2.4	3.1	3.6	58	52	47	60	56	60
No LPS (run 1)	20.8[f]	18.6	39.1	6.2	4.0	5.0	30	41	37	47	50	15
No LPS (run 2)	23.5[g]	NA	NA	5.0	NA	NA	34	NA	NA	48	NA	NA

SUPPLEMENTARY TABLE S3 *Thromboelastography: coagulation of LPS-stimulated whole blood in the presence of 20 µg/mL TF-011, TF-013 and TF-098. Raw data of three donors are presented.* [a]R = clotting lag time (time to initial fibrin formation). [b]K value = time (from initiation of fibrin formation) to reach a clot strength amplitude of 20 mm. [c]α angle = rate of fibrin build-up and cross-linking. [d]MA = maximum amplitude, representative of clot strength. [e]Average of isotype control values at all concentrations tested (1, 10 and 20 µg/mL). [f,g]For donor A, thromboelastography was performed in two separate runs. The isotype control IgG, TF-011 and TF-013 were included in run 1 ([f]), TF-098 was included in run 2 ([g]). NA, not applicable.

SUPPLEMENTARY FIGURES

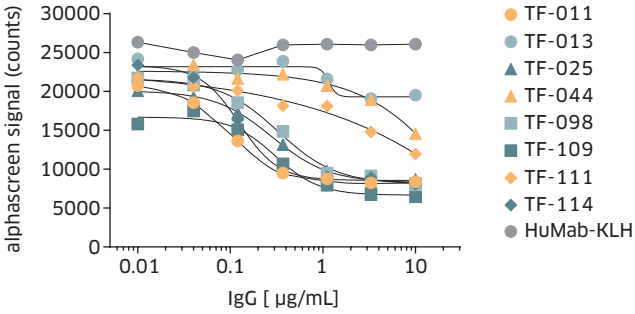

SUPPLEMENTARY FIGURE S1 *TF HuMab inhibit TF:FVIIa-induced ERK1/2 phosphorylation.* A431 cells were incubated with 50 nM recombinant FVIIa in the presence of TF HuMab. Phosphorylated ERK (p-ERK1/2) was measured in cell lysates using Alphascreen®. Counts on the y-axis indicate light emitted (at 520-620 nm) by acceptor beads, upon excitation of donor beads (680 nm). Light emission only occurs when donor and acceptor beads, both of which are coated with p-ERK1/2 specific antibodies, are in close proximity due to cross-linking by soluble p-ERK1/2. Results are representative of two independent experiments.

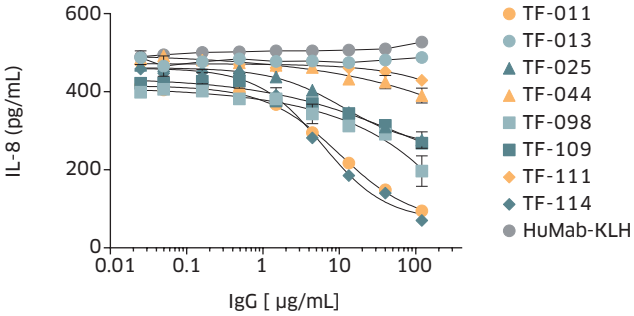

SUPPLEMENTARY FIGURE S2 *TF:FVIIa-induced IL-8 production in MDA-MB-231 cells is reduced in the presence of TF HuMab.* MDA-MB-231 cells were pre-incubated with 10 nM FVIIa, followed by addition of TF HuMab. IL-8 production was measured in cell culture supernatants using ELISA. FVIIa-induced IL-8 production in the absence of antibodies was 460 pg/mL and FVIIa-independent IL-8 production was 19 pg/mL. Results are representative of three individual experiments. Error bars indicate SEM.

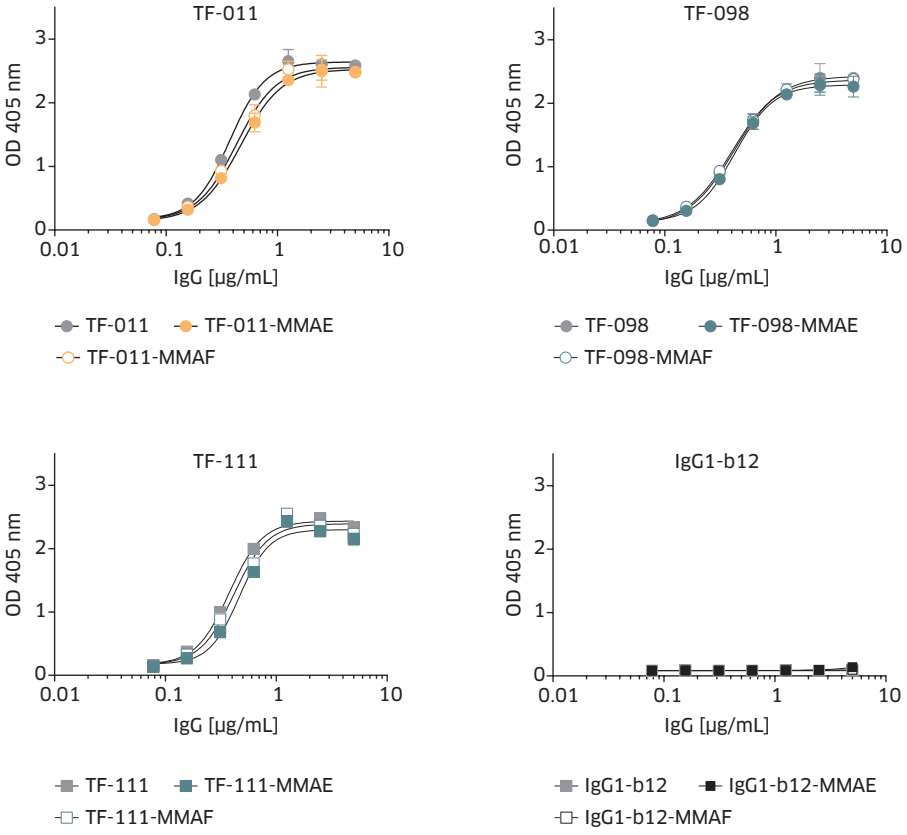

SUPPLEMENTARY FIGURE S3 *Binding of TF HuMab is unaltered after conjugation with vcMMAE or mcMMAF.* TF-ECDHis was immobilized on 96-well plates, and incubated with unconjugated HuMab (black circles), vcMMAE-conjugates (red triangles) or mcMMAF-conjugates (blue squares). Binding of TF HuMab or TF-ADCs was detected by ELISA, using an HRP-labeled mouse anti-human IgG1 antibody. IgG1-b12-MMAE and IgG1-b12-MMAF were included as isotype control ADCs, IgG1-b12 was included as an isotype control IgG. Error bars indicate SEM.

A

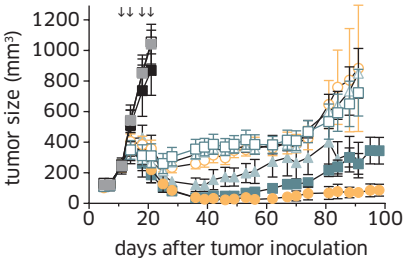

Treatment groups
(# mice with complete tumor regression/n):

- TF-011-MMAE (5/7)
- TF-011-MMAF (0/7)
- TF-098-MMAE (1/7)
- TF-098-MMAF (0/7)
- TF-111-MMAE (1/7)
- TF-111-MMAF (0/7)
- IgG1-b12-MMAE (0/7)
- IgG1-b12-MMAF (0/7)
- IgG1-b12 (0/7)
- ↓ treatment 3 mg/kg

B

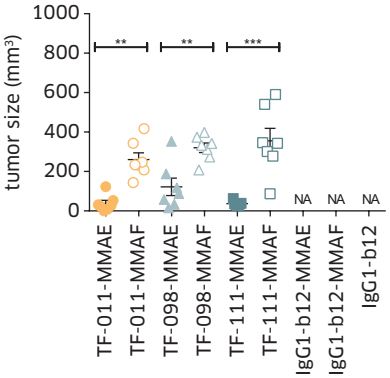

C

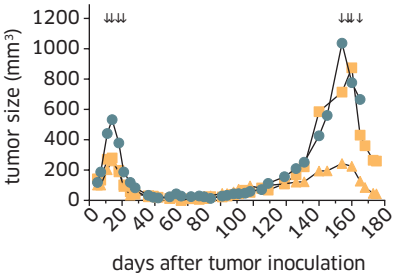

- TF-011-MMAE - mouse 652
- TF-011-MMAE - mouse 680
- TF-098-MMAE - mouse 694
- ↓ treatment 3 mg/kg

D

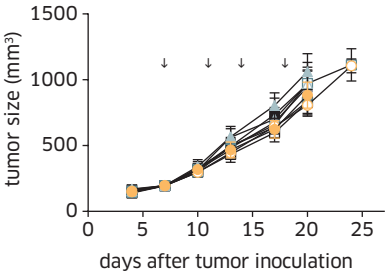

- TF-011-MMAE
- TF-011-MMAF
- TF-098-MMAE
- TF-098-MMAF
- TF-111-MMAE
- TF-111-MMAF
- IgG1-b12-MMAE
- IgG1-b12-MMAF
- IgG1-b12
- ↓ treatment 3 mg/kg

SUPPLEMENTARY FIGURE S4 *Anti-tumor activity of TF-ADCs in the A431 and HCT-116 xenograft models.* Xenografts were established by s.c. injection in SCID mice, and treatment with 3 mg/kg TF-ADCs was initiated 11 (A431) or 7 (HCT 116) days later. (**A**) Tumor growth in the different treatment groups in the A431 model. IgG1-b12-MMAE and IgG1-b12-MMAF were included as isotype control ADCs, IgG1-b12 was included as isotype control IgG. Curves represent mean tumor size per treatment group (7 mice per group), error bars indicate SEM. The number of mice that showed complete tumor regression (i.e. no measurable tumor remaining) in each of the treatment groups is indicated between brackets. (**B**) Tumor volumes in the A431 model at day 36. Differences in average tumor size between treatment groups were analyzed by one-way ANOVA, ** P<0.01, *** P<0.001. Mice in the control groups (IgG1-b12-MMAE, IgG1-b12-MMAF and IgG1-b12) were sacrificed before day 36 due to large tumor burden. (**C**) Mice in which initial treatment with TF-011-MMAE or TF-098-MMAE in the A431 xenograft model induced tumor regression, were kept in the study until tumors started growing again. Tumors were re-treated with four doses of the same ADC (at the indicated time points) as they had received in the first treatment cycle. Curves represent individual mice. (**D**) Tumor growth in the different treatment groups in the HCT-116 xenograft model. Curves represent mean tumor size per treatment group (7 mice per group), error bars indicate SEM.

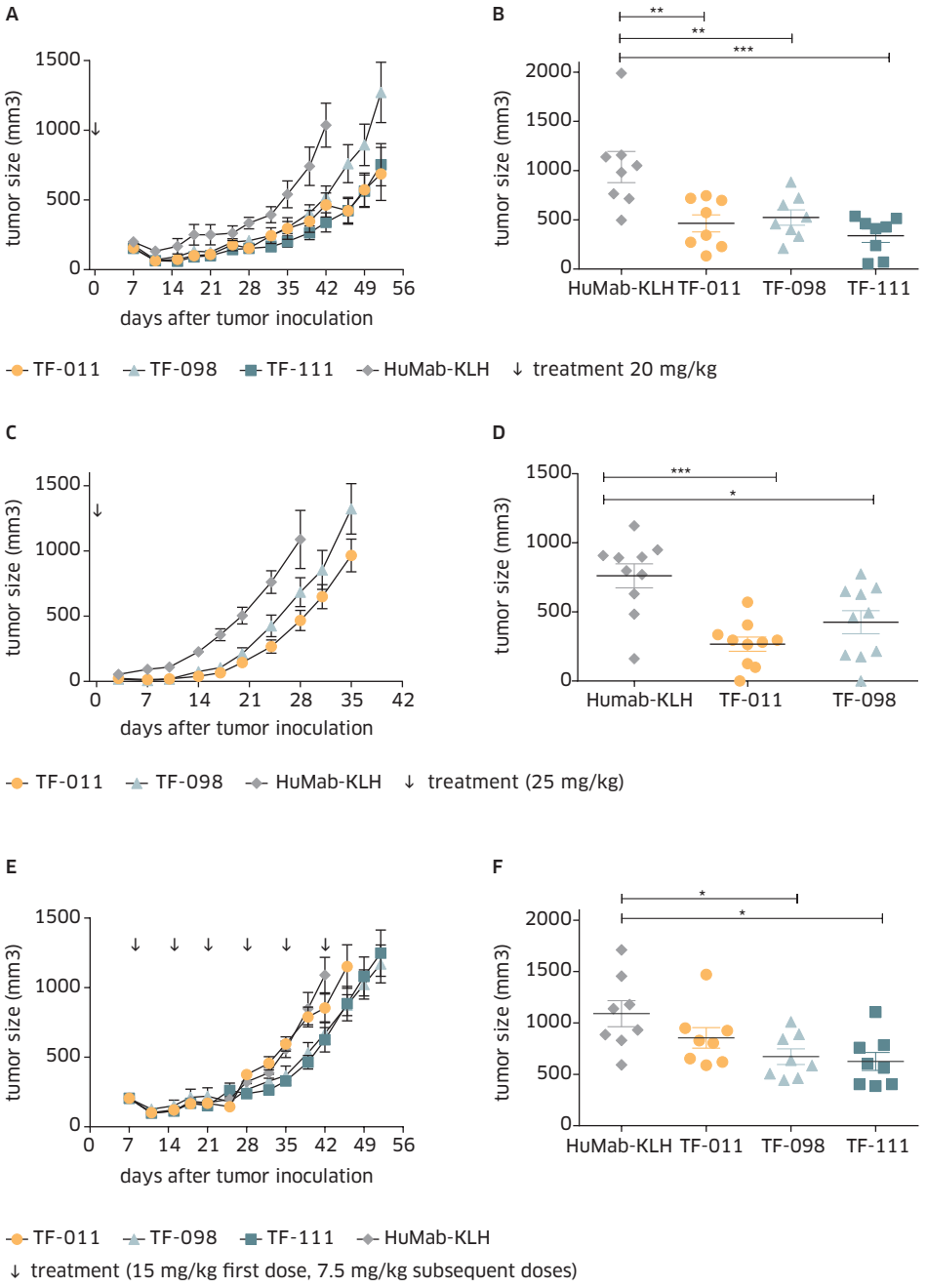
A
tumor size (mm3)
1500
1000
500
0
0 7 14 21 28 35 42 49 56
days after tumor inoculation
B
**
**
***
tumor size (mm3)
2000
1500
1000
500
0
HuMab-KLH TF-011 TF-098 TF-111
TF-011 TF-098 TF-111 HuMab-KLH ↓ treatment 20 mg/kg
C
tumor size (mm3)
1500
1000
500
0
0 7 14 21 28 35 42
days after tumor inoculation
D
***
*
tumor size (mm3)
1500
1000
500
0
Humab-KLH TF-011 TF-098
TF-011 TF-098 HuMab-KLH ↓ treatment (25 mg/kg)
E
tumor size (mm3)
1500
1000
500
0
0 7 14 21 28 35 42 49 56
days after tumor inoculation
F
*
*
tumor size (mm3)
2000
1500
1000
500
0
HuMab-KLH TF-011 TF-098 TF-111
TF-011 TF-098 TF-111 HuMab-KLH
↓ treatment (15 mg/kg first dose, 7.5 mg/kg subsequent doses)

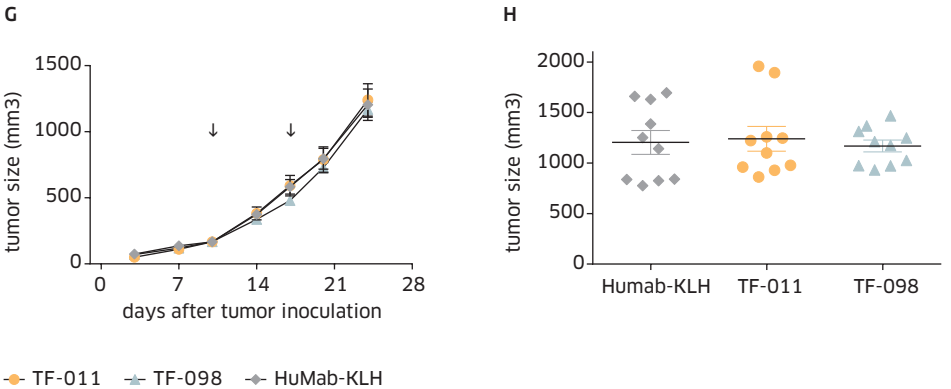

SUPPLEMENTARY FIGURE S5 *Anti-tumor activity of unconjugated TF HuMab in vivo.* BxPC-3 **(A,B,E,F)** or HPAF-II **(C,D,G,H)** xenografts were established by s.c. injection in SCID mice. Treatment was initiated within 1 h after tumor inoculation (prophylactic treatment), or when tumors had reached a size of 100-400 mm^3 (therapeutic treatment). **(A)** Tumor growth in BxPC-3 xenografts after prophylactic treatment with 20 mg/kg TF HuMab. **(B)** Tumor size at day 42 after tumor inoculation in the BxPC-3 prophylactic treatment model. **(C)** Tumor growth in the HPAF-II xenograft model, after prophylactic treatment with 20 mg/kg TF HuMab. **(D)** Tumor size at day 24 after tumor inoculation in the HPAF-II prophylactic treatment model. **(E)** Therapeutic treatment in the BxPC-3 xenograft model. Treatment was initiated on day 8 (15 mg/kg), when tumors had established, followed by weekly doses of 7.5 mg/kg. **(F)** Tumor size at day 43 after tumor inoculation in the BxPC-3 therapeutic treatment model. **(G)** Therapeutic treatment in the HPAF-II xenograft model. After tumors had established, mice were treated with 50 mg/kg TF HuMab on day 10, followed by 25 mg/kg on day 17. **(H)** Tumor size at day 24 after tumor inoculation in the HPAF-II therapeutic treatment model. Differences between treatment groups were analyzed using one-way ANOVA **(B,D,F,H)**; * P<0.05, ** P<0.01, *** P<0.001. Error bars **(A,C,E,G)** indicate SEM.

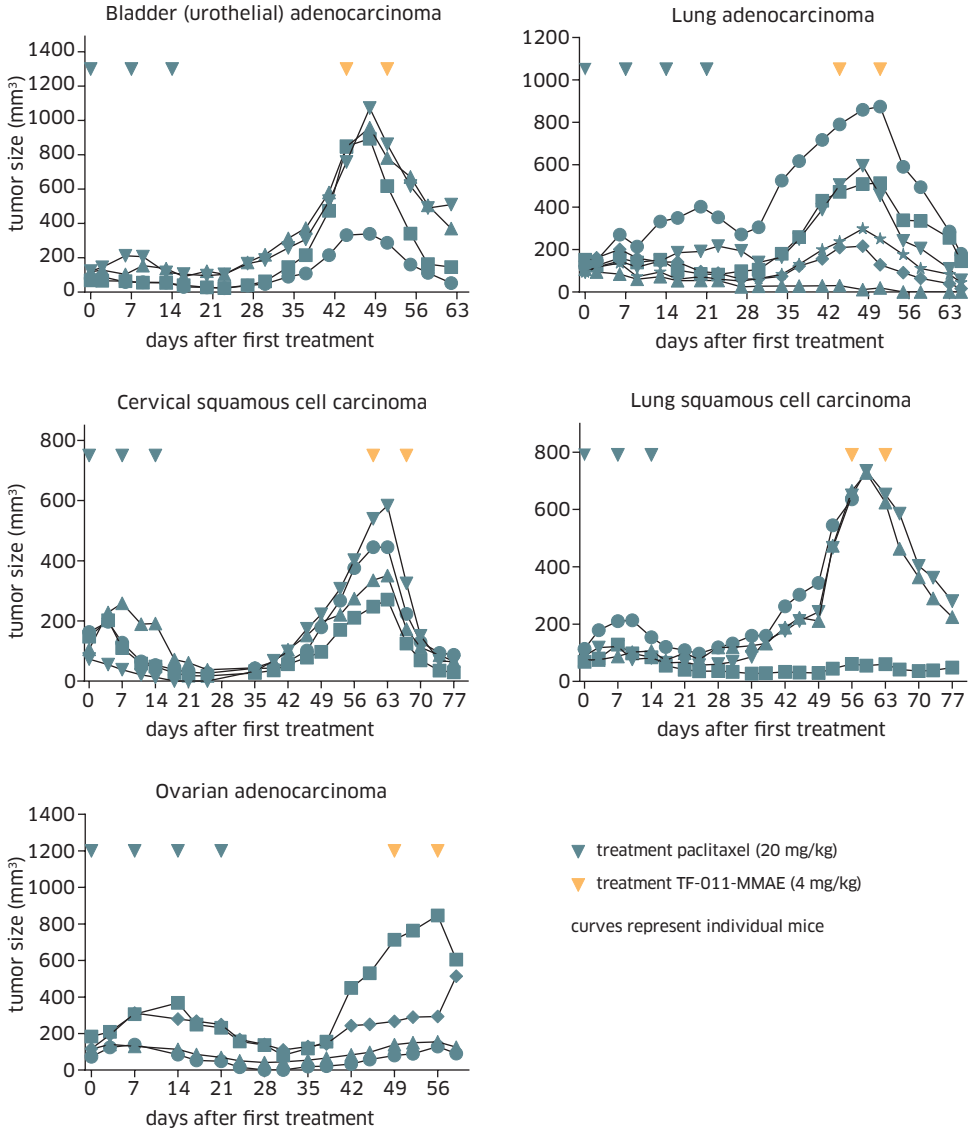

SUPPLEMENTARY FIGURE S6 *Post-paclitaxel treatment with TF-011-MMAE in PDX models.* PDX models were implanted s.c. in mice and when tumors had reached a size of 80-200 mm³, mice were randomized and treated with three or four doses of paclitaxel (20 mg/kg) at the indicated time points. Mice that showed tumor outgrowth after discontinuation of paclitaxel treatment were subsequently treated with two doses of 4 mg/kg TF-011-MMAE at the indicated time points. Curves and data points represent tumor sizes in individual mice.

Blot 1

Blot 3

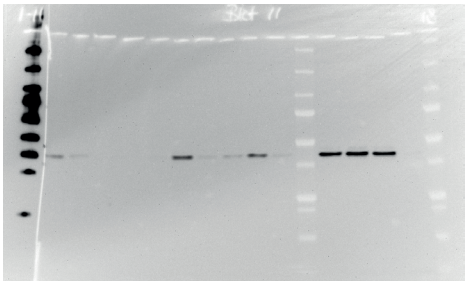

Blot 2

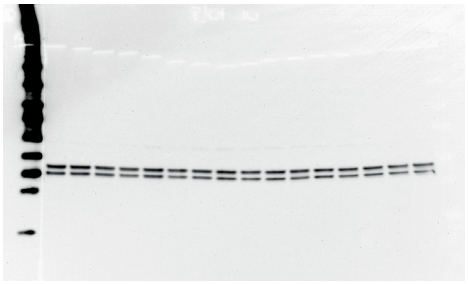

Blot 4

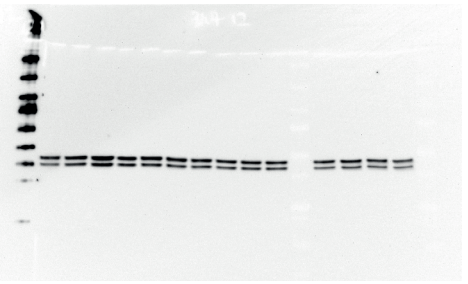

Legend blot 1,2: TF-011, TF-098, TF-114, TF-109		
Blot 1/2	**TF HuMab**	**FVIIa**
slot 1	protein marker	
slot 2	-	-
slot 3	TF-011	-
slot 4	TF-098	-
slot 5	TF-114	-
slot 6	TF-109	-
slot 7	-	10 nM FVIIa
slot 8	TF-011	10 nM FVIIa
slot 9	TF-098	10 nM FVIIa
slot 10	TF-114	10 nM FVIIa
slot 11	TF-109	10 nM FVIIa
slot 12	-	50 nM FVIIa
slot 13	TF-011	50 nM FVIIa
slot 14	TF-098	50 nM FVIIa
slot 15	TF-114	50 nM FVIIa
slot 16	TF-109	50 nM FVIIa
slot 17	-	-
slot 18	pre-stained marker	

Legend blot 3,4: TF-111, TF-044, TF-013, TF-025		
Blot 3/4	**TF HuMab**	**FVIIa**
slot 1	protein marker	
slot 2	-	-
slot 3	TF-111	-
slot 4	TF-044	-
slot 5	TF-013	-
slot 6	TF-025	-
slot 7	-	10 nM FVIIa
slot 8	TF-111	10 nM FVIIa
slot 9	TF-044	10 nM FVIIa
slot 10	TF-013	10 nM FVIIa
slot 11	TF-025	10 nM FVIIa
slot 12	pre-stained marker	
slot 13	TF-111	50 nM FVIIa
slot 14	TF-044	50 nM FVIIa
slot 15	TF-013	50 nM FVIIa
slot 16	TF-025	50 nM FVIIa
slot 17	pre-stained marker	
slot 18	-	

SUPPLEMENTARY FIGURE S7 *Full-length blots for figure 1C*. The cropped blots shown in the upper panel of Figure 1C (TF-011, TF-098, TF-114 and TF-109) were obtained from Blot 1 (p-ERK1/2) and Blot 2 (total ERK1/2). The cropped blots in the lower panel of Figure 1C (TF-111, -044, -013 and -25) were obtained from Blot 3 (p-ERK1/2) and Blot 4 (total ERK1/2).

5 Human kappa light chain targeted *Pseudomonas* exotoxin A – identifying human antibodies and Fab fragments with favorable characteristics for antibody-drug conjugate development

► J Immunol Methods. 2011 Aug 31;371 (1-2):122-33.

► Christian Kellner[1], Wim K. Bleeker[2], Jeroen J. Lammerts van Bueren[2], Matthias Staudinger[1], Katja Klausz[1], Stefanie Derer[1], Pia Glorius[1], Anja Muskulus[1], Bart E.C.G. de Goeij[2], Jan G.J. van de Winkel[2,3], Paul W.H.I. Parren[2], Thomas Valerius[1], Martin Gramatzki[1] and Matthias Peipp[1]

1 Division of Stem Cell Transplantation and Immunotherapy, 2nd Department of Medicine, Christian-Albrechts-University, Kiel.

2 Genmab, Utrecht, The Netherlands.

3 Immunotherapy Laboratory, Dept Immunology, University Medical Center Utrecht, Utrecht, The Netherlands

ABSTRACT

Antibody-drug conjugates (ADC) represent promising agents for targeted cancer therapy. To allow rational selection of human antibodies with favorable characteristics for ADC development a screening tool was designed obviating the need of preparing individual covalently linked conjugates. Therefore, α-kappa-ETA' was designed as a fusion protein consisting of a human kappa light chain binding antibody fragment and a truncated version of *Pseudomonas* exotoxin A. α-kappa-ETA' specifically bound to human kappa light chains of human or human-mouse chimeric antibodies and Fab fragments. Antibody-redirected α-kappa-ETA' specifically inhibited proliferation of antigen-expressing cell lines at low toxin and antibody concentrations. Selected antibodies that efficiently delivered α-kappa-ETA' in the novel assay system were used to generate scFv-based covalently linked immunotoxins. These molecules efficiently triggered apoptosis of target cells, indicating that antibodies identified in our assay system can be converted to functional immunoconjugates. Finally, a panel of human epidermal growth factor receptor (EGFR) antibodies was screened - demonstrating favorable characteristics with antibody 2F8. These data suggest that antibodies with potential for *Pseudomonas* exotoxin A-based ADC development can be identified using the novel α-kappa-ETA' conjugate.

INTRODUCTION

Antibody-drug conjugates (ADC) represent promising agents in tumor therapy, potentially overcoming some of the short-comings of "naked" antibodies or antibody derivatives that often are dependent on a functional host immune system [1-5]. ADC are bifunctional molecules that are composed of a targeting moiety represented by a monoclonal antibody or antibody fragment and a cytotoxic compound that is either chemically cross-linked or genetically fused [6-8]. The antibody moiety is used to deliver cytotoxic compounds to distinct antigen-positive cells recognized by the respective antibody. In the past, a variety of substances have been tested for ADC design. These include chemotherapeutic agents as well as toxins derived from plants or bacteria [9]. Often the toxic component only displays cytotoxicity when internalized. Therefore, for the development of ADC target antigens such as CD7, CD22, CD30 or CD33 on leukemias and lymphomas [6,10-12] and EGFR or HER2 on solid tumors were selected [13,14] due to a high internalization capacity after antibody binding or a high intrinsic turn over [6,7,9].

To date only a small number of ADC have been clinically approved with gemtuzumab-ozogamycin representing a prototypic conjugate composed of calicheamycin chemically linked to a CD33 IgG4 antibody [15,16]. Recently, novel ADC demonstrated impressive clinical results. Trastuzumab-DM1 (derivative of maytansine 1) showed

promising results in phase I and phase II clinical trials in patients with HER2-positive metastatic breast cancer [17-19]. Treatment with brentuximab vedotin, a chimeric CD30 antibody linked to the antimitotic agent monomethyl aurastatin E resulted in tumor regression for most patients with relapsed or refractory CD30-positive Hodgkin's lymphomas in a phase I study [20]. BL22, a CD22-directed ADC, representing a group of single-chain immunotoxins with scFv fragments fused to a truncated version of *Pseudomonas aeruginosa* exotoxin A, showed high response rates in phase II clinical trials in patients with hairy cell leukemia, achieving up to 47% complete remissions [21,22].

Irrespective of the ADC format, as chemical conjugate or single-chain fusion protein, selection of the targeting antibody is critical. Depending on epitope specificity, antibody binding to the targeted surface receptor may severely compromise surface redistribution, internalization and subsequently the intracellular routing of the receptor and potentially routing of the ADC / receptor complex. For example, different CD20 antibodies have been demonstrated to either recruit CD20 into lipid rafts or not, resulting in altered indirect effector functions such as CDC [23,24]. In addition, EGFR-directed antibodies have been demonstrated to significantly differ in their capacity to trigger receptor down modulation and internalization [25-27]. Furthermore, most toxic compounds only display potent cytoxicity when delivered to the correct intracellular compartment (e.g. the endoplasmatic reticulum (ER) for *Pseudomonas aeruginosa* exotoxin A) [28]. Therefore, different antibodies may significantly differ in their capacity to deliver selected cytotoxic compounds. As a consequence, selecting the most promising antibody at early developmental stages may reduce costs and obviates the need for testing many candidate conjugates in parallel in complex test systems such as animal models. Simple screening tools that allow identification of promising antibody candidates in an easy but highly predictive way may speed up the developing process. Cytotoxic compounds fused to an antibody-binding domain allowing formation of a stable non-covalent ADC may represent universal tools for fast screening of a large number of antibodies. Recently, fusion proteins of the IgG-binding motif from Streptococcal protein A or protein G and diphtheria toxin or *Pseudomonas aeruginosa* exotoxin A have been reported [29,30]. Although these molecules allowed formation of non-covalent ADC and screening of different murine and mouse/human chimeric antibodies for their potential to deliver a cytotoxic compound, this strategy displayed some limitations. As protein A and G display no species specificity and therefore also bind to bovine IgG present in high concentrations in most tissue culture media, establishing a high-throughput screening assay may be complicated, and may not allow screening by simple addition of antibody and antibody-binding toxin to the assay system [30]. Using antibody-binding domains with higher species specificity may overcome these shortcomings. Most therapeutic antibodies that enter clinical trials today are chimeric, humanized or fully human IgG antibodies containing human kappa light chains [31]. Therefore, in

the current report a novel *Pseudomonas aeruginosa* exotoxin A based fusion protein which specifically binds human kappa light chains was characterized as a screening tool to identify internalizing antibodies with potential in ADC development.

MATERIALS AND METHOD

Antibodies

Antibody	V-region	Constant region light chain	Constant region heavy chain	Specificity	Format	Source
Polyclonal rabbit serum	Rabbit	Rabbit kappa and lambda	Rabbit diff. isotypes	*Pseudomonas* exotoxin A	Igs	Sigma Aldrich
M225	Mouse	Mouse kappa	Mouse IgG1	Human EGFR	IgG1	ATCC
225-scFv-Fc	Mouse	None	Human IgG1 (CH2-CH3)	Human EGFR	scFv-Fc fusion	not published
4D5-scFv-Fc	Humanized	None	Human IgG1 (CH2-CH3)	Human HER2	scFv-Fc fusion	not published
CD16-Fab	Mouse	Human kappa	Human CH1	Human CD16	Fab fragment	not published
HM1.24-Fab	Mouse	Human kappa	Human CH1	Human HM1.24	Fab fragment	not published
Rituximab	Mouse	Human kappa	Human IgG1	Human CD20	Chimeric IgG1	Roche
Cetuximab	Mouse	Human kappa	Human IgG1	Human EGFR	Chimeric IgG1	Merck
2F8 (zalutumumab)	Human	Human kappa	Human IgG1	Human EGFR	IgG1	Genmab
018	Human	Human kappa	Human IgG1	Human EGFR	IgG1	Genmab
011	Human	Human kappa	Human IgG1	Human EGFR	IgG1	Genmab
008	Human	Human kappa	Human IgG1	Human EGFR	IgG1	Genmab
003	Human	Human kappa	Human IgG1	Human EGFR	IgG1	Genmab
panitumumab	Human	Human kappa	Human IgG2	Human EGFR	IgG2	Amgen
control IgG1	Human	Human kappa	Human IgG1	n.s.	IgG1	Sigma Aldrich
control IgG2	Human	Human kappa	Human IgG2	n.s.	IgG2	Sigma Aldrich
control IgA2	Human	Human kappa	Human IgA2	n.s.	IgA	Sigma Aldrich

Table 1. *Antibodies and antibody derivatives.* n.s. = not specified

Cell lines

Raji, Ramos, Daudi, ARH-77, CEM, L363 and A431 cells were obtained from the German Collection of Microorganisms and Cell Cultures (DSMZ, Braunschweig, Germany). JK-6L cells [32] were established in our laboratory. Cell lines were cultured in RPMI 1640-Glutamax-I medium (Invitrogen, Karlsruhe, Germany), containing 10% fetal calf serum, penicillin and streptomycin (R10+).

Construction of α-kappa-ETA'

AA truncated version of *Pseudomonas* exotoxin A (ETA') was synthesized according to published sequences (Entelechon GmbH; Regensburg, Germany). During that process, the codon usage was adjusted to *E.coli* and a mutation reported to enhance cytotoxicity (R490A) was introduced [33]. The KDEL endoplasmatic reticulum (ER)-retention motif was C-terminally introduced [34]. In addition, restriction sites allowing cloning into vector pet27b (Novagen) and the insertion of antibody binding domains such as scFv-fragments or domain antibodies as SfiI-cassettes were added [10,35]. The kappa light chain specific domain antibody was synthesized according to published sequences [36] and codon usage was adjusted to *E.coli*. The correct sequence of the final construct, pet27b-a- kappa-ETA', was verified by Sanger sequencing.

Expression and purification of immunotoxins

The ETA' fusion proteins were expressed under osmotic stress conditions as described [37]. Induced cultures were harvested 16–20 h after induction. The bacterial pellet from one liter culture was resuspended in 200 ml of extraction buffer (0.5 M sucrose, 0.1 M Tris, 1 mM EDTA, pH 8.0). The suspension was stirred for 3 h at 4°C and cleared by centrifugation for 30 min at 20.000 g. The ETA' fusion proteins were enriched by two step affinity chromatography using streptactin agarose matrix and Ni-NTA agarose (Qiagen, Hilden, Germany) according to the manufacturer's instructions. Final elution fractions containing recombinant protein were extensively dialyzed against PBS and stored at 4°C until use. Purified proteins were quantitated using capillary electrophoresis on an Experion™ system (BioRad, Hercules, USA) according to the manufacturer's protocol.

Flow cytometric analyses

For immunofluorescence staining, 3 x 10^5 target cells were washed in PBS supplemented with 1% bovine serum albumin (BSA; Sigma- Aldrich, Munich, Germany) and 0.1% sodium-azide (PBA buffer). To analyze immunotoxin binding, cells were incubated with either HM1.24-ETA', 225-ETA' or control proteins at indicated concentrations for 30 min on ice. After two times washing with 500 µl PBA buffer, cells were stained with Alexa-Fluor-488 coupled mouse anti-penta-his antibody (Qiagen, Hilden, Germany) or rabbit-anti-Exotoxin A polyclonal antibodies and FITC-labelled $F(ab')^2$-fragments of polyclonal goat anti-rabbit antibodies (Sigma-Aldrich). To investigate α-kappa-ETA' binding, cells were incubated with 20 µg/ml of the op-

sonising antibody or irrelevant control molecules diluted in PBA-buffer for 30 min on ice. After washing 20 µg/ml α-kappa-ETA' diluted in PBA-buffer was added and incubated for 30 min on ice. In the next step cells were washed as described. Polyclonal rabbit-anti-exotoxin A antibodies were added and cells were incubated for 30 min on ice. Following a washing step cells were incubated with FITC-conjugated polyclonal goat-anti-rabbit $F(ab')^2$ fragments. After a final washing step cells were fixed in 1% paraformaldehyde / PBS solution. Cells were analyzed by flow cytometry (Epics XL or FC500, Coulter) using appropriate scatter settings.

SDS-PAGE / Western blot analysis / Coomassie staining

1-2 µg of the respective purified recombinant protein was loaded on 4-12% Tris-Glycine gels (Invitrogen) under reducing conditions and were either directly stained with colloidal coomassie brilliant blue staining solution (Carl Roth GmbH) or blotted to PVDF membranes according to standard procedures. For the detection of purified exotoxin A-based fusion proteins membranes were blocked using 2% BSA / 2% non-fat dry milk in tris-buffered saline (TBS) for 1h at RT. Polyclonal rabbit anti-*Pseudomonas* exotoxin A antibodies (Sigma Aldrich) were added to a final dilution of 1:5000 and incubated for 1h at RT. Blots were washed with TBS-buffer containing 0.05% Tween 20 and 0.2% Triton X-100 three times for 5 min. HRP-conjugated polyclonal goat anti-rabbit antibodies were added in 2% BSA / 2% non-fat dry milk TBS solution for 1 h and washed as described above. Blots were finally developed using the ECL detection system (Pierce) and analyzed using a digital imaging system (Biorad). Detection of recombinant proteins by using anti-penta-his antibodies (Qiagen) was performed according to the manufacturer's instructions.

ELISA

Maxisorp ELISA plates were coated with 25 µl of the respective proteins diluted in PBS (final concentration of 10 µg/ml) for 1h at 37°C. Plates were washed with 125 µl of PBS and blocked with 100 µl of PBS / 3% BSA solution for 1 h at 37°C. α-kappa-ETA' (25 µl) was added at a concentration of 20 µg/ml diluted in PBS / 3% BSA. After 1 h incubation at 37°C wells were washed 3 times with PBS and polyclonal rabbit-anti-Exotoxin antibodies (Sigma-Aldrich) diluted in PBS / 3% BSA (1:2000) was added and incubated for 1 h at 37°C. Wells were washed as described above and polyclonal goat-anti-rabbit-IgG (H+L) HRP antibodies (Dianova; 1:2000 diluted in PBS / 3% BSA) were added. After a final 1h incubation step at 37°C wells were washed as described and developed by adding 50 µl ABTS solution (Roche). After 10 min incubation, absorbance was measured at 405 nm in a Tecan Rainbow plate reader. For control experiments demonstrating successful coating of proteins peroxidase-conjugated polyclonal $F(ab')^2$ fragments goat-anti-mouse IgG (H+L) (Dianova) or goat-anti-human-IgG-HRP (Sigma-Aldrich) diluted in PBS / 3% BSA (1:2000) were used.

Measurement of cytotoxic effects of immunotoxins

For detection of cytotoxic effects of immunotoxin, cells were seeded at 2 x 10^4 cells per 100 µl in 96-well plates.

ETA' fusion proteins in the presence or absence of antibodies were added at indicated concentrations. After 3 d of treatment, vital cell mass was measured using the MTT assay (Cell Proliferation Kit I; Roche, Mannheim, Germany). For the detection of early stages of apoptosis and cell death triggered by immunotoxin treatment, cells were seeded at 2 x 10^5 cells per ml in 24-well plates with varying immunotoxin concentrations. Cells were stained with FITC-conjugated Annexin V and 7-AAD (Beckman Coulter, Fullerton, USA) according to the manufacturers´ protocol, and subsequently analyzed by flow cytometry.

Statistical analyses

Statistical analysis was performed using GraphPad Prism. Experimental data were analyzed using the student's t-test, one- or two-way ANOVA repeated measures test with Bonferroni's post test when appropriate. The null hypothesis was rejected when $p < 0.05$.

RESULTS

Construction and purification of the kappa light chain-directed immunotoxin α-kappa-ETA'

In order to redirect *Pseudomonas* exotoxin A to human kappa light chain-containing antibodies or antibody derivatives, α-kappa-ETA', a kappa light chain-binding immunotoxin was designed. Therefore, a human kappa light chain-specific domain antibody was genetically fused to a truncated version of *Pseudomonas* exotoxin A (Fig.1A). The recombinant protein was secreted to the periplasm of *E.coli* and purified by two step affinity chromatography. Yields of the purified recombinant protein varied between 0.5-2 mg per liter of expression culture. Elution fractions from the second purification step were analyzed by SDS-PAGE and coomassie staining or western blot analysis. α-kappa-ETA' migrated with an apparent molecular mass of 55 kDa, closely resembling the calculated molecular mass (53.7 kDa; Fig. 1B). Western blot analysis further confirmed the identity of the purified protein (Fig. 1B).

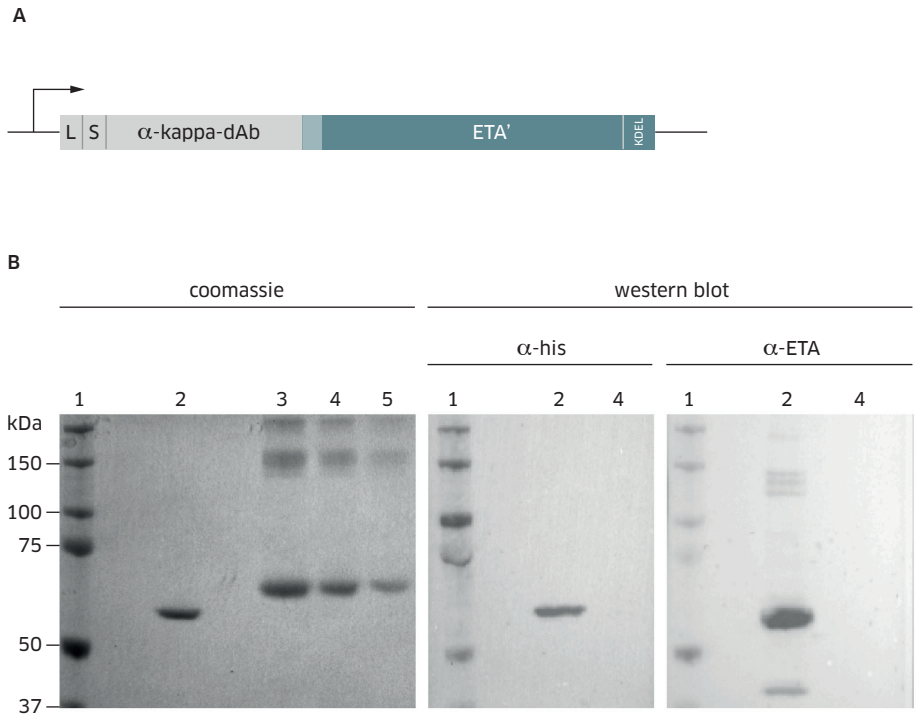

FIGURE 1 *Design and purification of α-kappa-ETA'.* **(A)** Scheme of α-kappa-ETA'. For secreted bacterial expression a pelB leader sequence (L) was introduced at the 5´-end. For purification a combined 6xhistidine- and strep-II-tag was added (S). ETA' = truncated version of *Pseudomonas* exotoxin A; KDEL = endoplasmatic reticulum retention motif; dAb = domain antibody with human kappa light chain specificity. **(B)** α-kappa-ETA' was expressed under osmotic stress conditions and purified from periplasmatic extracts using streptactin and Ni-NTA agarose beads. The purified protein was analyzed by SDS-PAGE and coomassie staining or western blot analysis using anti-penta-his or anti-exotoxin A specific antibodies. Lane 1 = molecular mass standard; lane 2 = purified α-kappa-ETA'; lane 3-5 = BSA as mass standard and specificity control for western blotting. Data are representative results from at least three experiments.

Kappa light chain-specific binding of α-kappa-ETA'

To demonstrate kappa light chain specific binding of α-kappa-ETA', ELISA experiments were performed. α-kappa-ETA' specifically bound to human kappa light chain containing antibodies of different isotype and Fab fragments, while no binding to fusion proteins containing a human IgG1-Fc domain but lacking the antibodies' constant kappa and CH1 regions (225-scFv-Fc and 4D5-scFv-Fc) or a murine IgG1 / kappa antibody was observed (Fig.2A). To further confirm human kappa light chain binding, cell lines expressing kappa or lambda light chain containing B cell receptors and cell lines lacking B cell receptor expression were analyzed for α-kappa-ETA' binding. As expected α-kappa-ETA' bound to kappa light chain-positive cell lines

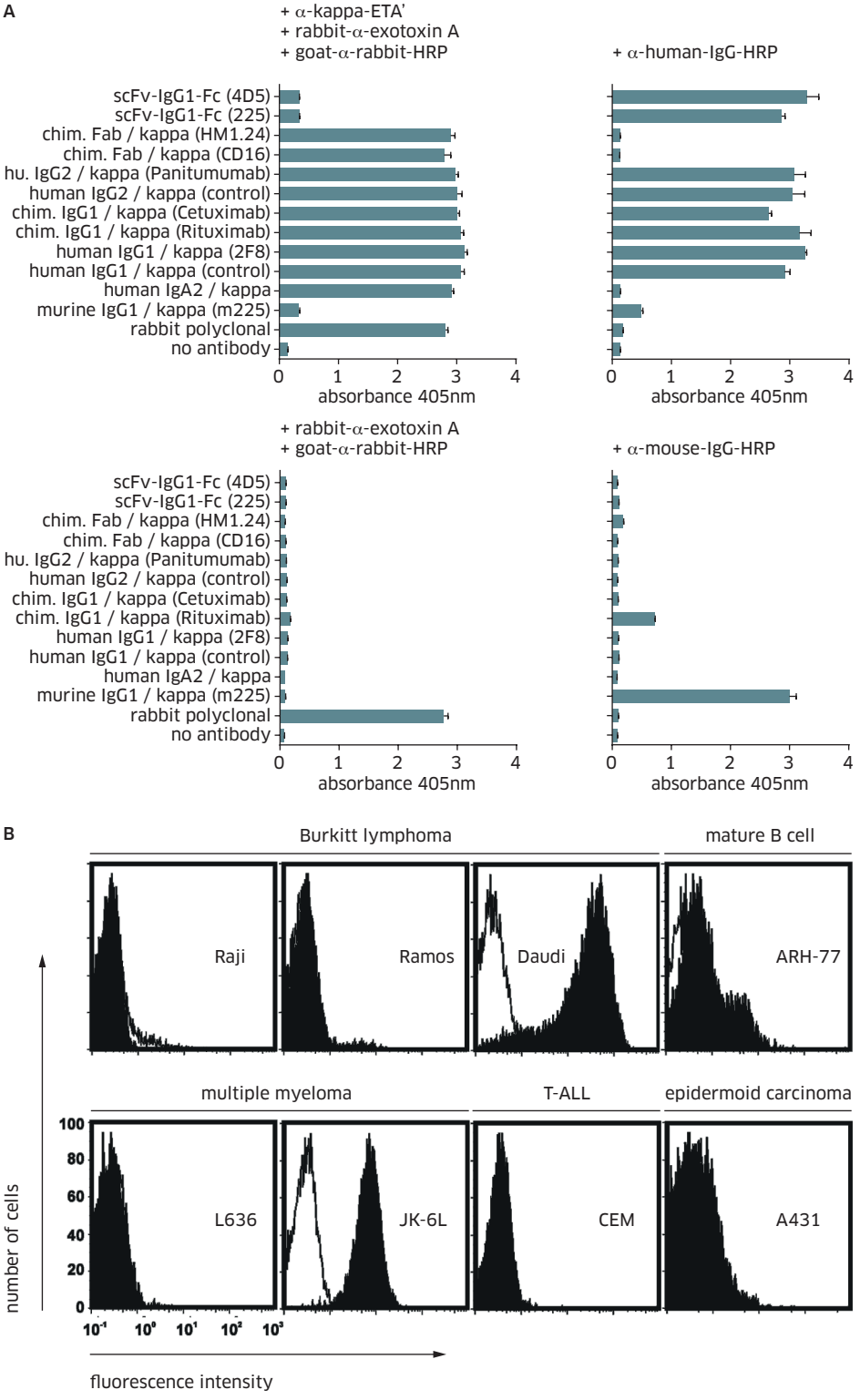
A
+ α-kappa-ETA'
+ rabbit-α-exotoxin A
+ goat-α-rabbit-HRP
+ α-human-IgG-HRP
scFv-IgG1-Fc (4D5)
scFv-IgG1-Fc (225)
chim. Fab / kappa (HM1.24)
chim. Fab / kappa (CD16)
hu. IgG2 / kappa (Panitumumab)
human IgG2 / kappa (control)
chim. IgG1 / kappa (Cetuximab)
chim. IgG1 / kappa (Rituximab)
human IgG1 / kappa (2F8)
human IgG1 / kappa (control)
human IgA2 / kappa
murine IgG1 / kappa (m225)
rabbit polyclonal
no antibody
0 1 2 3 4
absorbance 405nm
+ rabbit-α-exotoxin A
+ goat-α-rabbit-HRP
+ α-mouse-IgG-HRP
B
Burkitt lymphoma
mature B cell
Raji
Ramos
Daudi
ARH-77
multiple myeloma
T-ALL
epidermoid carcinoma
L636
JK-6L
CEM
A431
number of cells
100
80
60
40
20
0
10⁻¹ 10⁰ 10¹ 10² 10³
fluorescence intensity

FIGURE 2 *α-kappa-ETA' specifically binds to human kappa light chain containing antibodies and cell lines expressing cell-surface immunoglobulin with kappa light chains.* **(A)** Binding of α-kappa-ETA' to human kappa light chain was analyzed by ELISA using various human kappa light chain containing antibodies or control proteins. Identity of coated human, mouse and rabbit antibodies was further checked using anti-mouse-, anti-rabbit- or anti-human-HRP conjugates. **(B)** α-kappa-ETA' binding to cell lines expressing cell-surface-immunoglobulin with kappa light chains (Daudi; ARH-77; JK-6L), a cell line expressing cell-surface-immunoglobulin with l-light chains (Ramos) and cell lines that do not express cell-surface immunoglobulin (Raji; L363; CEM; A431) were analyzed by flow cytometry. α-kappa-ETA' was detected with a *Pseudomonas* exotoxin A specific polyclonal antibody and FITC- or HRP-conjugated rabbit-specific secondary reagents. For ELISA experiments, mean values +/- SEM from triplicate wells are given. Data are representative results from three experiments.

Daudi, ARH-77 and JK6-L while no binding was observed on lambda light chain expressing Ramos cells or B cell receptor-negative CEM, L363 and A431 cells. These results were in agreement with staining patterns observed with an anti-human kappa light chain-specific monoclonal antibody (data not shown). Together these data indicate that α-kappa-ETA' was successfully expressed and specifically bound antibodies containing human kappa light chains.

Kappa light chain-specific binding of α-kappa-ETA'

To demonstrate kappa light chain specific binding of α-kappa-ETA', ELISA experiments were performed. α-kappa-ETA' specifically bound to human kappa light chain containing antibodies of different isotype and Fab fragments, while no binding to fusion proteins containing a human IgG1-Fc domain but lacking the antibodies' constant kappa and CH1 regions (225-scFv-Fc and 4D5-scFv-Fc) or a murine IgG1 / kappa antibody was observed (Fig.2A). To further confirm human kappa light chain binding, cell lines expressing kappa or lambda light chain containing B cell receptors and cell lines lacking B cell receptor expression were analyzed for α-kappa-ETA' binding. As expected α-kappa-ETA' bound to kappa light chain-positive cell lines Daudi, ARH-77 and JK6-L while no binding was observed on lambda light chain expressing Ramos cells or B cell receptor-negative CEM, L363 and A431 cells. These results were in agreement with staining patterns observed with an anti-human kappa light chain-specific monoclonal antibody (data not shown). Together these data indicate that α-kappa-ETA' was successfully expressed and specifically bound antibodies containing human kappa light chains.

Antibody-dependent surface deposition of α-kappa-ETA'

To analyze antibody-dependent surface deposition of α-kappa-ETA', antibodies and Fab fragments directed against two highly internalized surface antigens were investigated. HM1.24 is a surface receptor expressed on multiple myeloma cells, while EGFR is expressed on a variety of solid tumors. To demonstrate α-kappa-ETA' binding to antibody-opsonized target cells, the kappa light chain-negative L363 myeloma cell line (HM1.24-positive) and the epidermoid carcinoma cell line A431 (EGFR-positive) were opsonized with target cell-specific mouse/human chimeric HM1.24-spe-

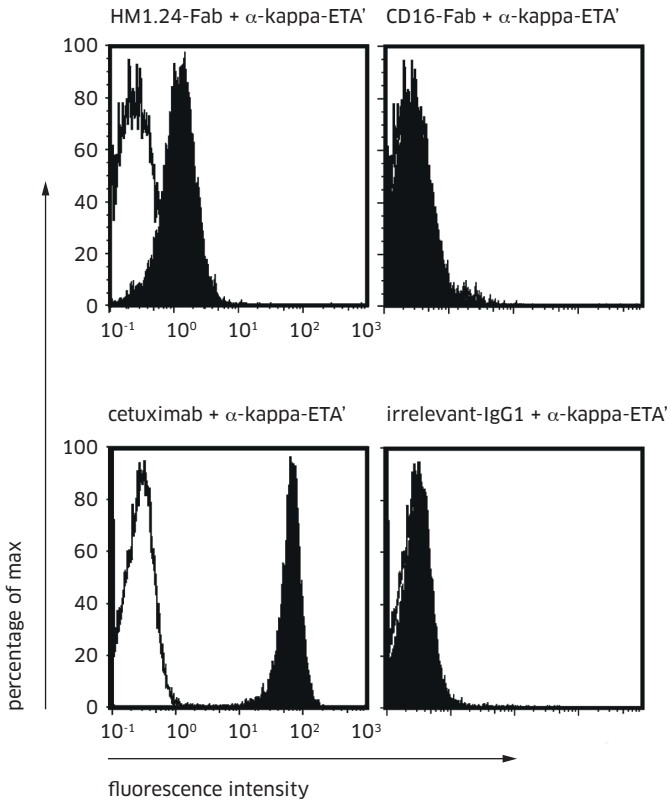

FIGURE 3 *α-kappa-ETA' specifically binds to target cells opsonized with human/mouse chimeric Fab fragments or IgG1 antibodies containing kappa light chains.* **(A)** To demonstrate specific redirected binding of α-kappa-ETA' to L363 cells (HM1.24+, EGFR-, kappa light chain-), cells were incubated with a chimeric HM1.24-directed Fab fragment that binds HM1.24, a surface marker expressed on multiple myeloma cell lines or with a CD16-specific control Fab. **(B)** Analogous experiments were performed with A431 cells (HM1.24low, EGFR+, kappa light chain-). After opsonization, α-kappa-ETA' was added and detected using anti-*Pseudomonas* exotoxin A antibodies and appropriate FITC-labeled secondary reagents. Data are representative results from three experiments that were performed.

cific Fab fragments or the EGFR-specifc mouse/human chimeric IgG1 antibody cetuximab, respectively. α-kappa-ETA' specifically bound to opsonized target cells, while no binding was observed when irrelevant matched control molecules that lack cell binding activity were used (Fig.3).

Cytotoxic effect of non-targeted α-kappa-ETA'

α-kappa-ETA' concentrations that do not show "unspecific" cytotoxic effects and consequently may be applicable for testing specific antibody-dependent delivery to kappa light chain-negative cell lines were determined. Therefore, kappa light chain negative cell lines L363 or A431 cells were incubated with increasing concentrations of α-kappa-ETA' and the direct growth inhibition effects were determined using the MTT assay. Interestingly, both cell lines differed significantly in sensitivity to non-targeted α-kappa-ETA'. L363 cells were quite resistant to α-kappa-ETA' up to 10 µg/ml, while A431 cells showed cytotoxic effects already at concentrations greater than 0.1 µg/ml (Fig.4). Therefore, for antibody-dependent delivery of α-kappa-ETA', 0.1 µg/ml was used for both cell lines.

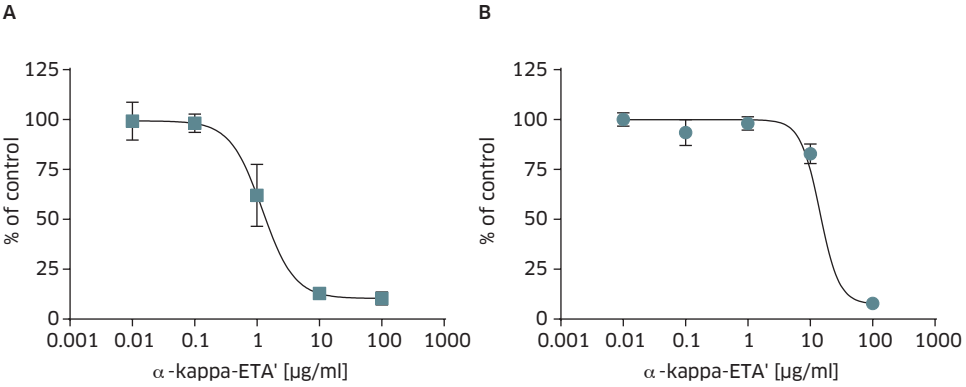

FIGURE 4 *Kappa light chain-negative cell lines show differences in sensitivity to "non-targeted" α-kappa-ETA'.* Kappa light chain-negative **(A)** A431 cells and **(B)** L363 cells were treated with increasing concentrations of α-kappa-ETA' to determine the maximally tolerated dose that does not lead to induction of non-specific cell death. After 72 h vital cell mass was measured by MTT assay. Untreated cells served as controls. Data are mean values +/- SEM of three independent experiments.

Antibody-dependent growth inhibition mediated by α-kappa-ETA'

To analyze whether antibody-dependent binding of α-kappa-ETA' leads to intracellular toxin delivery and growth inhibition of opsonized target cells, proliferation assays were performed. L363 cells or A431 cells were incubated with different target cell specific kappa light chain-containing antibody variants and isotypes, including Fab fragments, human/mouse chimeric IgG1, human IgG1, human IgG2 antibodies or corresponding isotype-matched control antibodies. In all cases analyzed strong inhibitory effects were observed when α-kappa-ETA' was incubated together with a target cell binding antibody variant but not when a matched control antibody molecule was used that does not bind to the respective target cell (Fig.5).

Antibody-dependent growth inhibition mediated by α-kappa-ETA' is human kappa light chain dependent

Experiments displayed in Fig.5 demonstrated that a strong inhibitory effect on cell proliferation of A431 cells was observed when α-kappa-ETA' was combined with the anti-EGFR antibody cetuximab or 2F8. Furthermore, significant inhibition of proliferation was also observed when the EGFR directed antibodies were tested without adding α-kappa-ETA'. To test whether the inhibitory effect mediated by the combination of α-kappa-ETA' and cetuximab was due to a kappa light chain-dependent delivery of α-kappa-ETA' and not due to the independent action of α-kappa-ETA' and the EGFR-directed antibody, experiments with the EGFR-directed murine IgG1 antibody m225 were performed. m225 is the parental murine antibody used for the generation of the mouse/human chimeric antibody cetuximab, and therefore shares identical v-regions. In proliferation assays m225 and cetuximab similarly inhibited growth of A431 cells in a dose-dependent manner. Importantly, when α-kappa-ETA' was added to m225 or cetuximab, a strong additional inhibitory effect was only observed in combination with cetuximab but not with the murine antibody m225 (Fig.6). These data indicated that most likely a noncovalent toxin / antibody complex was formed with the human kappa light chain containing antibody cetuximab but not with murine kappa light chain containing antibody m225 (in ELISA experiments α-kappa-ETA' did not bind to m225), resulting in the significant reduction in proliferation.

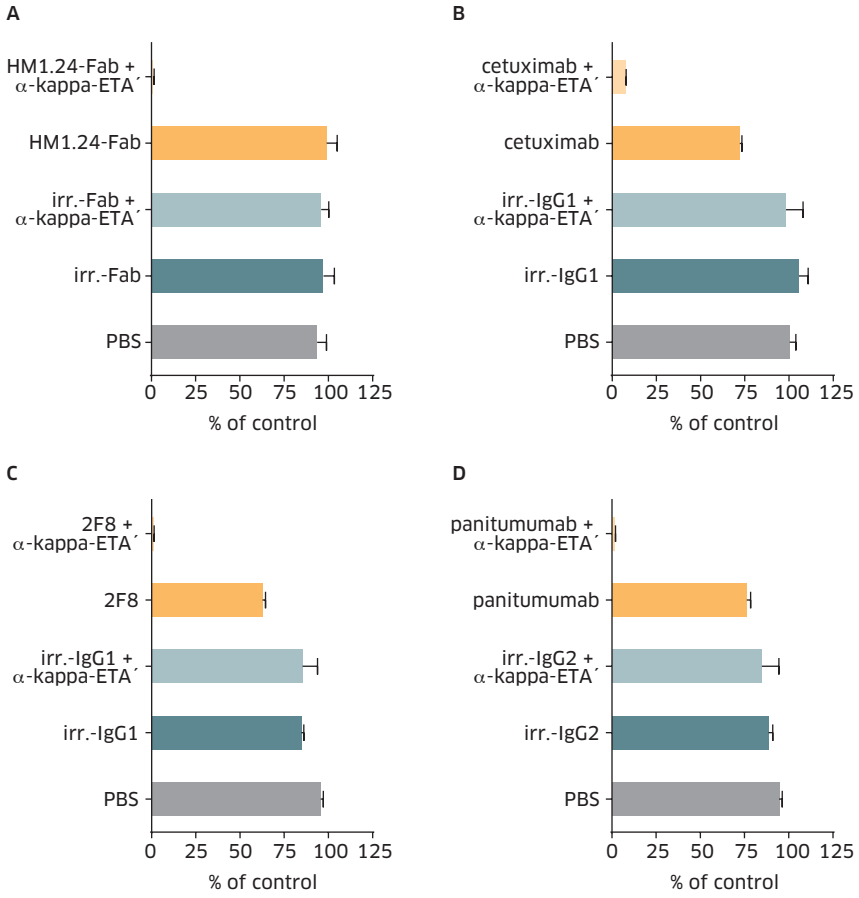

FIGURE 5 *α-kappa-ETA' induced inhibition of proliferation of opsonized target cells.* **(A)** L363 cells were incubated with recombinant HM1.24-specific mouse/human chimeric Fab fragments or an irrelevant similarly designed control molecule in the presence or absence of α-kappa-ETA'. **(B-D)** Similar experiments were performed with A431 cells and different EGFR-directed antibodies. **(B)** mouse/human chimeric IgG1/kappa antibody cetuximab; **(C)** fully human IgG1/kappa antibody 2F8; **(D)** fully human IgG2/kappa antibody panitumumab. Antibodies and Fab fragments were used at 1µg/ml, α-kappa-ETA' was used at 0.1 µg/ml final concentration. Isotype matched irrrelevant antibodies served as negative controls. After 72 h vital cell mass was determined by MTT assay. Data are mean values +/- SEM of **(A)** three or **(B-D)** five independent experiments. (*) statistically significant difference compared to PBS-treated control. (#) statistically significant difference compared to antibody-only treated cells. ($p<0.05$).

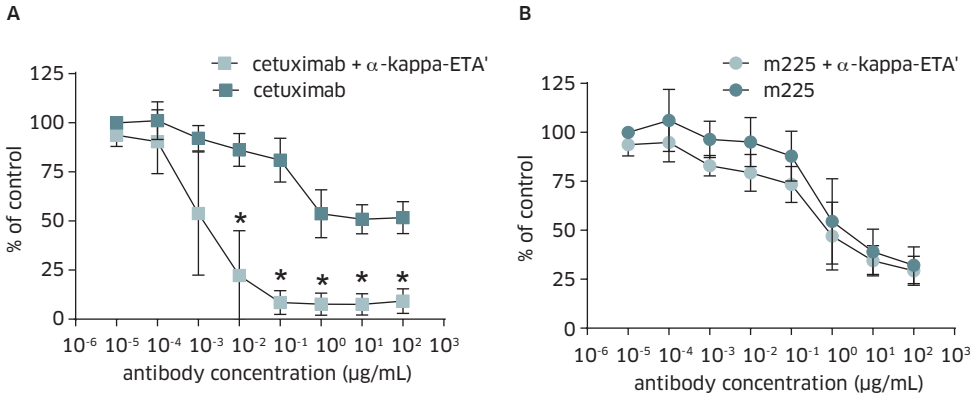

FIGURE 6 *Cytotoxic effect of kappa-directed ETA' is human kappa chain specific.* **(A)** A431 cells were incubated with increasing concentrations of **(A)** cetuximab or **(B)** with the parental murine IgG1/murine kappa antibody m225 (used for the generation of cetuximab) in the presence or absence of a constant concentration of α-kappa-ETA'. After 72 h vital cell mass was measured by MTT assay. Untreated cells served as controls. Data are mean values +/- SD of three independent experiments. (*) represents statistical difference between antibody vs antibody + α-kappa-ETA' treatment. α-kappa-ETA' was used at 0.1 µg/ml.

Cytotoxicity mediated by genetically linked single chain immunotoxins

In a next set of experiments it was tested whether antibodies which were able to potently deliver α-kappa-ETA' to antigen expressing cells can be converted to functionally active covalently linked immunotoxins. Therefore, scFv fragments derived from the v-regions of cetuximab or from a chimeric HM1.24-specific Fab fragment were genetically fused to the truncated version of *Pseudomonas* exotoxin A (Fig.7A). The two proteins HM1.24-ETA' and 225-ETA' were expressed in *E.coli* and purified (Fig.7A). 225-ETA' and HM1.24-ETA' specifically bound to antigen-expressing cells, while no binding was detected on antigen-negative cells (data not shown). HM1.24-ETA' induced apoptosis of HM1.24-expressing L363 cells at low concentrations (Fig.7B). This cytotoxic effect was completely inhibited by adding excess of the parental HM1.24-specific antibody demonstrating strict antigen-dependent induction of apoptosis (data not shown). No induction of apoptosis was observed with antigen negative Raji cells (Fig.7B). 225-ETA' mediated inhibition of proliferation of A431 cells, while an irrelevant control molecule did not show any inhibitory effect (Fig.7C). These data underline our hypothesis that antibodies which demonstrated strong inhibitory effects in our α-kappa-ETA' based screening assay can be successfully converted to functionally active covalently linked immunotoxins.

Screening a panel of human EGFR antibodies

A panel of seven novel human kappa light chain-containing IgG antibodies recognizing different epitopes on EGFR's extracellular domain (Fig.8A; Table II; [38]) was tested in the screening system. All antibodies tested in combination with α-kappa-ETA' showed significant inhibitory effects on growth of A431 cells, while only limited inhibitory effects were observed without addition of α-kappa-ETA' (Fig.8B). Clone 2F8 demonstrated the strongest inhibitory effect with IC50 values ~5-fold lower than clone 008 which showed the weakest effect in the test panel (Fig.8B). There was no obvious correlation between affinity / avidity and extend of cytotoxic effect (Table II). This observation was more closely in line with potency in internalization and EGFR down modulation previously observed for this antibody [39]. According to the presented data antibody 2F8 may be very well suited for the development of ADC.

Together these data suggest that α-kappa-ETA' may represent an interesting novel screening tool for the identification of promising candidate antibodies for the development of *Pseudomonas* exotoxin A-based immunotoxins and potentially other ADCs.

A

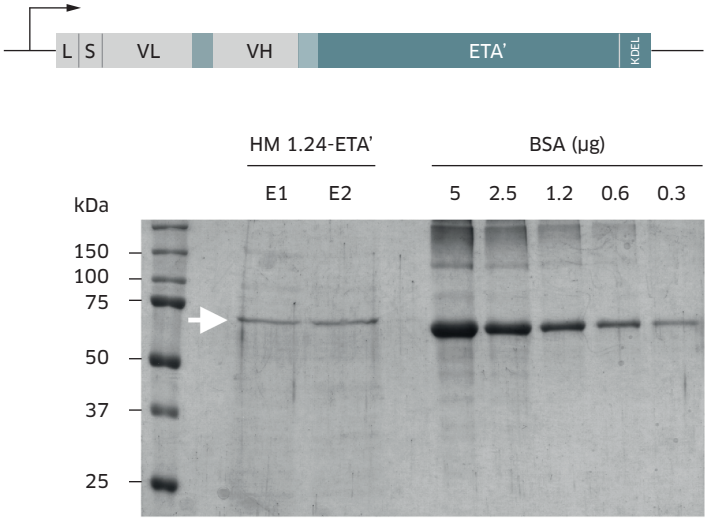
L
S
VL
VH
ETA'
KDEL
HM 1.24-ETA'
BSA (µg)
E1
E2
5
2.5
1.2
0.6
0.3
kDa
150
100
75
50
37
25

B

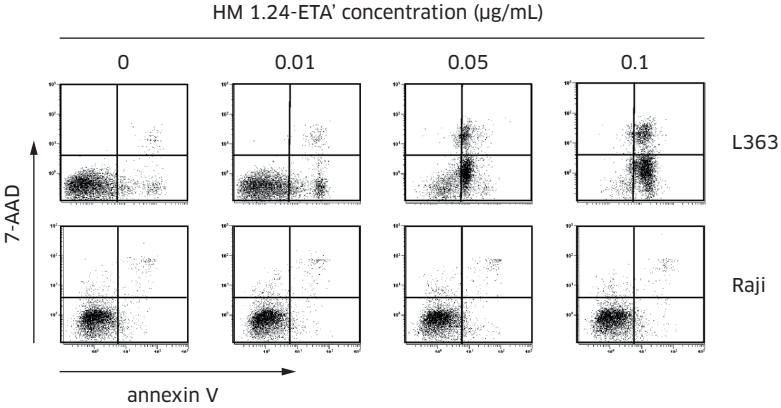
HM 1.24-ETA' concentration (µg/mL)
0
0.01
0.05
0.1
L363
Raji
7-AAD
annexin V

C

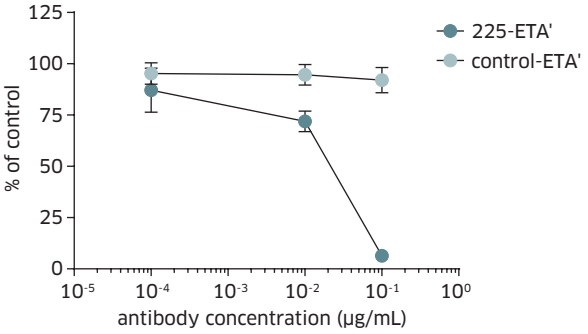
225-ETA'
control-ETA'
% of control
125
100
75
50
25
0
10-5
10-4
10-3
10-2
10-1
100
antibody concentration (µg/mL)

FIGURE 7 *Design and antigen-specific killing of scFv-based immunotoxins against tumor associated antigens.* **(A)** Design and purification of the recombinant scFv-based immunotoxins. L=pelB secretion leader; S = STREP-II-6xHis-tag; ETA' = truncated ETA fragment consisting of domain II and III of *Pseudomonas* exotoxin A; KDEL = endoplasmic reticulum retention motif; VL = V-region of the antibody light chain; VH = V-region of the antibody heavy chain. SDS-PAGE and coomassie staining was performed to analyze purity and integrity of 225-ETA' and HM1.24-ETA'. HM1.24-ETA' is shown as a representative result. **(B)** Dose-dependent induction of apoptosis and cell death of HM1.24-positive L363 multiple myeloma cells and antigen negative Raji cells was analyzed. 24h after treatment cells were analyzed by annexin V / 7-AAD staining and flow cytometry. **(C)** Antiproliferative activity of 225-ETA'. Tartget cells A431. After 72 h, vital cell mass was measured by MTT assay. Data are mean values +/- SEM of three independent experiments.

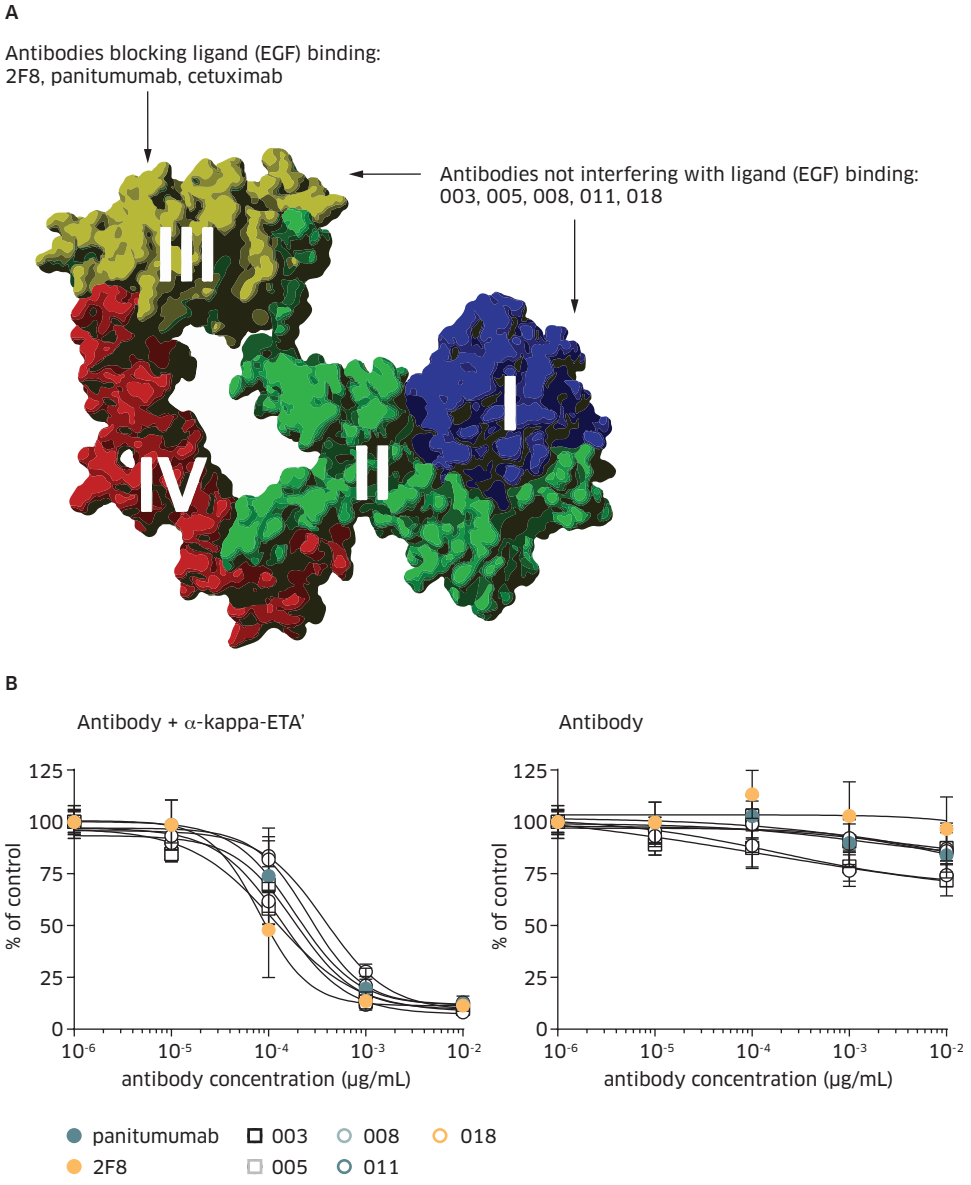

FIGURE 8 Fully human EGFR antibodies differ in their capacity to deliver α-kappa-ETA'. **(A)** Fully human antibodies directed against different subdomains I-IV of EGFR were analyzed in the novel screening assay. The 3D-model is based on protein structure pdb-file 1YY9 and was produced using the YASARA Structure software package. **(B)** A431 cells were incubated with increasing antibody concentrations in the presence (left graph) or absence (right graph) of a constant concentration of α-kappa-ETA'. After 72 h vital cell mass was measured by MTT assay. Untreated cells served as controls. Data are mean values +/- SEM of three independent experiments (each experiment set up in triplicates). α-kappa-ETA' was used at 0.1 µg/ml. * = significant difference between 008 and 2F8 ($p<0.05$). # = 2F8 significantly more effective compared to all other antibodies ($p<0.05$).

DISCUSSION

A novel human kappa light chain binding immunotoxin, α-kappa-ETA', was generated to allow screening for antibodies with potential in ADC development obviating the production of covalently linked individual conjugates. α-kappa-ETA' was specifically delivered and significantly inhibited proliferation of target cells that were opsonized with antibodies directed against internalized antigens HM1.24 and EGFR. Derived single-chain immunotoxins HM1.24-ETA' and 225-ETA' were highly active, indicating that antibodies identified in the screening approach can be successfully converted to genetically linked immunotoxins. Finally, a set of 7 fully human anti-EGFR antibodies was screened, with 2F8 identified as the most potent antibody in our novel screening assay.

Screening platforms allowing identification of antibody candidates for ADC in an easy but highly predictive way may speed up the developing process. To address this issue, recently fusion proteins of antibody binding proteins (IgG-binding motif from Streptococcal protein A or protein G) and diphtheria toxin or *Pseudomonas* exotoxin A were reported [29,30]. These molecules in contrast to α-kappa-ETA' bound the Fc part of complete antibodies. Although this strategy allowed screening of different antibodies for their potential to deliver the cytotoxic fusion protein, some caveats may limit its broad applicability. One of the proteins formed stable complexes only after further treatment with a chemical cross-linker [30]. In addition, the fusion proteins due to their protein A/G based design bind to the Fc part of different antibody isotypes with different affinities potentially compromising data interpretation when antibodies with different isotypes should be compared. Furthermore protein A/G based toxin fusions bind to bovine IgG in serum containing tissue culture medium if not covalently linked to the antibody [30]. Therefore, antibody screening with these molecules still requires pre-formation of the antibody-toxin-complex for reliable data interpretation or adaption of the target cell line to serum free conditions [30]. These procedures either require purified antibodies or adaption of tissue culture conditions, further complicating potential high throughput screenings. Due to its high specificity for human kappa light chain, α-kappa-ETA' may be ideally suited for screening different human antibodies, irrespective of the antibody isotype. A limitation of the presented concept is that potentially interesting murine antibodies from readily available hybridoma lines can not be tested, which is limited to human kappa light chain containing antibodies. Nevertheless, most therapeutic antibodies entering clinical trials today contain human kappa light chains, as reflected by the fact that to date all clinically approved chimeric, humanized and human antibodies are based on kappa constant regions. Consequently, although limited to human antibodies the novel screening tool may be widely applicable for screening large numbers of human antibodies isolated from human hybridoma lines or transgenic mice harboring human antibody genes, such as the Humab- or Xeno-mouse strains

[31,40,41]. In addition α-kappa-ETA' may represent an interesting tool for screening internalization characteristics of Fab or single-chain Fab fragments derived from phage display libraries [42,43]. In this setting α-kappa-ETA' in contrast to protein A / G based immunotoxins may obviate the need in converting isolated Fab fragments into complete antibodies. This assay system may easily be adapted for screening human lambda light chain containing or murine antibodies, by replacing the human kappa light chain-directed domain antibody by other antibody fragments with high immunoglobulin specificity. Whether antibodies with favorable characteristics identified by *in vitro* screening systems as described here will finally result in ADC with favorable *in vivo* characteristics ideally in a clinical setting has to be carefully evaluated in the future.

Antibody	EC_{50} (FACS) [µg/mL][a]	IC_{50} (MTT) [µg/mL]	Epitope location
2F8 (zalutumumab)	0.7	0.8×10^{-4}	Domain III
panitumumab	0.6	1.9×10^{-4}	Domain III
018	1.2	2.6×10^{-4}	Domain III
011	2.7	1.4×10^{-4}	Domain I/II
008	3.2	3.8×10^{-4}	Domain I/II
005	3.0	1.1×10^{-4}	Domain I/II
003	9.2	1.9×10^{-4}	Domain I/II

TABLE 2 *Characteristics of human IgG1/kappa EGFR antibodies.* a Dose dependent binding to EGFR-expressing cells was analyzed using indirect immunofluorescence staining and flow cytometry (data not show).

Acknowledgements

Heidi Bosse, Britta von Below and Daniela Hallack are acknowledged for expert technical assistance. This study was supported by research grant 2007.065.1 from the Wilhelm Sander-Stiftung, research grant DJCLS R 08/01 from the Deutsche José Carreras Leukaemie Stiftung e.V.; research grant VA124/7-1 from the Deutsche Forschungs Gemeinschaft (DFG); research grant from the Werner und Klara Kreitz-Stiftung and intramural funding from the Christian-Albrechts- University Kiel.

REFERENCE LIST

1 Carter PJ: Potent antibody therapeutics by design. *Nat Rev Immunol* 2006, 6(5):343-357.

2 Schrama D, Reisfeld RA, Becker JC: Antibody targeted drugs as cancer therapeutics. *Nat Rev Drug Discov* 2006, 5(2):147-159.

3 Weiner GJ: Monoclonal antibody mechanisms of action in cancer. *Immunol Res* 2007, 39(1-3):271-278.

4 Weiner LM, Dhodapkar MV, Ferrone S: Monoclonal antibodies for cancer immunotherapy. *Lancet* 2009, 373(9668):1033-1040.

5 Weiner LM, Surana R, Wang S: Monoclonal antibodies: versatile platforms for cancer immunotherapy. *Nat Rev Immunol* 2010, 10(5):317-327.

6 Pastan I, Hassan R, Fitzgerald DJ, Kreitman RJ: Immunotoxin therapy of cancer. *Nat Rev Cancer* 2006, 6(7):559-565.

7 Carter PJ, Senter PD: Antibody-drug conjugates for cancer therapy. *Cancer J* 2008, 14(3):154-169.

8 Schirrmann T, Krauss J, Arndt MA, Rybak SM, Dubel S: Targeted therapeutic RNases (ImmunoRNases). *Expert Opin Biol Ther* 2009, 9(1):79-95.

9 Wu AM, Senter PD: Arming antibodies: prospects and challenges for immunoconjugates. *Nat Biotechnol* 2005, 23(9):1137-1146.

10 Peipp M, Kupers H, Saul D, Schlierf B, Greil J, Zunino SJ, Gramatzki M, Fey GH: A recombinant CD7-specific single-chain immunotoxin is a potent inducer of apoptosis in acute leukemic T cells. *Cancer Res* 2002, 62(10):2848-2855.

11 Schwemmlein M, Peipp M, Barbin K, Saul D, Stockmeyer B, Repp R, Birkmann J, Oduncu F, Emmerich B, Fey GH: A CD33-specific single-chain immunotoxin mediates potent apoptosis of cultured human myeloid leukaemia cells. *Br J Haematol* 2006, 133(2):141-151.

12 Sutherland MS, Sanderson RJ, Gordon KA, Andreyka J, Cerveny CG, Yu C, Lewis TS, Meyer DL, Zabinski RF, Doronina SO *et al*: Lysosomal trafficking and cysteine protease metabolism confer target-specific cytotoxicity by peptide-linked anti-CD30-auristatin conjugates. *J Biol Chem* 2006, 281(15):10540-10547.

13 Wels W, Beerli R, Hellmann P, Schmidt M, Marte BM, Kornilova ES, Hekele A, Mendelsohn J, Groner B, Hynes NE: EGF receptor and p185erbB-2-specific single-chain antibody toxins differ in their cell-killing activity on tumor cells expressing both receptor proteins. *Int J Cancer* 1995, 60(1):137-144.

14 Wels W, Harwerth IM, Mueller M, Groner B, Hynes NE: Selective inhibition of tumor cell growth by a recombinant single-chain antibody-toxin specific for the erbB-2 receptor. *Cancer Res* 1992, 52(22):6310-6317.

15 Sievers EL, Larson RA, Stadtmauer EA, Estey E, Lowenberg B, Dombret H, Karanes C, Theobald M, Bennett JM, Sherman ML *et al*: Efficacy and safety of gemtuzumab ozogamicin in patients with CD33-positive acute myeloid leukemia in first relapse. *J Clin Oncol* 2001, 19(13):3244-3254.

16 Linenberger ML: CD33-directed therapy with gemtuzumab ozogamicin in acute myeloid leukemia: progress in understanding cytotoxicity and potential mechanisms of drug resistance. *Leukemia* 2005, 19(2):176-182.

17 Lewis Phillips GD, Li G, Dugger DL, Crocker LM, Parsons KL, Mai E, Blattler WA, Lambert JM, Chari RV, Lutz RJ *et al*: Targeting HER2-positive breast cancer with trastuzumab-DM1, an antibody-cytotoxic drug conjugate. *Cancer Res* 2008, 68(22):9280-9290.

18 Krop IE, Beeram M, Modi S, Jones SF, Holden SN, Yu W, Girish S, Tibbitts J, Yi JH, Sliwkowski MX *et al*: Phase I study of trastuzumab-DM1, an HER2 antibody-drug conjugate, given every 3 weeks to patients with HER2-positive metastatic breast cancer. *J Clin Oncol* 2010, 28(16):2698-2704.

19 Burris HA, 3rd, Rugo HS, Vukelja SJ, Vogel CL, Borson RA, Limentani S, Tan-Chiu E, Krop IE, Michaelson RA, Girish S *et al*: Phase II study of the antibody drug conjugate trastuzumab-DM1 for the treatment of human epidermal growth factor receptor 2 (HER2)-positive breast cancer after prior HER2-directed therapy. *J Clin Oncol* 2011, 29(4):398-405.

20 Younes A, Bartlett NL, Leonard JP, Kennedy DA, Lynch CM, Sievers EL, Forero-Torres A: Brentuximab vedotin (SGN-35) for relapsed CD30-positive lymphomas. *N Engl J Med* 2010, 363(19):1812-1821.

21 Kreitman RJ, Wilson WH, Bergeron K, Raggio M, Stetler-Stevenson M, FitzGerald DJ, Pastan I: Efficacy of the anti-CD22 recombinant immunotoxin BL22 in chemotherapy-resistant hairy-cell leukemia. *N Engl J Med* 2001, 345(4):241-247.

22 Kreitman RJ, Stetler-Stevenson M, Margulies I, Noel P, Fitzgerald DJ, Wilson WH, Pastan I: Phase II trial of recombinant immunotoxin RFB4(dsFv)-PE38 (BL22) in patients with hairy cell leukemia. *J Clin Oncol* 2009, 27(18):2983-2990.

23 Teeling JL, French RR, Cragg MS, van den Brakel J, Pluyter M, Huang H, Chan C, Parren PW, Hack CE, Dechant M *et al*: Characterization of new human CD20 monoclonal antibodies with potent cytolytic activity against non-Hodgkin lymphomas. *Blood* 2004, 104(6):1793-1800.

24 Glennie MJ, French RR, Cragg MS, Taylor RP: Mechanisms of killing by anti-CD20 monoclonal antibodies. *Mol Immunol* 2007, 44(16):3823-3837.

25 Lammerts van Bueren JJ, Bleeker WK, Bogh HO, Houtkamp M, Schuurman J, van de Winkel JG, Parren PW: Effect of target dynamics on pharmacokinetics of a novel therapeutic antibody against the epidermal growth factor receptor: implications for the mechanisms of action. *Cancer Res* 2006, 66(15):7630-7638.

26 Bhattacharyya S, Bhattacharya R, Curley S, McNiven MA, Mukherjee P: Nanoconjugation modulates the trafficking and mechanism of antibody induced receptor endocytosis. *Proc Natl Acad Sci U S A* 2010, 107(33):14541-14546.

27 Spangler JB, Neil JR, Abramovitch S, Yarden Y, White FM, Lauffenburger DA, Wittrup KD: Combination antibody treatment down-regulates epidermal growth factor receptor by inhibiting endosomal recycling. *Proc Natl Acad Sci U S A* 2010, 107(30):13252-13257.

28 Spooner RA, Smith DC, Easton AJ, Roberts LM, Lord JM: Retrograde transport pathways utilised by viruses and protein toxins. *Virol J* 2006, 3:26.

29 Mazor Y, Barnea I, Keydar I, Benhar I: Antibody internalization studied using a novel IgG binding toxin fusion. *J Immunol Methods* 2007, 321(1-2):41-59.

30 Kuo SR, Alfano RW, Frankel AE, Liu JS: Antibody internalization after cell surface antigen binding is critical for immunotoxin development. *Bioconjug Chem* 2009, 20(10):1975-1982.

31 Ruuls SR, Lammerts van Bueren JJ, van de Winkel JG, Parren PW: Novel human antibody therapeutics: the age of the Umabs. *Biotechnol J* 2008, 3(9-10):1157-1171.

32 Meister S, Schubert U, Neubert K, Herrmann K, Burger R, Gramatzki M, Hahn S, Schreiber S, Wilhelm S, Herrmann M *et al*: Extensive immunoglobulin production sensitizes myeloma cells for proteasome inhibition. *Cancer Res* 2007, 67(4):1783-1792.

33 Bang S, Nagata S, Onda M, Kreitman RJ, Pastan I: HA22 (R490A) is a recombinant immunotoxin with increased antitumor activity without an increase in animal toxicity. *Clin Cancer Res* 2005, 11(4):1545-1550.

34 Seetharam S, Chaudhary VK, FitzGerald D, Pastan I: Increased cytotoxic activity of Pseudomonas exotoxin and two chimeric toxins ending in KDEL. *J Biol Chem* 1991, 266(26):17376-17381.

35 Krebber A, Bornhauser S, Burmester J, Honegger A, Willuda J, Bosshard HR, Pluckthun A: Reliable cloning of functional antibody variable domains from hybridomas and spleen cell repertoires employing a reengineered phage display system. *J Immunol Methods* 1997, 201(1):35-55.

36 Hermans WJJ, Ten Haft MR, Overweel A: method for affinity purification. *WO 2006/059904 A1* 2006.

37 Barth S, Huhn M, Matthey B, Klimka A, Galinski EA, Engert A: Compatible-solute-supported periplasmic expression of functional recombinant proteins under stress conditions. *Appl Environ Microbiol* 2000, 66(4):1572-1579.

38 Dechant M, Weisner W, Berger S, Peipp M, Beyer T, Schneider-Merck T, Lammerts van Bueren JJ, Bleeker WK, Parren PW, van de Winkel JG *et al*: Complement-dependent tumor cell lysis triggered by combinations of epidermal growth factor receptor antibodies. *Cancer Res* 2008, 68(13):4998-5003.

39 Schneider-Merck T, Lammerts van Bueren JJ, Berger S, Rossen K, van Berkel PH, Derer S, Beyer T, Lohse S, Bleeker WK, Peipp M *et al*: Human IgG2 antibodies against epidermal growth factor receptor effectively trigger antibody-dependent cellular cytotoxicity but, in contrast to IgG1, only by cells of myeloid lineage. *J Immunol* 2010, 184(1):512-520.

40 Lonberg N: Human antibodies from transgenic animals. *Nat Biotechnol* 2005, 23(9):1117-1125.

41 Lonberg N: Fully human antibodies from transgenic mouse and phage display platforms. *Curr Opin Immunol* 2008, 20(4):450-459.

42 Hust M, Jostock T, Menzel C, Voedisch B, Mohr A, Brenneis M, Kirsch MI, Meier D, Dubel S: Single chain Fab (scFab) fragment. *BMC Biotechnol* 2007, 7:14.

43 Thie H, Meyer T, Schirrmann T, Hust M, Dubel S: Phage display derived therapeutic antibodies. *Curr Pharm Biotechnol* 2008, 9(6):439-446.

6 HER2 monoclonal antibodies that do not interfere with receptor heterodimerization-mediated signaling induce effective internalization and represent valuable components for rational antibody-drug conjugate design

► MAbs. 2014 Mar-Apr;6(2):392-402

► Bart ECG de Goeij[1], Matthias Peipp[2], Simone de Haij[1], Edward N van den Brink[1], Christian Kellner[2], Thilo Riedl[1], Rob de Jong[1], Tom Vink[1], Kristin Strumane[1], Wim K Bleeker[1] and Paul WHI Parren[1]

1 Genmab, Utrecht, The Netherlands

2 Division of Stem Cell Transplantation and Immunotherapy, 2nd Department of Medicine, Christian-Albrechts-University, Kiel

ABSTRACT

The human epidermal growth factor receptor (HER)2 provides an excellent target for selective delivery of cytotoxic drugs to tumor cells by antibody-drug conjugates (ADC) as has been clinically validated by ado-trastuzumab emtansine (Kadcyla™). While selecting a suitable antibody for an ADC approach often takes specificity and efficient antibody-target complex internalization into account, the characteristics of the optimal antibody candidate remain poorly understood. We studied a large panel of human HER2 antibodies to identify the characteristics that make them most suitable for an ADC approach. As a model toxin, amenable to *in vitro* high-throughput screening, we employed *Pseudomonas* exotoxin A (ETA') fused to an anti-kappa light chain domain antibody. Cytotoxicity induced by HER2 antibodies, which were thus non-covalently linked to ETA', was assessed for high and low HER2 expressing tumor cell lines and correlated with internalization and downmodulation of HER2 antibody-target complexes. Our results demonstrate that HER2 antibodies that do not inhibit heterodimerization of HER2 with related ErbB receptors internalize more efficiently and show greater ETA'-mediated cytotoxicity than antibodies that do inhibit such heterodimerization. Moreover, stimulation with ErbB ligand significantly enhanced ADC-mediated tumor kill by antibodies that do not inhibit HER2 heterodimerization. This suggests that the formation of HER2/ErbB-heterodimers enhances ADC internalization and subsequent killing of tumor cells. Our study indicates that selecting HER2 ADCs that allow piggybacking of HER2 onto other ErbB receptors provides an attractive strategy for increasing ADC delivery and tumor cell killing capacity to both high and low HER2 expressing tumor cells.

INTRODUCTION

The human epidermal growth factor receptor (HER)2 is a 185-kDa cell surface receptor tyrosine kinase and member of the epidermal growth factor receptor (EGFR) family that comprises four distinct receptors: EGFR/ErbB-1, HER2/ErbB-2, HER3/ErbB-3, and HER4/ErbB-4. Both homo- and heterodimers are formed by the four members of the EGFR family, with HER2 being the preferred and most potent dimerization partner for all other ErbBs [2,3]. HER2 has no known ligand, but can be activated via homodimerization when overexpressed, or by heterodimerization with other, ligand-occupied ErbB receptors [4]. Depending on the dimerization partner, HER2 induces activation of the MAPK pathway, thereby stimulating proliferation, or the PI3K-Akt pathway, which promotes cell survival [5]. Over-expression of HER2 has been described in a wide variety of cancers, including breast, ovarian, gastric and non-small cell lung cancer [5].

HER2 is a clinically well-validated target for antibody therapy and proven to be suitable for an antibody-drug conjugate (ADC) approach through ado-trastuzumab emtansine (Kadcyla™) [6,7]. Ado-trastuzumab emtansine, which is approved for therapy of metastatic HER2-positive breast cancer [8], consists of trastuzumab conjugated via a non-reducible thioether linker to the fungal toxin and tubulin inhibitor maytansine. This ADC was designed to release the drug upon complete degradation in the lysosomes of targeted cells, and demonstrated great efficacy against HER2 overexpressing tumors, without affecting healthy tissue with normal HER2 expression levels [6,7,9]. The drug was found to retain the mechanisms of action of unconjugated trastuzumab, including inhibition of PI3K/AKT signaling and HER2 ectodomain shedding, and induction of antibody-dependent cellular cytotoxicity (ADCC) [10].

While many antibody characteristics are taken into account when selecting a suitable antibody for HER2-targeted therapy, it is typically considered an advantage for an ADC approach if the HER2/antibody complex efficiently internalizes upon antibody binding. In healthy tissue, the intensity of ErbB receptor signaling in cells is controlled by accelerated receptor internalization and degradation upon ErbB ligand binding. However, for the orphan HER2 receptor, no such internalization mechanism exists and all expressed HER2 predominantly localizes to the plasma membrane [11-13]. Notably, increased EGFR or HER3 expression results in increased endocytosis of HER2, especially in the presence of ligand [14,15].

In this study, we analyzed a diverse panel of human HER2 monoclonal antibodies (mAbs) for their suitability as an ADC. Internalization and cytotoxicity of HER2 antibodies were studied in an *in vitro* test system by generating non-covalently linked immunotoxins using a human kappa light chain-directed truncated version of *Pseudomonas* exotoxin A. Receptor internalization and cytotoxicity was correlated with expression and activation levels of different ErbB receptors on tumor cells to identify HER2 antibodies that both internalize efficiently and, as an ADC, kill cells with a range of HER2 expression levels. In particular, HER2 antibodies that can utilize HER2 heterodimer-driven internalization seem very attractive for future HER2-targeted ADC therapeutics, especially to target tumor indications with lower HER2 expression.

MATERIALS AND METHOD

Antibodies and cell lines

Human MCF7 and AU565 (breast cancer), NCI-H747 and Colo 205 (colon cancer) cells were from American Type Culture Collection (ATCC). Human A431 (epithelial squamous carcinoma) cells were from the Deutsche Sammlung von Mikroorganismen und Zellkulturen (DSMZ). MCF7 cells were cultured in MEM (Lonza, BE12-169F) containing 10% heat inactivated calf serum (Hyclone, SH30087.04) and 0.01 mg/mL bovine

insulin (Sigma, I0516). Colo 205 and A431 cells were cultured in RPMI 1640 (Lonza, BE12-115F) containing 10% heat inactivated calf serum. AU565 and NCI-H747 cells were cultured in RPMI 1640, containing 10% heat inactivated calf serum, 2% sodium bicarbonate (Lonza, BE17-613E), 1% sodium pyruvate (Lonza, BE13-115E), and 0.5% glucose (Sigma, G8769).

Human IgG1,κ HER2 mAb were generated by immunizing HuMAb® mice (Medarex, Milpitas, CA) [16] alternating with NS0 cells transiently expressing full length HER2 (1255 aa, UniProt P04626) and a Keyhole Limpet Hemocyanin (KLH)-coupled C-terminal His6-tagged HER2 protein fragment comprising the HER2 extracellular domain (HER2ECDHis). MAb were obtained by fusing mouse splenocytes and lymph node cells with the mouse myeloma cell line SP2.0 (ATCC) by electrofusion using a CEEF 50 Electrofusion System (Cyto Pulse Sciences, Glen Burnie, MD, USA). Hybridomas were subcloned in semisolid medium using the ClonePix system (Genetix), and expanded and cultured based upon standard protocols [17]. Antibodies that bound HER2 expressing cell lines selectively were molecularly cloned and produced by transient transfection in HEK-293 cells, purified using protein A affinity chromatography (MabSelect SuRe, GE-Healthcare) and formulated in PBS containing Tween 80 and mannitol.

The HER2ECDHis constructs contained an optimal Kozak sequence and were cloned in the mammalian expression vector pEE13.4 (Lonza Biologics) [18,19] expressed in HEK-293F cells and purified using immobilized metal affinity chromatography. To allow a proper comparison, we also produced trastuzumab and pertuzumab in our transient HEK system. The variable region sequences of pertuzumab and trastuzumab described in US patents 6949245 and 7632924, respectively, were cloned and transfected in HEK-293 cells. Both were expressed as a human IgG1 (allotype f) antibody with a kappa light chain. These two mAb preparations are referred to as TH-pertuzumab and TH-trastuzumab, respectively. Clinical grade trastuzumab (Herceptin®) was purchased (Roche). Trastuzumab and TH-trastuzumab bound HER2 similarly (data not shown) and, as an additional control, Supplementary Figure 4 illustrates that clinical grade trastuzumab and TH-trastuzumab induced similar efficacy in our *in vitro* kappa-directed ETA' killing assay.

Cross-competition ELISA

ELISA plates were coated with HER2 antibodies at 4°C, 6–0.5 µg/mL. After blocking with PBSTC (PBS supplemented with 0.5% Tween 20 [Riedel-de-Haen, 63158] and 2% chicken serum [Invitrogen, 16110082]) for 1 hour at room temperature (RT), wells were incubated with 1 µg/mL soluble HER2ECDHis in the presence of an excess (10 µg/mL) of competitor HER2 antibody. Bound HER2ECDHis was detected with 0.5 µg/mL biotinylated rabbit-anti-6xhis antibody (Abcam, ab27025), followed by 0.1 µg/mL streptavidin-poly-HRP (Sanquin, M2032). The reaction was visualized using ABTS

(Roche) and stopped with 0.2% oxalic acid. Fluorescence at 405 nm was measured on a microtiter plate reader (Biotek Instruments) and residual HER2ECDHis binding was expressed as percentage relative to maximal binding observed in absence of competitor antibody.

HER2 ECD domain shuffle

Sequences of domains I–IV of the human HER2 extracellular domain were exchanged one-by-one from human to chicken HER2 (Gallus gallus isoform B NCBI: NP_001038126.1), generating 5 different constructs: 1) fully human HER2 (UniProt P04626), hereafter named hu-HER2; 2) hu-HER2 with chicken domain I (replacing amino acids (aa) 1-203 of human HER2 with the corresponding chicken HER2 region), named hu-HER2-ch(I); 3) hu-HER2 with chicken domain II (replacing amino acids (aa) 204-330 of human Her2 with the corresponding chicken Her2 region), named hu-HER2-ch(II); 4) hu-HER2 with chicken domain III (replacing aa 331-507 of human Her2 with the corresponding chicken Her2 region), named hu-HER2-ch(III); and 5) hu-HER2 with chicken domain IV (replacing aa 508-651 of human Her2 with the corresponding chicken Her2 region), named hu-HER2-ch(IV). The constructs were transiently transfected in Freestyle™ CHO-S (Invitrogen) cells using Freestyle MAX transfection reagent (Invitrogen, K9000-20). After culturing for 20 hours, HER2 antibody binding was analyzed by flow cytometry.

Flow cytometry

Binding of HER2 antibodies to membrane-bound HER2 on A431 cells was analyzed by flow cytometry as described [20]. Phycoerythrin (PE)-conjugated goat anti-human IgG (Jackson, 109-116-098) was used to detect binding of HER2 mAbs. EC_{50} values were determined by means of non-linear regression using GraphPad Prism (GraphPad Software V4.03).

Proliferation assay

AU565 cells were seeded in serum-free culture medium, 9,000 cells/well, in 96-wells tissue culture plates (Greiner bio-one, 655180) in the presence of 10 µg/mL antibody. MCF7 cells were seeded in complete growth medium, 2,500 cells/well. After 4 hours, medium was replaced with medium containing 1% serum, 10 µg/mL antibody and 1.5 ng/mL heregulin-β1 (PeproTech, 100-03). After 3 or 4 days incubation, 10% Alamarblue (Invitrogen, DAL110) was added, and fluorescence was monitored 4 hours later using the EnVision 2101 Multilabel reader (PerkinElmer). The Alamarblue signal in antibody-treated wells was plotted as a percentage relative to the signal in wells without antibody.

ERK-phosphorylation Alphascreen assay

AU565 cells were cultured overnight in 96-well plates (9,000 cells/well) in serum-free medium. The medium was replaced with DMEM (Sigma-Aldrich, D6546) and the cells

were cultured 2 hours. 10 µg/mL antibody dilutions (in DMEM) were added, 30 min prior to stimulation with 1.67 ng/mL EGF (Bioresource, PHG0311). After 10 min, the cells were washed twice with PBS, lysed and analyzed for the presence of phosphorylated ERK with the phospho-ERK specific AlphaScreen® assay, according to the manufacturer's protocol (PerkinElmer, TGRES500). Fluorescent units at 570 nm were measured with the EnVision 2101 Multilabel reader (PerkinElmer) using standard AlphaScreen® settings.

CypHer5E internalization assay

Cells were seeded in 384-well plates, 3,000 cells/well, in normal cell culture medium, containing 240 ng/mL goat anti-human-IgG Fab fragments (Jackson, 109-007-003) conjugated to CypHer5E (GE Healthcare, PA15401). CypHer5E is a pH-sensitive dye that is non-fluorescent at basic pH (extracellular: culture medium) and fluorescent at acidic pH (intracellular: endosomes, lysosomes). Serially-diluted antibodies (range 2500-4.9 ng/mL) were added and plates were incubated at RT for 9 hours. Mean fluorescent intensities (MFI) of intracellular CypHer5E were measured per well using homogeneous Fluorometric Microvolume Assay Technology (FMAT, Applied Biosystems). As read-out, fluorescence per cell was measured and multiplied with the number of positive cells per well (counts x fluorescence).

HER2 downmodulation ELISA

AU565 cells were seeded in 24-wells tissue culture plates (100,000 cells/well) in normal cell culture medium and cultured for 3 days at 37°C in the presence of 10 µg/mL HER2 antibody. Cells were lysed by incubating 30 min at RT with 25 µL Surefire Lysis buffer (Perkin Elmer, TGRA2510K). Total protein levels were quantified using bicinchoninic acid (BCA) protein assay reagent (Pierce, 23227). HER2 protein levels were analyzed using a HER2-specific sandwich ELISA. A 1000-fold dilution of rabbit anti-human HER2 intracellular domain antibody (Cell Signaling, 2165) was used to capture HER2 and 0.15 µg/mL biotinylated goat anti-human HER2 polyclonal antibody (R&D, BAF1129), followed by 0.1 µg/mL streptavidin-poly-HRP, were used to detect bound HER2. The reaction was visualized using ABTS and stopped with oxalic acid. Fluorescence at 405 nm was measured and the amount of HER2 was expressed as a percentage relative to untreated cells.

Cytotoxicity assay using α-kappa-ETA' toxin

Antibodies were pre-incubated with a predetermined concentration of α-kappa-ETA' (see supplementary methods for preparation of α-kappa-ETA') [21] that was not toxic for cells. This procedure allows formation of non-covalently linked immunotoxins, obviating the production of chemically conjugated toxins that may vary in toxin content and position of linkage. Cells were seeded in normal cell culture medium in 96-well tissue culture plates and serially diluted antibodies were added. As negative control, cells were incubated without antibody or with an isotype control antibody.

As a positive control for cytotoxicity, 10 µg/mL Staurosporin (Sigma, S6942) was added to cells without antibody. After 3 days, the amount of viable cells was quantified using Alamarblue or ATPlite (PerkinElmer, 6016941), both measured using the EnVision 2101 Multilabel reader. Viability was calculated according to (signal antibody-treated cells – signal positive control) / (signal untreated cells – signal positive control) x 100%.

Statistical analysis

Data analyses were done using GraphPad Prism 5 software. Group data were reported as mean ± SD. Dunett's test was applied for statistical analysis.

RESULTS

Characterization of HER2 antibody cross-competition groups.

A panel of 134 human HER2-specific antibodies was generated in human antibody transgenic mice using hybridoma technology [17]. Based on apparent affinities and sequence diversity, 72 HER2 mAbs were selected for further characterization in a cross-competition ELISA with the HER2 extracellular domain (HER2ECDHis). Four distinct cross-competition groups of mAbs were defined (Supplementary Table 1). Group 1 comprised 12 mAbs, including mAb-169 and trastuzumab (Herceptin®), which has previously been mapped to an epitope in domain IV of HER2 [22,23]. Group 2 comprised 17 mAbs, including mAb-025 and HEK-293-produced pertuzumab (TH-pertuzumab), which is known to recognize an epitope in domain II of HER2 [1,24]. MAb-169 and -025 were chosen as representative mAbs for their Group 1 and 2 respectively. Group 3 comprised 22 mAbs that did not compete for binding to HER2ECDHis with antibodies from other cross competition groups. Within Group 3 some variation was observed as some antibodies did not compete with each other for binding to HER2ECDHis, but did compete with the other Group 3 antibodies. Therefore we divided these antibodies in two subgroups, 3a and 3b, for which two representative antibodies, 098 and 153, were selected for further characterization. Finally, Group 4 comprised 21 mAbs that competed with each other for binding to HER2ECDHis, but not with any of the other cross-competition groups. MAb 005 was selected from Group 4 for further characterization.

To map the regions recognized and characterize epitope diversity between the four different groups of mAbs, a HER2 ECD shuffle experiment was performed. Five constructs were generated by swapping the sequences of domain I, II, III or IV of the extracellular domain of human HER2 with the corresponding sequence of chicken HER2. The wild-type construct is referred to as hu-HER2 and the mutants as hu-HER2-ch(I) to -(IV), respectively. The human and chicken HER2 orthologs show 67% homology in their ECD (62% homology in domain I, 72% in domain II, 63% in do-

main III and 68% in domain IV). The generated constructs were expected to result in a protein with domains that are sufficiently homologous to allow correct folding, but different enough to remove epitopes recognized by human HER2 specific mAbs. Group 1 mAbs trastuzumab and 169 showed loss of binding to Hu-HER2-ch(IV), but not to the other shuffle proteins, confirming that the epitopes of Group 1 mAbs reside in HER2 domain IV (Table I, Supplementary Figure 1). Group 2 antibody 025 only showed loss of binding for Hu-HER2-ch(II), confirming that its epitope resides in HER2 domain II. The distinction between Group 3a and 3b mAbs 098 and 153 was confirmed in the shuffle experiment in which mAb 098 showed loss of binding to Hu-HER2-ch(I) and a small decrease in binding to Hu-HER2-ch(II), whereas mAb 153 only showed strong loss of binding to Hu-HER2-ch(II). The Group 4 mAb 005 showed loss of binding upon substitution of HER2 domain III, and partially decreased binding to Hu-HER2-ch(II).

Next, the epitopes of HER2 antibodies 005 and 153 were predicted using Chemically Linked Immunogenic Peptides on Scaffolds (CLIPS™) technology [25,26]. Antibody binding was tested on linear and looped CLIPS of 15 to 35 amino acids, which were designed to allow for mapping of conformational epitopes on the human HER2 extracellular domain. Group 3 mAb 153 demonstrated binding to peptides including sequence RCKGPLPTD, suggesting binding to domain II on top of HER2 (Supplementary Figure 2). For the Group 4 mAb 005, two distinct peptides were predicted to be part of the epitope (GISWLGLRSLREL and IHHNTHLCFVHTVPW), which both reside in domain III distant from the dimerization regions (Supplementary Figure 2). We were unable to map the representative mAbs from the other groups using the CLIPS approach.

Taken together, our data demonstrated that the HER2 mAbs could be divided in four major groups based on their binding sites on HER2, with Group 1 antibodies binding epitopes in HER2 domain IV, Group 2 binding epitopes in HER2 domain II, Group 3a and 3b antibodies binding epitopes in a region overspanning HER2 domain I/II, and Group 4 antibodies that recognized epitopes in HER2 domain III.

		HER2-domain shuffle mapping				
clone	Group	wildtype	I	II	III	IV
Herceptin	1	+++	+++	+++	+++	-
169	1	+++	+++	+++	+++	++
025	2	+++	+++	-	+++	+++
098	3a	+++	-	++	+++	+++
153	3b	+++	+++	-	+++	+++
005	4	+++	+++	++	-	+++

TABLE 1 *Summary of antibody binding to different HER2 receptor constructs.* Wild-type; hu-HER2, I; hu-HER2-ch(I), II; hu-HER2-ch(II), III; hu-HER2-ch(III), IV; hu-HER2-ch(IV) +++ Indicates wild-type binding or binding similar to wild-type binding, ++ indicates reduced EC50 but similar maximal binding compared to wild-type binding, - indicates no binding detected. See Supplementary Figure 1 for dose-response binding curves.

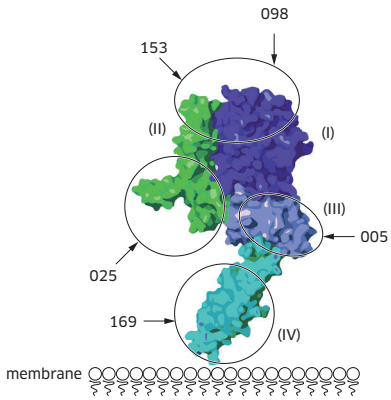

	HER2 mAb Cross-blocking group					
	1		2	3		4
	Herc	169	025	098	153	005
Apparent affinity EC_{50} (nM)	5.7	6.1	3.9	2.3	4.2	5.3
Inhibition of ligand-independent growth	+	+	-	-*	-	-
Inhibition of ligand-induced growth	-/+	-	+	-	+	-
Internalization	-/+	-/+	+	++	++	+
Downmodulation	-/+	-/+	-/+	++	++	+
Kappa-ETA' toxicity AU565	-/+	+	++	++	++	++
Kappa-ETA' toxicity A431	-	-	++	++	++	++
Effect EGF on killing	-	-	-	+	-	+

TABLE 2 *Summary antibody characteristics.* Summary of the different antibody characteristics and representation of the different HER2 epitopes recognized. Flow cytometry was applied to determine the apparent antibody affinities on A431 cells which were depicted as EC50 value. HER2 structure was obtained from Franklin et al.[1] *Significantly agonistic.

Proliferation inhibition by HER2 antibodies.

Representative antibodies from each cross-competition group were tested for their ability to inhibit HER2-driven proliferation. Because HER2 is an orphan receptor, it normally requires ligand-induced heterodimerization with other ErbB family members for its signaling, such as EGF-induced EGFR/HER2 or heregulin-induced HER2/HER3 heterodimerization [2]. However, when highly overexpressed, HER2 can signal as a homodimer in a ligand-independent fashion. HER2 homodimerization-induced signaling was distinguished from heterodimerization-induced signaling by analyzing ligand-independent and ligand-induced proliferation. The ability of HER2 mAbs to inhibit ligand-independent proliferation was tested in AU565 cells, which express very high HER2 levels (Supplementary Table 2). Group 1 antibodies demonstrated significant inhibition of AU565 cell proliferation (Figure 1A), consistent with what has previously been described for trastuzumab [23]. MAb from Group 2 or 4 did not show any effect on ligand-independent AU565 proliferation. In contrast, both Group 3 mAb enhanced proliferation of HER2-overexpressing AU565 cells. These data indicate that Group 1 mAb, which bind HER2 domain IV, can interfere with signaling induced by HER2 homodimerization when the receptor is highly overexpressed.

The potential of HER2 mAbs to inhibit HER2 heterodimerization-driven proliferation was tested in MCF7 cells, which express comparable levels of HER2 and HER3 (Supplementary Table 2) and are responsive to the HER3 ligand heregulin-β1 [27]. Figure 1B demonstrates that heregulin-β1-induced proliferation of MCF7 cells was inhibited by the HER2 domain II binding Group 2 mAbs and Group 3b mAb 153. The Group 3a mAb 098, for which the epitope was mainly defined to residues in HER2 domain I and only displayed limited binding to domain II, did not affect heregulin-β1-induced MCF-7 proliferation. Group 1 and 4 antibodies also had no effect on heregulin-β1-induced proliferation, with the exception of trastuzumab, which demonstrated some inhibitory effect, although with lower significance.

HER2 can also signal through ligand-activated EGFR [2]. Therefore, our conclusions for HER2 heterodimerization-dependent signaling were confirmed by assessing EGF-induced EGFR/HER2 heterodimerization and downstream ERK phosphorylation in AU565 cells (Figure 1C). Here again, Group 2 mAb inhibited ligand-dependent signaling most prominently. These data suggest that binding to HER2 domain II is critical for the ability of HER2 antibodies to interfere with ligand-induced HER2 heterodimerization and signaling, consistent with what has previously been described for pertuzumab [1,24].

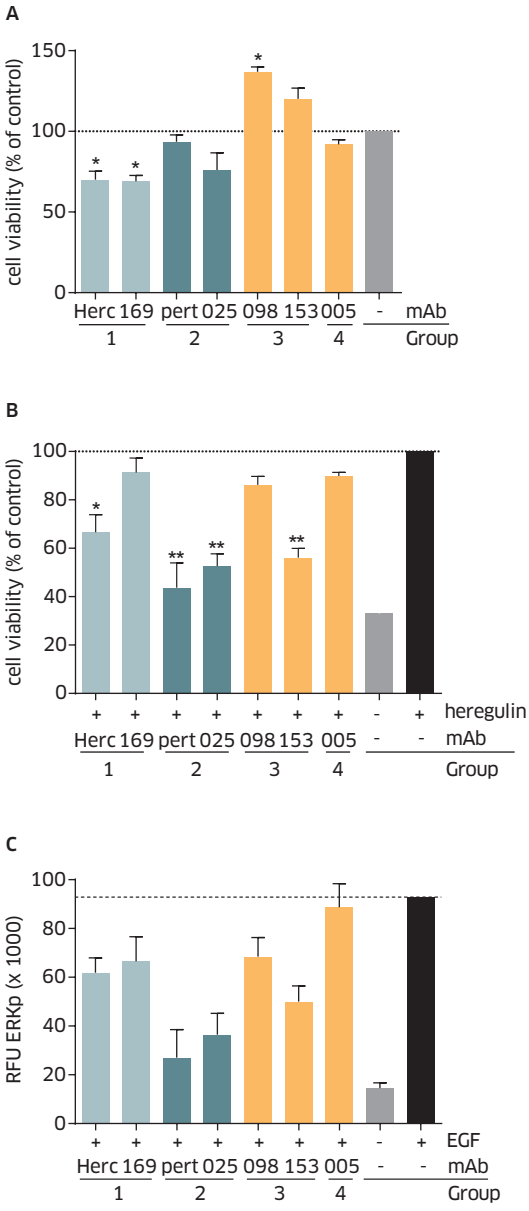

FIGURE 1 *In vitro inhibition of proliferation and ERK phosphorylation by HER2 antibodies.* **A)** Inhibition of proliferation of AU565 cells. Cell viability is presented as a percentage relative to untreated cells (± SD, n=3), (*P <0.05). **B)** Inhibition of proliferation of MCF7 Cell viability is presented as a percentage relative to cells stimulated with Heregulin-β1 only (± SD, n=3), (*P <0.05, **P <0.01). **C)** Inhibition of ERK phosphorylation in AU565. The amount of phosphorylated ERK was quantified using a phospho-ERK specific AlphaScreen® assay. Values depicted are the mean of at least two experiments ± SD.

HER2 antibody-induced internalization and HER2 downmodulation

A prerequisite for an ADC approach is efficient internalization of the antibody-target complex. A CypHer5E-based internalization assay was performed to investigate the internalization capacity of the mAbs. All 72 HER2 mAbs of the four cross-competition groups described above were tested. AU565 cells were incubated with HER2 mAbs that were indirectly labeled with the pH-sensitive dye CypHer5E conjugated to Fab fragments of a goat anti-human IgG antibody, which becomes fluorescent in the acid environment of the endosomal/lysosomal compartments upon internalization (Figure 2A,B). Group 3 mAbs clearly showed enhanced receptor internalization compared to the other cross-competition groups. Group 1 mAbs, in contrast, induced receptor internalization relatively poorly. This was further illustrated by the dose response curves generated for the representative mAbs of each cross-competition group (Figure 2B). These data show that antibody internalization was strongly induced by Group 3 HER2 antibodies in particular, and to a lesser extent by antibodies from the other cross-competition groups.

Upon internalization, antibody-target complexes enter the endosomal compartment, and are either transported to the lysosomes for degradation, or are recycled back to the plasma membrane. We investigated for representative mAbs of each cross-competition group whether HER2 mAb binding induced degradation of the HER2 target. The total amount of HER2 protein in AU565 cells was quantified by ELISA after a 3-days antibody treatment. AU565 cells were seeded to confluence at the beginning of the experiment to minimize antibody-induced effects on proliferation. Both Group 3 antibodies induced HER2 downmodulation (~50% of untreated cells; Figure 3). In contrast, Group 1 and 2 antibodies hardly induced any downmodulation, whereas Group 4 antibody 005 induced intermediate HER2 downmodulation. Except for the Group 2 HER2 mAb 025, these data are in line with the internalization results, suggesting that internalization upon HER2 mAb binding results in degradation of the antibody-target complexes for Group 1, Group 3 and Group 4 antibodies. HER2 antibody 025 behaved differently in that it showed internalization comparable to Group 4 mAb 005, but induced limited HER2 downmodulation. This might suggest that the antibody-target complex formed by mAb 025 is primarily directed towards the recycling pathway instead of the lysosomal degradation pathway.

HER2-mAb activity in an *in vitro* kappa-directed ETA' killing assay

To further investigate which antibodies were suitable for an ADC approach, an *in vitro* cell-based killing assay using the *Pseudomonas* exotoxin A (ETA') fused to an anti-kappa light chain domain antibody (α-kappa-ETA') amenable to high throughput screening was used [21]. This fusion protein allows formation of non-covalently-linked immunotoxins with antibodies containing human kappa light chains. The α-kappa-ETA' fusion protein needs to undergo furin-mediated proteolytic cleavage in the endosomes to separate the catalytic exotoxin part from the antibody binding

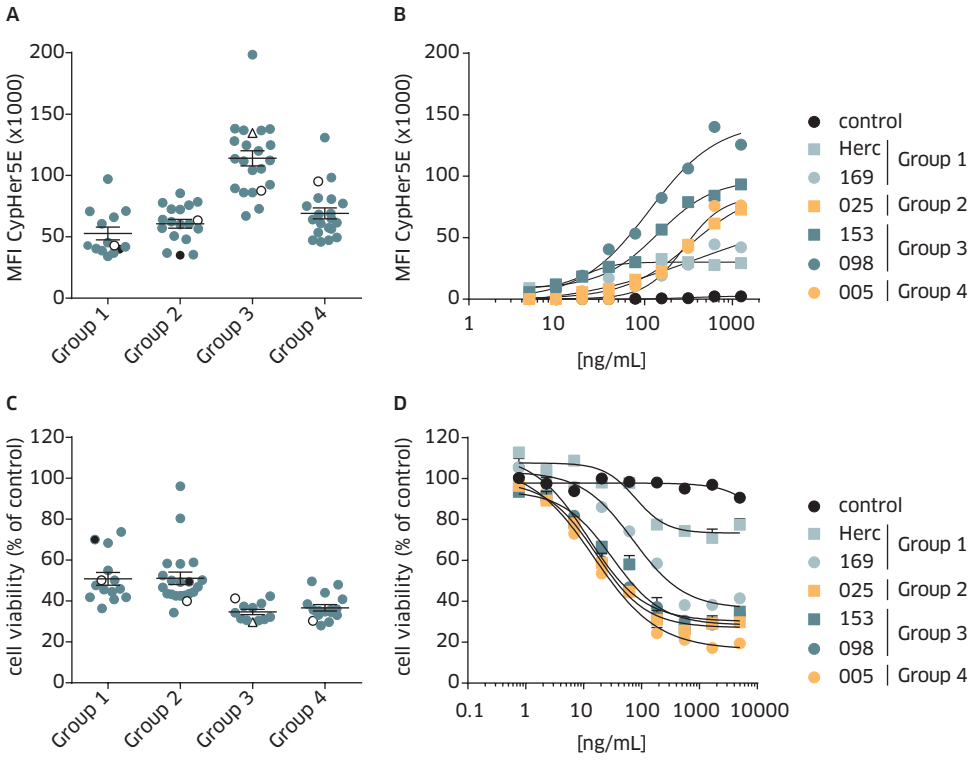

FIGURE 2 *Internalization and HER2-mAb α-kappa-ETA' induced killing of AU565 cells.* **A/B)** Cells were seeded and incubated for 9 hours at RT with CypHer5E-conjugated Fab fragments of goat anti-human IgG and serially diluted HER2 antibodies. **(A)** Maximal 'counts x fluorescence' is plotted. Each dot represents a different antibody. In black are trastuzumab (Group 1) and TH-pertuzumab (Group 2). The open symbols represent the representative mAbs from each Group. Within Group 3, mAb 098 was depicted as triangle and mAb 153 as circle. Antibodies from Group 3 induced significantly more CypHer5E fluorescence compared to mAbs from Groups 1, 2 and 4 ($P < 0.001$). **B)** Dose-response curves of mAbs representing each of the Groups (n=2). **C/D)** Viability of AU565 cells after 3 days incubation with HER2 antibodies pre-incubated with 0.1 µg/mL α-kappa-ETA'. Antibodies from Groups 3 and 4 induced significantly more cytotoxicity compared to mAbs from Groups 1 and 2 ($P < 0.001$). **C)** Each dot represents the maximal reduction in cell viability induced by a different antibody. In black are trastuzumab and TH-pertuzumab. The open symbols represent the representative mAbs from each Group. **D)** Dose-response curves of mAbs representing each of the Groups (± SD, n=2). An isotype control mAb (control) was used as negative control.

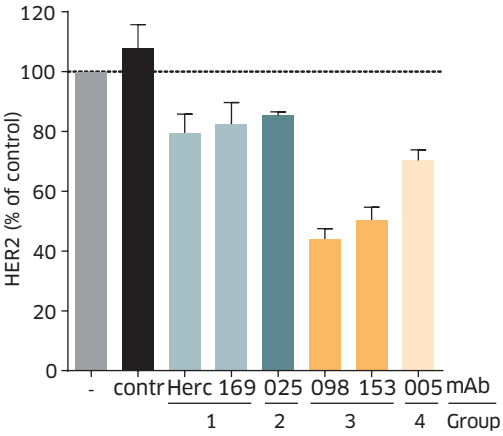

FIGURE 3 *Antibody induced downmodulation of HER2*. Relative percentage of HER2 expressed in AU565 cell lysate after 3 days incubation 10 µg/mL HER2 mAb. The amount of HER2 was quantified using a HER2-specific capture ELISA and plotted as a percentage relative to untreated cells indicated with - (± SD, N=3). An isotype control mAb (contr) was used as negative control.

domain. The released toxin is then transported to the endoplasmic reticulum and redirected to the cytosol where it inhibits protein synthesis and induces apoptosis [28]. We investigated whether there was a correlation between the efficiency of antibody-induced internalization, HER2-downmodulation and cytotoxicity mediated by immunotoxins derived from HER2 mAbs of the different cross-competition groups.

We screened our complete panel of 72 HER2 mAbs for inhibition of AU565 cell viability when pre-incubated with α-kappa-ETA'. In general, α-kappa-ETA' pre-incubated Group 3 and Group 4 antibodies induced higher toxicity (lower cell viability) in AU565 cells compared to α-kappa-ETA' pre-incubated antibodies from Group 1, including trastuzumab, and Group 2, including TH-pertuzumab, (Figure 2C). Reduced cell viability was evidently due to cellular toxicity rather than inhibition of proliferation, as effects of unconjugated antibodies on proliferation in the 3-days assay were observed only at concentrations above 100 ng/mL (data not shown), at which α-kappa-ETA' pre-incubated antibodies already demonstrated maximal efficacy (Figure 2C). Moreover, microscopic inspection of the cells revealed morphologic characteristics typical for apoptotic cells, such as cell shrinkage, membrane blebbing and loss of membrane asymmetry. The dose-response curves of different mAbs of each cross-competition group again show that Group 1 antibodies induced less efficient cell killing than mAbs from the other cross-competition groups (Figure 2D).

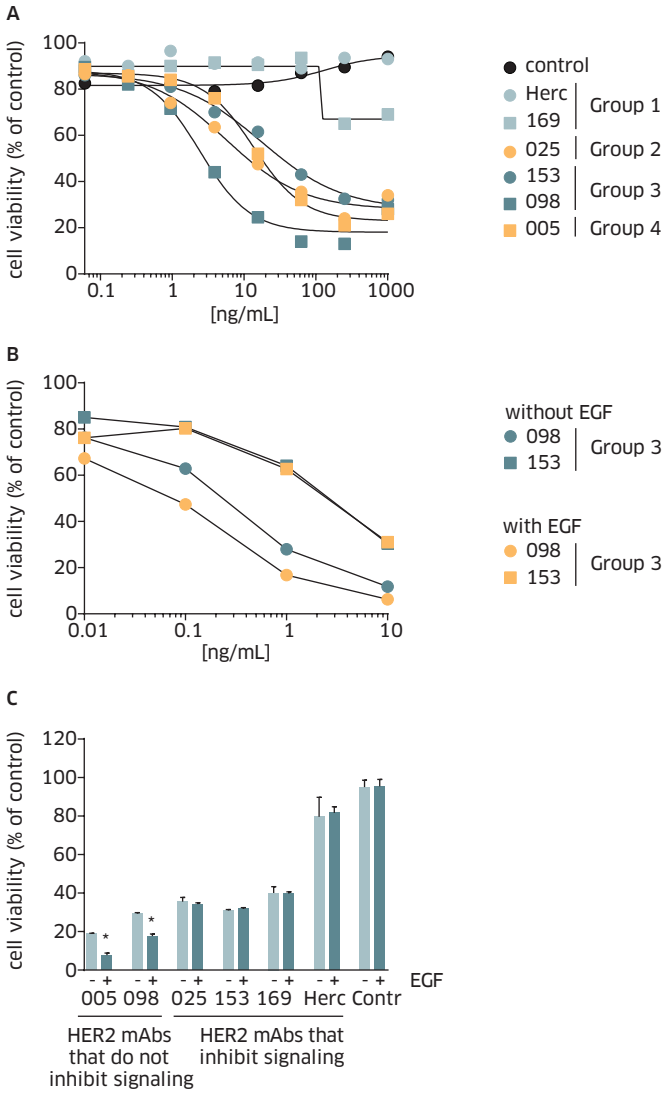

FIGURE 4 *The effect of EGFR and its ligand EGF on HER2-mAb α-kappa-ETA' induced toxicity.* **(A)** A431 cells were seeded in presence of HER2 antibodies pre-incubated with 0.1 µg/mL α-kappa-ETA'. After 3 days, cell viability was quantified using Alamarblue and plotted as a percentage relative to untreated cells (n=2). **(B/C)** Colo 205 cells were seeded in presence or absence of HER2 antibodies pre-incubated with 0.25 µg/mL α-kappa-ETA'. After 30 minutes 1.5 ng/mL EGF (+) or medium (-) was added and after 3 days, cell viability was quantified using ATPlite and plotted as a percentage relative to untreated cells (n=2). **(C)** The amount of viable cells after treatment with HER2 antibody pre-incubated with 0.25 µg/mL α-kappa-ETA' was plotted. Dark grey bars represent cell viability after treatment with 100 ng/mL HER2 antibody. Increased cell survival after treatment with 10 ng/mL HER2 antibody was plotted as light grey bars. 10 µg/mL Staurosporin was used as positive control to determine 0% cell viability. * indicates that viability in presence of EGF was significantly lower compared to viability in absence of EGF ($P<0.05$).

The selected mAb from Group 2 (025) was one of the more effective antibodies from this group and thus also induced efficient dose-dependent cytotoxicity. These results were consistent with internalization data in AU565 cells for each antibody.

The effects of EGFR and its ligand EGF on HER2-mAb α-kappa-ETA' induced toxicity

The efficacy of α-kappa-ETA' pre-incubated HER2 mAbs was further investigated using the low-HER2 expressing cell line A431 (Supplementary Table 2). After three days, cell viability was efficiently decreased by the Group 2, 3 and 4 antibodies, while Group 1 antibodies demonstrated minimal to no efficacy (Figure 4A). These results were comparable to what was observed for AU565 cells; however, differences between mAbs from Group 1 and other Groups were much more pronounced in A431. Because A431 cells have very high EGFR expression (Supplementary Table 2), resulting in EGFR/HER2 heterodimerization [29], we hypothesized that this might accelerate internalization of HER2, thereby increasing cell killing induced via α-kappa-ETA' pre-incubated HER2 antibodies. Since Group 1 antibodies inhibit ligand-independent dimerization and thus also the formation of EGFR/HER2 heterodimers on A431 cells, these antibodies may not be able to benefit from this internalization route and therefore are reduced in their ability to induce ADC-mediated toxicity. Together, these data might then suggest that high EGFR expression and thus EGFR/HER2 heterodimerization in A431 cells is involved in increased α-kappa-ETA'-mediated cytotoxic efficacy of the HER2 mAbs of Group 2, 3 and 4 compared to AU565 cells with low EGFR expression.

Ligand binding to EGFR typically causes accelerated internalization of the receptor [12,30-34]. Therefore, we tested our hypothesis by assessing the cytotoxic capacity of α-kappa-ETA' pre-incubated HER2 mAbs on Colo205 cells in the absence or presence of EGF. Colo205 cells show low levels of both EGFR and HER2 on the cell surface (Supplementary Table 2), although the density of both receptors may be somewhat higher than expected due to the small size of these cells. More importantly, Colo205 cells are responsive to EGFR activation by EGF. Results with kappa-ETA' pre-incubated HER2 mAbs on Colo205 cells in the absence of EGF were comparable to AU565 and A431 cells, i.e., Group 1 mAbs showed less cell killing than the representative mAbs from the other Groups (Figure 4C). Upon EGF stimulation, only Group 3a HER2 mAb 098 and Group 4 mAb 005 showed enhanced α-kappa-ETA'-mediated cytotoxicity (Figure 4B/C), whereas EGF did not affect α-kappa-ETA'-mediated cytotoxicity induced by Group 1 or 2 or the Group 3b mAb (153).

These results support our hypothesis that the formation of HER2/ErbB-heterodimers is beneficial for HER2 antibody-mediated drug delivery into target cells. Therefore, antibodies that inhibit the formation of ligand-induced or ligand-independent HER2/ErbB-heterodimers seem less suitable for an ADC approach compared to antibodies that do not interfere with HER2 heterodimerization.

DISCUSSION

In the present study, we characterized a broad panel of human HER2 antibodies generated in human antibody transgenic mice and studied their effects on receptor signaling, internalization and downmodulation of antibody-receptor complexes. To investigate which HER2 antibodies were most suitable for an ADC approach, we used an assay sytem based on a high affinity kappa light chain-specific domain antibody fused to a truncated form of *Pseudomonas* exotoxin A (α-kappa ETA') [21]. Toxicity induced by non-covalently linked toxin/HER2 antibody conjugates was tested on tumor cells with different expression levels of the ErbB receptors. Our results indicated that the formation of HER2/ErbB-heterodimers is beneficial to achieve sufficient HER2 antibody-mediated drug delivery into target cells.

Especially on tumor cells that do not over-express HER2 to extremely high levels, the formation of HER2/ErbB heterodimers may represent an attractive approach for HER2 antibodies to deliver an ADC.

Most ADCs, including ado-trastuzumab emtansine, make use of non-cleavable linkers, or linkers that require proteolytic cleavage in lysosomes for drug release, such as thioether, disulfide and peptide-based valine-citrulline (SGN-35) linkers [9,35]. This differs from *Pseudomonas* exotoxin A-based conjugates, which are cleaved by furin in the endosomes, resulting in separation of the catalytic domain from the antibody-binding domain. Although the kinetics are not entirely understood, it should be noted that rapid lysosomal transport of *Pseudomonas* exotoxin A-based conjugates may hamper furin mediated cleavage and consequently reduce cytotoxicity [36]. Antibodies that deliver kappa-ETA' more effectively into the lysosome, might therefore induce a lesser degree of killing, because of toxin degradation. The kappa-ETA' assay could therefore underestimate the potential value of such antibodies for an ADC approach. Nevertheless, in our panel of antibodies, we did not identify antibodies that were ineffective in the kappa-toxin assay while inducing rapid internalization as shown by strong CypHer5E fluorescence (Supplementary Figure 3). Furthermore, *Pseudomonas* exotoxin A has been used by a variety of investigators in preclinical and clinical testing to enhance the efficacy of antibody-based drugs [37-41], e.g., scFv[FRP5]-ETA (single chain Fv directed against HER2) [41], VB4-845 (scFv targeting EpCAM) [37], SS1P (dsFv directed against mesothelin) [40] and CAT-8015 (stabilized Fv fragment targeting CD22) [28]. Therefore the exotoxin A-based screening system should reliably identify antibodies with favorable characteristics for ADC development.

Based on cross-competition ELISA, HER2 extracellular domain shuffle and CLIPS™ technology, a panel of 72 HER2 antibodies was divided into four different cross-competition groups. It was observed that antibodies from Groups 2, 3 and 4, which did

not inhibit ligand-independent HER2 dimerization, induced enhanced internalization and α-kappa-ETA'-mediated cytotoxicity compared to antibodies from Group 1, which inhibited ligand-independent HER2 dimerization. This contrast was most prominent for cells with low HER2 expression but increased EGFR expression (AU565 cells -HER2 high, EGFR low- versus A431 cells -HER2 low, EGFR high-), demonstrating that toxicity induced by α-kappa-ETA' pre-incubated Group 1 antibodies, such as trastuzumab, cannot be enhanced via co-expression with EGFR. Due to over-expression of EGFR on A431 cells, internalization of HER2 was mostly driven by the formation of ligand-independent HER2/EGFR heterodimers. Various studies have demonstrated that internalization of HER2 is dependent on expression levels of other ErbB family members, especially EGFR [11,14,42], and that degradation of HER2 could be enhanced through co-expression of EGFR or HER3 [15]. However, no correlation has been observed thus far between cytotoxicity of anti-HER2 immunotoxins and the relative antibody affinities, epitopes recognized or amount of immunotoxin internalized [43]. Also here, no correlation was observed between antibody affinities and toxicity induced in a α-kappa-ETA' model system. However, a clear correlation was observed between the different HER2 cross-competition groups and the amount of toxicity induced in the α-kappa-ETA' model system.

Trastuzumab's ability to inhibit the formation of ligand-independent HER2/HER3 dimers has been described [23]. It may very well be that trastuzumab also inhibits formation of ligand-independent EGFR/HER2 dimers. This could explain why antibodies from Groups 2, 3 and 4, which did not disrupt ligand-independent EGFR/HER2 dimerization on A431 cells, still induced efficient killing of these cells. It should be noted, however, that besides differences in ErbB expression levels, other differences caused by the distinct origins of A431 (epithelial carcinoma) and AU565 (breast cancer) may influence the outcome of the results as well. Moreover, *Pseudomonas* exotoxin A exerts its cytotoxic activity by inhibiting protein synthesis [44]. Because Group 3 antibodies enhanced proliferation of high HER2 expressing tumor cells, this may also enhance the cytotoxic effects induced by ETA'. In addition, antibody-induced receptor activation has been demonstrated to enhance endocytic degradation of HER2 [45,46]. Antibody 005, however, had no effect on HER2-mediated proliferation, but demonstrated enhanced internalization and α-kappa-ETA'-mediated cell killing. This result indicates that receptor crosslinking may be favorable, but not crucial for enhancing receptor internalization.

The relevance of HER2 heterodimerization on internalization of antibody-receptor complexes was further supported by the observation that stimulation with EGF enhanced toxicity of α-kappa-ETA' pre-incubated HER2 antibodies 005 and 098, which did not inhibit heterodimerization of HER2. Toxicity induced via antibodies 025 and 153, which do inhibit ligand induced HER2 heterodimerization, was unaffected. The observation that EGF-induced activation of HER2 can potentiate the

action of a HER2-directed immunotoxin was also observed by Wels et al [47]. Notably, toxicity induced by α-kappa-ETA' pre-incubated antibodies 169 and trastuzumab was also unaffected upon EGF stimulation, supporting the findings that HER2 domain IV may be involved in stabilization of ligand-induced HER2/EGFR heterodimers [48]. The possibility that differences observed between clinical grade trastuzumab and other HER2 antibodies were due to differences in the constant antibody domains, was excluded by comparing clinical grade trastuzumab with HEK-293-produced trastuzumab (TH-trastuzumab). No differences in toxicity were observed between the two batches when tested in the α-kappa-ETA' toxin assay with AU565 cells (Supplementary Figure 4).

It is generally believed that trastuzumab drives internalized HER2 away from the recycling pathway toward the lysosomal degradation pathway, although the contribution of this mechanism to the anti-tumor effect of trastuzumab is not fully understood [11-13]. We have demonstrated that antibodies that inhibit HER2/EGFR signaling, also showed reduced internalization, as observed with trastuzumab. By using antibodies that do not inhibit HER2 heterodimerization, it was possible to kill lower HER2-expressing tumor cells. This illustrates that the most effective unconjugated antibodies are not necessarily the most effective ADCs. Since HER2 expression and expression of other ErbBs is required to enhance the efficacy of these HER2-ADCs, they may be more tumor-specific while targeting a broader range of tumor indications. In this case, however, we were not able to demonstrate superiority of particular antibody groups *in vivo* because the non-covalent interaction of α-kappa-ETA' with IgG does not hold *in vivo* and covalent conjugation of α-kappa-ETA' to IgG failed.

In conclusion, these results demonstrate that maximum HER2-ADC delivery and tumor kill requires the formation of HER2/ErbB heterodimers. Therefore, inhibition of receptor signaling seems less favorable for an ADC approach. Especially on low-HER2 expressing tumors, piggybacking with other ErbBs may represent an attractive approach to increase intracellular delivery of an ADC.

REFERENCE LIST

1 Franklin MC, Carey KD, Vajdos FF, Leahy DJ, de Vos AM, Sliwkowski MX: Insights into ErbB signaling from the structure of the ErbB2-pertuzumab complex. *Cancer Cell* 2004, 5(4):317-328.

2 Graus-Porta D, Beerli RR, Daly JM, Hynes NE: ErbB-2, the preferred heterodimerization partner of all ErbB receptors, is a mediator of lateral signaling. *EMBO J* 1997, 16(7):1647-1655.

3 Tao RH, Maruyama IN: All EGF(ErbB) receptors have preformed homo- and heterodimeric structures in living cells. *J Cell Sci* 2008, 121(Pt 19):3207-3217.

4 Riese DJ, 2nd, Stern DF: Specificity within the EGF family/ErbB receptor family signaling network. *Bioessays* 1998, 20(1):41-48.

5 Baselga J, Swain SM: Novel anticancer targets: revisiting ERBB2 and discovering ERBB3. *Nat Rev Cancer* 2009, 9(7):463-475.

6 Lewis Phillips GD, Li G, Dugger DL, Crocker LM, Parsons KL, Mai E, Blattler WA, Lambert JM, Chari RV, Lutz RJ *et al*: Targeting HER2-positive breast cancer with trastuzumab-DM1, an antibody-cytotoxic drug conjugate. *Cancer Res* 2008, 68(22):9280-9290.

7 Krop IE, Beeram M, Modi S, Jones SF, Holden SN, Yu W, Girish S, Tibbitts J, Yi JH, Sliwkowski MX *et al*: Phase I study of trastuzumab-DM1, an HER2 antibody-drug conjugate, given every 3 weeks to patients with HER2-positive metastatic breast cancer. *J Clin Oncol*, 28(16):2698-2704.

8 A P: F.D.A. Approves a new drug for advanced breast cancer. In: *The New York Times.* New York; 2013.

9 Senter PD: Potent antibody drug conjugates for cancer therapy. *Curr Opin Chem Biol* 2009, 13(3):235-244.

10 Junttila TT, Li G, Parsons K, Phillips GL, Sliwkowski MX: Trastuzumab-DM1 (T-DM1) retains all the mechanisms of action of trastuzumab and efficiently inhibits growth of lapatinib insensitive breast cancer. *Breast Cancer Res Treat*.

11 Austin CD, De Maziere AM, Pisacane PI, van Dijk SM, Eigenbrot C, Sliwkowski MX, Klumperman J, Scheller RH: Endocytosis and sorting of ErbB2 and the site of action of cancer therapeutics trastuzumab and geldanamycin. *Mol Biol Cell* 2004, 15(12):5268-5282.

12 Yarden Y, Sliwkowski MX: Untangling the ErbB signalling network. *Nat Rev Mol Cell Biol* 2001, 2(2):127-137.

13 Longva KE, Pedersen NM, Haslekas C, Stang E, Madshus IH: Herceptin-induced inhibition of ErbB2 signaling involves reduced phosphorylation of Akt but not endocytic down-regulation of ErbB2. *Int J Cancer* 2005, 116(3):359-367.

14 Sorkin A, Goh LK: Endocytosis and intracellular trafficking of ErbBs. *Exp Cell Res* 2008, 314(17):3093-3106.

15 Pedersen NM, Breen K, Rodland MS, Haslekas C, Stang E, Madshus IH: Expression of epidermal growth factor receptor or ErbB3 facilitates geldanamycin-induced down-regulation of ErbB2. *Mol Cancer Res* 2009, 7(2):275-284.

16 Fishwild DM, O'Donnell SL, Bengoechea T, Hudson DV, Harding F, Bernhard SL, Jones D, Kay RM, Higgins KM, Schramm SR *et al*: High-avidity human IgG kappa monoclonal antibodies from a novel strain of minilocus transgenic mice. *Nat Biotechnol* 1996, 14(7):845-851.

17 Yokoyama WM: Production of monoclonal antibodies. *Curr Protoc Cytom* 2006, Appendix 3:Appendix 3J.

18 Kozak M: Initiation of translation in prokaryotes and eukaryotes. *Gene* 1999, 234(2):187-208.

19 Bebbington CR, Renner G, Thomson S, King D, Abrams D, Yarranton GT: High-level expression of a recombinant antibody from myeloma cells using a glutamine synthetase gene as an amplifiable selectable marker. *Biotechnology (N Y)* 1992, 10(2):169-175.

20 Lammerts van Bueren JJ, Bleeker WK, Bogh HO, Houtkamp M, Schuurman J, van de Winkel JG, Parren PW: Effect of target dynamics on pharmacokinetics of a novel therapeutic antibody against the epidermal growth factor receptor: implications for the mechanisms of action. *Cancer Res* 2006, 66(15):7630-7638.

21 Kellner C, Bleeker WK, Lammerts van Bueren JJ, Staudinger M, Klausz K, Derer S, Glorius P, Muskulus A, de Goeij BE, van de Winkel JG *et al*: Human kappa light chain targeted Pseudomonas exotoxin A--identifying human antibodies and Fab fragments with favorable characteristics for antibody-drug conjugate development. *J Immunol Methods* 2011, 371(1-2):122-133.

22 Cho HS, Mason K, Ramyar KX, Stanley AM, Gabelli SB, Denney DW, Jr., Leahy DJ: Structure of the extracellular region of HER2 alone and in complex with the Herceptin Fab. *Nature* 2003, 421(6924):756-760.

23 Junttila TT, Akita RW, Parsons K, Fields C, Lewis Phillips GD, Friedman LS, Sampath D, Sliwkowski MX: Ligand-independent HER2/HER3/PI3K complex is disrupted by trastuzumab and is effectively inhibited by the PI3K inhibitor GDC-0941. *Cancer Cell* 2009, 15(5):429-440.

24 Landgraf R: HER2 therapy. HER2 (ERBB2): functional diversity from structurally conserved building blocks. *Breast Cancer Res* 2007, 9(1):202.

25 Teeling JL, Mackus WJ, Wiegman LJ, van den Brakel JH, Beers SA, French RR, van Meerten T, Ebeling S, Vink T, Slootstra JW *et al*: The biological activity of human CD20 monoclonal antibodies is linked to unique epitopes on CD20. *J Immunol* 2006, 177(1):362-371.

26 de Weers M, Tai YT, van der Veer MS, Bakker JM, Vink T, Jacobs DC, Oomen LA, Peipp M, Valerius T, Slootstra JW *et al*: Daratumumab, a novel therapeutic human CD38 monoclonal antibody, induces killing of multiple myeloma and other hematological tumors. *J Immunol* 2011, 186(3):1840-1848.

27 Agus DB, Akita RW, Fox WD, Lewis GD, Higgins B, Pisacane PI, Lofgren JA, Tindell C, Evans DP, Maiese K *et al*: Targeting ligand-activated ErbB2 signaling inhibits breast and prostate tumor growth. *Cancer Cell* 2002, 2(2):127-137.

28 Kreitman RJ: Recombinant immunotoxins containing truncated bacterial toxins for the treatment of hematologic malignancies. *BioDrugs* 2009, 23(1):1-13.

29 Brennan PJ, Kumagai T, Berezov A, Murali R, Greene MI: HER2/neu: mechanisms of dimerization/ oligomerization. *Oncogene* 2000, 19(53):6093-6101.

30 Cao Z, Wu X, Yen L, Sweeney C, Carraway KL, 3rd: Neuregulin-induced ErbB3 downregulation is mediated by a protein stability cascade involving the E3 ubiquitin ligase Nrdp1. *Mol Cell Biol* 2007, 27(6):2180-2188.

31 Sundvall M, Korhonen A, Paatero I, Gaudio E, Melino G, Croce CM, Aqeilan RI, Elenius K: Isoform-specific monoubiquitination, endocytosis, and degradation of alternatively spliced ErbB4 isoforms. *Proc Natl Acad Sci U S A* 2008, 105(11):4162-4167.

32 Baulida J, Carpenter G: Heregulin degradation in the absence of rapid receptor-mediated internalization. *Exp Cell Res* 1997, 232(1):167-172.

33 Baulida J, Kraus MH, Alimandi M, Di Fiore PP, Carpenter G: All ErbB receptors other than the epidermal growth factor receptor are endocytosis impaired. *J Biol Chem* 1996, 271(9):5251-5257.

34 Wiley HS, Herbst JJ, Walsh BJ, Lauffenburger DA, Rosenfeld MG, Gill GN: The role of tyrosine kinase activity in endocytosis, compartmentation, and down-regulation of the epidermal growth factor receptor. *J Biol Chem* 1991, 266(17):11083-11094.

35 Chiron MF, Fryling CM, FitzGerald DJ: Cleavage of pseudomonas exotoxin and diphtheria toxin by a furin-like enzyme prepared from beef liver. *J Biol Chem* 1994, 269(27):18167-18176.

36 Weldon JE, Pastan I: A guide to taming a toxin--recombinant immunotoxins constructed from Pseudomonas exotoxin A for the treatment of cancer. *FEBS J* 2011, 278(23):4683-4700.

37 MacDonald GC, Rasamoelisolo M, Entwistle J, Cuthbert W, Kowalski M, Spearman MA, Glover N: A phase I clinical study of intratumorally administered VB4-845, an anti-epithelial cell adhesion molecule recombinant fusion protein, in patients with squamous cell carcinoma of the head and neck. *Med Oncol* 2009, 26(3):257-264.

38 Wayne AS, Kreitman RJ, Findley HW, Lew G, Delbrook C, Steinberg SM, Stetler-Stevenson M, Fitzgerald DJ, Pastan I: Anti-CD22 immunotoxin RFB4(dsFv)-PE38 (BL22) for CD22-positive hematologic malignancies of childhood: preclinical studies and phase I clinical trial. *Clin Cancer Res*, 16(6):1894-1903.

39 Biggers K, Scheinfeld N: VB4-845, a conjugated recombinant antibody and immunotoxin for head and neck cancer and bladder cancer. *Curr Opin Mol Ther* 2008, 10(2):176-186.

40 Hassan R, Bullock S, Premkumar A, Kreitman RJ, Kindler H, Willingham MC, Pastan I: Phase I study of SS1P, a recombinant anti-mesothelin immunotoxin given as a bolus I.V. infusion to patients with mesothelin-expressing mesothelioma, ovarian, and pancreatic cancers. *Clin Cancer Res* 2007, 13(17):5144-5149.

41 von Minckwitz G, Harder S, Hovelmann S, Jager E, Al-Batran SE, Loibl S, Atmaca A, Cimpoiasu C, Neumann A, Abera A *et al*: Phase I clinical study of the recombinant antibody toxin scFv(FRP5)-ETA specific for the ErbB2/HER2 receptor in patients with advanced solid malignomas. *Breast Cancer Res* 2005, 7(5):R617-626.

42 Hendriks BS, Opresko LK, Wiley HS, Lauffenburger D: Quantitative analysis of HER2-mediated effects on HER2 and epidermal growth factor receptor endocytosis: distribution of homo- and heterodimers depends on relative HER2 levels. *J Biol Chem* 2003, 278(26):23343-23351.

43 Boyer CM, Pusztai L, Wiener JR, Xu FJ, Dean GS, Bast BS, O'Briant KC, Greenwald M, DeSombre KA, Bast RC, Jr.: Relative cytotoxic activity of immunotoxins reactive with different epitopes on the extracellular domain of the c-erbB-2 (HER-2/neu) gene product p185. *Int J Cancer* 1999, 82(4):525-531.

44 Pastan I, FitzGerald D: Pseudomonas exotoxin: chimeric toxins. *J Biol Chem* 1989, 264(26):15157-15160.

45 Klapper LN, Vaisman N, Hurwitz E, Pinkas-Kramarski R, Yarden Y, Sela M: A subclass of tumor-inhibitory monoclonal antibodies to ErbB-2/HER2 blocks crosstalk with growth factor receptors. *Oncogene* 1997, 14(17):2099-2109.

46 Guillemard V, Nedev HN, Berezov A, Murali R, Saragovi HU: HER2-mediated internalization of a targeted prodrug cytotoxic conjugate is dependent on the valency of the targeting ligand. *DNA Cell Biol* 2005, 24(6):350-358.

47 Wels W, Beerli R, Hellmann P, Schmidt M, Marte BM, Kornilova ES, Hekele A, Mendelsohn J, Groner B, Hynes NE: EGF receptor and p185erbB-2-specific single-chain antibody toxins differ in their cell-killing activity on tumor cells expressing both receptor proteins. *Int J Cancer* 1995, 60(1):137-144.

48 Wehrman TS, Raab WJ, Casipit CL, Doyonnas R, Pomerantz JH, Blau HM: A system for quantifying dynamic protein interactions defines a role for Herceptin in modulating ErbB2 interactions. *Proc Natl Acad Sci U S A* 2006, 103(50):19063-19068.

49 Seetharam S, Chaudhary VK, FitzGerald D, Pastan I: Increased cytotoxic activity of Pseudomonas exotoxin and two chimeric toxins ending in KDEL. *J Biol Chem* 1991, 266(26):17376-17381.

50 Poncelet P, Carayon P: Cytofluorometric quantification of cell-surface antigens by indirect immunofluorescence using monoclonal antibodies. *J Immunol Methods* 1985, 85(1):65-74.

SUPPLEMENTARY METHODS

Preparation of α-kappa-ETA'

The human kappa light chain-directed toxin contains a truncated version of exotoxin A (ETA') from *Pseudomonas aeroginosa* comprising domains Ib, II, and III [44] Domain Ia was replaced by a high affinity domain antibody with human kappa light chain specificity. The C-terminal located endogenous endoplasmatic reticulum retention motif REDLK was replaced by the KDEL motif to improve intracellular retrograde transport [49] A combined 6xhistidine- and strep-II tag was added at the N-terminus for purification purposes. A pelB leader sequence was introduced at the 5´-end of the construct for directing protein expression to the periplasmatic space. The immunotoxin was expressed under osmotic stress conditions and purified from periplasmatic extracts by two step affinity chromatography using streptactin and Ni-NTA agarose beads as described [21] The purified protein was analyzed by SDS-PAGE and coomassie staining, capillary electrophoresis or western blot analysis.

Supplementary Method 2: Epitope mapping

Epitope mapping was performed at Pepscan using their proprietary CLIPS™ technology, as described by Teeling et al [25] Over 5,000 different Chemically Linked Immunogenic Peptides on Scaffolds (CLIPS™) were generated; linear or looped with sizes ranging from 15 to 35 amino acids, which functionally mimic overlapping epitopes of the extracellular domain of HER2. The peptides were synthesized using standard Fmoc-chemistry and deprotected using trifluoric acid with scavengers. Subsequently, the deprotected peptides were reacted on microarrays for 30-60 min, the microarrays were washed extensively with excess of millipore H_2O and sonicated in disrupt-buffer containing 1% sodium dodecylsulfate / 0.1% betamercaptoethanol in phosphate buffered saline (PBS) at 70°C for 30 min, followed by sonication in millipore H_2O for another 45 min. Subsequently, 1 μg/mL antibody in PBS/1% Tween was added to detect binding to CLIPS using an ELISA-type read-out. 1/1000 diluted HRP-conjugated rabbit anti-human Ab and 2,2'-azino-bis(3-ethylbenzthiazoline-6-sulphonic acid substrate (ABTS) were used to detect and visualize antibody binding.

Supplementary Method 3: Quantitative determination of cell surface antigens

Qifikit (DAKO) was used to detect and quantify cell surface expression of EGFR, HER2 and HER3, according to manufacturer's protocol [50]. In brief; cells were stained with 10 μg/mL mouse anti-human EGFR (BD), mouse anti-human HER2 (R&D systems), mouse anti-human HER3 (Oncogene), following incubation with polyclonal goat anti-mouse IgG FITC (DAKO). In parallel a series of bead populations, containing a well-defined number of antibody molecules per bead, was stained with the polyclonal goat anti-mouse IgG FITC antibody. Mean fluorescence intensities (MFI) were measured using flow cytometry, and a calibration curve with the MFI of the individual

bead populations was plotted against the number of mAb molecules on the beads. This curve was used to interpolate the number of EGFR, HER2 or HER3 molecules per cell.

SUPPLEMENTARY TABLES

Immobilized mAb ↓	competing mAb →						
	Herc	169	pert	025	098	153	005
Herc	6	15	100	107	101	101	137
169	19	45	101	98	105	102	97
pert	104	100	9	20	103	100	151
025	98	98	8	18	102	99	99
098	107	102	104	108	17	110	126
153	134	111	121	97	115	28	174
005	126	103	115	109	117	121	18
Cross-competition group	1	1	2	2	3a	3b	4

75 - >100% competition 25 - 74% competition 0 - 24% competition

SUPPLEMENTARY TABLE 1 *Cross-competition ELISA.* Cross-competition ELISA reveals at least 4 distinct cross-competition groups. HER2 antibodies were coated at their predetermined coat-concentrations, and incubated with HER2ECDHis in absence or presence of an excess of a second (competitor) HER2 antibody. Bound Her2ECDHis was detected using a biotinylated rabbit-anti-6xhis antibody in combination with streptavidin-poly-HRP. Depicted values are mean binding percentages relative to the binding observed in the absence of competitor antibody, of three individual experiments. Shaded boxes indicate competition (e.g. HER2ECDHis in the presence of soluble Herceptin only shows 6% of total binding to immobilized Herceptin; which therefore provides a 94% inhibition as indicated by the dark shading). Cross-competition group designations are indicated at the bottom (Herc = Herceptin; Pert = TH-pertuzumab).

	EGFR	HER2	HER3
AU565	35,000	1,000,000	27,000
Colo 205	10,000	30,000	6,000
A431	1,000,000	15,000	15,000
MCF7	n.d.	19,000	22,000

SUPPLEMENTARY TABLE 2 *Quantitative flow cytometry.* Number of EGFR, HER2 and HER3 molecules per cell quantified with quantitative flow cytometry analysis (n.d.: not detected).

SUPPLEMENTARY FIGURES

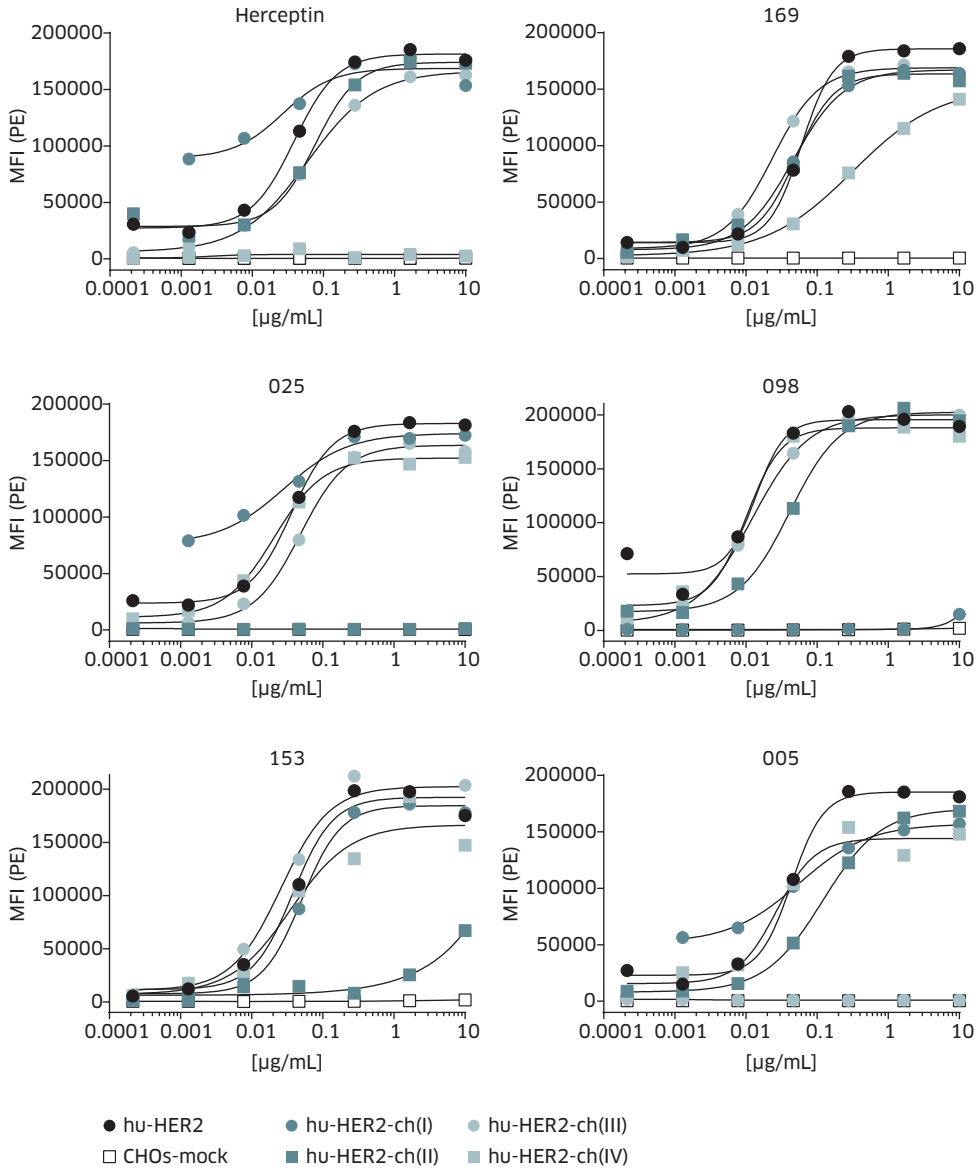

SUPPLEMENTARY FIGURE 1 *HER2 shuffle analysis.* Loss of HER2 antibody binding to CHO-S cells transfected with hu-HER2 (●), hu-HER2-ch(I) (●), hu-HER2-ch(II) (■), hu-HER2-ch(III) (●) or hu-HER2-ch(IV) (■) constructs analyzed by means of flow cytometry. Constructs were generated by swapping the sequences of domains I, II, III, IV of the extracellular domain of human HER2 with the corresponding sequence of chicken HER2. Cells transfected with empty vector were used as control (□).

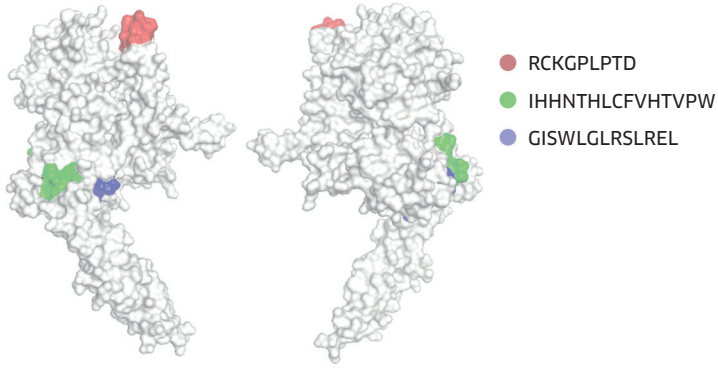

SUPPLEMENTARY FIGURE 2 *Analysis of binding of antibodies 005 and 153 to HER2-ECD CLIPS.* Model depicting the binding epitopes of antibodies 005 and 153 as mapped by use of CLIPS technology. Two epitopes were visualized in two different representations of the crystal structure of HER2ECD by use of VMD molecular modeling software. The epitope for antibody 005 was located at the rear end of HER2 domain III, whereas the epitope for antibody 153 was located on top of the receptor at HER2 domain II.

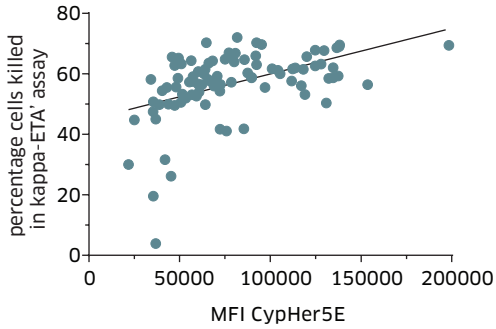

SUPPLEMENTARY FIGURE 3 *Correlation analysis.* Correlation between the percentage of AU565 cells killed in the kappa-ETA' assay and the MFI of CypHer5E. Spearman's coefficient r = 0.5373.

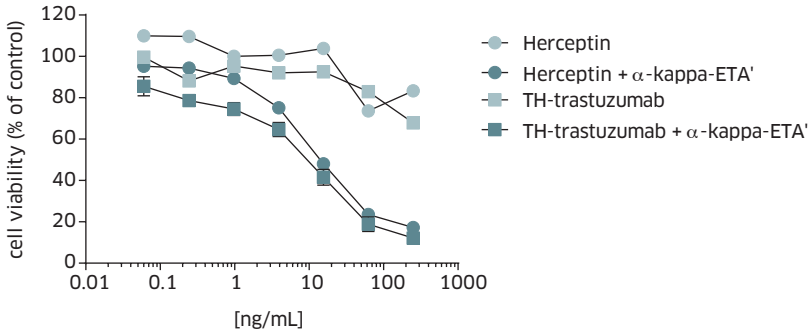

SUPPLEMENTARY FIGURE 4 *CHO vs. HEK produced trastuzumab in the α-kappa-ETA' model system.* Cell kill induced by clinical grade Herceptin compared with HEK-293 produced Herceptin in α-kappa-ETA' assay with AU565 cells. A final concentration of 0.5 µg/mL α-kappa-ETA' was used. Viability was plotted as a percentage relative to untreated cells. 10 µg/mL Staurosporin was used as positive control.

7 Efficient payload delivery by a bispecific antibody targeting HER2 and CD63

► To be submitted

► Bart ECG de Goeij[1], Tom Vink[1], Hendrik ten Napel[1], Esther CW Breij[1], David Satijn[1], Richard Wubbolts[2], David Miao[3] and Paul WHI Parren[1,4,5]

1 Genmab, Yalelaan 60, 3584 CM, Utrecht, The Netherlands

2 Dept. of Biochemistry and Cell Biology, Faculty of Veterinary Medicine, Utrecht University, Yalelaan 2, 3584 CM, Utrecht, The Netherlands

3 Concortis Biosystems Corp., San Diego, 11760 Sorrento Valley, CA 92121 USA

4 Dept. of Cancer and Inflammation Research, Institute of Molecular Medicine, University of Southern Denmark, Odense, Denmark

5 Dept. of immunohematology and Blood Transfusion, Leiden University Medical Center, 2333 ZA Leiden, The Netherlands

ABSTRACT

Antibody drug conjugates (ADC) are designed to be stable in circulation and to release potent cytotoxic drugs intracellularly following antigen-specific binding, uptake and degradation in tumor cells. Efficient internalization and routing to lysosomes where proteolysis can take place is therefore essential. For many cell surface proteins and carbohydrate structures on tumor cells, however, the magnitude of these processes is insufficient to allow for an effective ADC approach. We hypothesized that we could overcome this limitation by enhancing lysosomal ADC delivery via a bispecific antibody (bsAb) approach, in which one binding domain would provide tumor specificity, whereas the other binding domain would facilitate targeting to the lysosomal compartment. We therefore designed a bsAb in which one binding arm specifically targeted the lysosome-associated membrane glycoprotein 3 (LAMP3 or CD63), a protein that is described to shuttle between the plasma membrane and intracellular compartments. We optimized the targeting characteristics of the CD63 antibody and combined it in a bsAb with a HER2 binding arm, which was selected as model antigen for tumor specific binding. The resulting bsHER2xCD63$_{his}$ demonstrated strong binding, internalization and lysosomal accumulation in HER2-positive tumor cells, and minimal internalization into HER2-negative cells. By conjugating bsHER2xCD63$_{his}$ to the microtubule-disrupting agent duostatin-3, we were able to demonstrate potent cytotoxicity of bsHER2xCD63$_{his}$-ADC against HER2-positive tumors, which was not observed with monovalent HER2- and CD63-specific ADCs. Our data demonstrate, for the first time, that intracellular trafficking of ADCs can be improved using a bsAb approach that targets the lysosomal membrane protein CD63 and provide a rationale for the development of novel bsADCs that combine tumor-specific targeting with targeting of rapidly internalizing antigens.

Introduction

Antibody Drug Conjugates (ADCs) are emerging as powerful anti-cancer treatments. Over 50 different ADCs are currently in clinical evaluation, while brentuximab vedotin (Adcetris) and trastuzumab emtansine (Kadcyla) have already been approved for the treatment of Hodgkin lymphoma and metastatic breast cancer, respectively [1]. These ADCs, as well as virtually all other ADCs in clinical development, are designed to be stable in circulation and to release their cytotoxic payload after internalization and lysosomal processing of the antigen/ADC complex [2]. The requirement for antigen- and antibody-mediated internalization limits the number of suitable ADC targets. In many cases, intracellular processing of ADCs is inefficient. Following internalization, receptors such as transferrin [3], HER2 [4,5], cell adhesion molecule L1 [6] and integrins [7], are continuously recycled back from the endosomal compartment to the plasma membrane. High antigen expression and highly toxic payloads are required to ensure activity of ADCs. Therefore approaches that increase internalization, lysosomal targeting and intratumoral processing of ADCs are highly desired.

We previously demonstrated that ADCs that are more efficiently internalized and transported to the lysosomes induce more effective cytotoxicity [8]. Therefore, we set out to improve ADC-mediated drug release by improving their intracellular delivery. We generated an ADC based on a bispecific antibody [9], in which one binding arm was responsible for tumor cell binding and the other binding arm was designed to facilitate internalization and lysosomal delivery of the toxic payload. Ideally, such a bispecific ADC would allow utilization of tumor antigens that do not or poorly internalize for an ADC approach, thereby greatly enhancing the pool of potential ADC targets. An antibody specific for the lysosome-associated membrane glycoprotein 3 (LAMP3 or CD63) was selected to provide a Fab arm that facilitates internalization and lysosomal transport. CD63 is a member of the tetraspanin superfamily and is ubiquitously expressed. The major pool of CD63 resides in intracellular compartments such as endosomes and lysosomes, but some expression can be found on the cell surface. Although the biology of CD63 is not completely understood, CD63 has been described to regulate transport of other proteins typically through endocytosis [10]. For example, complex formation between CD63 and the gastric H,K-ATPase β-subunit, results in the redistribution of H,K-ATPase from the cell surface to CD63-positive intracellular compartments [11]. Furthermore, CD63 has been described to regulate surface expression of membrane-type 1 matrix metalloproteinase by targeting the enzyme for lysosomal degradation [12], and silencing of CD63 in endothelial cells prevents internalization of vascular endothelial growth factor receptor 2 (VEGFR2) in response to its ligand VEGF [13]. Also across different tumor types, CD63 has been demonstrated to continuously shuttle between the plasma membrane and lysosomes, which was dependent on the presence of AP2 and clathrin [14]. Thus CD63 seems an attractive antigen to facilitate internalization and lysosomal delivery.

To study our hypothesis that a CD63-specific Ab-arm could promote internalization and lysosomal targeting of a bsAb also including a tumor-specific, poorly internalizing binding arm, we generated a bsAb recognizing CD63 and the human epidermal growth factor receptor 2 (HER2). HER2 is a clinically well validated ADC target through the clinical experience and approval of trastuzumab emtansine [15]. However, for internalization to be most effective HER2 requires cross-linking of HER2 molecules. Especially on tumor cells that highly overexpress HER2, Ab-induced cross-linking has been described to improve internalization of HER2 [5,16,17]. The notion that monomeric HER2 does not internalize well suggested to us that a bsAb with monovalent HER2 binding characteristics may represent a suitable model system for testing whether internalization of cell surface molecules can be increased through binding to CD63.

We found that a bsAb targeting HER2 and CD63 was efficiently transported to lysosomes of HER2-positive tumor cells. This effect was not observed with monovalent

control antibodies only targeting HER2 or CD63. By conjugating bsHER2xCD63 with the microtubule disrupting agent duostatin-3, we were able to demonstrate that a bsHER2xCD63-ADC induced potent *in vitro* and *in vivo* cytotoxicity of HER2-positive tumor cells. Monovalent ADCs targeting HER2 or CD63 alone had no effect on tumor growth which demonstrates that CD63 targeting can be used to improve payload delivery of poorly internalizing ADCs.

MATERIALS AND METHOD

Cell lines

Human SK-OV-3 (ovarian cancer), HCC1954 (breast ductal carcinoma) and Colo 205 (colorectal adenocarcinoma) cells were obtained from American Type Culture Collection (ATCC). SK-OV-3 cells were cultured in Minimal Essential Medium Eagles (ATCC) containing 10% heat inactivated calf serum (Hyclone). HCC1954 and Colo 205 cells were cultured in RPMI 1640 (Lonza) containing 10% heat inactivated calf serum. To guarantee cell line authenticity, cell lines were aliquoted and banked, and cultures were grown and used for a limited number of passages before starting a new culture from stock. Cell lines were routinely tested for mycoplasma contamination. HER2 cell surface expression was quantified by QIFIKIT analysis (DAKO) according to the manufacturer's guidelines, using a mouse anti-human HER2 antibody (R&D) as described previously [8].

Antibody generation, site-directed mutagenesis and conjugation

Cloning and production of HER2 antibody IgG1-153 has been described elsewhere [16]. The variable domain heavy and light chain regions of CD63 antibody 2192 were obtained from hybridoma 2.19 [18], by 5'-RACE of the variable regions from hybridoma derived RNA and sequencing. Variable regions were cloned in the mammalian expression vector pcDNA3.3 (Invitrogen) containing the relevant constant domains (codon optimized, Invitrogen) with the relevant heavy chain constant domain mutations (K409R or F405L). CD63 antibody mutations were introduced either by site directed mutagenesis or direct gene synthesis. Antibodies were produced by cotransfection of heavy chain and light chain vectors and transient expression in HEK-293 freestyle cells (Invitrogen) as described by Vink et al [19]. Bispecific antibodies (Duobody) were made by controlled Fab-arm exchange as described by Labrijn et al [20]. The IgG1-b12 antibody was included as isotype control [21].

Duostatin-3 conjugated antibodies were generated by covalent conjugation of valine-citrulline-duostatin-3 (Duo3) on antibody lysine groups of IgG1-HER2-F405L and IgG1-b12-F405L as described previously [8]. After conjugation, IgG1-HER2-F405L-Duo3 and IgG1-b12-F405L-Duo3 were Fab-arm exchanged with IgG1-HER2-K409R, IgG1-CD63-K409R and IgG1-b12-K409R, to generate bsHER2xCD63-Duo3,

bsHER2xb12-Duo3, bsCD63xb12-Duo3, and IgG1 b12-Duo3 and IgG1 Her2-Duo3 controls all having an equal DAR of one duostatin-3 molecule per Ab, as determined by hydrophobic interaction chromatography (HIC).

CD63 binding ELISA

The binding of Histidine-mutated IgG1-2192 to CD63 was tested by ELISA. In short, ELISA plates (Greiner) were coated overnight at 4°C with 0.8 µg/mL goat anti-human IgG (Jackson). The plates were blocked with 2% chicken serum and incubated with 1 µg/mL histidine-mutated IgG1-2192. Serially diluted (1-0.0005 µg/mL) recombinant human CD63 (Creative Biomart) was added followed by 1 µg/mL mouse anti-poly-histidine-biotin (R&D). The reaction was visualized using ABTS and stopped with oxalic acid. Fluorescence at 405 nm was measured and depicted using GraphPad Prism 5 software.

CD63 affinity measurements

Kinetics of human His-tagged CD63 (1 µg/ml, 77 nM) (Creative BioMart) were assessed using label-free Bio-Layer Interferometry on an Octet RED384 (ForteBio). Anti-CD63 wild type or mutants containing histidine substitutions were immobilized on Anti-Human IgG Fc Capture Biosensors (ForteBio) at 1 µg/mL. Association and dissociation kinetics were determined in citric acid/Na2HPO4 buffer pH7.4 supplemented with 0.1 % BSA Fraction V (Roche) and 0.02% Tween-20 (Sigma-Aldrich), using a shaker speed of 1000 rpm at 30°C. The dissociation constant KD (M) was determined with ForteBio Data Analysis v7.0, using the 1:1 model in combination with a local full fit. The six clones with lowest KD values were measured twice, other clones were measured once.

mAb-FITC accumulation assay with whole blood

Whole blood samples from healthy donors were collected in Heparin tubes. Whole blood was diluted 1:2 in RPMI-1640 supplemented with 10% heat inactivated cosmic calf serum. CD63 antibodies were conjugated with FITC (Thermo Scientific) according to manufacturer's instruction and added at final concentration of 10 µg/mL, to whole blood cells. Following 1 hour incubation at 4°C or 3 and 16 hours incubation at 37°C, erythrocytes were lysed by incubating 15 minutes at 4°C with erythrocyte lysis buffer (155 mM NH4Cl, 10 mM KHCO3 and 0.1 mM EDTA at pH 7.4). Fluorescence intensities of FITC were measured on a flow cytometer (BD). Granulocytes were gated using mouse anti-human CD66b-PerCP-Cy5.5 (BD) and thrombocytes were gated using mouse anti-human CD62-APC (BD).

Confocal microscopy

SK-OV-3 cells were grown on glass coverslips (Thermo Fisher Scientific) at 37˚C for 16 hours. One hour prior to antibody treatment, cells were pre-incubated with 50 µg/mL leupeptin (Sigma) to block lysosomal activity. Antibody (1 µg/mL) was added and cells were incubated for 1, 3 or 16 hours at 37˚C. Cells were fixed, permeabilized and incubated 45 min with goat anti-human IgG1-FITC (Jackson) to stain for human IgG and mouse anti-human CD107a-APC (BD) to stain for lysosomes. Coverslips were mounted (Calbiochem) on microscope slides and imaged with a Leica SPE-II confocal microscope (Leica Microsystems) equipped with LAS-AF software. 12-bit grayscale TIFF images were analyzed for colocalisation using MetaMorph® software (Molecular Devices). Colocalisation was depicted as arbitrary units [AU] representing the total pixel intensity of antibody overlapping with the lysosomal marker LAMP1. This value was divided by the total pixel intensity of LAMP1, to correct for differences in cell densities between different pictures.

HER2 downmodulation assay

HCC1954, SK-OV-3 and Colo 205 cells were seeded (1 million cells/flask) in T25 flasks (Greiner) and incubated overnight at 37°C to obtain a confluent monolayer. Antibodies were added (10 µg/mL) and cells were cultured for another 3 days at 37°C, washed and lysed. Total protein levels were quantified using bicinchoninic acid (BCA) protein assay reagent (Pierce), according to manufacturer's instruction. Next, ELISA plates (Greiner) were coated with 1 µg/mL rabbit anti-human HER2 (Cell Signalling Technology), blocked with 2% chicken serum (Hyclone) and incubated with 50 µL cell lysate. Goat anti-human HER2-biotin (R&D, 50 ng/mL) was added to detect HER2, followed by streptavidin-poly-HRP (Sanquin, 100 ng/mL). The reaction was visualized using ABTS and stopped with oxalic acid. Fluorescence at 405 nm was measured and the amount of HER2 was expressed as a percentage relative to untreated cells.

Cytotoxicity assay

Cells were seeded in 96-well tissue culture plates (5,000 cells/well) and incubated for 6 hours at 37°C. Serially diluted ADCs (10-0.0005 µg/mL) were added and the cells were incubated for 3 days at 37°C. Cell viability was assessed using CellTiter-GLO (Promega), according to the manufacturer's guidelines. The percentage of viable cells was depicted as a percentage relative to untreated cells.

Tumor xenograft model

6-11 week old female SCID mice (C.B-17/IcrPrkdc-scid/CRL) were purchased from Charles River. Subcutaneous tumors were induced by inoculation of 5 x 10^6 SK-OV-3 cells in the right flank of the mice. Tumor volumes were calculated from digital caliper measurements as 0.52 x length x $width^2$ (mm^3). When tumors reached 200–400 mm^3, mice were grouped into groups of 7 mice with equal tumor size distribution and mAbs

were injected intraperitoneally (8 mg/kg). During the study, blood samples were collected into heparin-containing tubes to confirm the presence of human IgG in plasma. IgG levels were quantified using a nephelometer (Siemens Healthcare). Mice that did not show human IgG in plasma were excluded from the analysis.

Statistical analysis

Data analysis was done using GraphPad Prism 5 software. Group data were reported as mean ± SD. Statistical analysis of xenograft studies was done with one-way ANOVA at the last day that all groups were complete. Mantel-Cox analysis of Kaplan-Meier curves was performed to analyze statistical differences in progression-free survival time.

RESULTS

Generation of a low affinity CD63 antibody

To improve intracellular trafficking of ADCs, we set out to generate a bispecific ADC that specifically binds to tumor cells with one Fab-arm, while its second Fab-arm is being used to facilitate internalization and lysosomal delivery of the cytotoxic payload. The resulting bsADC should only induce cytotoxicity in tumor cells expressing both antigens. A bsAb targeting HER2 and CD63 was selected as a model for such an ADC. CD63 is ubiquitously expressed and expression is found predominantly in the endosomal and lysosomal compartment, although some expression was also described on the plasma membrane [10,18]. To ensure tumor specificity of the bsAb, the CD63 arm of the bsHER2xCD63 should not bind and internalize in absence of the tumor-specific arm. We hypothesized that a CD63 antibody with low affinity target binding would fulfill these criteria. Therefore we first set out to generate a panel of mutated CD63 antibodies with variable CD63 affinity. It has been demonstrated that single amino acid histidine substitutions can be used to alter Ab affinity [22,23]. Hence site-directed mutagenesis was applied to introduce histidine substitutions in the variable heavy and light chain domains of CD63-specific monoclonal Ab 2192. The resulting clones were screened for binding to soluble CD63 with ELISA (Figure 1A) and label-free Octet (Figure 1B). Antibodies that showed diminished but detectable binding to CD63 were further analyzed with confocal microscopy to visualize internalization and lysosomal targeting. SK-OV-3 cells were grown on glass coverslips and incubated with histidine-mutated CD63 antibody ($CD63_{his}$). As a control we also tested monovalent bsCD63xb12 that recognizes CD63 with one Fab-arm, while the second Fab-arm recognizes an irrelevant antigen in this context (HIV-1 gp120). After 1 and 16 hours incubation, cells were fixed and permeabilized and human IgG1 was stained with an anti-human IgG-FITC antibody while lysosomes were stained with an anti-LAMP1-APC antibody. Figure 2 demonstrates the lysosomal accumulation of the wild type CD63

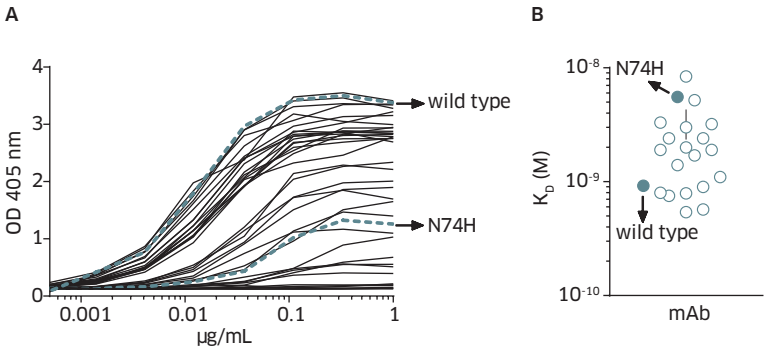

FIGURE 1 *Binding of CD63 antibody affinity variants to CD63.* **(A)** ELISA plates coated with goat anti-human IgG1 were incubated with a fixed concentration of Histidine-mutated antibody variants of CD63 mAb 2192. Serially diluted recombinant human CD63 was added to determine Ab binding and depicted as OD405 values in correlation to CD63 concentration. The dose response of the selected N74H mutant is indicated. **(B)** Anti-CD63 antibodies containing histidine substitutions were immobilized on anti-human IgG Fc Capture Biosensors and the affinity for human His-tagged CD63 was determined using Bio-Layer Interferometry. The dissociation constant KD (M) was calculated and plotted for each mutant. For a number of antibody variants the KD could not be measured accurately because insignificant CD63 binding was detected. As a result the KD values of these antibodies are not depicted.

Ab and the asparagine into histidine (N74H)-mutated CD63 Ab (IgG1-CD63$_{his}$) that was selected for the development of a low affinity CD63 arm.

After 1 hour incubation, no IgG1-CD63 was detected at the plasma membrane or intracellularly (Figure 2A). However after 16 hours of antibody exposure, IgG1-CD63 and the low affinity IgG1-CD63$_{his}$ were abundantly present in the lysosomes of SK-OV-3 cells, as indicated by the colocalisation with LAMP1 (Figure 2B and 2D). This highlights the transient expression of CD63 at the plasma membrane and its constitutive endocytosis and trafficking to the lysosomes. Monovalent bsCD63xb12 also showed substantial transport to lysosomes after 16 hours incubation (Figure 2C). In contrast, hardly any lysosomal transport was observed for the low affinity monovalent bsCD63$_{his}$xb12, as shown in Figure 2E. This indicates the successful generation of a CD63 Fab-arm that should not induce internalization in tissues only expressing CD63.

Binding and internalization of CD63 antibodies in healthy tissue was assessed by measuring intracellular accumulation of FITC-conjugated CD63 antibodies in granulocytes and thrombocytes [10,18]. Whole blood from healthy donors was incubated with FITC conjugated antibodies for 1 hour at 4°C or for 3 and 16 hours at 37°C. Erythrocytes were lysed and remaining lymphocytes and thrombocytes were ana-

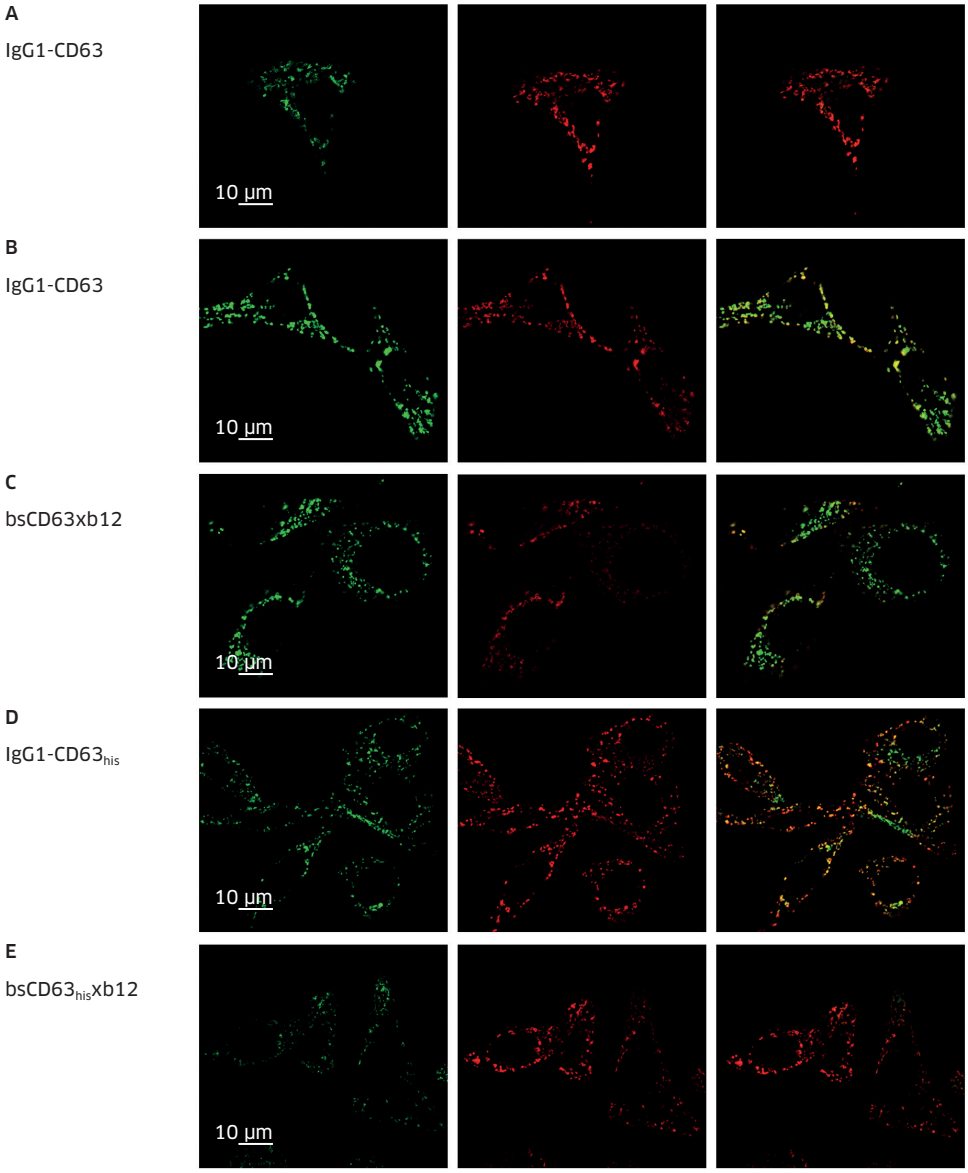

FIGURE 2 *Intracellular accumulation of CD63 antibody variants in tumor cells.* SK-OV-3 cells were incubated 1 hour **(A)** or 16 hours **(B-E)** with IgG1-CD63 **(A, B)** bsCD63xb12 **(C)**, IgG1-CD63$_{his}$ **(D)** or bsCD63$_{his}$xb12 **(E)**. Lysosomes were stained with mouse anti-human LAMP1-APC (red), CD63 antibodies were stained with goat anti-human IgG1-FITC (green). Colocalisation of anti-human IgG1-FITC with anti-human LAMP1-APC is depicted in orange (bottom panel).

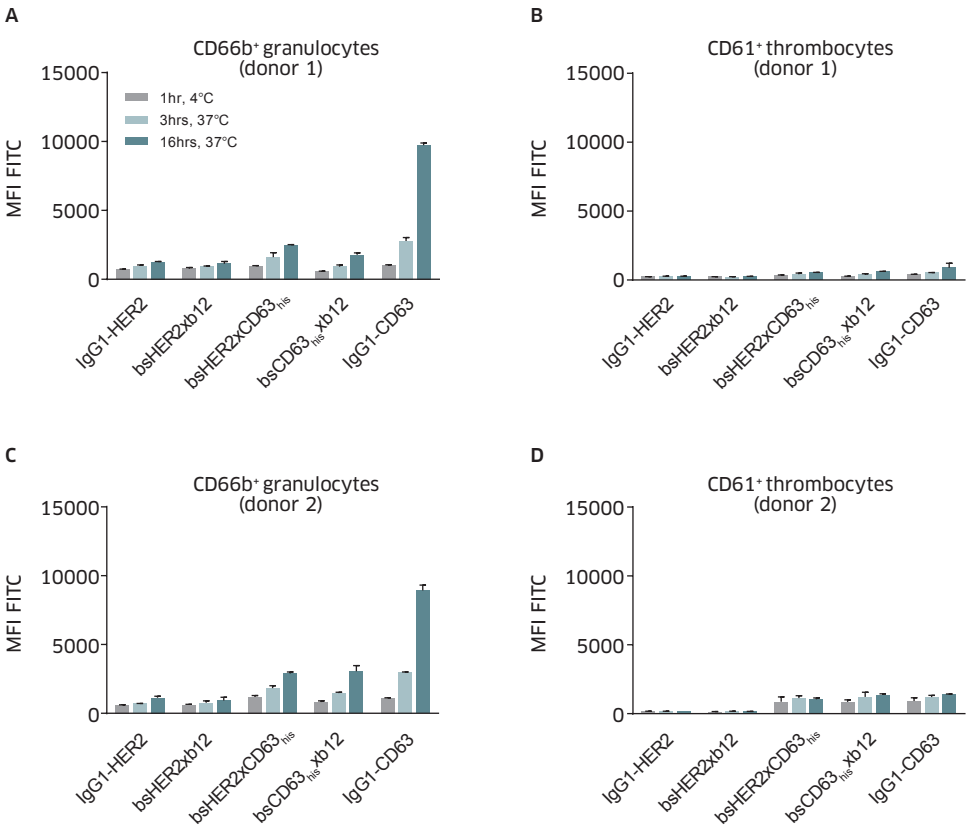

FIGURE 3 *Binding and intracellular accumulation of IgG1-CD63$_{his}$ in whole blood cells.* Whole blood samples from two healthy donors were incubated 1 hour at 4°C, 3 hours at 37°C or 16 hours at 37°C with 10 µg/mL of FITC-conjugated CD63 antibody. After incubation, erythrocytes were lysed and fluorescence intensities of FITC were measured for the granulocyte **(A, C)** and thrombocyte **(B, D)** populations using a flow cytometer. Data shown are mean ± standard deviation of 2 measurements, obtained in two separate donors.

lyzed on a flow cytometer to measure intracellular accumulation of FITC conjugated antibodies. Figure 3 shows no detectable binding of CD63 antibodies to granulocytes or thrombocytes after 1 hour. However, FITC fluorescence of IgG1-CD63 on granulocytes was clearly increased after 16 hours of incubation, indicating accumulation of IgG1-CD63 into granulocytes. In contrast, FITC fluorescence of bsCD63$_{his}$xb12 was hardly increased after 16 hours. Thus, by using a low affinity CD63-specific Fab-arm, we were able to minimize binding and intracellular accumulation of a monovalent CD63 Ab into healthy cells.

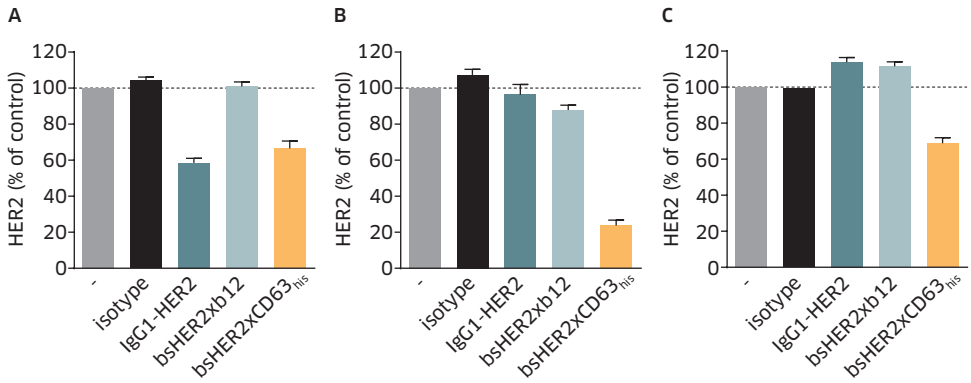

FIGURE 4 *Antibody-dependent downmodulation of HER2 in tumor cell lines.* Relative percentage of HER2 expressed in AU565 **(A)**, SK-OV-3 **(B)** and Colo205 **(C)** cell lysates after three days incubation with 10 µg/mL antibody. The amount of HER2 was quantified using a HER2-specific capture ELISA and plotted as a percentage relative to untreated cells (-). Data shown are mean ± standard deviation of 2 experiments.

A CD63-specific Fab-arm facilitates lysosomal targeting of poorly internalizing antibodies

Next, we investigated whether the $CD63_{his}$-specific Fab-arm could be used to facilitate internalization and lysosomal targeting of a HER2-specific Fab-arm. HER2 antibody 153 (IgG1-HER2), which is known to internalize as bivalent IgG [16], was used to generate a bispecific IgG1 (bsHER2x$CD63_{his}$) that can bind to both, HER2 and CD63. To validate the use of a monovalent HER2-specific IgG (bsHER2xb12) as a model for an IgG with poor internalization characteristics, we first investigated Ab-induced downmodulation of the monovalent bsHER2xb12. For this, the total amount of HER2 protein in tumor cell lines with different expression levels of HER2; HCC1954 (500,000 HER2/cell), SK-OV-3 (200,000 HER2/cell) and Colo205 (50,000 HER2/cell) was quantified after three days of incubation with HER2 antibody and compared with untreated cells. IgG1-HER2 induced ~40% downmodulation of total HER2 in HCC1954 cells that express high levels of HER2 (Figure 4A), which was in line with previously published results [16]. Despite the fact that the monovalent bsHER2xb12 showed dose-dependent binding to HER2-positive SK-OV-3 cells (Supplementary Figure S1), no downmodulation of HER2 was observed (Figure 4A). This highlights that antibody-dependent receptor cross-linking was critical for increasing the degradation of HER2. The bsHER2x$CD63_{his}$ was able to restore the downmodulation of HER2 on HCC1954 cells. Moreover, on cell lines with lower HER2 expression, such as SK-OV-3 (Figure 4B) and Colo205 (Figure 4C), bsHER2x$CD63_{his}$ also induced downmodulation of HER2, whereas IgG1-HER2 did not affect HER2 protein levels.

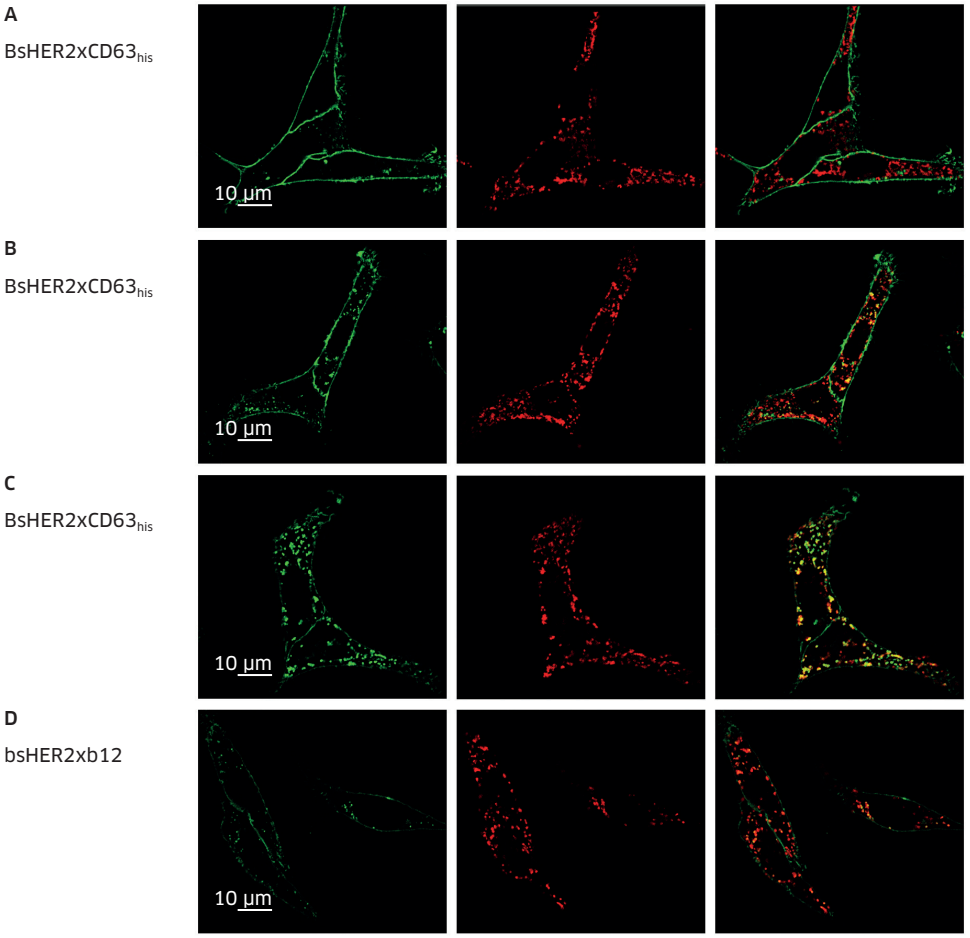

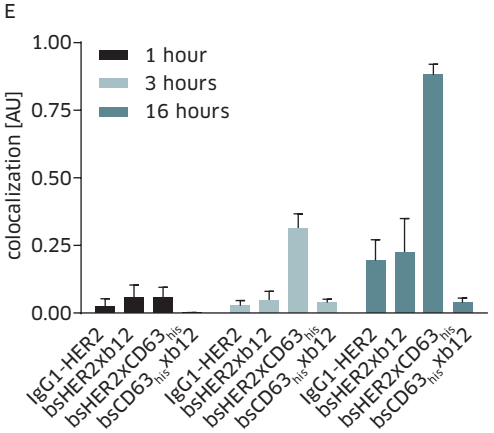

FIGURE 5 *BsHER2xCD63$_{his}$ colocalizes with lysosomes in SK-OV-3 cells.* SK-OV-3 cells were incubated 1 hour **(A)**, 3 hours **(B)** or 16 hours **(C, D)** with bsHER2xCD63$_{his}$ **(A-C)**, and bsHER2xb12 **(D)**. Lysosomes were stained with mouse anti-human LAMP1-APC (red), CD63 antibodies were stained with goat anti-human IgG1-FITC (green). Colocalisation of anti-human IgG1-FITC with anti-human LAMP1-APC is depicted in orange. **(E)** Arbitrary units [AU] represent the total pixel intensity of antibody overlapping with the lysosomal marker LAMP1, divided by the total pixel intensity of LAMP1. Data shown are mean ± standard deviation of 3 images.

We next investigated lysosomal transport of bsHER2xCD63$_{his}$ using confocal microscopy. SK-OV-3 cells were incubated with bsAb and left for 1, 3 and 16 hours at 37°C. Following fixation and permeabilization, human IgG1 was stained with an anti-human IgG-FITC antibody and lysosomes were stained with an anti-LAMP1-APC antibody. Figure 5A and 5B demonstrate that after 1 and 3 hours of incubation, bsHER2xCD63$_{his}$ predominantly localized to the plasma membrane. Whereas after 16 hours (Figure 5C), plasma membrane staining of bsHER2xCD63$_{his}$ was reduced while colocalization with the lysosomal marker LAMP1 was increased. The lysosomal colocalisation of bsHER2xCD63$_{his}$ was more abundant as compared to control Abs only targeting HER2 or CD63 (Figure 5D and 5E). These data indicate that binding of bsHER2xCD63$_{his}$ predominantly occurs through interaction with HER2 while interaction with CD63 induces sub-sequential transport to lysosomes.

BsHER2xCD63$_{his}$-duostatin-3 effectively kills HER2-positive tumor cell lines

To investigate whether the strong lysosomal targeting observed with bsHER2xCD63$_{his}$ results in increased cytotoxicity of a bsHER2xCD63$_{his}$-ADC, we conjugated bsHER2xCD63$_{his}$ with the antimitotic agent duostatin-3 [8], using a valine-citrulline linker that is cleaved by lysosomal proteases [24]. The resulting duostatin-3 conjugated antibodies were incubated with tumor cell lines after which cell viability was assessed using CellTiter-GLO. The decrease in viable tumor cells was expressed as percentage compared to untreated cells. The high HER2-expressing HCC1954 cell line was efficiently killed by bsHER2xHER2-ADC and bsHER2xCD63$_{his}$-ADC (Figure 6A). The monovalent bsHER2xb12-ADC also induced cytotoxicity of HCC1954 cells, but the IC$_{50}$ value was considerably higher. A marked difference between the ADCs was found on SK-OV-3 cells (Figure 6B). BsHER2xHER2-ADC and bsHER2xb12-ADC induced modest cytotoxicity of SK-OV-3 cells, while cytotoxicity induced by bsHER2xCD63$_{his}$-ADC was considerably higher. Viability of the low HER2-expressing cell line Colo 205 was not affected by any of the ADCs (Figure 6C). The cytotoxicity assay with bsHER2xCD63$_{his}$-ADC was also performed in presence of an excess of unconjugated IgG1-CD63 and unconjugated IgG1-HER2, to block CD63 and HER2 binding at the cell surface, respectively (Figure 6D). Both conditions increased the IC$_{50}$ value of bsHER2xCD63$_{his}$-ADC induced cytotoxicity, indicating that binding to both HER2 and CD63 at the plasma membrane is required to induce maximal cytotoxicity.

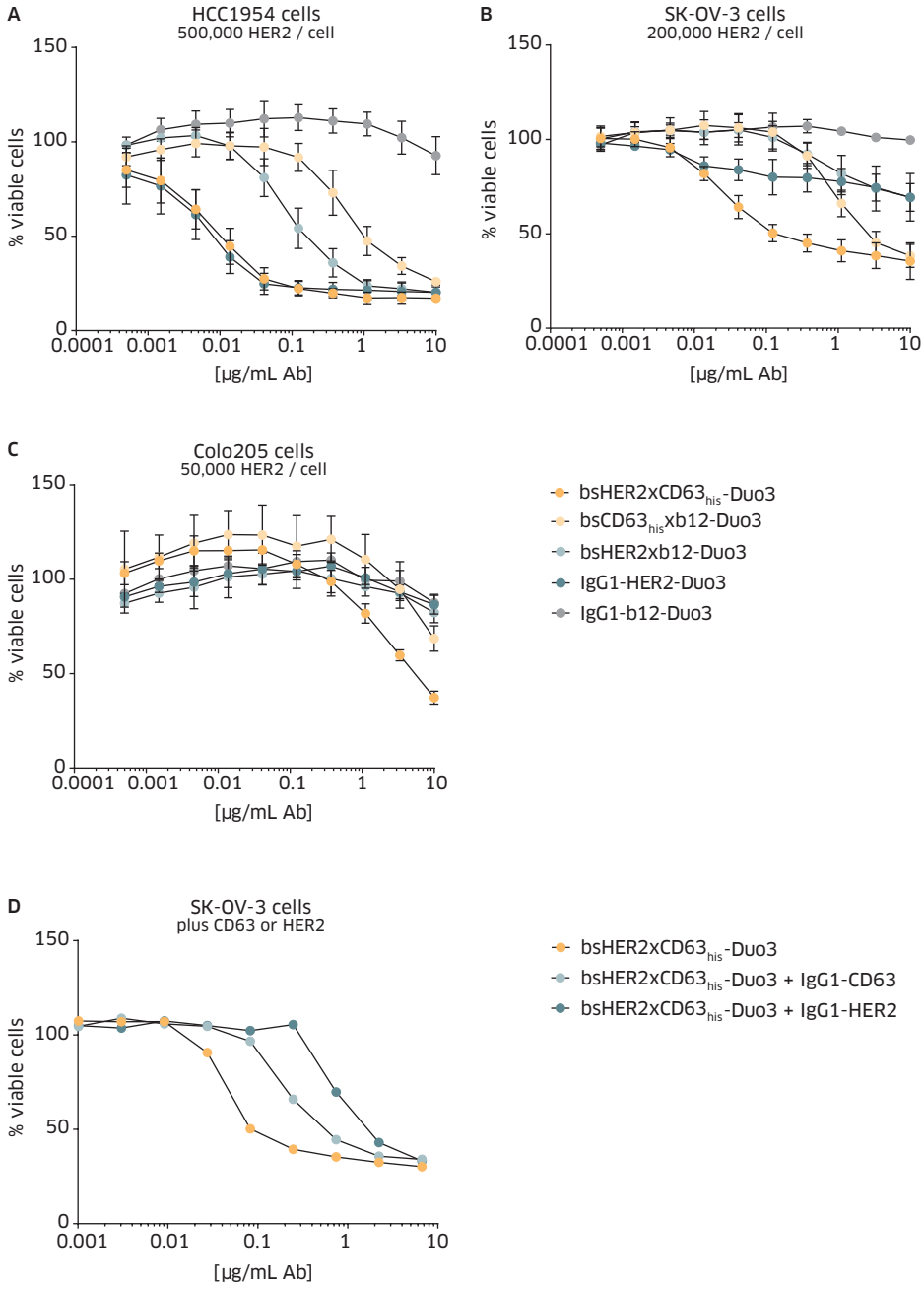

FIGURE 6 *Cytotoxicity of bsHER2xCD63$_{his}$-Duo3, bsHER2xb12-Duo3, bsCD63$_{his}$xb12-Duo3, IgG1 HER2-Duo3 and IgG1 b12-Duo3 in vitro.* HCC1954 **(A)**, SK-OV-3 **(B)** and Colo205 **(C)** cells were seeded in 96-well tissue culture plates together with serially diluted ADCs. SK-OV-3 **(D)** cells were also incubated with serially diluted ADCs plus 10 µg/mL unconjugated IgG1-HER2 or IgG1-CD63. After three days incubation at 37°C viability was assessed using CellTiter-GLO and depicted as a percentage relative to untreated cells. **(A-C)** Data shown are mean ± standard deviation of at least 2 different experiments.

The *in vivo* anti-tumor activity of a monomeric HER2-ADC is rescued by dual targeting of HER2 and CD63

The strong cytotoxicity of bsHER2xCD63$_{his}$-ADC in SK-OV-3 cells *in vitro*, led us to investigate the anti-tumor effect of bsHER2xCD63$_{his}$-ADC on SK-OV-3 tumor xenografts. SCID mice were inoculated subcutaneously with 5 million SK-OV-3 cells. When tumors reached an average size of 200 mm^3, mice were treated with a single dose of 8 mg/kg ADC. Figure 7 demonstrates that bsHER2xCD63$_{his}$-ADC induced significant inhibition of tumor growth, while the monovalent bsHER2xb12-ADC or bsCD63$_{his}$xb12-duo3, had no effect on tumor growth. This provides a strong proof-of-concept and demonstrates that a low affinity CD63-specific Fab-arm can be used to induce lysosomal delivery and toxin release of a poorly internalizing ADC in tumors *in vivo*.

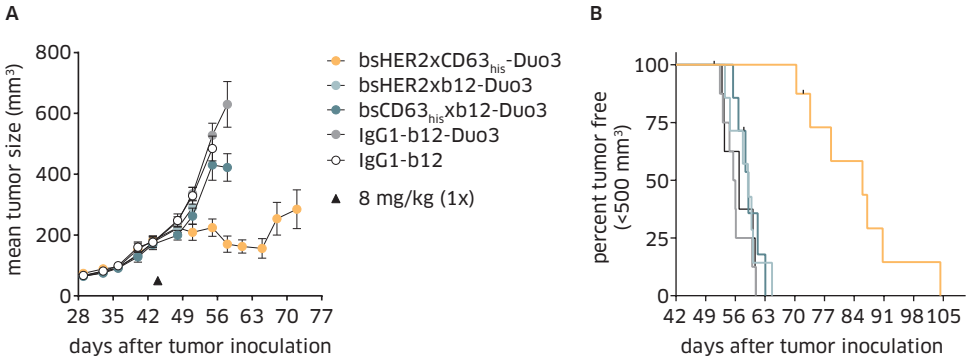

FIGURE 7 *Efficacy of bsHER2xCD63$_{his}$-Duo3, bsHER2xb12-Duo3, bsCD63$_{his}$xb12-Duo3, IgG1 b12-Duo3 and IgG1-b12 in a SK-OV-3 xenograft model.* Mice were inoculated subcutaneously with 5 x 10^6 SK-OV-3 cells. When average tumor volume reached >200 mm^3, mice were divided in groups of 7 mice with equal tumor size distribution and injected intraperitoneally at indicated time points with 8 mg/kg ADC. Tumors were measured twice a week by using calipers and the mean tumor volume ± SEM (mm^3) was plotted against time **(A)**, as well as time to progression indicated by the percentage of mice with tumors <500mm^3 **(B)**.

DISCUSSION

In the present study, we tested the possibility of enhancing lysosomal delivery of ADCs by targeting a tumor-specific antigen in combination with an antigen that facilitates trafficking to the lysosomes. To this end, a bispecific ADC was generated that combines tumor-specific targeting through HER2, with enhanced lysosomal delivery through CD63. The binding affinity of the CD63 arm was modified in order to limit monovalent target binding and to direct the targeting characteristics of the bsAb to tumor cells that co-express HER2 and CD63. The resulting bsHER2xCD63$_{his}$ demonstrated binding and lysosomal accumulation into HER2-positive tumor cells, but not CD63-positive granulocytes or thrombocytes.

By conjugating bsHER2xCD63$_{his}$ with Duostatin-3, we were able to generate an ADC that induced *in vitro* and *in vivo* cytotoxicity of HER2-positive tumor cells. While treatment with monovalent CD63 and HER2 ADCs had no effect on growth of SK-OV-3 tumors *in vivo*, bsHER2xCD63$_{his}$-ADC showed clear inhibition of tumor growth. This demonstrates that a bispecific Fab-arm recognizing an antigen involved in intracellular trafficking can be used in combination with a tumor-specific Fab-arm, to facilitate intracellular delivery of ADCs.

The use of bispecific antibodies to improve efficacy of ADCs has been investigated by others previously. However by recognizing two separate tumor-specific targets, these bispecific ADCs were designed to target tumors with heterogeneous target expression. Thus, the ADCs would be able to recognize and kill tumors that express either one of the tumor targets, or both, broadening anti-tumor activity and reducing escape from therapy. A bispecific fusion protein targeting epithelial cell adhesion molecule (EpCAM) and CD133 was investigated in preclinical studies to deliver a bacterial toxin to EpCAM-positive tumor cells as well as cancer stem cells expressing CD133 [25]. Similarly, a fusion protein targeting the EGF receptor and the urokinase receptor (uPAR) was used to target tumor cells through EGFR and tumor stroma through uPAR [26]. While DT2219, a bispecific recombinant immunotoxin targeting CD19 and CD22 positive B-cell tumors, demonstrated broader reactivity against B-cell malignancies as compared to individual immunotoxins targeting CD19 or CD22 alone [27,28].

Our bsHER2xCD63$_{his}$-ADC has a different mechanism of action and can only induce efficient cytotoxicity when both antigens are expressed on the same cell. However this approach can be applied to tumor antigens with poor or suboptimal internalization, thereby strongly expanding the number of tumor antigens that could be targeted by an ADC. For HER2, an antigen that only shows Ab induced downmodulation at high expression levels, bsHER2xCD63$_{his}$ was able to induce downmodulation of HER2 even on low HER2-expressing cell lines. This suggests that this approach may

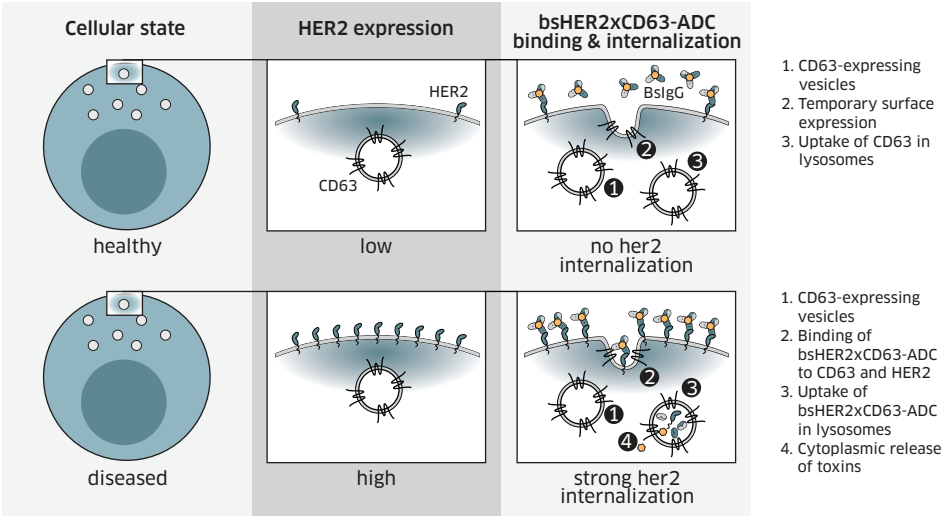

FIGURE 8 *Proposed model of the mechanism of action of bsHER2xCD63$_{his}$-ADC on healthy and diseased cells.*

also be applicable to cell lines expressing low copy numbers of the targeted tumor antigen. However, exposure of Colo205 cells to bsHER2xCD63-ADC did not result in substantial cytotoxicity despite down modulation of HER2 on these cells. This may in part be due to the low drug-to-antibody ratio (DAR) of our ADCs. Tubulin inhibitor conjugated antibodies usually contain on average 3-4 drug molecules per antibody [29], while our ADCs had a DAR of one. Increasing the DAR of bsHER2xCD63-ADC may therefore result in further improving the cytotoxicity so that also low HER2-expressing tumor cells can be killed. However, as more potent ADCs might also affect normal cells expression low levels of HER2, the decreased therapeutic window of such constructs should be carefully considered.

Another explanation for the lack of efficacy against low HER2-expressing tumors may be related to the mechanism of action of bsHER2xCD63$_{his}$-ADC. The affinity of the CD63-specific Fab-arm was reduced to prevent uptake of bsHER2xCD63$_{his}$-ADC by healthy tissues that express CD63 [10,18]. On tumor cell lines that also expressed high numbers of HER2 molecules, CD63 binding was restored. We hypothesize that on these cells, bsHER2xCD63$_{his}$-ADC first bound to HER2, resulting in high density of bsHER2xCD63$_{his}$-ADC on the plasma membrane (Figure 8). This enabled bsHER2x-CD63$_{his}$-ADC to bind to CD63 once it shuttles to the plasma membrane. On cell lines with low HER2 expression, the likelihood that HER2 and CD63 binding occurs simultaneously is probably lower, because the proximity between both receptors

is decreased. As a consequence bsHER2xCD63$_{his}$-ADC can no longer bind to both HER2 and CD63. There are no reports describing complex formation between HER2 and CD63. While CD63 expression at the plasma membrane has been described to concentrate to tetraspanin-enriched microdomains [30], HER2 has been described to localize to lipid rafts [31]. A proteomics approach used to identify proteins in lipid rafts did not reveal any tetraspanins amongst the 241 identified proteins [32]. Thus at low copy number both receptors may very well be expressed in different microdomains at the cell surface. Selection of tumor-specific antigens that are known to interact with CD63 may improve bivalent binding of bsADC at low copy numbers. For example, CD63 has been described to interact with other tetraspanins (CD81, CD82, CD9 and CD151), integrins, MHCII, CXCR4, TM4SF5, syntenin-1, TIMP-1, H, K-ATPase and MT1-MMP [10]. Furthermore, antigens that are highly overexpressed, but lack lysosomal transport, may also represent attractive candidates. Glycosylphosphatidylinositol (GPI) anchored proteins [3,33], adhesion molecules [6] and integrins [7] often recycle back to the plasma membrane after endocytosis, with only a minor fraction being targeted for lysosomal degradation. Using HER2 as a model antigen we have demonstrated that such antigens can be redirected for lysosomal degradation by a bsAb that also targets an antigen that is involved in intracellular trafficking CD63. Hence these antigens may represent attractive targets for the development of a bsADC that combines tumor-specific targeting with enhanced lysosomal delivery through CD63.

Acknowledgements
We would like to thank Ester van 't Veld for technical support.

REFERENCE LIST

1 Burris HA: Developments in the use of antibody-drug conjugates. *Am Soc Clin Oncol Educ Book* 2013.

2 Perez HL, Cardarelli PM, Deshpande S, Gangwar S, Schroeder GM, Vite GD, Borzilleri RM: Antibody-drug conjugates: current status and future directions. *Drug Discov Today* 2014, 19(7):869-881.

3 Dautry-Varsat A, Ciechanover A, Lodish HF: pH and the recycling of transferrin during receptor-mediated endocytosis. *Proc Natl Acad Sci U S A* 1983, 80(8):2258-2262.

4 Harari D, Yarden Y: Molecular mechanisms underlying ErbB2/HER2 action in breast cancer. *Oncogene* 2000, 19(53):6102-6114.

5 Baulida J, Kraus MH, Alimandi M, Di Fiore PP, Carpenter G: All ErbB receptors other than the epidermal growth factor receptor are endocytosis impaired. *J Biol Chem* 1996, 271(9):5251-5257.

6 Kamiguchi H, Lemmon V: Recycling of the cell adhesion molecule L1 in axonal growth cones. *J Neurosci* 2000, 20(10):3676-3686.

7 Pellinen T, Ivaska J: Integrin traffic. *J Cell Sci* 2006, 119(Pt 18):3723-3731.

8 de Goeij BE, Satijn D, Freitag CM, Wubbolts R, Bleeker WK, Khasanov A, Zhu T, Chen G, Miao D, van Berkel PH *et al*: High turnover of Tissue Factor enables efficient intracellular delivery of antibody-drug conjugates. *Mol Cancer Ther* 2015.

9 Labrijn AF, Meesters JI, de Goeij BE, van den Bremer ET, Neijssen J, van Kampen MD, Strumane K, Verploegen S, Kundu A, Gramer MJ *et al*: Efficient generation of stable bispecific IgG1 by controlled Fab-arm exchange. *Proc Natl Acad Sci U S A* 2013, 110(13):5145-5150.

10 Pols MS, Klumperman J: Trafficking and function of the tetraspanin CD63. *Exp Cell Res* 2009, 315(9):1584-1592.

11 Duffield A, Kamsteeg EJ, Brown AN, Pagel P, Caplan MJ: The tetraspanin CD63 enhances the internalization of the H,K-ATPase beta-subunit. *Proc Natl Acad Sci U S A* 2003, 100(26):15560-15565.

12 Takino T, Miyamori H, Kawaguchi N, Uekita T, Seiki M, Sato H: Tetraspanin CD63 promotes targeting and lysosomal proteolysis of membrane-type 1 matrix metalloproteinase. *Biochem Biophys Res Commun* 2003, 304(1):160-166.

13 Tugues S, Honjo S, Konig C, Padhan N, Kroon J, Gualandi L, Li X, Barkefors I, Thijssen VL, Griffioen AW *et al*: Tetraspanin CD63 promotes vascular endothelial growth factor receptor 2-beta1 integrin complex formation, thereby regulating activation and downstream signaling in endothelial cells *in vitro* and *in vivo*. *J Biol Chem* 2013, 288(26):19060-19071.

14 Janvier K, Bonifacino JS: Role of the endocytic machinery in the sorting of lysosome-associated membrane proteins. *Mol Biol Cell* 2005, 16(9):4231-4242.

15 Jelovac D, Emens LA: HER2-directed therapy for metastatic breast cancer. *Oncology (Williston Park)* 2013, 27(3):166-175.

16 de Goeij BE, Peipp M, de Haij S, van den Brink EN, Kellner C, Riedl T, de Jong R, Vink T, Strumane K, Bleeker WK *et al*: HER2 monoclonal antibodies that do not interfere with receptor heterodimerization-mediated signaling induce effective internalization and represent valuable components for rational antibody-drug conjugate design. *MAbs* 2014, 6(2):392-402.

17 Albanell J, Codony J, Rovira A, Mellado B, Gascon P: Mechanism of action of anti-HER2 monoclonal antibodies: scientific update on trastuzumab and 2C4. *Adv Exp Med Biol* 2003, 532:253-268.

18 Metzelaar MJ, Schuurman HJ, Heijnen HF, Sixma JJ, Nieuwenhuis HK: Biochemical and immunohistochemical characteristics of CD62 and CD63 monoclonal antibodies. Expression of GMP-140 and LIMP-CD63 (CD63 antigen) in human lymphoid tissues. *Virchows Arch B Cell Pathol Incl Mol Pathol* 1991, 61(4):269-277.

19 Vink T, Oudshoorn-Dickmann M, Roza M, Reitsma JJ, de Jong RN: A simple, robust and highly efficient transient expression system for producing antibodies. *Methods* 2014, 65(1):5-10.

20 Labrijn AF, Meesters JI, Priem P, de Jong RN, van den Bremer ET, van Kampen MD, Gerritsen AF, Schuurman J, Parren PW: Controlled Fab-arm exchange for the generation of stable bispecific IgG1. *Nat Protoc* 2014, 9(10):2450-2463.

21 Parren PW, Ditzel HJ, Gulizia RJ, Binley JM, Barbas CF, 3rd, Burton DR, Mosier DE: Protection against HIV-1 infection in hu-PBL-SCID mice by passive immunization with a neutralizing human monoclonal antibody against the gp120 CD4-binding site. *AIDS* 1995, 9(6):F1-6.

22 Igawa T, Ishii S, Tachibana T, Maeda A, Higuchi Y, Shimaoka S, Moriyama C, Watanabe T, Takubo R, Doi Y *et al*: Antibody recycling by engineered pH-dependent antigen binding improves the duration of antigen neutralization. *Nat Biotechnol* 2010, 28(11):1203-1207.

23 Chaparro-Riggers J, Liang H, DeVay RM, Bai L, Sutton JE, Chen W, Geng T, Lindquist K, Casas MG, Boustany LM *et al*: Increasing serum half-life and extending cholesterol lowering *in vivo* by engineering antibody with pH-sensitive binding to PCSK9. *J Biol Chem* 2012, 287(14):11090-11097.

24 Doronina SO, Toki BE, Torgov MY, Mendelsohn BA, Cerveny CG, Chace DF, DeBlanc RL, Gearing RP, Bovee TD, Siegall CB *et al*: Development of potent monoclonal antibody auristatin conjugates for cancer therapy. *Nat Biotechnol* 2003, 21(7):778-784.

25 Waldron NN, Barsky SH, Dougherty PR, Vallera DA: A bispecific EpCAM/CD133-targeted toxin is effective against carcinoma. *Target Oncol* 2014, 9(3):239-249.

26 Oh S, Tsai AK, Ohlfest JR, Panoskaltsis-Mortari A, Vallera DA: Evaluation of a bispecific biological drug designed to simultaneously target glioblastoma and its neovasculature in the brain. *J Neurosurg* 2011, 114(6):1662-1671.

27 Vallera DA, Oh S, Chen H, Shu Y, Frankel AE: Bioengineering a unique deimmunized bispecific targeted toxin that simultaneously recognizes human CD22 and CD19 receptors in a mouse model of B-cell metastases. *Mol Cancer Ther* 2010, 9(6):1872-1883.

28 Bachanova V, Frankel AE, Cao Q, Lewis D, Grzywacz B, Verneris MR, Ustun C, Lazaryan A, McClune B, Warlick ED *et al*: Phase I Study of a Bispecific Ligand-Directed Toxin Targeting CD22 and CD19 (DT2219) for Refractory B-cell Malignancies. *Clin Cancer Res* 2015, 21(6):1267-1272.

29 Lewis Phillips GD, Li G, Dugger DL, Crocker LM, Parsons KL, Mai E, Blattler WA, Lambert JM, Chari RV, Lutz RJ *et al*: Targeting HER2-positive breast cancer with trastuzumab-DM1, an antibody-cytotoxic drug conjugate. *Cancer Res* 2008, 68(22):9280-9290.

30 Nydegger S, Khurana S, Krementsov DN, Foti M, Thali M: Mapping of tetraspanin-enriched microdomains that can function as gateways for HIV-1. *J Cell Biol* 2006, 173(5):795-807.

31 Nagy P, Vereb G, Sebestyen Z, Horvath G, Lockett SJ, Damjanovich S, Park JW, Jovin TM, Szollosi J: Lipid rafts and the local density of ErbB proteins influence the biological role of homo- and heteroassociations of ErbB2. *J Cell Sci* 2002, 115(Pt 22):4251-4262.

32 Foster LJ, De Hoog CL, Mann M: Unbiased quantitative proteomics of lipid rafts reveals high specificity for signaling factors. *Proc Natl Acad Sci U S A* 2003, 100(10):5813-5818.

33 Gamage DG, Hendrickson TL: GPI transamidase and GPI anchored proteins: oncogenes and biomarkers for cancer. *Crit Rev Biochem Mol Biol* 2013, 48(5):446-464.

SUPPLEMENTAL FIGURES

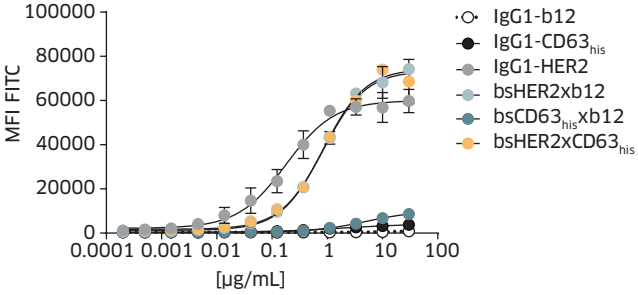

SUPPLEMENTARY FIGURE S1 *Binding of bsHER2xCD63$_{his}$ to SK-OV-3 cells as assessed by flow cytometry.* SK-OV-3 cells were incubated with serially diluted antibodies followed by incubation with goat anti-human IgG1-FITC to detect binding. Mean fluorescence intensities of FITC are depicted in relation to the antibody concentration. Data shown are mean ± standard deviation of 2 experiments.

8 General discussion

Owing to improved conjugation technologies and appropriate targeting, the clinical landscape of ADCs is rapidly expanding. Over 50 ADCs are in the clinic and many more are in preclinical development. To ensure the clinical success of ADCs it is important to find the right combination of tumor antigen, targeting antibody, conjugation linker and cytotoxic drug. The aim of this thesis was to improve our understanding of antibody - antigen requirements that are needed for the development of safe and effective ADC treatments. For the first generation of ADCs that were generated, the antibody selection criteria focused on differential antibody binding to tumor cells relative to normal tissue [1,2]. However it was soon appreciated that certain antibody-drug conjugates require internalization and lysosomal processing to be effective [3]. The first clinically approved ADC gemtuzumab ozogamycin (Mylotarg), made use of a CD33-specific hinge-stabilized IgG4 antibody (hP67.6) that, by itself, did not induce cytotoxicity, ADCC or CDC [4]. The antigen was selected based on its expression on acute myeloid leukemia (AML) cells and lack of expression outside the myeloid cell lineages and pluripotent stem cells, while the antibody showed to be rapidly internalized upon target binding [5]. Thus antigen and antibody selection were driven by criteria needed for the development of an ADC. However this was not always the case. Brentuximab vedotin (Adcetris) was generated by conjugating the CD30 antibody cAC10 with MMAE. This antibody was selected because it was able to inhibit proliferation and induce apoptosis of Hodgkin lymphoma cells [6]. Unfortunately the unconjugated antibody showed minimal clinical activity, which spurred efforts to enhance antitumor activity through the development of an ADC [7]. Likewise, trastuzumab was conjugated with maytansin to overcome resistance to treatment with the unconjugated antibody [8] and the PSMA antibody huJ591 (a humanized version of MLN591) was selected for development of MLN2704-ADC, because huJ591 was clinically validated [9,10]. Previously existing monoclonal antibodies were therefore used for the development of these ADCs. This approach had the following advantages (A) lower cost of development (Ab production and screening were no longer needed and production cell lines potentially were already available); (B) shorter development time lines; (C) reduced clinical safety risk (Ab pharmacokinetics, biodistribution and potential antibody-dependent adverse effects were known); (D) it potentially allowed for combining cytotoxic effects of payload delivery with optimal inhibition of receptor signaling or engagement of immune effector mechanisms. Nevertheless, such repurposing of unconjugated antibodies for an ADC approach has the disadvantage that internalization was not always included as a criterion in the selection of the mAb. Using the α-kappa-ETA' assay, we found that HER2 antibodies that bind different HER2 domains differ in their capacity to deliver α-kappa-ETA' to tumor cells. HER2 Abs that did not interfere with receptor heterodimerization and did not inhibit tumor growth, induced the highest amount of cytotoxicity in the α-kappa-ETA' assay [11] (**chapter 5**). Others have also demonstrated that screening for internalizing HER2 antibodies results in selection of clones that recognize distinctive non-overlapping epitopes in comparison to trastuzumab [12,13].

Thus combining antagonistic antibodies with cytotoxic payloads may not always result in the most optimal payload delivery. Furthermore, to completely block receptor signaling *in vivo*, target binding should be saturated, which may require relatively high dosing of unconjugated antibodies *in vivo* [14]. ADCs usually have a lower maximum tolerated dose (MTD) compared to unconjugated antibodies, which could result in lower dosing of ADCs and limit their ability to saturate target binding and induce antagonism. This would make selection of tumor inhibitory antibodies even less critical. That noted, however, dosing regimens of trastuzumab (4 mg/kg followed by a weekly maintenance dose of 2 mg/kg [15]) and trastuzumab emtansine (Kadcyla) (3.6 mg/kg every three weeks [16]) are not that different.

ANTIBODY SELECTION

The importance of proper antibody selection for ADC development was also demonstrated for other antigens than HER2. Studies with the CD22 expressing Burkit lymphoma cell line BJAB have demonstrated that large differences in anti-tumor efficacy between different CD22 antibodies conjugated with MCC-DM1 may occur [17]. In addition, inotuzumab ozogamicin, a calicheamicin-conjugated CD22 ADC, was generated through conjugation of mAb G5/44 that was selected because of its high endocytosis capacity [18]. Likewise antibodies targeting different epitopes on neural cell adhesion molecule (NCAM) [19], mucin-1 [20] and TF [21,22] showed differential capacity to induce endocytosis.

For TF-specific antibodies, bivalent antibody binding seemed more critical for antibody internalization than Ab affinity. This was demonstrated by clones TF-011 and TF-098, which differed ~100-fold in TF binding affinity but showed comparable internalization, while internalization of Fab fragments of TF-011 was clearly less efficient [21,22] (**Chapter 3**). Similar results were found for HER2 clone 153, which could downmodulate HER2 as bivalent IgG1, but not as monovalent IgG1 (**Chapter 7**). Another study, comparing bivalent and monovalent HER2-ADCs demonstrated a 100-fold greater cytotoxicity of IgG1-HER2-mcMMAF compared to Fab-HER2-mcMMAF [23]. Studies with Fab fragments of the EGFR antibody cetuximab also demonstrated that antibody-induced crosslinking was required to induce significant endocytosis of EGFR [24,25]. This demonstrates that the choice of ADC format can have significant impact on the rate of endocytosis.

Similar to ADCs, immunotoxins are designed to facilitate delivery of toxic payloads to tumor cells. Immunotoxins are typically composed of single-chain variable fragments (scFv) fused to bacterial toxins. They have entered clinical testing more than two decades ago, but toxicity at low dosing and strong immunogenicity have hampered the approval of immunotoxins as anti-cancer agents. Moreover unlike ADCs,

immunotoxins lack the capacity to crosslink their targeted antigen, which may limit their efficacy. Nevertheless, monovalent immunotoxins targeting EGFR and HER2 have demonstrated effective delivery of their cytotoxic payload to tumor cells [26,27]. This may seem contradictory with our observation that Fab fragments of TF-011 and HER2-153 were not internalized [22]. However, although Fab fragments of TF-011 and HER2-153 cannot increase endocytosis of TF and HER2 respectively, endocytosis of Fab fragments can still take place through piggybacking with the regular turnover of the targeted antigen.

Indeed, some receptors do not require Ab induced crosslinking for maximal payload delivery. Studies comparing internalization of IgG1 and Fab fragments directed against CD73, demonstrated that mAb IgG1-AD2 caused CD73 to cluster and internalize. This effect was also observed with Fab fragments of AD2, but not with another IgG1-CD73 mAb recognizing a distinct epitope [28]. Likewise, studies comparing efficacy of Ricin A-conjugated anti-CD22 IgG1 and Fab fragments demonstrated that cytotoxicity was mostly dependent on the antibody epitopes recognized and not so much on the antibody format used. IgG1 and Fab fragments induced similar cytotoxicity with only a difference in IC_{50} value that correlated with loss of avidity for the Fab fragments [29,30]. One could hypothesize that for such antigens a monovalent ADC may be more effective compared to a bivalent ADC (assuming that drug-to-antibody ratios are equal), because a bivalent ADC may occupy two binding sites and thus two antigens, whereas a monovalent ADC can only bind one antigen. Thus for antigens that are not dependent on bivalent antibody binding for Ab-induced internalization, the same amount of antigen may internalize two times more monovalent ADCs as compared to bivalent ADCs.

In summary, selection of antibodies that recognize distinctive epitopes or have the ability to crosslink their antigen may affect the redistribution of Ab/antigen complexes from the plasma membrane into intracellular compartments. Depending on the internalization characteristics of the targeted antigen, different antibody formats may be preferred.

ANTIGEN SELECTION

Ideally a successful ADC should target an antigen that is exclusively and homogenously expressed on tumor cells, present at high copy numbers on the plasma membrane and well internalized and targeted to the lysosomes following antibody binding. Unfortunately these requirements are rarely met in a single antigen. Most tumor antigens are also expressed to some extent on healthy tissues, tumor expression is often heterogeneous between and within tumors, and internalization and lysosomal targeting are relatively inefficient. Luckily the rapid ADC developments help us to

redefine these parameters. Tumor specificity for example, although preferred, is not an absolute requirement for ADC development. Firstly, potential toxicity to normal cells is affected by the nature of the payload selected. Tubulin targeting agents are only effective against proliferating cells, thus some expression of the targeted antigen on healthy tissue that is non-dividing can be tolerated when using these agents. Secondly, antigens may not always be accessible for antibodies. Either because the organ or tissue in which it is expressed is less accessible for antibodies (e.g.; brain [31]), or because the antigen is only present in intracellular compartments (e.g.; TF expression in resting monocytes [32]). Thirdly, many tumor antigens are differentially expressed, with cell surface copy numbers in tumor tissue exceeding those in normal tissue. Thus, by selecting the right mAb-toxin combination some expression in healthy tissues can be tolerated. This was also demonstrated by the approval of trastuzumab emtansine. Expression of HER2 has been described for various healthy organs such as: heart, skin and epithelial cells of the gastrointestinal tracts [33]. However, for trastuzumab emtansine no related toxicity has been reported in these tissues [16]. Also various other ADCs that have progressed to phase II clinical testing, show expression of the targeted antigen in healthy tissue: EGFR (basal layer skin) [34], GPNMB (brain [rats], basal layer skin, bone osteoclasts) [35], CEACAM5 (colon, stomach) [36], TROP2 (skin, pancreas, liver, kidney) [37,38], NaPi2b (liver, lung, breast) [39] and PSMA (endothelium, prostate) [40].

The prerequisite that an ADC target should be well internalized holds true, however, also this parameter is not fixed. The CD30 antibody cAC10 has been demonstrated to internalize into CD30-positive Hodgkin lymphoma cells, but a large part of the antibody is still present on the plasma membrane after 20 hours incubation [41]. Similar results were obtained when HER2 positive breast cancer cells were incubated with radiolabeled ^{125}I-trastuzumab. Antibody internalization was clearly demonstrated, but the majority of ^{125}I-trastuzumab was still present on the cell membrane after 24 hours incubation [42]. Despite the fact that only a portion of these antibodies was internalized, both antibodies demonstrated impressive preclinical and clinical activity when conjugated with cytotoxic payloads [7,16]. This can be explained by the high surface expression of both receptors on tumor cells that compensates for the partial internalization [22,43]. Furthermore the inefficient endocytosis of HER2 may contribute to the tumor specificity of trastuzumab emtansine by sparing healthy tissues that moderately express HER2 [22,44,45]. More recently ADCs targeting the carcinoembryonic antigen-related cell adhesion molecule 5 (CEACAM5) have entered phase II clinical development. This antigen was long considered to be non-internalizing. Later studies have demonstrated that some internalization does occur, presumably through the normal turnover of the cell membrane. Together with the high number of CEACAM5 molecules at the surface of tumor cells this enables sufficient payload delivery to kill the targeted tumor cell [46-48]. Likewise, the B-lymphocyte antigen CD20 that is highly expressed in chronic lymphocytic leukemia can be uti-

lized for an ADC approach, even though it shows moderate internalization [49,50]. Also here the high expression of the targeted antigen made it possible to induce cytotoxicity through vcMMAE-conjugated CD20 antibodies [51].

Thus poorly internalizing tumor antigens can be utilized for an ADC approach provided that they are highly overexpressed (> 10^5 molecules/cell). Our studies comparing EGFR, HER2 and TF as targets for an ADC approach support these findings. We demonstrated that a duostatin-3 conjugated HER2-ADC was only effective against tumor cell lines expressing at least 2 x 10^5 HER2/cell [22] (**chapter 3**). In contrast, TF-011 conjugated with duostatin-3 was already effective against cell lines with ≥2 x 10^4 TF/cell. Confocal experiments revealed that in contrast to HER2-antibodies, virtually all extracellular bound TF-antibodies were transported to lysosomes within 16 hours incubation [22]. Furthermore, high expression of TF was found on a large number of cancer indications, with limited expression on healthy tissues [21]. Hence TF represents an attractive ADC target that combines high expression on tumor cells with strong internalization and lysosomal targeting.

Also for TF some expression has been reported on healthy tissues such as cells in the sub-endothelial vessel wall (e.g. pericytes, smooth muscle cells and fibroblasts) that interact with FVIIa when vascular integrity is disrupted [52]. The subendothelial localization is thought to limit TF exposure to clotting factors present in the blood. Subendothelial TF expression is found in a variety of vital organs, including the brain, heart, intestine, kidney, lung, placenta, uterus and testes However imaging studies in cynomolgus monkeys, that were shown to have TF tissue expression comparable to humans (Genmab, data on file), only revealed minor accumulation of radiolabeled TF-011 in testis of male cynomolgus monkeys. Furthermore, tisotumab vedotin showed an acceptable toxicity profile in cynomolgus monkeys, with a relatively narrow range of findings. When treated with a dose of 3 mg/kg, moderate and reversible neutropenia was observed, in addition to mild and reversible skin and testicular toxicity. No toxicity was observed at a dose of 1 mg/kg tisotumab vedotin. Xenograft studies in mice demonstrated efficacy at doses as low as 0.5 mg/kg of tisotumab vedotin, with tumor regression being observed at doses of 2 and 4 mg/kg [21]. The safety of tisotumab vedotin is currently being tested in a Phase I clinical trial. The dose escalation phase of the study is still ongoing but at the highest dose reported thus far (1.8 mg/kg) the MTD in humans was not yet reached [53]. Usually the MTD of vcMMAE conjugated antibodies does not exceed 2.5 mg/kg (**chapter 2**), indicating that the therapeutic index of tisotumab vedotin is expected to be narrow. Unfortunately this seems to hold true for all ADCs that are currently being tested in the clinic. Therefore approaches to improve the therapeutic index of ADCs seem mandatory (**chapter 2**).

TUMOR PENETRATION

Tumor-specific antigens that are highly over-expressed represent attractive targets for an ADC approach, yet they also pose a challenge. The high expression may create a barrier for antibodies to penetrate deeper into the tumor [54-56]. This so called "binding site barrier" was first described in 1990 [57]. It was hypothesized that mAbs with high affinity for their tumor antigen, stably bind to the first encountered antigen, making transport across the vasculature a considerable barrier. High antigen density and rapid antibody internalization and degradation may further increase the barrier effect. To overcome the impaired tumor penetration of antibodies, one could simply increase the dosage. However, this may also result in accumulation in normal tissues [58]. Especially for ADCs the elevated blood concentration, may result in off-target toxicity before therapeutic efficacy is reached. Consequently, various researchers have demonstrated that reducing the antibody affinity improves tumor penetration [54-56]. However, this may also negatively affect antibody retention in the tumor as well as antibody internalization and degradation [56].

Using immunohistochemistry, we also demonstrated that HER2 is highly and homogeneously expressed in various tumor xenografts (Figure 1A). Similarly, in human tumor biopsies, over 75% of the cells that stained positive for cytokeratin, a marker for human epithelial cells, also stained positive for HER2, which was determined with the Herceptest [59]. This homogeneous staining pattern was also observed for tumor xenografts with lower HER2 expression, such as NCI-H441. To examine whether the high and homogeneous expression of HER2 poses a binding site barrier, mice bearing SKOV3 tumor xenografts were treated with 3 and 30 mg/kg trastuzumab. After two days, tumors were harvested and stained with rabbit anti-human IgG to detect trastuzumab. Figure 1B shows a homogeneous staining pattern for tumors treated with 30 mg/kg trastuzumab. However when tumors were treated with 3 mg/kg trastuzumab, antibody staining was restricted to tumor cells surrounding the blood vessels. This clearly demonstrates that tumor penetration of HER2 antibodies can be hampered by a binding site barrier. This may limit the potency of HER2-specific ADCs, such as T-DM1 which is dosed at 3.6 mg/kg [16], a dose that may not be sufficient to overcome this barrier. Therefore approaches to improve tumor penetration of ADCs or their cytotoxic payloads may improve anti-tumor efficacy. One such method is the selection of linker-drugs that have bystander activity, which was successfully demonstrated for TF-011-MMAE [21], or by selecting more potent linker drugs that require a more limited accumulation in tumor cells to induce cytotoxicity.

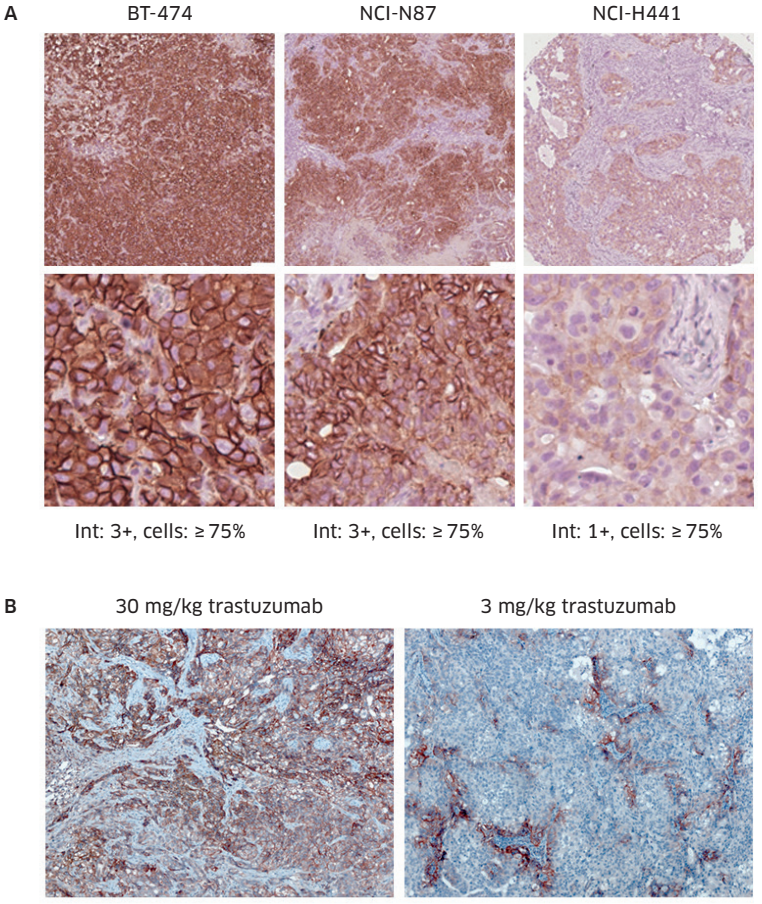

FIGURE 1 *HER2 binding site barrier.* **(A)** BT-474, NCI-N87 and NCI-H441 tumor xenograft biopsies were stained for HER2 using the Herceptest (DAKO). Staining intensities and percentage positive cells is depicted for representative images. **(B)** SKOV3 tumor xenografts treated with 3 and 30 mg/kg trastuzumab were excised and stained with anti-hu-IgG to detect trastuzumab.

CYTOTOXIC PAYLOAD

The development of novel payloads may help to improve the therapeutic index of ADCs. Currently there are two main classes of ADC payloads; the tubulin targeting agents (maytansin, auristatin and tubulysin) and the DNA-damaging agents (calicheamicin, duocarmycin, pyrrolobenzodiazepine (PBD), doxorubicin and SN-38) (Table 1). The tubulin targeting agents are most abundantly used and are available as the auristatin-derivatives MMAE and MMAF and the maytansine-derivatives DM1 and DM4. Their mitotic spindle inhibition primarily affects proliferating cells, which makes tubulin-targeting agents generally less toxic than DNA damaging agents, that also act on non-proliferating cells. From a tumor killing perspective this has the drawback that tubulin targeting agents do not target non-proliferating tumor cells. Furthermore tubulin-targeting agents are usually substrates for multidrug resistance (MDR) pumps [60,61]. The latter can be avoided by using different conjugation linkers that, after intracellular processing, give rise to slightly different metabolites which are less susceptible to MDR pumps [61]. In general tubulin targeting agents are used for development of ADCs that target tumor-enriched antigens with some expression on healthy tissues.

DNA-targeting agents have a broader spectrum of efficacy, ranging from highly potent DNA minor groove binders calicheamicin, duocarmycin and PBD dimers, to the less potent topoisomerase inhibitors SN-38 (active form of irinotecan [62]) and doxorubicin. Up to now, the DNA minor groove binders have been employed for ADCs directed against hematological tumors that are easily accessible and show limited expression on healthy tissue. In addition, a calicheamicin-conjugated EphrinA ADC (PF-06647263) has recently entered clinical development [63]. This antigen was selected because of its selective overexpression on cancer stem cells (CSC). The relative low proliferation rate and the high expression of drug efflux mechanisms on CSC set hurdles for tubulin targeting agents. This can be overcome by using DNA damaging agents such as duocarmycin and PBD dimers that have demonstrated efficacy against multidrug resistant cell lines [62,64]. Calicheamicins are generally less active in cells expressing the multidrug resistance phenotype [65], but this can be overcome by selecting different linkers [66], though it is not clear whether such linker design was used here [63].

Payload	Linker	Mechanism of action	Phase	Effective against non-dividing cells	Bystander activity
monomethyl auristatin E (MMAE), vedotin	valine citrulline (vc)	Blocks tubulin polymerization by binding vinca binding domain of α-tubulin	approved	No	Yes
Maytansine (DM1), emtansine	succinimidyl *trans*-4-(*N*- maleimidylmethyl) cyclohexane-1-carboxylate (SMCC)	Blocks tubulin polymerization by binding near vinca binding domain of tubulin	approved	No	No
Calicheamicin, ozogamicin	acetyl butyrate (AcBu)	DNA-alkylating agent (binds in the minor groove)	3	Yes	Yes
monomethyl auristatin F (MMAF), mafodotin	maleimidocaproyl (MC)	Blocks tubulin polymerization by binding vinca binding domain of α-tubulin	2	No	No
Maytansine (DM4), ravtansine	N-succinimidyl-4-(2-pyridyldithio)butanoic acid maytansine (SPDB)	Blocks tubulin polymerization by binding near vinca binding domain of tubulin	2	No	Yes
SN-38, govitecan	CL2A (pH sensitive linker)	Irinotecan metabolite that inhibits topoisomerase I	2	Yes	Yes
Doxorubicin	hydrazone (pH sensitive linker)	Topoisomerase II inhibitor	1, 2	Yes	Yes
D6.5 (PBD)	dipeptide	DNA targeting agent	1, 2	Yes	Yes
Tubulysin B hydrazide (TubBH)	enzyme cleavable linker	Blocks tubulin polymerization by binding peptide binding domain of tubulin	1	No	Yes
Duocarmycin	valine citrulline (vc)	DNA-alkylating agent (binds in the minor groove)	1	Yes	Yes
pyrollobenzodiazepine dimers (PBD)	valine citrulline (vc)	Cross-linking of opposing DNA strands	1	Yes	Yes
α-Amanitin	?	RNA polymerase II inhibitor	0	Yes	No
PNU-159682	valine citrulline (vc)	Nemorubicin metabolite that inhibits topoisomerase I	0	Yes	unknown
Duostatin-3	valine citrulline (vc)	Tubulin targeting agent	0	No	No

TABLE 1 *Overview of different linker-drugs used for ADC development.*

The choice of linker can also impact the bystander kill activity of ADCs. Bystander cytotoxicity occurs when the cytotoxic payload is released from the ADC by antigen positive tumor cells, after which it can diffuse into neighboring, potentially target-negative, tumor cells and induce cytotoxicity. This can be convenient when targeting solid tumors with heterogeneous antigen expression but it also has the potential to harm normal cells. Cytotoxic payloads like MMAE, DM1, DM4, duocarmycin and PBDs are highly membrane permeable and have the intrinsic capacity to diffuse into other nearby tumor cells to induce bystander kill [22,67-69]. However, the bystander capacity of ADCs can be manipulated by carefully selecting the combination of the cytotoxic payload and the linker (linker-drug combination). Studies comparing efficacy of DM1-conjugated CanAg-ADCs demonstrated that the use of a non-cleavable linker (SMCC) prevents bystander kill induced by anti-CanAg-SMCC-DM1, presumably because the DM1 metabolite that is released after intracellular processing of the ADC is less permeable [68]. Alternatively, the membrane permeability of the payload itself can be modified. This was demonstrated for the auristatin analog MMAF, which is negatively charged preventing uptake of the unconjugated toxin by healthy cells [21]. Similar to this, the tubulin targeting agent duostatin3, that was used in our preclinical studies, lacks the ability to induce bystander killing, but was highly active against antigen positive tumor cells [22].

For the development of TF-011-MMAE, a tubulin targeting agent was preferred over a DNA damaging agent because TF expression was not limited to tumor cells. For example, expression of TF was found on sub-endothelial cells surrounding the blood vessels and on mature keratinocytes in the skin. These cells are generally slow or non-proliferating which makes them less sensitive to treatment with the tubulin targeting agents. We also compared efficacy between vcMMAE and mcMMAF conjugates of TF-011. The linker-drug combinations were equally effective *in vitro*, however TF-011-vcMMAE outperformed TF-011-mcMMAF *in vivo*. We believe this can be attributed to the heterogeneous expression of TF *in vivo*, which was counteracted by the bystander activity of TF-011-MMAE. Similar to our observations in xenograft models, TF expression appears to be heterogeneous in human cancer, thus, a linker-drug combination with bystander activity was selected for our TF-specific ADC.

TOXICITY

The selection of a linker-drug combination with bystander activity has the potential downside of inducing bystander damage to healthy tissues. Clinical studies with bivatuzumab mertansine, a CD44v6 antibody conjugated through a cleavable disulfide linker with DM1, demonstrated skin toxicity. These skin reactions were generally reversible but because of a fatal skin toxicity (epidermal necrolysis), clinical development of bivatuzumab mertansine was halted [70]. It was demonstrated that

keratinocytes, which reside in the basal layer of the skin, had high expression of CD44v6. These cells are not dividing, however they are in close proximity to highly proliferating epidermal stem cells that reside in the lower part of the epidermis. Unlike trastuzumab-emtansine which was conjugated through a non-cleavable SMCC linker, bivatuzumab mertansine has the potential to induce bystander kill. Therefore DM1 released by CD44v6 positive keratinocytes may have leaked into nearby epidermal stem cells causing damage to these highly proliferating cells. In nonclinical toxicity studies with tisotumab vedotin, reversible skin toxicity was observed. Although TF was not expressed by proliferating cells in the basal layer of the skin, these cells may be exposed to MMAE through release of free MMAE by TF-positive mature keratinocytes.

For most ADCs currently in clinical development, dose-limiting toxicities such as neutropenia are described as unrelated to the targeted antigen (**chapter 2**). However it can not be excluded that these toxicities partly arise from a bystander effect induced by targeting antigen-positive tumor cells. Various ADCs targeting hematological malignancies such as brentuximab vedotin, inotuzumab ozogamicin, gemtuzumab ozogamicin, polatuzumab vedotin and coltuximab ravtansin have been reported to induce neutropenia and thrombocytopenia. These ADCs also have the ability to induce bystander killing. Thus bystander activity in the bone marrow where both tumor cells and myeloid progenitor cells are present may contribute to these observed toxicities. However similar dosing of ADCs that did not target tumor cells located in the bone marrow also induced neutropenia and thrombocytopenia (i.e. trastuzumab emtansine, glembatumumab vedotin, indusatumab vedotin and DMUC5754A). This may come from toxicity of the free payload released by ADCs processed elsewhere in the body. Although these toxins are usually hydrophobic and are easily absorbed by the nearest cell, which would limit localization to the bone marrow, free MMAE can be measured in plasma from patients treated with ADC, peaking 2-3 days after dosing [71]. On the other hand, trastuzumab emtansine does not have bystander activity and needs to be absorbed by the cell to induce toxicity. FcγRIIa binding has been described to facilitate "unspecific" uptake of trastuzumab emtansine by megakaryocytes, ultimately leading to intracellular concentrations of ADC that are above the threshold for cytotoxicity [72]. The affinity of FcγRIIa for monovalent IgG is very low (>10^{-7} M), and requires extremely high IgG concentrations for FcR-mediated binding to take place. However the leaky vasculature of the bone marrow (and also spleen) may result in high local concentrations of ADC that might enable antigen independent uptake mechanisms via Fc-receptors or pinocytosis.

Alternatively, toxicity may be the result of circulating ADC-containing immune complexes, that can be rapidly cleared through FcR binding [73]. The conjugation of antibodies with small molecule payloads creates a hapten-like structure. When administered by itself, the small molecule payload does not induce immunogenicity, but

conjugated to a carrier (antibody) these structures may show increased immunogenicity, resulting in the production of anti-payload antibodies. These antibodies may bind to circulating ADCs, resulting in the formation of immune complexes, especially for ADCs conjugated with high DAR's. These immune complexes can be cleared by macrophages in the liver, spleen, but also the bone marrow, which may expose myeloid progenitor cells to the toxic payload. A study comparing biodistribution and pharmacokinetics of an anti-Lewis Y antibody and ADC in cancer patients, showed increased uptake of the ADC in the liver. Furthermore the ADC was rapidly cleared from the bloodstream and showed less uptake in the tumor as compared to the naked antibody [74]. However, anti-drug antibodies or immune complexes were not detected.

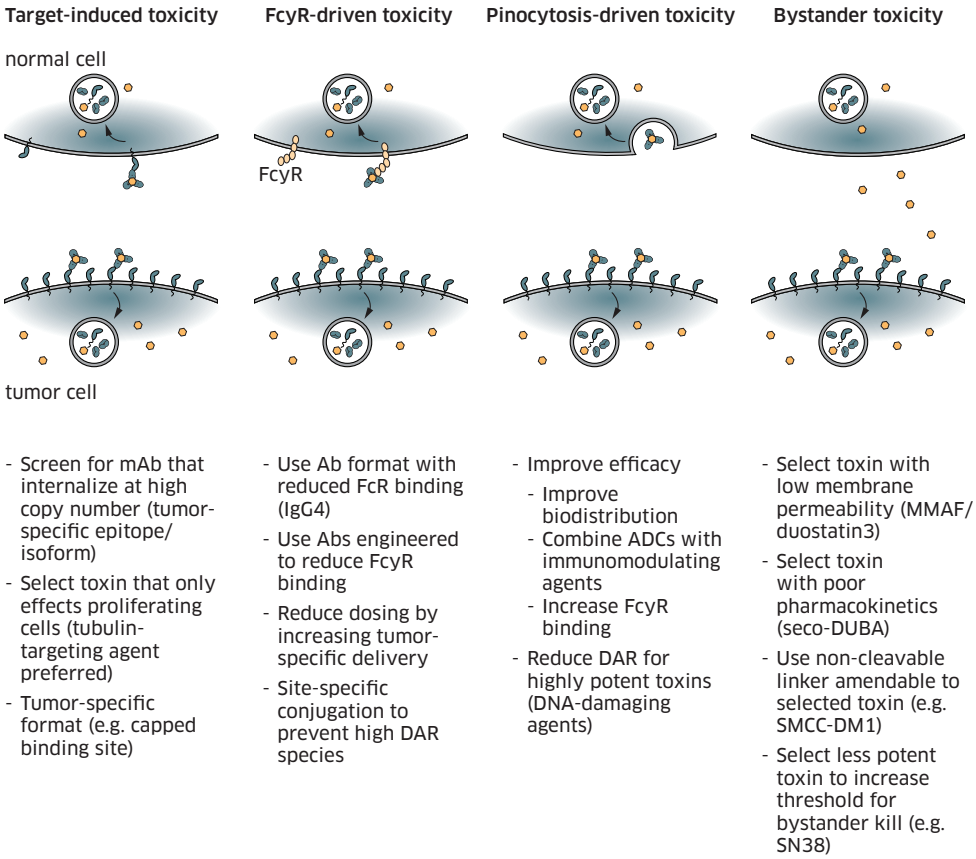

FIGURE 2 *Overview of potential mechanism of toxicity induced by ADCs and strategies to minimize these toxic effects.*

Although the mechanism behind the toxicity of ADCs remains poorly understood, strategies to improve tumor specificity, control bystander activity or prevent uptake by FcR expressing cells may help to improve the therapeutic window of ADCs (Figure 2). Alternatively improvements in linker stability, DAR and the site of conjugation have been proposed to reduce systemic toxicity of ADCs.

NOVEL FORMATS

The use of novel antibody platforms may help to improve the efficacy of ADCs. We have used bsAb technology to improve internalization and lysosomal targeting of poorly internalizing tumor antigens. The bsAb made use of a binding arm directed against the lysosomal membrane protein CD63, to facilitate internalization and lysosomal transport of a second binding arm directed against the model antigen HER2. The resulting bsHER2xCD63 demonstrated efficient internalization, lysosomal targeting and toxin mediated killing of HER2-positive tumor cells, which was not observed with control ADCs only targeting either HER2 or CD63 (**chapter 7**). Although not yet demonstrated, this approach has the potential to improve payload delivery of various poorly internalizing tumor antigens, thereby broadening the number of suitable ADC targets. Tumor antigens that are considered non- or poorly internalizing can only be utilized for an ADC approach when they are highly over-expressed. Using the bsAb approach, these tumor antigens may already be internalized at lower copy number which may increase the number of patients eligible to ADC treatment.

Internalization of mAb/receptor complexes can also be increased by using a bsAb that targets two different epitopes on the same antigen [75]. This was demonstrated through generation of a bsAb that binds two non-overlapping epitopes on HER2, represented by mAbs 153 and 169 (bsAb-$HER2_{153}$xHER_{169}) [11]. The bsAb-$HER2_{153}$x-HER_{169} induced strong degradation of HER2 as well as inhibition of tumor growth *in vivo*. This effect was thought to result from enhanced clustering of HER2 at the cell surface, induced by bsAb-$HER2_{153}$xHER_{169}. This was supported by other studies showing that the combinations of HER2 antibodies that recognize distinct non-overlapping epitopes induced strong receptor endocytosis and degradation [76-79]. In addition, clustering of surface receptors can also be induced using IgM antibodies. Binding of IgM antibodies to the FcμR results in clustering of cell surface receptors leading to rapid lysosomal degradation [80]. Unfortunately the poor pharmacokinetics of IgM antibodies are unfavourable for an ADC approach. HexaBody, a novel antibody formats that combines the PK of IgG1 antibodies with the formation of hexamers after antigen binding on cells, may overcome this limitation [81]. This platform is based on an IgG1 antibody containing a single point mutation that enhances the formation of hexamers through enhanced Fc:Fc clustering. Unlike IgM molecules

this interaction does not occur in solution but requires antigen binding before hexamerization can take place.

Alternatively novel ADC formats can be used to combine targeting of different tumor antigens to enhance the efficacy in tumors with heterogeneous target expression. This has been demonstrated with a bispecific fusion protein targeting the tumor bulk through epithelial cell adhesion molecule (EpCAM) and cancer stem cells through CD133 [82], and a bispecific fusion protein targeting the tumor bulk through EGFR and tumor stroma through the urokinase receptor (uPAR) [83]. This approach however requires that both tumor antigens are well internalized upon monovalent binding. DT2219, a bispecific recombinant immunotoxin targeting CD19 and CD22 positive B-cell tumors may fulfill these criteria as both antigens are considered to be rapidly internalizing independent of antibody induced cross-linking [29,30]. The bsADC DT2219 demonstrated broader reactivity against B-cell malignancies as compared to individual immunotoxins targeting CD19 or CD22 alone [84,85]. Furthermore, the use of a bsADC instead of the combination of the individual ADCs has the advantage that tumor cell kill induced by the bsADC may be increased without increasing toxicity to healthy tissues. Whereas the combination of two individual immunotoxins likely combines improved tumor cell kill with an increase in toxicity because both ADCs have to be distributed to the tumor, increasing the concentration of untargeted ADC in circulation.

Another novel antibody format that may help to improve ADC treatment is based on a masking peptide that blocks antigen binding in circulation. Various well internalizing tumor antigens can not be targeted with ADCs because of their expression on healthy tissues, which may result in unwanted toxicity [70] or introduce a 'sink-effect' that limits the exposure of the tumor to the ADC. By blocking antibody-binding sites in the circulation and enhancing local binding at the tumor-site, toxicity of ADCs may be reduced while improving their PK. This was demonstrated through introduction of a masking peptide linked to the binding site of an antibody through a matrix metalloproteinase (MMP)-sensitive – linker peptide. The masking peptide blocks antibody binding in circulation, however when localized to the tumor, the masking peptide is cleaved by MMPs, that are highly expressed in the tumor microenvironment, thus exposing the antibody binding site and allowing target binding by the ADC. This approach was successfully demonstrated by conjugating a masking peptide to the N-terminus of the light chain of the EGFR antibody cetuximab [86]. When conjugated with the masking peptide, cetuximab demonstrated improved safety and increased half-life in nonhuman primates as well as tumor specific accumulation in xenografted mice. These results suggest that the use of ADCs with masked binding sites may broaden the number of suitable ADC targets.

FUTURE PERSPECTIVE

The goal of this thesis was to better understand the antibody and antigen requirements needed for effective ADC treatment. Ideal ADC targets are rare, however antibodies, linkers and payloads can be used to optimize efficacy of ADCs targeting existing and novel tumor antigens. Considerations for ADC development are summarized in Figure 3. By carefully selecting the most suitable combination of antigen, antibody, linker and payload, novel tumor antigens can be utilized for ADC development. Novel antibody platforms such as, bispecific antibodies, antibodies with capped binding sites and antibodies with modulated FcR binding may help to further improve the exciting and developing field of ADCs.

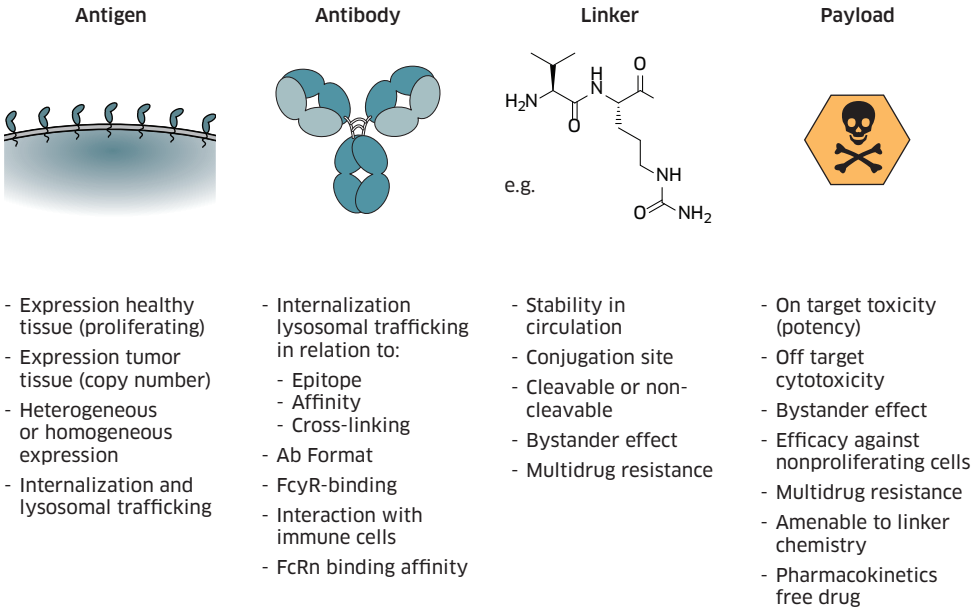

FIGURE 3 *Considerations for ADC development.*

REFERENCES

1 Ford CH, Newman CE, Johnson JR, Woodhouse CS, Reeder TA, Rowland GF, Simmonds RG: Localisation and toxicity study of a vindesine-anti-CEA conjugate in patients with advanced cancer. *Br J Cancer* 1983, 47(1):35-42.

2 Ghose T, Nigam SP: Antibody as carrier of chlorambucil. *Cancer* 1972, 29(5):1398-1400.

3 Pietersz GA, Krauer K: Antibody-targeted drugs for the therapy of cancer. *J Drug Target* 1994, 2(3):183-215.

4 Caron PC, Co MS, Bull MK, Avdalovic NM, Queen C, Scheinberg DA: Biological and immunological features of humanized M195 (anti-CD33) monoclonal antibodies. *Cancer Res* 1992, 52(24):6761-6767.

5 Bernstein ID: Monoclonal antibodies to the myeloid stem cells: therapeutic implications of CMA-676, a humanized anti-CD33 antibody calicheamicin conjugate. *Leukemia* 2000, 14(3):474-475.

6 Francisco JA, Cerveny CG, Meyer DL, Mixan BJ, Klussman K, Chace DF, Rejniak SX, Gordon KA, DeBlanc R, Toki BE *et al*: cAC10-vcMMAE, an anti-CD30-monomethyl auristatin E conjugate with potent and selective antitumor activity. *Blood* 2003, 102(4):1458-1465.

7 Foyil KV, Bartlett NL: Anti-CD30 Antibodies for Hodgkin lymphoma. *Curr Hematol Malig Rep* 2010, 5(3):140-147.

8 Lewis Phillips GD, Li G, Dugger DL, Crocker LM, Parsons KL, Mai E, Blattler WA, Lambert JM, Chari RV, Lutz RJ *et al*: Targeting HER2-positive breast cancer with trastuzumab-DM1, an antibody-cytotoxic drug conjugate. *Cancer Res* 2008, 68(22):9280-9290.

9 Nanus DM, Milowsky MI, Kostakoglu L, Smith-Jones PM, Vallabahajosula S, Goldsmith SJ, Bander NH: Clinical use of monoclonal antibody HuJ591 therapy: targeting prostate specific membrane antigen. *J Urol* 2003, 170(6 Pt 2):S84-88; discussion S88-89.

10 Henry MD, Wen S, Silva MD, Chandra S, Milton M, Worland PJ: A prostate-specific membrane antigen-targeted monoclonal antibody-chemotherapeutic conjugate designed for the treatment of prostate cancer. *Cancer Res* 2004, 64(21):7995-8001.

11 de Goeij BE, Peipp M, de Haij S, van den Brink EN, Kellner C, Riedl T, de Jong R, Vink T, Strumane K, Bleeker WK *et al*: HER2 monoclonal antibodies that do not interfere with receptor heterodimerization-mediated signaling induce effective internalization and represent valuable components for rational antibody-drug conjugate design. *MAbs* 2014, 6(2):392-402.

12 Owen SC, Patel N, Logie J, Pan G, Persson H, Moffat J, Sidhu SS, Shoichet MS: Targeting HER2+ breast cancer cells: lysosomal accumulation of anti-HER2 antibodies is influenced by antibody binding site and conjugation to polymeric nanoparticles. *J Control Release* 2013, 172(2):395-404.

13 Poul MA, Becerril B, Nielsen UB, Morisson P, Marks JD: Selection of tumor-specific internalizing human antibodies from phage libraries. *J Mol Biol* 2000, 301(5):1149-1161.

14 Bleeker WK, Lammerts van Bueren JJ, van Ojik HH, Gerritsen AF, Pluyter M, Houtkamp M, Halk E, Goldstein J, Schuurman J, van Dijk MA *et al*: Dual mode of action of a human anti-epidermal growth factor receptor monoclonal antibody for cancer therapy. *J Immunol* 2004, 173(7):4699-4707.

15 Goldenberg MM: Trastuzumab, a recombinant DNA-derived humanized monoclonal antibody, a novel agent for the treatment of metastatic breast cancer. *Clin Ther* 1999, 21(2):309-318.

16 Krop IE, Beeram M, Modi S, Jones SF, Holden SN, Yu W, Girish S, Tibbitts J, Yi JH, Sliwkowski MX *et al*: Phase I study of trastuzumab-DM1, an HER2 antibody-drug conjugate, given every 3 weeks to patients with HER2-positive metastatic breast cancer. *J Clin Oncol* 2010, 28(16):2698-2704.

17 Polson AG, Williams M, Gray AM, Fuji RN, Poon KA, McBride J, Raab H, Januario T, Go M, Lau J *et al*: Anti-CD22-MCC-DM1: an antibody-drug conjugate with a stable linker for the treatment of non-Hodgkin's lymphoma. *Leukemia* 2010, 24(9):1566-1573.

18 DiJoseph JF, Popplewell A, Tickle S, Ladyman H, Lawson A, Kunz A, Khandke K, Armellino DC, Boghaert ER, Hamann P *et al*: Antibody-targeted chemotherapy of B-cell lymphoma using calicheamicin conjugated to murine or humanized antibody against CD22. *Cancer Immunol Immunother* 2005, 54(1):11-24.

19 Kwa HB, Wesseling J, Verhoeven AH, van Zandwijk N, Hilkens J: Immunoscintigraphy of small-cell lung cancer xenografts with anti neural cell adhesion molecule monoclonal antibody, 123C3: improvement of tumour uptake by internalisation. *Br J Cancer* 1996, 73(4):439-446.

20 Pietersz GA, Wenjun L, Krauer K, Baker T, Wreschner D, McKenzie IF: Comparison of the biological properties of two anti-mucin-1 antibodies prepared for imaging and therapy. *Cancer Immunol Immunother* 1997, 44(6):323-328.

21 Breij EC, de Goeij BE, Verploegen S, Schuurhuis DH, Amirkhosravi A, Francis J, Miller VB, Houtkamp M, Bleeker WK, Satijn D *et al*: An antibody-drug conjugate that targets tissue factor exhibits potent therapeutic activity against a broad range of solid tumors. *Cancer Res* 2014, 74(4):1214-1226.

22 de Goeij BE, Satijn D, Freitag CM, Wubbolts R, Bleeker WK, Khasanov A, Zhu T, Chen G, Miao D, van Berkel PH *et al*: High turnover of tissue factor enables efficient intracellular delivery of antibody-drug conjugates. *Mol Cancer Ther* 2015, 14(5):1130-1140.

23 Axup JY, Bajjuri KM, Ritland M, Hutchins BM, Kim CH, Kazane SA, Halder R, Forsyth JS, Santidrian AF, Stafin K *et al*: Synthesis of site-specific antibody-drug conjugates using unnatural amino acids. *Proc Natl Acad Sci U S A* 2012, 109(40):16101-16106.

24 Perez-Torres M, Guix M, Gonzalez A, Arteaga CL: Epidermal growth factor receptor (EGFR) antibody down-regulates mutant receptors and inhibits tumors expressing EGFR mutations. *J Biol Chem* 2006, 281(52):40183-40192.

25 Fan Z, Lu Y, Wu X, Mendelsohn J: Antibody-induced epidermal growth factor receptor dimerization mediates inhibition of autocrine proliferation of A431 squamous carcinoma cells. *J Biol Chem* 1994, 269(44):27595-27602.

26 Wels W, Biburger M, Muller T, Dalken B, Giesubel U, Tonn T, Uherek C: Recombinant immunotoxins and retargeted killer cells: employing engineered antibody fragments for tumor-specific targeting of cytotoxic effectors. *Cancer Immunol Immunother* 2004, 53(3):217-226.

27 von Minckwitz G, Harder S, Hovelmann S, Jager E, Al-Batran SE, Loibl S, Atmaca A, Cimpoiasu C, Neumann A, Abera A *et al*: Phase I clinical study of the recombinant antibody toxin scFv(FRP5)-ETA specific for the ErbB2/HER2 receptor in patients with advanced solid malignomas. *Breast Cancer Res* 2005, 7(5):R617-626.

28 Terp MG, Olesen KA, Arnspang EC, Lund RR, Lagerholm BC, Ditzel HJ, Leth-Larsen R: Anti-human CD73 monoclonal antibody inhibits metastasis formation in human breast cancer by inducing clustering and internalization of CD73 expressed on the surface of cancer cells. *J Immunol* 2013, 191(8):4165-4173.

29 Shen GL, Li JL, Ghetie MA, Ghetie V, May RD, Till M, Brown AN, Relf M, Knowles P, Uhr JW *et al*: Evaluation of four CD22 antibodies as ricin A chain-containing immunotoxins for the *in vivo* therapy of human B-cell leukemias and lymphomas. *Int J Cancer* 1988, 42(5):792-797.

30 Ghetie MA, May RD, Till M, Uhr JW, Ghetie V, Knowles PP, Relf M, Brown A, Wallace PM, Janossy G *et al*: Evaluation of ricin A chain-containing immunotoxins directed against CD19 and CD22 antigens on normal and malignant human B-cells as potential reagents for *in vivo* therapy. *Cancer Res* 1988, 48(9):2610-2617.

31 Tabrizi M, Bornstein GG, Suria H: Biodistribution mechanisms of therapeutic monoclonal antibodies in health and disease. *AAPS J* 2010, 12(1):33-43.

32 Osterud B, Bjorklid E: Blood-Borne Tissue Factor (Including Microparticles). *Madame Curie Bioscience Database*.

33 Press MF, Cordon-Cardo C, Slamon DJ: Expression of the HER-2/neu proto-oncogene in normal human adult and fetal tissues. *Oncogene* 1990, 5(7):953-962.

34 Li T, Perez-Soler R: Skin toxicities associated with epidermal growth factor receptor inhibitors. *Target Oncol* 2009, 4(2):107-119.

35 Maric G, Rose AA, Annis MG, Siegel PM: Glycoprotein non-metastatic b (GPNMB): A metastatic mediator and emerging therapeutic target in cancer. *Onco Targets Ther* 2013, 6:839-852.

36 Hammarstrom S: The carcinoembryonic antigen (CEA) family: structures, suggested functions and expression in normal and malignant tissues. *Semin Cancer Biol* 1999, 9(2):67-81.

37 Eisenwort G, Jurkin J, Yasmin N, Bauer T, Gesslbauer B, Strobl H: Identification of TROP2 (TACSTD2), an EpCAM-like molecule, as a specific marker for TGF-beta1-dependent human epidermal Langerhans cells. *J Invest Dermatol* 2011, 131(10):2049-2057.

38 Stepan LP, Trueblood ES, Hale K, Babcook J, Borges L, Sutherland CL: Expression of Trop2 cell surface glycoprotein in normal and tumor tissues: potential implications as a cancer therapeutic target. *J Histochem Cytochem* 2011, 59(7):701-710.

39 Kiyamova R, Shyian M, Lyzogubov VV, Usenko VS, Gout T, Filonenko V: Immunohistochemical analysis of NaPi2b protein (MX35 antigen) expression and subcellular localization in human normal and cancer tissues. *Exp Oncol* 2011, 33(3):157-161.

40 Silver DA, Pellicer I, Fair WR, Heston WD, Cordon-Cardo C: Prostate-specific membrane antigen expression in normal and malignant human tissues. *Clin Cancer Res* 1997, 3(1):81-85.

41 Sutherland MS, Sanderson RJ, Gordon KA, Andreyka J, Cerveny CG, Yu C, Lewis TS, Meyer DL, Zabinski RF, Doronina SO *et al*: Lysosomal trafficking and cysteine protease metabolism confer target-specific cytotoxicity by peptide-linked anti-CD30-auristatin conjugates. *J Biol Chem* 2006, 281(15):10540-10547.

42 Austin CD, De Maziere AM, Pisacane PI, van Dijk SM, Eigenbrot C, Sliwkowski MX, Klumperman J, Scheller RH: Endocytosis and sorting of ErbB2 and the site of action of cancer therapeutics trastuzumab and geldanamycin. *Mol Biol Cell* 2004, 15(12):5268-5282.

43 Higuchi M, Matsuda T, Mori N, Yamada Y, Horie R, Watanabe T, Takahashi M, Oie M, Fujii M: Elevated expression of CD30 in adult T-cell leukemia cell lines: possible role in constitutive NF-kappaB activation. *Retrovirology* 2005, 2:29.

44 Kallab V, Benz C, Kirpotin J, Marks J, Park J: Novel evaluation of targeted receptor internalization as a predictive tool for HER2/EGFR antibody-based therapeutics. *Journal of Clinical Oncology, 2004 ASCO, Vol 22, No 14S (July 15 Supplement), 2004: 3157.*

45 Baulida J, Kraus MH, Alimandi M, Di Fiore PP, Carpenter G: All ErbB receptors other than the epidermal growth factor receptor are endocytosis impaired. *J Biol Chem* 1996, 271(9):5251-5257.

46 Ford CH, Tsaltas GC, Osborne PA, Addetia K: Novel flow cytometric analysis of the progress and route of internalization of a monoclonal anti-carcinoembryonic antigen (CEA) antibody. *Cytometry* 1996, 23(3):228-240.

47 Tsaltas G, Ford CH, Gallant M: Demonstration of monoclonal anti-carcinoembryonic antigen (CEA) antibody internalization by electron microscopy, western blotting and radioimmunoassay. *Anticancer Res* 1992, 12(6B):2133-2142.

48 Govindan SV, Cardillo TM, Moon SJ, Hansen HJ, Goldenberg DM: CEACAM5-targeted therapy of human colonic and pancreatic cancer xenografts with potent labetuzumab-SN-38 immunoconjugates. *Clin Cancer Res* 2009, 15(19):6052-6061.

49 Li ZH, Zhang Q, Wang HB, Zhang YN, Ding D, Pan LQ, Miao D, Xu S, Zhang C, Luo PH *et al*: Preclinical studies of targeted therapies for CD20-positive B lymphoid malignancies by Ofatumumab conjugated with auristatin. *Invest New Drugs* 2014, 32(1):75-86.

50 Law CL, Cerveny CG, Gordon KA, Klussman K, Mixan BJ, Chace DF, Meyer DL, Doronina SO, Siegall CB, Francisco JA *et al*: Efficient elimination of B-lineage lymphomas by anti-CD20-auristatin conjugates. *Clin Cancer Res* 2004, 10(23):7842-7851.

51 Engelberts PJ, Badoil C, Beurskens FJ, Boulay-Moine D, Grivel K, Parren PW, Moulard M: A quantitative flow cytometric assay for determining binding characteristics of chimeric, humanized and human antibodies in whole blood: proof of principle with rituximab and ofatumumab. *J Immunol Methods* 2013, 388(1-2):8-17.

52 Abe K, Shoji M, Chen J, Bierhaus A, Danave I, Micko C, Casper K, Dillehay DL, Nawroth PP, Rickles FR: Regulation of vascular endothelial growth factor production and angiogenesis by the cytoplasmic tail of tissue factor. *Proc Natl Acad Sci U S A* 1999, 96(15):8663-8668.

53 Lassen UN, Hong DS, Diamantis N, Subbiah V, Kumar R, Sorensen M, Lisby S, Coleman RL, De Bono JS: A phase I, first-in-human study to evaluate the tolerability, pharmacokinetics and preliminary efficacy of HuMax-tissue factor-ADC (TF-ADC) in patients with solid tumors. *J Clin Oncol 33, 2015 (suppl; abstr 2570)*.

54 Ritchie M, Tchistiakova L, Scott N: Implications of receptor-mediated endocytosis and intracellular trafficking dynamics in the development of antibody drug conjugates. *MAbs* 2013, 5(1):13-21.

55 Adams GP, Schier R, McCall AM, Simmons HH, Horak EM, Alpaugh RK, Marks JD, Weiner LM: High affinity restricts the localization and tumor penetration of single-chain fv antibody molecules. *Cancer Res* 2001, 61(12):4750-4755.

56 Rudnick SI, Lou J, Shaller CC, Tang Y, Klein-Szanto AJ, Weiner LM, Marks JD, Adams GP: Influence of affinity and antigen internalization on the uptake and penetration of Anti-HER2 antibodies in solid tumors. *Cancer Res* 2011, 71(6):2250-2259.

57 Fujimori K, Covell DG, Fletcher JE, Weinstein JN: A modeling analysis of monoclonal antibody percolation through tumors: a binding-site barrier. *J Nucl Med* 1990, 31(7):1191-1198.

58 Saga T, Neumann RD, Heya T, Sato J, Kinuya S, Le N, Paik CH, Weinstein JN: Targeting cancer micrometastases with monoclonal antibodies: a binding-site barrier. *Proc Natl Acad Sci U S A* 1995, 92(19):8999-9003.

59 Jacobs TW, Gown AM, Yaziji H, Barnes MJ, Schnitt SJ: Specificity of HercepTest in determining HER-2/neu status of breast cancers using the United States Food and Drug Administration-approved scoring system. *J Clin Oncol* 1999, 17(7):1983-1987.

60 Chen R, Hou J, Newman E, Kim Y, Donohue C, Liu X, Thomas SH, Forman SJ, Kane SE: CD30 Downregulation, MMAE Resistance, and MDR1 Upregulation Are All Associated with Resistance to Brentuximab Vedotin. *Mol Cancer Ther* 2015, 14(6):1376-1384.

61 Kovtun YV, Audette CA, Mayo MF, Jones GE, Doherty H, Maloney EK, Erickson HK, Sun X, Wilhelm S, Ab O *et al*: Antibody-maytansinoid conjugates designed to bypass multidrug resistance. *Cancer Res* 2010, 70(6):2528-2537.

62 Ogasawara H, Nishio K, Kanzawa F, Lee YS, Funayama Y, Ohira T, Kuraishi Y, Isogai Y, Saijo N: Intracellular carboxyl esterase activity is a determinant of cellular sensitivity to the antineoplastic agent KW-2189 in cell lines resistant to cisplatin and CPT-11. *Jpn J Cancer Res* 1995, 86(1):124-129.

63 Damelin M, Bankovich A, Park A, Aguilar J, Anderson WC, Santaguida M, Aujay M, Fong S, Khandke K, Pulito V *et al*: Anti-EFNA4 Calicheamicin Conjugates Effectively Target Triple-Negative Breast and Ovarian Tumor-Initiating Cells To Result In Sustained Tumor Regressions. *Clin Cancer Res* 2015.

64 Kung Sutherland MS, Walter RB, Jeffrey SC, Burke PJ, Yu C, Kostner H, Stone I, Ryan MC, Sussman D, Lyon RP *et al*: SGN-CD33A: a novel CD33-targeting antibody-drug conjugate using a pyrrolobenzodiazepine dimer is active in models of drug-resistant AML. *Blood* 2013, 122(8):1455-1463.

65 Walter RB, Raden BW, Hong TC, Flowers DA, Bernstein ID, Linenberger ML: Multidrug resistance protein attenuates gemtuzumab ozogamicin-induced cytotoxicity in acute myeloid leukemia cells. *Blood* 2003, 102(4):1466-1473.

66 Hamann PR, Hinman LM, Beyer CF, Greenberger LM, Lin C, Lindh D, Menendez AT, Wallace R, Durr FE, Upeslacis J: An anti-MUC1 antibody-calicheamicin conjugate for treatment of solid tumors. Choice of linker and overcoming drug resistance. *Bioconjugate Chem* 2005, 16(2):346-353.

67 van der Lee MM, Groothuis PG, Ubink R, van der Vleuten MA, van Achterberg TA, Loosveld EM, Damming D, Jacobs DC, Rouwette M, Egging DF *et al*: The Preclinical Profile of the Duocarmycin-Based HER2-Targeting ADC SYD985 Predicts for Clinical Benefit in Low HER2-Expressing Breast Cancers. *Mol Cancer Ther* 2015.

68 Kovtun YV, Audette CA, Ye Y, Xie H, Ruberti MF, Phinney SJ, Leece BA, Chittenden T, Blattler WA, Goldmacher VS: Antibody-drug conjugates designed to eradicate tumors with homogeneous and heterogeneous expression of the target antigen. *Cancer Res* 2006, 66(6):3214-3221.

69 Smith LM, Nesterova A, Alley SC, Torgov MY, Carter PJ: Potent cytotoxicity of an auristatin-containing antibody-drug conjugate targeting melanoma cells expressing melanotransferrin/p97. *Mol Cancer Ther* 2006, 5(6):1474-1482.

70 Tijink BM, Buter J, de Bree R, Giaccone G, Lang MS, Staab A, Leemans CR, van Dongen GA: A phase I dose escalation study with anti-CD44v6 bivatuzumab mertansine in patients with incurable squamous cell carcinoma of the head and neck or esophagus. *Clin Cancer Res* 2006, 12(20 Pt 1):6064-6072.

71 Younes A, Bartlett NL, Leonard JP, Kennedy DA, Lynch CM, Sievers EL, Forero-Torres A: Brentuximab vedotin (SGN-35) for relapsed CD30-positive lymphomas. *N Engl J Med* 2010, 363(19):1812-1821.

72 Uppal H, Doudement E, Mahapatra K, Darbonne WC, Bumbaca D, Shen BQ, Du X, Saad O, Bowles K, Olsen S *et al*: Potential mechanisms for thrombocytopenia development with trastuzumab emtansine (T-DM1). *Clin Cancer Res* 2015, 21(1):123-133.

73 Chen K, Nishi H, Travers R, Tsuboi N, Martinod K, Wagner DD, Stan R, Croce K, Mayadas TN: Endocytosis of soluble immune complexes leads to their clearance by FcgammaRIIIB but induces neutrophil extracellular traps via FcgammaRIIA *in vivo*. *Blood* 2012, 120(22):4421-4431.

74 Herbertson RA, Tebbutt NC, Lee FT, MacFarlane DJ, Chappell B, Micallef N, Lee ST, Saunder T, Hopkins W, Smyth FE *et al*: Phase I biodistribution and pharmacokinetic study of Lewis Y-targeting immunoconjugate CMD-193 in patients with advanced epithelial cancers. *Clin Cancer Res* 2009, 15(21):6709-6715.

75 Labrijn AF, Meesters JI, de Goeij BE, van den Bremer ET, Neijssen J, van Kampen MD, Strumane K, Verploegen S, Kundu A, Gramer MJ *et al*: Efficient generation of stable bispecific IgG1 by controlled Fab-arm exchange. *Proc Natl Acad Sci U S A* 2013, 110(13):5145-5150.

76 Friedman LM, Rinon A, Schechter B, Lyass L, Lavi S, Bacus SS, Sela M, Yarden Y: Synergistic down-regulation of receptor tyrosine kinases by combinations of mAbs: Implications for cancer immunotherapy. *Proceedings of the National Academy of Sciences of the United States of America* 2005, 102(6):1915-1920.

77 Nahta R, Hung M-C, Esteva FJ: The HER-2-Targeting Antibodies Trastuzumab and Pertuzumab Synergistically Inhibit the Survival of Breast Cancer Cells. *Cancer Research* 2004, 64(7):2343-2346.

78 Ben-Kasus T, Schechter B, Lavi S, Yarden Y, Sela M: Persistent elimination of ErbB-2/HER2-overexpressing tumors using combinations of monoclonal antibodies: Relevance of receptor endocytosis. *Proceedings of the National Academy of Sciences* 2009, 106(9):3294-3299.

79 Spangler JB, Neil JR, Abramovitch S, Yarden Y, White FM, Lauffenburger DA, Wittrup KD: Combination antibody treatment down-regulates epidermal growth factor receptor by inhibiting endosomal recycling. *Proceedings of the National Academy of Sciences* 2010, 107(30):13252-13257.

80 Vire B, Skarzynski M, Thomas JD, Nelson CG, David A, Aue G, Burke TR, Jr., Rader C, Wiestner A: Harnessing the fcmu receptor for potent and selective cytotoxic therapy of chronic lymphocytic leukemia. *Cancer Res* 2014, 74(24):7510-7520.

81 Diebolder CA, Beurskens FJ, de Jong RN, Koning RI, Strumane K, Lindorfer MA, Voorhorst M, Ugurlar D, Rosati S, Heck AJ *et al*: Complement is activated by IgG hexamers assembled at the cell surface. *Science* 2014, 343(6176):1260-1263.

82 Waldron NN, Barsky SH, Dougherty PR, Vallera DA: A bispecific EpCAM/CD133-targeted toxin is effective against carcinoma. *Target Oncol* 2014, 9(3):239-249.

83 Oh S, Tsai AK, Ohlfest JR, Panoskaltsis-Mortari A, Vallera DA: Evaluation of a bispecific biological drug designed to simultaneously target glioblastoma and its neovasculature in the brain. *J Neurosurg* 2011, 114(6):1662-1671.

84 Vallera DA, Oh S, Chen H, Shu Y, Frankel AE: Bioengineering a unique deimmunized bispecific targeted toxin that simultaneously recognizes human CD22 and CD19 receptors in a mouse model of B-cell metastases. *Mol Cancer Ther* 2010, 9(6):1872-1883.

85 Bachanova V, Frankel AE, Cao Q, Lewis D, Grzywacz B, Verneris MR, Ustun C, Lazaryan A, McClune B, Warlick ED *et al*: Phase I Study of a Bispecific Ligand-Directed Toxin Targeting CD22 and CD19 (DT2219) for Refractory B-cell Malignancies. *Clin Cancer Res* 2015, 21(6):1267-1272.

86 Desnoyers LR, Vasiljeva O, Richardson JH, Yang A, Menendez EE, Liang TW, Wong C, Bessette PH, Kamath K, Moore SJ *et al*: Tumor-specific activation of an EGFR-targeting probody enhances therapeutic index. *Sci Transl Med* 2013, 5(207):207ra144.

Summary

Antibody-Drug Conjugates (ADCs) represent a new class of anti-cancer therapeutics that combine the tumor specificity, pharmacokinetics and biodistribution of antibodies with the cytotoxic capacity of chemotherapeutic payloads. Currently over 50 ADCs are in clinical development with variable success. Clinical efficacy is driven by the right combination of tumor antigen, targeting antibody, conjugation linker and cytotoxic payload. The expression level of ADC targets on tumor cells and healthy tissue as well as the intracellular trafficking of the antibody component are crucial parameters for selection of the linker-drug combination. This thesis addresses the selection criteria of tumor specific antibodies and antigens for the development of ADCs.

Chapter 1 provides an introduction on the general biology of antibodies and ADCs, as well as the main objective of this thesis. **Chapter 2** is a review that deliberates the target requirements for ADC development and the therapeutic window of currently existing ADCs. Dosing regimens of ADCs are often hampered by toxicities unrelated to the targeted antigen. Strategies to overcome these toxicities, such as the use of novel DNA damaging payloads with picomolar efficacy as well as adapting the interaction of ADCs with the immune system may help to increase the therapeutic window of ADCs. However, studies addressing the safety and establishing the maximum tolerated dose (MTD) of such ADC approaches are mandatory.

In **Chapter 3** we explored Tissue Factor (TF) as a novel ADC target. Intracellular routing of TF was compared with the targets of two clinically applied ADCs, human epidermal growth factor receptor 2 (HER2) and epidermal growth factor receptor (EGFR). We found rapid and constitutive transport of TF to lysosomes of tumor cells which translated into effective cytotoxicity induced by Duostatin-3 conjugated TF-antibodies. Furthermore, unlike HER2-vcDuo3, TF-vcDuo3 required relatively low surface expression of the target antigen to be effective. This was further emphasized in **Chapter 4**, where TF-011 was selected as the preferred TF-specific antibody for the development of tisotumab vedotin (TF-011-MMAE). TF-011 was able to induce antibody dependent cellular cytotoxicity (ADCC) and to inhibit TF:FVIIa-mediated intracellular signaling without interfering with the role of TF in coagulation. Although the unconjugated antibody had minimal anti-tumor efficacy *in vivo*, the same antibody conjugated with vcMMAE demonstrated almost complete tumor regression in a wide variety of patient-derived xenograft (PDX) models, despite the heterogeneous target expression in some of these models. This may in part be due to a so-called by-

stander effect, where antigen-negative tumor cells are killed through toxins released by antigen-positive tumor cells.

In **Chapter 5** we describe the development of a high throughput *in vitro* assay that can be used for the identification and selection of internalizing antibodies capable of delivering a cytotoxic payload to tumor cells. For this, a modified version of the *Pseudomonas* exotoxin-A was used. The alpha-2-macroglobulin receptor binding domain of *Pseudomonas* exotoxin-A was replaced with a human kappa light chain binding domain. By combining the resulting fusion protein (α-kappa-ETA') with antibodies targeting EGFR or HM1.24, we were able to demonstrate α-kappa-ETA' mediated cytotoxicity of tumor cells expressing EGFR or HM1.24. These results support the identification and selection of antibodies with favorable internalization characteristics for ADC development. In **Chapter 6** the α-kappa-ETA' assay was used to screen a large panel of HER2 Abs for their ability to deliver α-kappa-ETA' into tumor cells. Substantial differences in cytotoxicity were found between HER2 Abs from different cross-competition groups, when non-covalently linked to α-kappa-ETA'. By correlating α-kappa-ETA' mediated cytotoxicity with inhibition of ErbB signaling and inhibition of HER2 driven proliferation we found that Abs that did not interfere with heterodimerization of HER2 induced greater α-kappa-ETA' mediated cytotoxicity. These results demonstrated that the characteristics of antibodies that are favorable for an ADC approach, i.e. internalization and capacity to induce toxin-mediated cell kill, may differ from those that are favorable for therapy with naked antibodies, such as inhibition of receptor signaling. Therefore antibodies that are effective without drug-conjugation may not always represent the best antibody candidates for an ADC approach.

Because some tumor targets are less optimal for an ADC approach due to poor internalization characteristic, we developed an alternative strategy to improve internalization of poorly internalizing antibodies or antigens, which is described in **Chapter 7**. As a model, we generated a bispecific ADC (bsHER2xCD63-Duo3) that combines tumor-specific targeting through HER2, with targeting of CD63 to facilitate trafficking to the lysosome. The monovalent HER2-specific Fab-arm, by itself, was unable to induce internalization, and consequently, the monovalent HER2-specific ADC showed poor anti-tumor activity. The affinity of the CD63 Fab-arm was chosen such that monovalent CD63 binding was inefficient, in order to limit CD63 targeting to tumor cells that co-express HER2 and CD63. While monovalent ADCs targeting HER2 or CD63 had no effect on tumor growth, bsHER2xCD63-Duo3 showed strong anti-tumor efficacy against HER2-positive xenografts, which provides a rationale for the development of novel bsADCs that combine tumor specific targeting with targeting of rapidly internalizing antigens.

In conclusion, the work in this thesis describes the Ab and antigen requirements for optimal payload delivery and supports the development of novel and improved ADCs. Important considerations for ADC development, such as antigen expression and internalization, Ab format and epitopes as well as the type of linker-payload used, are summarized in **Chapter 8**. There is no such thing as the perfect ADC. However by increasing our knowledge on the requirements for successful ADC development we may enable the development of next generation ADCs with a superior therapeutic window.

Samenvatting in het Nederlands

De gemene deler

Kanker is een verzamelnaam voor ziektes die ontstaan door lichaamseigen cellen waarvan de celdeling is ontspoord. In ons lichaam bevinden zich allerlei verschillende typen cellen die qua uiterlijk en functie erg van elkaar kunnen verschillen. In theorie kan vanuit elk van deze gezonde cellen een kankercel ontstaan. De kans hierop is erg klein, maar wanneer er veranderingen (mutaties) optreden in het DNA van een gezonde cel, kan deze cel transformeren tot een kankercel. Deze mutaties vinden continu plaats en worden meestal door de cel zelf opgespoord en hersteld. Bekende risicofactoren voor kanker zoals roken, ongezond eten en ouderdom vergroten het aantal mutaties in het DNA waardoor de kans ook groter wordt dat er een kankercel ontstaat. Veel van deze mutaties hebben geen gevolgen voor de celdeling waardoor ze geen kwaadaardige gevolgen hebben. Mocht er toch een cel ontstaan met een kwaadaardige mutatie dan gaat deze cel normaal gesproken in apoptose. Dit is een soort zelfmoordproces waarbij de cel zijn eigen DNA kapotmaakt, dood gaat en vervolgens wordt opgeruimd door gespecialiseerde cellen van ons afweersysteem (het immuunsysteem). In het geval van een kankercel werkt dit mechanisme niet goed. Hierdoor krijgt de kankercel vrij spel en kan deze naar hartenlust gaan delen, waardoor een tumor kan ontstaan.

Antilichamen als anti-kanker therapie

Ons immuunsysteem is gespecialiseerd in het herkennen en bestrijden van lichaamsvreemde indringers zoals virussen en bacteriën, maar omdat een kankercel ontstaat vanuit een lichaamseigen cel heeft ons immuunsysteem moeite om deze cellen op te sporen. De twee belangrijkste wapens van het immuunsysteem zijn witte bloedcellen en antilichamen, die er samen voor zorgen dat lichaamsvreemde indringers worden bestreden. Om de behandeling van kanker te bevorderen, ontwikkelen veel bedrijven antilichamen (ook wel immunoglobulinen) die specifiek in staat zijn om kankercellen te herkennen. Zulke tumor-specifieke antilichamen kunnen het immuunsysteem vertellen waar zich in ons lichaam kankercellen bevinden, en vervolgens bijdragen aan het opruimen van die kankercellen. In Hoofdstuk 1, Figuur 1 is een schematische weergave te zien van een antilichaam. Elk antilichaam bestaat uit twee delen: het Fab-domein en het Fc-domein. Het Fab-domein, of antigeen bindend domein, is het gedeelte waarmee het antilichaam eiwitstructuren kan herkennen die op een kankercel voorkomen. Het Fc-domein is het gedeelte waarmee een antilichaam het immuunsysteem kan activeren. Cellen van ons immuunsysteem hebben receptoren op hun oppervlak die specifiek in staat zijn om te binden aan het Fc-domein van een antilichaam. Deze interactie kan ervoor zorgen dat gespecialiseerde cellen van ons

immuunsysteem (NK-cellen, granulocyten en macrofagen), de tumor cel doden en opruimen. Het Fc-domein van een antilichaam kan ook worden herkend door complement factoren. Dit zijn eiwitten die zich in onze bloedbaan bevinden. Zodra deze eiwitten aan antilichamen binden ontstaat er een gat in de tumor cel waardoor de cel dood gaat. Daarnaast zijn sommige tumor-specifieke antilichamen in staat om de groei van tumor cellen te remmen zonder hulp van de andere componenten van het immuunsysteem. Dit gebeurt bijvoorbeeld als het antilichaam bindt aan een eiwit dat is betrokken bij de groei van tumor cellen. De behandeling van kankerpatiënten met antilichamen kan erg goed werken. Op dit moment worden vooral patiënten met specifieke vormen van leukemie succesvol behandeld met antilichamen. Helaas zijn er ook vormen van kanker waarbij behandeling met antilichamen tot nu toe minder succesvol is. Bijvoorbeeld in situaties waarin de kankercellen ongevoelig (resistent) zijn of worden voor deze behandeling.

Antilichaam-drug conjugaten

Een methode om de anti-tumor activiteit van antilichamen te vergroten is door er giftige stoffen (toxines), zoals chemotherapeutica, aan te koppelen. Chemotherapie is naast het bestralen en het chirurgisch verwijderen van tumoren de meest voorkomende behandeling tegen kanker. Er zijn allerlei verschillende soorten chemotherapeutica die de groei van tumoren kunnen remmen. Helaas beschadigen deze medicijnen ook gezonde cellen in ons lichaam. Door deze toxines te koppelen aan tumor-specifieke antilichamen proberen we ervoor te zorgen dat de chemotherapie zijn dodelijke werking alleen nog maar uitoefent op tumor cellen. Deze vorm van medicijnen noemen we antilichaam-drug conjugaten (ADC's). Het antilichaam wordt hierbij gebruikt als een soort transportmiddel om de chemotherapie in de tumorcel te krijgen, en daarbij zo min mogelijk schade aan te richten aan gezonde cellen. Dit idee is niet nieuw en werd ruim 100 jaar gelden al beschreven door Nobelprijs winnaar Paul Ehrlich. Sindsdien hebben diverse onderzoekers geprobeerd om ADC's te maken, maar pas in 2000 kwam het eerste ADC (Mylotarg®) op de markt. Helaas werd dit ADC door tegenvallende resultaten in kankerpatiënten ook weer terug getrokken van de markt. Tegenwoordig zijn de conjugatiemethodes sterk verbeterd waardoor ADC's veiliger en effectiever zijn en daadwerkelijk kunnen worden gebruikt voor de behandeling van kankerpatiënten. Er zijn inmiddels twee nieuwe ADC's op de markt. Adcetris® voor de behandeling van patiënten met lymfeklierkanker en Kadcyla® voor de behandeling van patiënten met borstkanker. Daarnaast is in Hoofdstuk 2, Tabel 1 een overzicht te zien van de verschillende ADC's die op dit moment in kankerpatiënten worden getest. In de laatste kolom staat de maximaal tolereerbare dosis (MTD) voor kankerpatiënten weergegeven. Dit is de maximale hoeveelheid van het medicijn die kan worden gegeven aan patiënten, zonder dat er ernstige bijwerkingen optreden. Hoofdstuk 2 van dit proefschrift beschrijft een literatuurstudie waaruit blijkt dat de minimale dosis waarbij ADC's tumorgroei remmen in een diermodel, nagenoeg gelijk is aan de MTD van de ADC's in patiënten. Dit betekent dat we voor

optimale behandeling van kanker patiënten het liefst een hogere dosis van de ADC zouden willen geven, maar dit is voor de huidige ADC's niet mogelijk omdat de ADC dan ook gezonde cellen aantast. Als gevolg wordt er een lagere dosis van het medicijn gegeven, en dat belemmert de effectiviteit van de behandeling.

Promotieonderzoek

Gedurende mijn promotie onderzoek heb ik onderzocht hoe we de effectiviteit van ADC's kunnen verbeteren. Voor een effectieve ADC behandeling is het van belang dat ADC's worden opgenomen door de tumor cel en worden afgebroken in een specifiek compartiment binnenin de cel; het lysosoom. Als de ADC wordt afgebroken komt het toxine vrij en kan het toxine zijn werk doen en de tumorcel doden (zie ook Hoofdstuk 1, Figuur 2). Echter, veel eiwitten worden niet goed door de tumor cel opgenomen en komen daardoor niet in het lysosoom terecht. Een ADC dat zo'n eiwit herkent op de tumorcel, zal dus ook niet in het lysosoom terecht komen waardoor het toxine niet vrijkomt, en het ADC geen effectiviteit laat zien. In Hoofdstuk 3 hebben we onderzocht welke eiwitten het beste door de tumor cel worden opgenomen, om zo te kijken welke eiwitten het meest geschikt zijn voor het ontwikkelen van een ADC. In deze studie hebben we gevonden dat tissue factor, een eiwit wat op veel tumoren voorkomt, heel efficiënt wordt opgenomen door tumor cellen. We denken daarom dat antilichamen die tissue factor herkennen, heel geschikt zijn voor het maken van ADC's. In Hoofdstuk 4 wordt beschreven hoe we verschillende antilichamen gericht tegen tissue factor hebben gemaakt en hoe we het beste antilichaam (TF-011) hebben geselecteerd voor het maken van een ADC. Door een toxine te koppelen aan dit antilichaam, laten we onder andere zien dat een ADC die tissue factor herkent erg sterke remming van tumor groei geeft. Het ADC wordt op dit moment getest in kankerpatiënten, waarbij we vooral onderzoeken of het medicijn veilig is.

In Hoofdstuk 5 wordt een methode beschreven die kan worden gebruikt om grote hoeveelheden antilichamen te vergelijken als ADC, om zo het meest geschikte antilichaam te selecteren voor de ontwikkeling van een ADC. Het is erg veel werk om een ADC te maken. Daarom hebben we een truc bedacht waarmee we eenvoudig kunnen testen of antilichamen in staat zijn om een toxine in een tumor cel te krijgen. Hiervoor gebruiken we een toxine dat wordt uitgescheiden door een bacterie. Dit toxine kan niet aan tumor cellen binden en is daardoor niet schadelijk. Echter het toxine kan wel specifiek aan onze antilichamen binden. Als zo'n antilichaam wordt opgenomen door een tumor cel, dan kan het toxine met het antilichaam meeliften en de tumor cel alsnog doden. Door het toxine te mengen met verschillende antilichaam is het mogelijk om te testen welke combinatie van antilichaam en toxine in staat is om tumorcellen te doden. In Hoofdstuk 5 laten we zien dat deze truc goed werkt. Vervolgens wordt deze truc in Hoofdstuk 6 gebruikt om een grote hoeveelheid antilichamen gericht tegen een specifiek tumor eiwit te testen. Hoewel deze antilichamen allemaal hetzelfde tumoreiwit herkennen, vonden we grote verschillen

in de mate waarin deze antilichamen in staat waren cellen te doden in combinatie met het bacteriële toxine. Hiermee hebben we aangetoond dat niet elk antilichaam geschikt is om een ADC te maken. Het is daarom belangrijk om verschillende antilichamen te testen om zo de het beste antilichaam te selecteren voor de ontwikkeling van een ADC.

Voor sommige tumor eiwitten lukt het niet om een antilichaam te vinden wat goed wordt opgenomen door de tumorcel en uiteindelijk terecht komt in het lysosoom. Dit maakt het niet gemakkelijk om een ADC te ontwikkelen. Toch zouden we ook deze eiwitten graag willen gebruiken om tumorcellen te kunnen doden met behulp van een ADC. Hoofdstuk 7 beschrijft een methode waarmee de opname van antilichamen door tumor cellen, en het transport naar lysosomen, kan worden verbeterd. Hierbij maken we gebruik van een techniek om bispecifieke antilichamen te maken. Dit zijn antilichamen die twee verschillende eiwitten kunnen herkennen. Door een antilichaam te maken wat naast een tumoreiwit, ook een eiwit kan herkennen dat zorgt voor transport naar het lysosoom, proberen we de opname van antilichamen door tumor cellen te verbeteren. De studie in Hoofstuk 7 toont aan dat dit bispecifieke antilichaam veel beter wordt opgenomen door tumor cellen in vergelijking tot een antilichaam dat alleen het tumor eiwit herkent. Daarnaast zien we dat dit bispecifieke antilichaam beter in staat is om tumor cellen te doden, zodra we het koppelen aan een toxine.

Samengevat laten de resultaten beschreven in dit proefschrift zien dat we door de juiste tumor eiwitten en antilichamen te selecteren, de effectiviteit van ADC's in tumormodellen kunnen verbeteren. Daarnaast hebben we meer inzicht gekregen in welke eigenschappen van tumoreiwitten en antilichamen, belangrijk zijn voor de ontwikkeling van ADC's. Deze kennis kan ons helpen om de ontwikkeling van toekomstige ADC's te verbeteren.

Dankwoord

En dan nu het meest gelezen deel van menig proefschrift. Dit proefschrift bestaat uit maar liefst zes wetenschappelijke artikelen waarvan vier reeds gepubliceerd. Dit alles had ik natuurlijk niet kunnen doen zonder hulp van al mijn Genmab collega's! Ik hoop dan ook dat iedereen bij Genmab zich aangesproken voelt als ik zeg bedankt! Een aantal van jullie wil ik graag even persoonlijk benoemen.

Laat ik beginnen bij het begin, mijn stage bij Jeroen en Wim. Ik wil jullie bedanken voor het vertrouwen dat jullie in mij hebben geschonken en het feit dat jullie een goed woordje voor me hebben gedaan bij Jan en Paul. Zonder jullie was ik waarschijnlijk nooit als promovendus bij Genmab aan het werk gegaan.

Tijdens mijn promotietraject heb ik het genoegen gehad om met veel verschillende collega's te mogen samenwerken. In mijn eerste jaar ben ik ondergebracht bij Edward en later Joost en Luus, waarbij we hartstochtelijk opzoek zijn gegaan naar antagonistische cMet antilichamen. Vervolgens ben ik overgestapt naar het HER2 project en daar heb ik samen met Simone en Wim gewerkt aan het karakteriseren van een panel HER2 antistoffen. Tijdens deze periode kwam ik ook in contact met het anti-kappa toxine van Matthias en Christian, en hiermee werd voorzichtig een link gelegd naar de ADCs. Vanaf dat moment begonnen de artikelen binnen te stromen en werd de definitieve overstap naar de ADCs gemaakt. Hier heb ik me onder toeziend oog van Wim, Patrick, David, Michel en Esther mogen ontpoppen tot ADC expert. Gedurende deze periode heb ik ontzettend veel van jullie geleerd, vooral ook omdat een ieder van jullie het onderzoek op geheel eigen wijze inricht. Met Wim kon ik uren lang discussiëren over een bindingscurve, terwijl David vanuit vogelperspectief het onderzoek de juiste richting in stuurde. Ik wil jullie allemaal bedanken voor de leerzame en leuke periode. Terwijl de directe begeleiding steeds veranderde was er één constante factor gedurende mijn promotie onderzoek, en dat is mijn promotor Paul. Wat het onderwerp ook was, jij kwam altijd met goede adviezen aanzetten en wist lijn aan te brengen in mijn steeds veranderende onderzoek, waarvoor zeer veel dank!

Gedurende mijn promotie onderzoek is er een enorme berg werk verricht, en dat had ik niet kunnen doen zonder de hulp van een aantal zeer getalenteerde studenten Pascal, Maarten en Claudia. Maarten bedankt voor het opzetten van de confocale microscopie experimenten, deze lopen als een rode draad door mijn boekje en succes met Labficience. Claudia (CLF) bedankt voor je hulp op het TF project, het heeft

een mooie publicatie opgeleverd en het had niet veel gescheeld of we hadden het gebruik van biseksuele antistoffen gepatenteerd.

Dan is er nog iemand die inmiddels wel heel veel werk heeft verzet… Hendrik! Naast de enorme berg experimenten die je hebt uitgevoerd, ben je ook een zeer goede sparringpartner en een zeer prettige collega om mee samen te werken. Je hebt het als rustige Urker jongen niet gemakkelijk gehad toen je op één kamer kwam te zitten met Patrick en mij, maar inmiddels heb je alle schroom van je afgezet en je ontwikkeld tot steunpilaar binnen ons cluster. Daarmee is ook meteen de link gelegd naar die andere persoon die het werken bij Genmab tot een feestje maakt… Patrick! Vanaf de eerste dag bij Genmab was er meteen een goede klik, waardoor we zowel binnen als buiten Genmab een hoop mooie dingen hebben meegemaakt. Daarnaast is je parate kennis over B-cell tumoren een grote waarde voor Genmab waar we hopelijk nog lang gebruik van mogen maken.

“I'm pretty sure there's a lot more to life than being really, really, ridiculously smart. And I plan on finding out what that is”, Antonio, Georg en Jelte-Jan, bedankt! Daarnaast wil ik ook graag Marije bedanken voor het goede voorbeeld wat ze heeft gegeven, Mina voor de ontelbare batches die ze voor me heeft vrij gegeven, Tom voor zijn CD63 connectie, Aran, Joyce en Janine voor hun hulp bij de Fab-arm exchange proeven. Richard, Esther en Rob voor het beschikbaar stellen van de confocale microscoop en hun hulp bij het opzetten van de proeven, John voor zijn hulp bij het schrijven van de review, Esther B. voor het vele review werk en Joost (scicomvisuals) voor zijn hulp bij het vervaardigen van dit mooie boekje.

Als afsluiting wil ik mijn lieve vriendin Brenda bedanken voor haar steun. Je hebt me geleerd dat het leven niet alleen draait om werk en bier, er zijn ook andere zaken die nog belangrijker zijn…

List of publications

Bart E.C.G. de Goeij, John M. Lambert. New developments for antibody drug conjugate based therapeutic approaches. *Invitation by Current Opinion in Immunology, June 2016, volume 40.*

Bart E.C.G. de Goeij, Tom Vink, Hendrik ten Napel, Esther C.W. Breij, David Satijn, Richard Wubbolts, David Miao and Paul W.H.I. Parren. Efficient payload delivery by a bispecific antibody that targets HER2 and CD63. *To be submitted.*

Bart E.C.G. de Goeij, David Satijn, Claudia M. Freitag, Richard Wubbolts, Wim K. Bleeker, Alisher Khasanov, Tong Zhu, Gary Chen, David Miao, Patrick H.C. van Berkel, and Paul W.H.I. Parren. High turnover of Tissue Factor enables efficient delivery of antibody-drug conjugates. *Mol Cancer Ther. 2015 May;14(5):1130-40.*

Bart E.C.G. de Goeij, Matthias Peipp, Simone de Haij, Edward N. van den Brink, Christian Kellner, Thilo Riedl, Rob de Jong, Tom Vink, Kristin Strumane, Wim K. Bleeker and Paul W.H.I. Parren. HER2 monoclonal antibodies that do not interfere with receptor heterodimerization-mediated signaling induce effective internalization and represent valuable components for rational antibody-drug conjugate design. *MAbs. 2014 Mar-Apr;6(2):392-402.*

Esther C.W. Breij, **Bart E.C.G. de Goeij**, Sandra Verploegen, Danita H. Schuurhuis, Ali Amirkhosravi, John Francis, Vibeke Breinholt Miller, Mischa Houtkamp, Wim K. Bleeker, David Satijn, and Paul W.H.I. Parren. An antibody-drug conjugate that targets tissue factor exhibits potent therapeutic activity against a broad range of solid tumors. *Cancer Res. 2014 Feb 15;74(4):1214-26.*

Aran F. Labrijn, Joyce I. Meesters, **Bart E. C. G. de Goeij**, Ewald T. J. van den Bremer, Joost Neijssen, Muriel D. van Kampen, Kristin Strumane, Sandra Verploegen, Amitava Kundu, Michael J. Gramer, Patrick H. C. van Berkel, Jan G. J. van de Winkel, Janine Schuurman, and Paul W. H. I. Parren Efficient generation of stable bispecific IgG1 by controlled Fab-arm exchange. *Proc Natl Acad Sci U S A. 2013 Mar 26;110(13):5145-50.*

Christian Kellner, Wim K. Bleeker, Jeroen J. Lammerts van Bueren, Matthias Staudinger, Katja Klausz, Stefanie Derer, Pia Glorius, Anja Muskulus, **Bart E.C.G. de Goeij**, Jan G.J. van de Winkel, Paul W.H.I. Parren, Thomas Valerius, Martin Gramatzki and Matthias Peipp. Human kappa light chain targeted Pseudomonas exotoxin A – identifying human antibodies and Fab fragments with favorable characteristics for antibody-drug conjugate development. *J Immunol Methods. 2011 Aug 31;371(1-2):122-33.*

Laura A. Smit, Delfine Y.H. Hallaert, René Spijker, **Bart de Goeij**, Annelieke Jaspers, Arnon P. Kater, Marinus H.J. van Oers, Carel J.M. van Noesel and Eric Eldering. Differential Noxa/Mcl-1 balance in peripheral versus lymph node chronic lymphocytic leukemia cells correlates with survival capacity. *Blood. 2007 Feb 15;109(4):1660-8.*